A Controlled Release Microchip

by

John Thomas Santini, Jr.

B.S.E., Chemical Engineering
University of Michigan, 1994

Submitted to the Department of Chemical Engineering
in Partial Fulfillment of the Requirements for the Degree of

Doctor of Philosophy in Chemical Engineering

at the

Massachusetts Institute of Technology
September 1999

Signature of Author .....
John T. Santini, Jr.
Department of Chemical Engineering
July 28, 1999

Certified by .....
Robert S. Langer
Kenneth J. Germeshausen Professor of Chemical and Biomedical Engineering
Thesis Supervisor

Certified by .....
Michael J. Cima
Sumitomo Electric Industries Professor of Engineering
Thesis Supervisor

Accepted by .....
Robert E. Cohen
St. Laurent Professor of Chemical Engineering
Chairman, Committee for Graduate Students

A Controlled Release Microchip
by
John Thomas Santini, Jr.

Submitted to the Department of Chemical Engineering
on July 28, 1999, in partial fulfillment of the requirements for the degree of
Doctor of Philosophy in Chemical Engineering

ABSTRACT

It is well known that the method by which a drug is delivered can have a significant effect on the drug's therapeutic efficacy. There exist numerous cases where constant release is not the optimal method of drug delivery; instead, delivery of pulses of drug at variable time intervals is the preferred method. This method is commonly referred to as pulsatile delivery, and it is preferred in some cases because it closely mimics the way in which the human body naturally produces the compounds.

The objectives of this thesis were to design, fabricate, and characterize a microchip capable of achieving both pulsatile and continuous release of multiple chemical substances on demand. Each prototype microchip consisted of an array of reservoirs etched into and extending through a silicon wafer. Each reservoir was covered on one end by a thin conductive membrane that served as the anode in an electrochemical reaction. The reservoir was filled with chemicals through the other side of the reservoir and was then sealed. The proposed release mechanism had no moving parts and was based on the electrochemical dissolution of a thin anode membrane covering each reservoir. Each reservoir was independently addressable, and the electric potential was applied to an anode membrane using wires and a potentiostat. Future integration of microelectronic components may allow reservoirs to be opened on demand by a preprogrammed microprocessor, remote control, or by biosensors and biofeedback controllers. Potential advantages of the microchip for the release of drugs and other chemicals may include its small size, low power consumption, and the absence of moving parts. Such microchips may find application in a wide array of fields such as drug delivery, medical diagnostics, chemical detection, industrial process monitoring and control, and micro-scale chemical synthesis.

A process was developed for producing prototype microchips using microfabrication methods such as ultraviolet photolithography, chemical vapor deposition (CVD), reactive ion etching (RIE), and electron beam evaporation. An important component of this process was a procedure for making thin (1000-3000 Å), unsupported, metal membrane anodes on silicon. In addition, the fabrication process was designed so that the chemicals to be released would never be exposed to solvents, acids, bases, or high temperatures. This was accomplished by completing all device fabrication steps before reservoir filling. This important process feature would be especially useful when dealing with easily denatured molecules such as proteins or DNA.

Gold was selected as the model membrane and electrode material for the prototype controlled release microchips primarily due to its unique electrochemical properties. It is easily deposited and patterned, has a low reactivity with other substances, and resists spontaneous corrosion in most aqueous solutions over the entire pH range. However, the presence of a small amount of chloride ion in solution creates an electric potential/pH region that thermodynamically favors the dissolution of gold as water soluble gold chloride complexes. Experiments showed

that gold thin films are rapidly corroded in saline solution and that corrosion occurs preferentially in the grain boundaries.

Release studies were conducted to demonstrate that single and multiple substances could be released from microchip devices on demand. Sodium fluorescein (a fluorescent dye) and radioactive calcium (in the form, $^{45}CaCl_2$) were chosen as model substances for release due to their simplicity of detection in solution. Prototype devices were filled with one or both substances, sealed, and submerged in either phosphate buffered saline or 0.145 M NaCl solution. A potential of +1.04 volts relative to a saturated calomel reference electrode (SCE) was applied between a gold membrane anode covering a filled reservoir and a cathode. Electrochemical dissolution of the gold membrane anode typically occurred within 10-20 seconds of application of the potential. Once the reservoir was opened, the compound in the reservoir was able to diffuse into the surrounding solution and was detected by fluorescence spectroscopy or scintillation counting. This process was repeated to obtain multiple releases from a single device.

Disintegration refers to the "falling apart" of a gold membrane over a reservoir resulting from gold corrosion and possibly, applied physical stresses. The visualization of the membrane disintegration process was achieved by videotaping the corrosion of gold membranes through a microscope. The observations from these *in situ* membrane disintegration experiments were then combined with gold corrosion concepts and data to develop a qualitative mechanism for the disintegration of thin, gold membranes covering chemical reservoirs.

Future work should focus on materials science issues, microelectronics fabrication and packaging, and *in vivo* studies.

Thesis Supervisor: Robert Langer
Title: Kenneth J. Germeshausen Professor of Chemical and Biomedical Engineering

Thesis Supervisor: Michael J. Cima
Title: Sumitomo Electric Industries Professor of Engineering

ACKNOWLEDGMENTS

I'm very thankful that I had the opportunity to do my graduate study at MIT. My five years here have been challenging at times, but the knowledge and experience that I have acquired while at MIT will benefit me in the years to come. I am also thankful for the wonderful friendships and fond memories that I will take away from MIT. These will remain with me for the rest of my life.

Before I say goodbye to the my home away from home in the basement of building 12, the infinite corridor, Lobdell food, and Laverdes' subs, I would like to thank a number of people that helped to make my time at MIT enjoyable and productive.

Bob Langer and Michael Cima, for the opportunity to work on the controlled release microchip project and your mentorship over the years.

My thesis committee, Klavs Jensen, Carl Thompson, and Ron Latanision, for helpful discussions and suggestions about my research.

My UROPS, Nishla Keiser and Allie Lin, for all the time and hard work they put into their experiments. The data they collected were an important part of this thesis.

All the members of the Cima and Langer Labs, for their advice, suggestions, and support over the years, you all were a great help when my research seemed to hit a brick wall. I also want to thank them for their friendship and the fun that we had together both in and out of the office and the lab. These memories are very special to me.

Lenny Rigione and John Centorino, for always being willing to spend their valuable time to help me with trying new experiments or working with new equipment.

Barbara Layne, Pam Brown, and Connie Beal, for putting up with me and all my questions about administrative stuff.

Rich Perilli, formerly of the Bldg. 13 Microlab, for getting me started in the field of microfabrication.

Vicky Diadiuk and the others at MTL, for helping with my many microfabrication processing questions.

All the students in H-entry at MacGregor House when I was a graduate resident tutor, I appreciate the friendships we formed and enjoyed watching you as you grew while at MIT.

The graduate resident tutors, housemasters, and building manager at MacGregor House, it was a great three years working with you.

Most important of all, Cathy (my wife-to-be), my parents - John and Pat Santini, my brother Andrew, and my love for God and the Catholic faith, none of this would have been possible without the love, strength, and support that you have given me. You are all truly a blessing.

TABLE OF CONTENTS

LIST OF FIGURES

LIST OF TABLES

1. INTRODUCTION

1.1 Overview of controlled release.

1.1.1 Definition. Controlled release, as used in this thesis, refers to a field of study focused on developing technologies having the ability to release chemicals in a controlled way. This can include controlling the release time of a chemical, the release rate, or both. Controlled release technology has proved useful in a number of areas such as food products and fragrance delivery, but it has had its largest impact in the field of drug delivery.

1.1.2 Background. It is well known that the method by which a drug is delivered can have a significant effect on the drug's therapeutic efficacy[1]. For some drugs, there exists an optimum range of concentrations in which the maximum therapeutic benefit is derived. Drug concentrations above this range can be toxic, while concentrations below this range may produce no therapeutic effect at all. Conventional drug delivery systems such as tablets or injections typically result in a drug delivery profile initially marked by a sharp increase in concentration to a peak above the therapeutic range. The drug concentration then continues to decrease until it falls below the therapeutic range. Therefore, the time spent in the optimum concentration range is short. For potent drugs, initial concentration peaks can pose a serious risk of toxicity. For drugs such as antibiotics, a minimum concentration must be maintained for an extended period. If the concentration falls below this minimum level, there is a risk of creating dangerous, drug-resistant strains of bacteria. The field of controlled release initially focused on achieving a nearly constant release of drug over an extended period of time with minimal influence by outside factors such as pH[2]. Much of this work involved the use or development of polymers that released drug at a constant rate due to drug diffusion out of the polymer or by the degradation of the polymer over time. Some examples of commercially available polymeric devices for constant drug release are Gliadel®[3] (poly(anhydride) wafers that release BCNU at a constant rate as the polymer degrades—for the treatment of malignant brain tumors) and Norplant®[4] (silicone rods that release birth control drugs at a constant rate via diffusion out of the polymer—for contraception).

However, there exist numerous cases where constant release is not the optimal method of drug delivery. Instead, delivery of pulses of drug at variable time intervals is the preferred method and is commonly referred to as pulsatile delivery. This delivery method works better in some cases because it closely mimics the way in which the human body naturally produces the compounds. Insulin is a well-known example of a compound secreted by the body in a pulsatile manner[5]. Another example of compounds produced by the body in a pulsatile or periodic manner are the hormones of the anterior pituitary gland (adenohypophysis). Adenohypophyseal hormones such as gonadotropin, growth hormone, and thyrotropin are important in reproduction, growth, and the regulation of other body systems such as the cardiovascular system. Many compounds and environmental factors can stimulate or inhibit the production of these hormones. However, compounds secreted by the hypothalamus, called releasing factors or hormones, play a primary role in the regulation of adenohypophyseal hormones. For instance, women suffering from gonadotropin releasing hormone (GnRH) deficiency may not ovulate normally, making it difficult to conceive a child. Growth hormone releasing hormone (GHRH) deficiency in children may lead to dwarfism. Research has shown that the pulsatile administration of GnRH and GHRH can help reduce the severity of these deficiencies[6,7]. In fact, it has been shown that continuous administration of GnRH results in desensitization of GnRH receptors on the pituitary gland and may actually suppress the release of gonadotropins[8].

Much previous work in methods of achieving pulsatile release has focused on polymeric materials that respond to specific stimuli[9]. Researchers have developed ways to take advantage of changes in a polymer's physical properties to release drugs or other compounds in response to changes in electric[10-13] or magnetic[14,15] fields, exposure to ultrasound[15,16], light[17], or enzymes[18], and changes in pH[19] or temperature[20-22]. However, in some cases the stimuli source can be large, expensive, or too complex for frequent use and in other cases the baseline or "off" release rate is usually non-zero. Application of the stimuli will cause a large increase in release (the "on" state), but removal of the stimuli (the "off" state) will not stop release completely. As a result, few of these polymeric pulsatile release systems have been commercially viable.

An alternative method of pulsatile release involves the use of pumps and catheters. Pumps work well for pulsatile release and can be programmed to deliver pulses of drug solutions to a patient through a catheter at variable times. In fact, one of the current methods for treating

GnRH deficiency in women involves wearing a pump (about the size of an adult fist) on the belt with a catheter inserted into the woman, either subcutaneously or intravenously[23-25]. This pump delivers a pulse of a solution containing 5 μg of GnRH every 90 minutes continuously for several weeks to months. However, pump and catheter systems such as this can be inconvenient and uncomfortable, can limit a patient's mobility and activity, are limited to delivering solutions only, and may result in infections at the catheter site.

1.2 Overview of microfabrication technology.

1.2.1 Definition. Microfabrication technology, as used in this thesis, "is denoted by the use of photolithographic pattern transfer methods to produce micron-scale features in a manufacturing method that is compatible with batch fabrication and has a high degree of reproduction accuracy."[26] Microfabrication technology has traditionally been used to produce microelectronic devices such as computer microprocessors. However, microfabrication technology has been used increasingly to produce micron-scale devices whose primary function may be mechanical, chemical, or optical in nature. Such devices include microreactors, micropumps, accelerometers, and micromirrors, and are commonly referred to as MEMS, or microelectromechanical systems.

1.2.2 Background. Microfabrication technology and microfabricated devices have found use in a number of fields. Two of the most notable examples include the fabrication of nozzles for ink jet printers[27] and accelerometers for automotive applications[28]. More recent examples include the fabrication of microreactors for the production of chemicals[29,30] and micro-turbine engines for aerospace applications[31,32].

Microfabricated devices for biological applications can generally be placed into one of two categories, microfluidic devices and non-microfluidic devices. Microfluidics is an area of microfabrication that focuses on the miniaturization of fluid handling systems such as pumps, valves, and flow channels. The concept of fabricating an entire chemical "lab-on-a-chip" including pumps, valves, mixers, reactors, and separators has generated a lot of interest in microfluidics over the last several years[33,34]. The interest in microfluidics for biological applications has focused largely on developing microsystems for chemical[35-37] or DNA[38-40]

analysis. The fabrication of such systems has resulted in the development of numerous microfluidic components such as micropumps and microvalves[41,42]. These micropumps can be based on moving parts such as diaphragms or piezoelectric components that mechanically pump liquids[36,43-45]. Some micropumps may not have moving parts, but may move ionic fluids using electric fields (i.e. electrophoresis)[46-48]. Microfabricated valves may be reversible, as in the case of pneumatic[49] and thermoelectric[50] valves, or they may be irreversible. A theoretical example of an irreversible microvalve involves placing a dissolvable membrane between two solutions. Dissolving the membrane in the presence of a pressure gradient irreversibly opens the membrane and allows liquids to flow from one side of the valve to the other[51]. Unfortunately, a limitation of micropumps, microvalves, and other microfluidic components is that they can only be used with liquid materials. There are even limitations on the types of liquids that can be used with electrophoretic micropumps. Microfluidic components involving moving parts suffer from reliability concerns, while other components are disadvantaged by complex fabrication schemes. For example, the presence of a single air bubble in a micropump containing moving parts may cause the pump to fail. The operation of some microfluidic components, such as the irreversible microvalves mentioned previously[51], have never been demonstrated.

Non-microfluidic devices for biological applications include "DNA chips"[52]. These devices do not involve the pumping or movement of fluids on the microchip, but instead use immobilized materials on the device surface to identify genetic material or other chemicals[53,54]. The relative simplicity of these devices and their ease of manufacture has made them popular with pharmaceutical companies for high throughput drug screening and combinatorial chemistry.

The use of microfabrication in the field of controlled release has been limited. One could envision using microfluidic devices to achieve pulsatile drug release, but the limitations of delivering only liquid drug formulations, the complexity of fabrication schemes, and the presence of moving parts that are subject to breakdown, are significant and may present obstacles to their clinical and commerical use. As a result, the field of controlled release has not been able to take full advantage of microfabrication technology.

1.3 Thesis objectives. The specific objectives of this Ph.D. thesis are:

(1) To propose the design of a microfabricated device having the ability to release multiple chemical substances in a highly controlled manner. (Chapter 2)

   (a) The device should not be limited to the release of liquids, but should have the potential to release solids and gels as well.

   (b) The release mechanism should be simple and contain no moving parts.

(2) To select materials and develop a method of fabricating the devices proposed in objective (1). (Chapters 3 & 4)

(3) To design and conduct chemical release studies to prove the principle of operation of the devices proposed in objective (1) is feasible. (Chapter 5)

(4) To present observations and propose a qualitative mechanism for the disintegration of the gold membrane reservoir caps in the devices proposed in objective (1). (Chapter 6)

1.4 References.

1. Bakken, E.E. & Heruth, K. "Temporal control of drugs, an engineering perspective." *Ann. New York Acad.Sci.* **618**, 422-427 (1991).
2. Langer, R. "New methods of drug delivery." *Science* **249**, 1473-1624 (1990).
3. "Gliadel Wafer" in *Physicians' Desk Reference* (ed. Arky, R.) 2365-2367 (Medical Economics Company, Inc., Montvale, NJ, 1998).
4. "Norplant System" in *Physicians' Desk Reference* (ed. Arky, R.) 3085-3089 (Medical Economics Company, Inc., Montvale, NJ, 1998).
5. Matthews, D.R., Lang, D.A., Burnett, M.A. & Turner, R.C. "Control of pulsatile insulin secretion in man." *Diabetologia* **24**, 231-237 (1983).
6. Gelato, M.C. & Merriam, G.R. "Growth hormone releasing hormone." *Ann. Rev. Physiol.* **48**, 569-591 (1986).
7. Reid, R.L., Fretts, R. & Vugt, D.A.V. "The theory and practice of ovulation induction with gonadotropin-releasing hormone." *American Journal of Obstentrics and Gynocology* **158**, 176-185 (1988).
8. Kuret, J.A. & Murad, F. "Adenohypophyseal hormones and related substances" in *Goodman and Gillman's, The Pharmacological Basis of Therapeutics* 1334-1360 (Pergamon Press, New York, NY, 1990).
9. Kost, J. & Langer, R. "Responsive polymeric delivery systems." *Advanced Drug Delivery Reviews* **6**, 19-50 (1991).
10. Miller, L.L. "Electrochemically controlled release of drug ions from conducting polymers." *Mol. Cryst. Liq. Cryst.* **160**, 297-301 (1988).
11. Kwon, I.C., Bae, Y.H. & Kim, S.W. "Electrically erodible polymer gel for controlled release of drugs." *Nature* **354**, 291-293 (1991).

12. Bae, Y.H., Kwon, I.C. & Kim, S.W. "Pulsatile drug release by electrical stimulus" in *Polymeric Drugs and Drug Administration, ACS Symposium Series No. 545* (ed. Ottenbrite, R.M.) 98-110 (Americal Chemical Society, Washington, DC, 1994).
13. Hepel, M. & Fijalek, Z. "Electrorelease of drugs from composite polymeric films" in *Polymeric Drugs and Drug Administration, ACS Symposium Series No. 545* (ed. Ottenbrite, R.M.) 79-97 (Americal Chemical Society, Washington, DC, 1994).
14. Edelman, E.R., Kost, J., Bobeck, H. & Langer, R. "Regulation of drug release from polymeric matrices by oscillating magnetic fields." *Journal of Biomedical Materials Research* **19**, 67-83 (1985).
15. Kost, J. & Langer, R. "Magnetically and ultrasonically modulated drug delivery systems" in *Pulsed and Self-Regulated Drug Delivery* (ed. Kost, J.) 3-15 (CRC Press, Boca Raton, 1990).
16. Kost, J., Leong, K. & Langer, R. "Ultrasound-enhanced polymer degredation and release of incorporated substances." *Proc. Natl. Acad. Sci. USA* **86**, 7663-7666 (1989).
17. Mathiowitz, E. & Cohen, M.D. "Polyamide microcapsules for controlled release. V. Photochemical release." *Journal of Membrane Science* **40**, 67-86 (1989).
18. Fischel-Ghodsian, F., Brown, L., Mathiowitz, E., Brandenburg, D. & Langer, R. "Enzymatically controlled drug delivery." *Proc. Natl. Acad. Sci. USA* **85**, 2403-2406 (1988).
19. Siegel, R.A., Falamarzian, M., Firestone, B.A. & Moxley, B.C. "pH-controlled release from hydrophobic/polyelectrolyle copolymer hydrogels." *Journal of Controlled Release* **1988**, 179-182 (1988).
20. Hoffman, A.S., Afrassiabi, A. & Dong, L.C. "Thermally reversible hydrogels: II. Delivery and selective removal of substances from aqueous solutions." *Journal of Controlled Release* **4**, 213-222 (1986).
21. Bae, Y.H., Okano, T., Hsu, R. & Kim, S.W. "Thermo-sensitive polymers as on-off switches for drug release." *Makromol. Chem., Rapid Commun.* **8**, 481-485 (1987).
22. Okano, T., Bae, Y.H. & Kim, S.W. "Temperature responsive controlled drug delivery" in *Pulsed and Self-Regulated Drug Delivery* (ed. Kost, J.) 17-45 (CRC Press, Boca Raton, 1990).
23. Santoro, N. "Efficacy and safety of intraveneous pulsatile gonadotropin-releasing hormone: Lutrepulse for injection." *American Journal of Obstetrics and Gynecology* **163**, 1759-1764 (1990).
24. Creasy, G.W. & Jaffe, M.E. "Pulsatile delivery systems." *Ann. New York Acad. Sci.* **618**, 548-557 (1991).
25. Creasy, G.W. & Jaffe, M.E. "Endocrine/reproductive pulsatile delivery systems." *Advanced Drug Delivery Reviews* **6**, 51-56 (1991).
26. Schmidt, M.A. "Personal communication" (1999).
27. Bassous, E., Taub, H.H. & Kuhn, L. "Ink jet printing nozzle arrays etched in silicon." *Applied Physics Letters* **31**, 135-137 (1977).
28. Roylance, L.M. & Angell, J.B. "A batch fabricated silicon accelerometer." *IEEE Transactions on Electron Devices* **ED-26**, 1911-1917 (1979).
29. Srinivasan, R., *et al.* "Micromachined chemical reactors for surface catalyzed oxidation reactions" in *IEEE Proc. Solid State Sensor and Actuator Workshop* 15-18 (IEEE, Hilton Head, SC, 1996).
30. DeWitt, S.H. "Microreactors for chemical synthesis." *Current Opinions in Chemical Biology* **3**, 350-356 (1999).

31. Epstein, A.H. & Senturia, S.D. "Macro power from micro machinery." *Science* **276**, 1211 (1997).
32. Epstein, A.H., *et al.* "Micro-heat engines, gas turbines, and rocket engines" in *28th AIAA Fluid Dynamics Conference, 4th AIAA Shear Flow Control Conference* (American Institute of Aeronautics and Astronautics, Snowmass Village, CO, 1997).
33. Freemantle, M. "Downsizing chemistry, chemical analysis and synthesis on microchips promise a variety of potential benefits" in *Chemical and Engineering News* 27-36 (1999).
34. Service, R.F. "Coming soon: The pocket DNA sequencer." *Science* **282**, 399-401 (1998).
35. Nakagawa, S., Shoji, S. & Esashi, M. "A micro chemical analyzing system integrated on a silicon wafer" in *Proc. IEEE Microelectromechanical systems (MEMS 90)* 89-94 (IEEE, Napa Valley, CA, 1990).
36. van der Schoot, B.H., Jeanneret, S., Berg, A.v.d. & Rooij, N.F.d. "A modular miniaturized chemical analysis system." *Sensors and Actuators B.* **13-14**, 333-335 (1993).
37. Blankenstein, G. & Larsen, U.D. "Modular concept of a laboratory on a chip for chemical and biochemical analysis." *Biosensors & Bioelectronics* **13**, 427-438 (1998).
38. Burns, M.A., *et al.* "Microfabricated structures for integrated DNA analysis." *Proc. Natl. Acad. Sci. USA* **93**, 5556-5561 (1996).
39. Burns, M.A., *et al.* "An integrated nanoliter DNA analysis device." *Science* **282**, 484-487 (1998).
40. Mastrangelo, C.H., Burns, M.A. & Burke, D.T. "Microfabricated devices for genetic diagnostics." *Proceeding of the IEEE* **86**, 1769-1787 (1998).
41. Gravesen, P., Branebjerg, J. & Jensen, O.S. "Microfluidics-a review." *J. Micromech. Microeng.* **3**, 168-182 (1993).
42. Shoji, S. & Esashi, M. "Microflow devices and systems." *J. Micromech. Microeng.* **4**, 157-171 (1994).
43. Smits, J.G. "Piezoelectric micropump with three valves working peristaltically." *Sensors and Actuators* **A21-A23**, 203-206 (1990).
44. Schomburg, W K., Fahrenberg, J., Maas, D. & Rapp, R. "Active valves and pumps for microfluidics." *J. Micromech. Microeng.* **3**, 216-218 (1993).
45. Bourouina, T., Bosseboeuf, A. & Grandchamp, J.-P. "Design and simulation of an electrostatic micropump for drug-delivery applications." *J. Micromech. Microeng.* **7**, 186-188 (1997).
46. Fuhr, G., Hagedorn, R., Muller, T., Benecke, W. & Wagner, B. "Microfabricated electrohydrodynamic (EHD) pumps for liquids of higher conductivity." *Journal of Microelectromechanical Systems* **1**, 141-146 (1992).
47. Harrison, D.J., *et al.* "Micromachining a miniaturized capillary electrophoresis-based chemical analysis system on a chip." *Science* **261**, 895-897 (1993).
48. Manz, A., *et al.* "Electroosmotic pumping and electrophoretic separations for miniaturized chemical analysis systems." *J. Micromech. Microeng.* **4**, 257-265 (1994).
49. Vieider, C., Ohman, O. & Elderstig, H. "A pneumatic actuated microvalve with a silicon rubber membrane for integration with fluid-handling systems" in *Dig. Int. Conf. Sensors and Actuators (Transducers '95)* 284-286 (Stockholm, Sweden, 1995).
50. Franz, J., Baumann, H. & Trah, H.-P. "A silicon microvalve with integrated flow sensor" in *Dig. Int. Conf. Sensors and Actuators (Transducers '95)* 313-316 (Stockholm, Sweden, 1995).

51. Madou, M. in *Fundamentals of Microfabrication* 485-486 (CRC Press, Boca Raton, FL, 1997).
52. Service, R.F. "Microchip arrays put DNA on the spot." *Science* **282**, 396-399 (1998).
53. Eggers, M., *et al.* "A microchip for quantative detection of molecules utilizing luminescent and radioisotope reporter groups." *Biotechniques* **17**, 516-524 (1994).
54. Yershov, G., *et al.* "DNA analysis and diagnostics on oligonucleotide microchips." *Prod. Natl. Acad. Sci. USA* **93**, 4913-4918 (1996).

2. A CONTROLLED RELEASE MICROCHIP

2.1 Theory of operation. The controlled release microchip consists of an array of reservoirs extending through an electrolyte-impermeable substrate material. Each of these reservoirs is sealed on one end by a thin membrane of material that serves as an anode in an electrochemical reaction. The anode consists of a conductive material that electrochemically dissolves when an electric potential is applied to it in an electrolyte. There are several other electrodes on the device surface that serve as cathodes in the electrochemical reaction. These cathodes can be made of any conductive material but are usually made of the same material as the anodes in order to simplify fabrication procedures. The reservoirs are filled through the open end (i.e. the end not covered with the anode membrane) with the chemical to be released. The open ends of the reservoirs are then sealed with a waterproof material after filling.

The device is submerged in an electrolyte containing ions that form a soluble complex with the anode material in its ionic form. A potential is applied to an anode membrane when release is desired from its corresponding reservoir. This causes the anode material to oxidize and form the soluble complex with the electrolyte ions. The soluble complex then dissolves into the electrolyte, causing the membrane to disappear. The chemical in the newly opened reservoir is now exposed to the surrounding electrolyte and is free to dissolve in the electrolyte and diffuse out of the reservoir. A cross section of a typical controlled release microchip is given in figure 2-1 to help illustrate the device concept.

Any complex chemical release pattern can be broken down into a combination of two parameters: release rate and release time. A unique feature of the controlled release microchip is the ability to control both the release rate and release time of chemicals from the device. The release rate is a function of the dissolution rate of the chemical while it's in the reservoir and the diffusion rate of the material out of the reservoir. The composition and properties of the material placed in the reservoir will determine if the dissolution or diffusion process is limiting. For example, the release of a chemical from a reservoir can be dissolution limited if its pure form is only slightly soluble in the electrolyte or if it's mixed with a polymer that dissolves slowly in the electrolyte. Conversely, the release can be diffusion controlled when the chemical is soluble in its pure form or is mixed with polymers that are soluble in the electrolyte. In either case,

agitation of the electrolyte can aid in chemical release from a reservoir by preventing the build up of chemicals outside of the reservoir opening, which would decrease the driving force for dissolution of the chemical in the electrolyte or diffusion of the chemical out of the reservoir. In other words, agitation helps maintain sink conditions in the electrolyte.

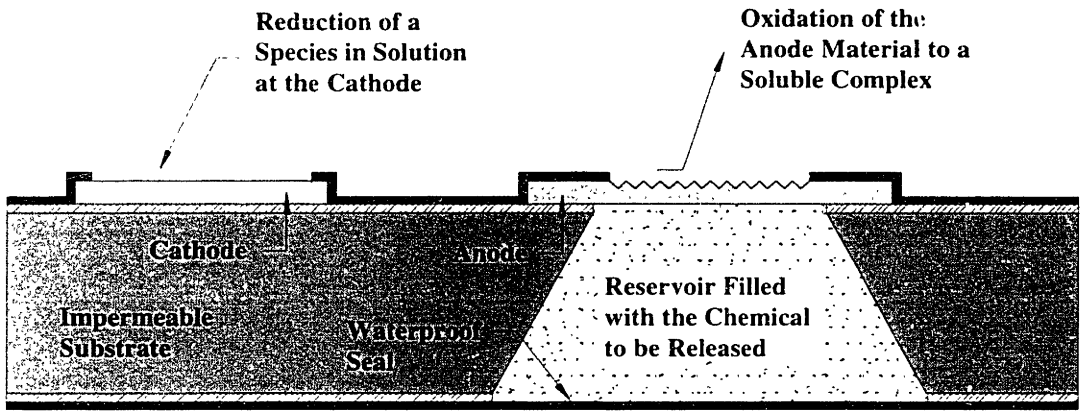

Figure 2-1. Cross section of a typical controlled release microchip.

The time at which release is begun from any reservoir can also be controlled with the microchip. Spontaneous release from a reservoir will not occur if the anode membrane material is stable in the electrolyte solution. Therefore, an anode membrane material is selected that will not dissolve and open until the correct electric potential is applied. The anode membranes covering the reservoirs each have their own conducting path to the power source. This makes each reservoir (or group of reservoirs) "independently addressable," allowing electric potentials to be applied to any combination of reservoirs at any given time.

2.2 Potential advantages. We demonstrated for the first time, the storage and release of multiple chemical substances from a microchip device having no moving parts[1]. This new method of chemical delivery could represent, with further study, a substantial step forward in the development of "smart" drug delivery systems. Other fields besides drug delivery where this technology may find use include medical diagnostics, analytic chemistry, chemical detection, industrial process monitoring and control, combinatorial chemistry, microbiology, and fragrance

delivery. The controlled release microchip can best be understood by examining some of its potential advantages, as listed in the next several paragraphs. (Note: The term "microchip" as used herein, refers to the microfabricated silicon-based devices we've developed for controlled release applications.)

Chemicals in any form (solid, liquid, or gel) can be delivered by the microchip. Microfluidic devices such as pumps are limited to delivering only liquids. The controlled release microchip consists of a reservoir covered by a thin membrane of material that can be dissolved on demand. The form of the chemical or drug inside the reservoir has little or no effect on the electrochemical behavior of the membrane. Therefore, the microchip is not limited to delivering only liquids.

The microchip has no moving parts. A thin barrier membrane covers each reservoir filled with one or more chemicals. These chemicals can be released from the microchip by the disintegration of the membrane. The membrane is removed by the application of an electric potential, which causes the membrane to dissolve by a simple electrochemical reaction. The absence of moving parts increases device reliability by decreasing the possibility of mechanical breakdown.

Complex release patterns (such as simultaneous continuous and pulsatile release) can be achieved from the microchip. Each chemical filled reservoir in the microchip can be activated and opened independently of all the other reservoirs on the microchip. This allows complete control over the time of chemical release from the device. The rate of chemical release from each individual reservoir can be controlled by the properties of the material in that reservoir. For example, chemicals can theoretically be released from a reservoir for an extended period at a constant rate if the chemical is mixed with a polymer that dissolves slowly over time. However, this constant release will not begin until the moment the reservoir is opened. Therefore, both the time at which release begins and the rate of release from a reservoir can be theoretically controlled. This type of control could be achieved using preprogrammed microprocessors, remote control units, or biosensors.

A variety of highly potent drugs can potentially be delivered from the microchip in a safe manner. It is important that the amount of drug delivered to a patient matches the amount prescribed, especially for highly potent compounds. It is difficult to accurately measure small

quantities of drug for incorporation into conventional drug delivery vehicles such as pressed tablets. This leads to a large uncertainty relative to the total amount of drug in the tablet. However, each reservoir of a microchip can be accurately filled with a small amount of the highly potent compound using micro-injection or ink jet printing techniques. The amount of drug administered can be tightly controlled and accidental overdose is unlikely because release from active devices can only occur when an electric potential is applied to that reservoir. Larger doses can be administered by simply opening multiple reservoirs simultaneously.

The microchip can be made small enough to make local delivery of chemicals possible. An advantage of local drug delivery is that high concentrations of drug can be achieved at the site where it is needed, while keeping the systemic concentration of the drug at a low level. This is particularly helpful if the drug has adverse side effects if administered systemically in high doses. For example, BCNU (Carmustine) is used extensively in the treatment of malignant brain tumors[2]. Large amounts of BCNU must be administered to a patient systemically to achieve the minimum acceptable concentration of BCNU at the tumor site in the brain. This is largely due to the impermeability of the blood-brain barrier to most drugs. The resulting large systemic concentration of BCNU causes many extreme side effects affecting the liver, kidneys, and spleen. Implantation of polymer wafers containing BCNU at the tumor site (after tumor removal) allows the local concentration of BCNU at the tumor site to be 1000 times higher than that possible with systemic delivery. However, the systemic concentration of BCNU is kept quite low, greatly reducing the side effects normally associated with BCNU therapy. This treatment is not a cure for brain cancer. However, this therapy does extend life and greatly improve the quality of life of the patient during treatment and is a good illustration of the benefits of local drug delivery.

Multiple chemicals can be stored and released from the microchip. Each reservoir can be filled with a different chemical or combination of chemicals. The development of a "pharmacy-on-a-chip" has become a future possibility because there is enough room on a dime-sized microchip for over 1000 reservoirs.

Some new protein-based drugs have limited stability (i.e. shelf life). Water penetration into these protein drug formulations is the most frequent cause of their instability. The membrane covering filled reservoirs will prevent water penetration into the reservoirs. The

stability of protein drugs is theoretically enhanced by the microchip because the drug can be isolated from the outside environment (i.e. hermetically sealed).

2.3 Potential applications. The goal of this thesis was to demonstrate fabrication and operational proof-of-principle for a microchip device for chemical and drug delivery. However, the feasibility of using a microchip for drug delivery applications was examined and the microchip's operational space was defined before beginning the proof-of-principle studies. As used herein, operational space refers to the combination of number of doses and amount per dose that could be utilized in a prototype microchip. The results of this feasibility survey are displayed in figure 2-2. Figure 2-2 shows the relationship between the number of doses and the amount of drug per dose for a small sampling of drugs representing several large families of compounds such as antibiotics, steroids, and hormones. Treatment with some drugs may continue indefinitely and are represented on the plot by horizontal arrows. Other therapies are continued for a limited period of time and are represented on the plot by distinct points. Typical, systemic drug dosages can range from 5 μg or less to more than one gram per dose[3-5]. The elapsed time between each dose can vary anywhere from a few minutes to several weeks, depending on the nature of the compound and its potency. The delineation of the operational space of the microchip delivery device is vital for selecting possible applications for the device and understanding its place among the conventional drug delivery methods. The operational spaces for 17 mm by 17 mm prototype microchips of differing thickness (based on approximately 1156 reservoirs per microchip) are indicated by the dashed diagonal lines in figure 2-2. Any chemical substances found below and to the left of these dashed lines are possible candidates for delivery by the prototype microchips. Notice that the microchips represented on this plot would be useful for delivering potent drugs such as hormones and steroids. Additional potent drugs that could potentially be delivered by the microchip, but are not indicated in the plot, include drugs for cancer chemotherapy, gene therapy, and the treatment of chronic pain (using potent pain killers such as the morphine derivatives). However, some drugs on the plot are currently delivered in large systemic doses because there exists no good method to deliver them by another route. It may be possible to use microchip technology to change the drug's route of administration from systemic to local. Local delivery could possibly decrease the amount of drug

required, thereby increasing the number of drugs that fall within the microchip's operational space.

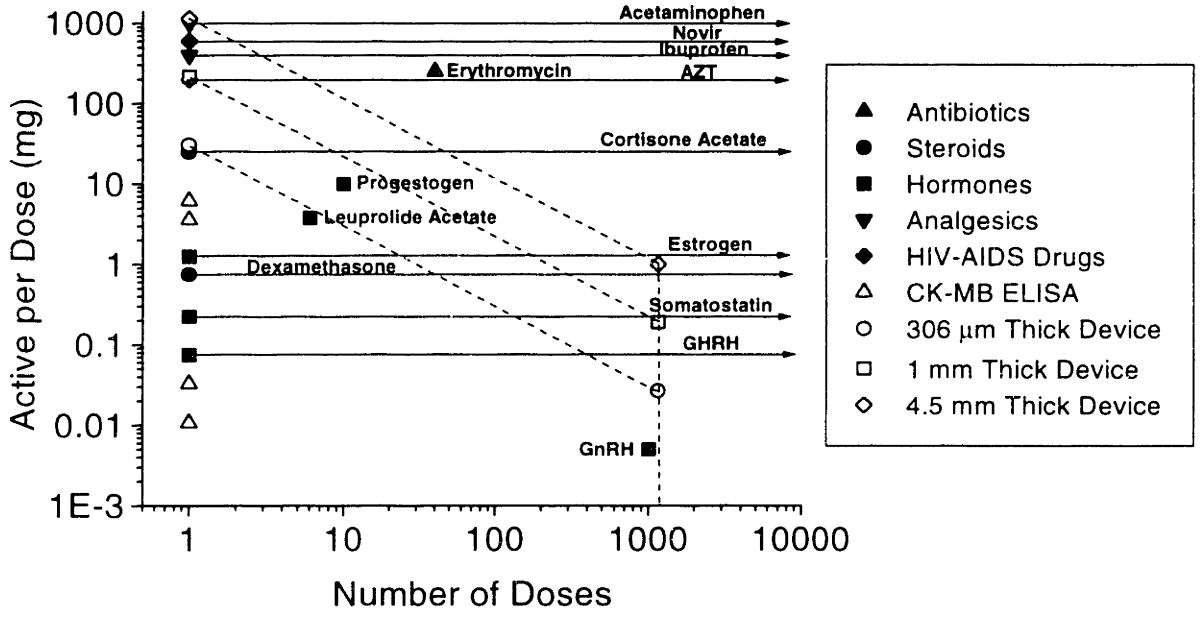

Figure 2-2. Operational space for a 17 mm by 17 mm microchip drug delivery device having 1156 reservoirs.

The microchip has many other possible uses outside of drug delivery, even though figure 2-2 focuses primarily on that field. In general, the microchip could be used in any application where small amounts of chemicals had to be controllably released. An example outside of drug delivery where this technology would be useful is in diagnostics. A tiny, disposable microchip could be fabricated and filled with all of the reagents needed for a particular diagnostic assay. A tiny microprocessor on the microchip could be preprogrammed to release the reagents in the correct amounts and in the proper sequence so that the assay could be automated. All the reagents for a typical immunoassay (ELISA) used to detect creatine kinase-MB (CK-MB) (Sigma Kit 49-A), an enzyme released by heart muscle in response to a heart attack, are shown on the graph to demonstrate that reagent usage in today's diagnostic technology is within the operational space of the microchip.

2.4 Device design. Two different prototype designs of the controlled release microchip were used during this Ph.D. project. One was fabricated in the Building 13 Microlab at MIT and will be referred to in this thesis as a "Microlab prototype." The other microchip was fabricated in the Technology Research Laboratory (TRL) of MIT's Microsystems Technology Laboratory (MTL) and will be referred to in this thesis as a "TRL prototype." The two prototypes have several features in common. Both prototypes contain reservoirs in a substrate, anode membranes covering one end of each of the reservoirs, cathodes on the surface of the device, and both prototypes must be in a chloride containing electrolyte to operate. A few of the differences include the number and placement of the electrodes, some aspects of fabrication, and device reliability. The following two sections of this chapter provide the general design and structure for both prototypes. The fabrication methods and materials for each prototype are presented in detail in chapter 3.

2.4.1 Microlab prototype. 2" diameter silicon wafers were used as the substrate material for the Microlab prototypes. The use of silicon in the controlled release microchip design allowed the utilization of microelectronics processing techniques such as ultraviolet photolithography, electron beam evaporation, reactive ion etching, and chemical vapor deposition. These techniques enabled the reservoirs and electrodes to be made more precisely and much smaller than was possible using macroscopic fabrication techniques.

Figure 2-3 shows a photograph of a Microlab prototype. Figure 2-4a shows a cut away portion of a typical Microlab prototype containing reservoirs filled with a chemical to be released. The Microlab prototype device consisted of a 20 mm by 20 mm square silicon device containing six reservoirs that extended completely through the silicon. The reservoirs were square pyramidal in shape (i.e. contained one large and one small square opening, see figure 2-4b) due to the potassium hydroxide etching method used to fabricate them. The small reservoir opening was approximately 50 μm by 50 μm and the large opening was approximately 480 μm by 480 μm. The silicon substrate thickness varied between 295 to 315 μm, resulting in each reservoir having a volume of approximately 25 nL. Each reservoir was sealed on the small square end by a 1,000 Å (0.1 μm) thick membrane anode and surrounded by its own cathode. Early Microlab prototypes used copper as the anode material. However, copper can corrode

without an applied potential, especially if chloride ions are present in electrolyte. Consequently, later Microlab prototypes used gold as the anode material. Gold was chosen as a model membrane material because it is easily deposited and patterned, has a low reactivity with other substances, and resists spontaneous corrosion in many solutions over the entire pH range. Details of the fabrication of the Microlab prototypes are given in section 3.2.1.1. The selection of gold as the model anode membrane material and gold corrosion studies are discussed in chapter 4. Release study results for a Microlab prototype are presented in section 5.3.1.1.

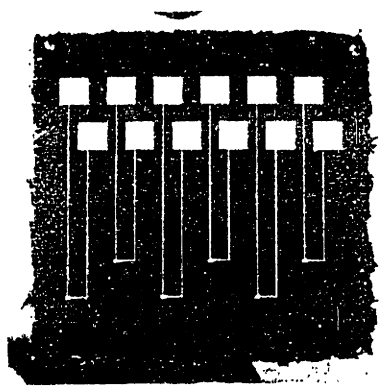

Figure 2-3. Photograph of a Microlab prototype controlled release microchip. (Photograph by Richard Holman.)

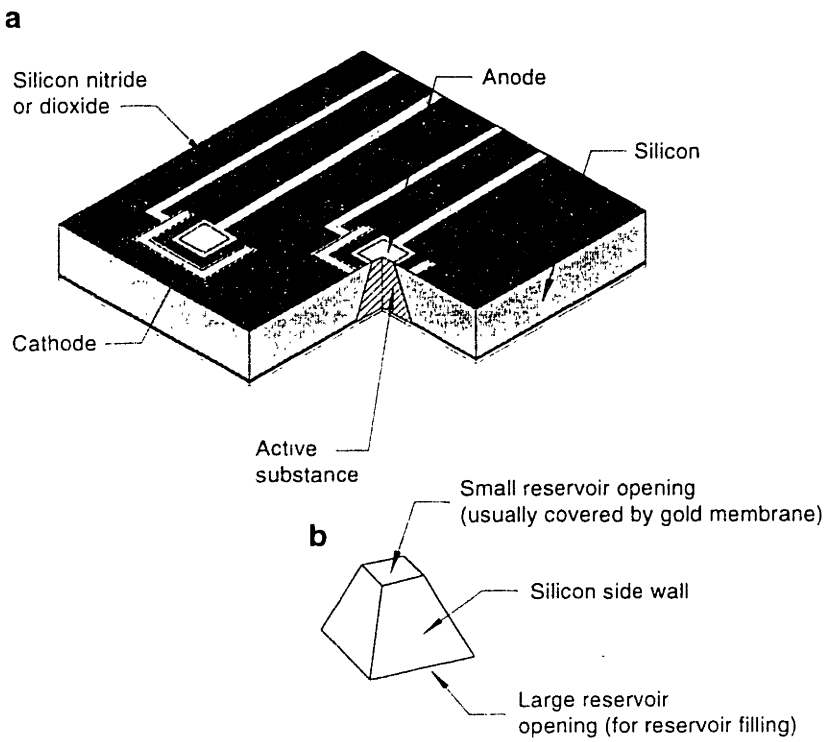

Figure 2-4. Schematic of a typical Microlab prototype, (a) a cross section showing a reservoir and two anode-cathode pairs and (b) a diagram showing the shape of each reservoir.

2.4.2 TRL prototype. 4" diameter silicon wafers were used as the substrate material for the TRL prototypes. Figure 2-5 is a photograph of a TRL prototype. Figure 2-6 shows a cut away portion of a TRL prototype containing reservoirs filled with a chemical to be released. The TRL prototype consisted of a 17 mm by 17 mm square silicon device containing 34 reservoirs that extended completely through the silicon. The reservoirs were square pyramidal in shape (i.e. contained one large and one small square opening, same as Fig. 2-4b) due to the potassium hydroxide etching method used to fabricate them. The small reservoir opening was approximately 50 μm by 50 μm and the large opening was approximately 480 μm by 480 μm. The silicon substrate thickness varied between 295 to 315 μm, resulting in each reservoir having a volume of approximately 25 nL. Each reservoir was sealed on the small square end by a 2,000-3,000 Å (0.2-0.3 μm) thick, gold membrane that served as an anode in an electrochemical reaction. There were also three thin-film gold cathodes spaced at different intervals across the surface of the device. The TRL device had only three cathodes for 34 anodes while the Microlab

device had one cathode for each of its six anodes. This difference simplified the packaging of the TRL prototype by decreasing the number of wirebonds (i.e. electrical connections) required per reservoir. (Note: The TRL prototype had 34 anode membranes, but only 29 anode connections to the power source. The reason is that several anode membranes were connected together so that the electric potential could be applied to those electrodes simultaneously via one conducting path.)

The sizes of both types of prototype devices were selected strictly for ease of handling during release experiments and compatibility with available device packaging. The number of wirebonds required for operation of the Microlab prototype was small enough (12 wirebonds) that simple packaging could be used. The device packaging of the TRL prototype was more complicated due to the larger number of electrodes on the chip surface (32 total wirebonds, as opposed to 12 for the Microlab prototypes). Therefore, the size of the TRL prototype was dictated by the availability of a commercial microchip package having at least 32 bonding pads on one side. A 144 pin, pin-grid array (PGA) package with a 17.3 mm by 17.3 mm die cavity was selected for the TRL prototypes. The TRL prototypes were fabricated to be 17 mm by 17 mm to fit easily into the PGA package. However, it should be noted that devices do not need to be that large and could be reduced to less than two millimeters, depending on the particular application. As a point of reference, a device of the size used in these studies (17 mm by 17 mm) has enough surface area to accommodate over 1000 reservoirs. Details of the fabrication and packaging of the TRL prototypes are given in section 3.2.1.2. Release study results for TRL prototypes are presented in sections 5.3.1.2, 5.3.1.3, and 5.3.2.

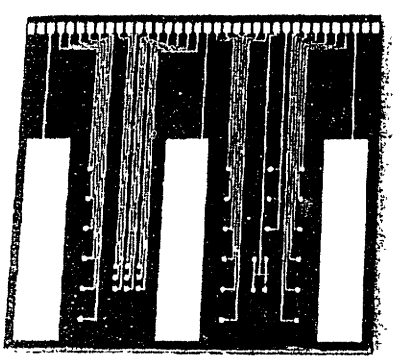

Figure 2-5. Photograph of a TRL prototype controlled release microchip. (Photograph by Paul Horwitz.)

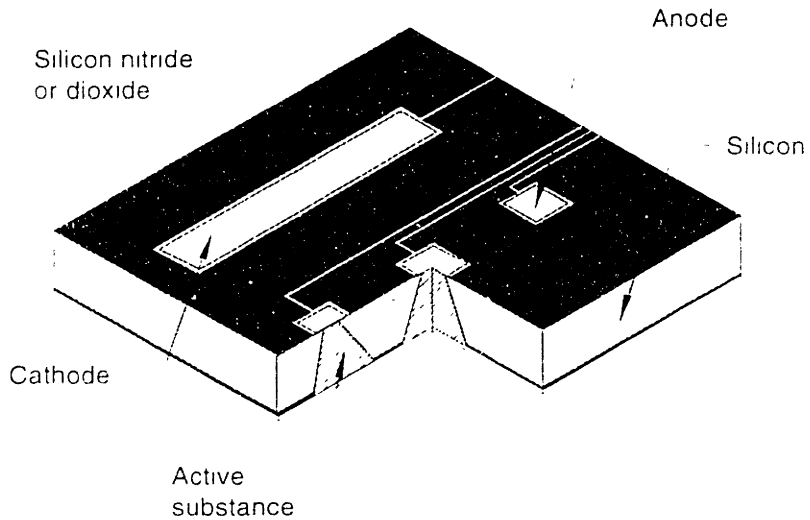

Figure 2-6. Schematic of a typical TRL prototype showing two reservoirs, one cathode, and three anodes.

2.5 References.

1. Santini, J.T., Jr., Cima, M.J. & Langer, R. "A controlled-release microchip." *Nature* **397**, 335-338 (1999).

2. Sampath, P. & Brem, H. "Implantable slow-release chemotherapeutic polymers for the treatment of malignant brain tumors." *Cancer Control: JMMC* **5**, 130-137 (1998).

3. *Martindale, The Extra Pharmacopoeia* (The Pharmaceutical Press, London, England, 1982).

4. *Physicians' Desk Reference* (Medical Economics Data Production Company, Montvale, NJ, 1995).

5. Kuret, J.A. & Murad, F. "Adenohypophyseal hormones and related substances" in *Goodman and Gillman's, The Pharmacological Basis of Therapeutics* 1334-1360 (Pergamon Press, New York, NY, 1990).

3. MICROCHIP FABRICATION

3.1 Introduction. The controlled release microchip design proposed in chapter 2 was based on silicon as the substrate material. This chapter presents procedures for fabricating prototype controlled release microchips utilizing standard microelectronic processing techniques such as ultraviolet photolithography, chemical vapor deposition, reactive ion etching, and electron beam evaporation. This chapter also details the use of inkjet printing and microinjection methods for filling reservoirs for subsequent release studies. Methods for reservoir sealing and device packaging are also presented.

3.2 Experimental methods.

3.2.1 Prototype fabrication.

3.2.1.1 Microlab prototype. The Building 13 Microlab is a facility operated by the Center for Materials Science and Engineering (CMSE) at MIT. The Microlab has the processing equipment necessary to make microchips, but it is not a controlled environment cleanroom. Particulates are reduced by the use of laminar flow hoods, lab coats, hair nets, and booties, but the particulate count is not controlled below a specific value.

Fabrication of the Microlab prototypes began by cleaning the wafers using the RCA process. The RCA process is a wet chemical cleaning process for silicon wafers comprised of three main steps[1]. The first step removes organic contaminants, the second removes silicon dioxide from the silicon surface, and the third removes ionic contaminants. Table 3-1 lists the details of each of the steps in the RCA process.

Table 3-1. RCA wafer cleaning process.

(1) Place the wafers in a 5:1:1 (volume ratio) H_2O:NH_4OH:H_2O_2 solution at 80°C for 10-15 minutes, then rinse with de-ionized (DI) water for 1 minute.
(2) Place the wafers in a 10:1 (volume ratio) H_2O:HF solution at room temperature for 15 seconds, then rinse with DI water for 20-30 seconds. However, do not let wafers dry before the next step. (Note that the reagent grade HF used to make the above (10:1) solution is supplied commercially as a 49% solution.)
(3) Place the wafers in a 6:1:1 (volume ratio) H_2O:HCl:H_2O_2 solution at 80°C for 10-15 minutes, then rinse to the desired resistivity in DI water and dry with heated N_2 (in a spin-rinse-dryer).

Approximately 3,000 Å (0.3 μm) of silicon nitride was deposited on both sides of 4" diameter, 295-310 μm thick, prime grade, (100) silicon wafers using a Plasma Enhanced Chemical Vapor Deposition (PECVD) system at MIT Lincoln Labs (Electrotech Delta 201 PECVD System, now manufactured by Trikon). The nitride was deposited at approximately 100 Å/sec at the conditions listed in table 3-2. The 4" wafers were scored and broken into four, equal-sized pieces for use in the Microlab contact alligner (Karl Suss MJB-3), which could only hold 3" diameter silicon wafers or smaller. The pieces were cleaned by sonication in acetone and methanol for 5 minutes each. The wafers were spin coated (Headway Research PWM 101 spinner) at 4,000 rpm for 30 seconds with a liquid photoresist adhesion promoter (Shipley Microposit Primer), which is essentially hexamethyldisilazne (HMDS). A positive photoresist (Shipley S1822) was spin coated at 4,000 rpm for 30 seconds onto the silicon nitride layer on one side of each piece of silicon and "soft" baked at 90°C for 25 min. in an oven (Blue M). The "soft" baked photoresist was exposed to ultraviolet (UV) light in the range of 365-405 nm for 15 seconds in a contact alligner (Karl Suss MJB-3) through an iron oxide photolithography mask (Advance Reproductions Corporation). The UV exposed photoresist was developed for 65 seconds using an ammonium hydroxide based developer (Shipley CD-30) and rinsed with de-ionized (DI) water. The developed wafers were "hard" baked at 120°C for 25 minutes in an oven (Blue M). The photolithographically patterned wafers were inserted into a parallel plate, reactive ion etching (RIE) unit (Plasma-Therm 700 Series Waf'r/Batch Dual Chamber Plasma Processing System) to etch the portions of the silicon nitride layer not masked by photoresist. The silicon

nitride was etched for 11 minutes at the conditions listed in table 3-3. Any residual photoresist on the surface of the wafer after etching was removed by a sequential solvent rinse using acetone and methanol, in that order. The nitride layer of each wafer had a single 20 mm square device etched into it, with each device containing six, 480 μm square reservoirs.

Table 3-2. PECVD silicon nitride deposition parameters for the Electrotech Delta 201 PECVD System.

Gas Flows	
N_2 =	3500 sccm
NH_3 =	500 sccm
SiH_4 =	300 sccm
RF Power =	550 W
Pressure =	850 mtorr
Showerhead Temp. =	350°C
Platen Temp. =	300°C

Table 3-3. Parameters for the reactive ion etching of PECVD silicon nitride in the Plasma-Therm 700 Series Waf'r/Batch Dual Chamber Plasma Processing system.

Gas Flows	
CHF_3 =	45 sccm
O_2 =	2 sccm
RF Bias =	300 V
Pressure =	45 mtorr
Temperature =	25°C

Silicon is readily etched by aqueous potassium hydroxide (KOH) solutions at high temperatures[2,3]. Silicon nitride is etched only slightly by the same solution. Therefore, the PECVD nitride was used as a mask to protect the silicon from etching in KOH, except for those areas where reservoirs were to be located. The patterned nitride wafers were etched in a 40% (by weight) solution of KOH (Mallinckrodt #6984, pellets) at 85°C. The resulting silicon etch rate

was calculated to be approximately 1 μm/min. The KOH solution anisotropically etched square pyramidal reservoirs (as shown in fig 2-4b) into the silicon along the (111) crystal planes until the silicon nitride film on the opposite side of the wafer was reached. The newly fabricated silicon nitride membranes completely covered the 40-60 μm square openings of the reservoir. The KOH also etched away the silicon around the 20 mm by 20 mm device, leaving this small square piece of silicon as the substrate for all subsequent processing steps.

The next step in Microlab prototype fabrication was the formation of the gold anodes and cathodes. The wafers were coated with liquid HMDS as described in the first photolithgraphy step in Microlab prototype fabrication. A negative photoresist (Futurrex NR8-3000) was spin coated (Headway Research PWM 101 spinner) at 3,500 rpm for 60 seconds onto the side of the silicon wafers having the nitride membranes over the small opening of the reservoirs. The photoresist was "soft" baked at 115-120°C for 60 seconds on a hotplate located under a laminar flow hood. The "edge bead" (accumulation of photoresist around the outside edges of the silicon piece) was removed using acetone and a cleanroom swab. The "soft" baked photoresist was exposed to UV light in the range of 365-405 nm for 40 seconds in a contact alligner (Karl Suss MJB-3) through an iron oxide photolithography mask (Advance Reproductions Corporation). The negative photoresist was developed for 210 seconds using an ammonium hydroxide based developer (Futurrex RD2) and rinsed with de-ionized (DI) water. The photoresist was "overdeveloped" for 75 seconds after the photoresist had cleared (approximately 135 seconds) to ensure that the patterned photoresist sidewalls had the negative slope required for the gold liftoff process. No "hard" bake was performed with negative photoresist wafers.

The wafers patterned with the negative photoresist were placed in the vacuum chamber of an electron beam evaporator (Sloan Pak-8 controller, the rest of the unit was made of parts from numerous manufacturers). The wafers were secured to a flat plate positioned above the crucible containing the metal to be evaporated (see figure 3-1). The chamber was pumped down to a base vacuum of approximately 2.4×10^{-6} torr. First, a 100 Å (0.01 μm) thick layer of chromium was deposited at a rate of 2 Å/sec on the wafers to serve as an adhesion layer for gold[4]. Next, a 1,000 Å (0.1 μm) thick layer of gold was deposited at a rate of 5 Å/sec. Both metals were deposited with no external heating or cooling. The wafers were allowed to cool for 10 minutes under vacuum and removed from the vacuum chamber. Each wafer was submerged in acetone to

dissolve the negative photoresist and "lift off" the metals from wafer except in those areas where the metals were deposited directly on exposed silicon nitride. Any residual photoresist on the surface of the wafer after lift off was removed by a sequential solvent rinse using acetone and methanol, in that order. The devices were also exposed to an oxygen plasma at the conditions listed in table 3-4 for 6 minutes to help remove residual photoresist.

Table 3-4. Oxygen plasma parameters for device cleaning in the Plasma-Therm 700 Series Waf'r/Batch Dual Chamber Plasma Processing system.

Gas Flows	
O_2 =	50 sccm
RF Power =	100 W
Pressure =	45 mtorr
Temperature =	25°C

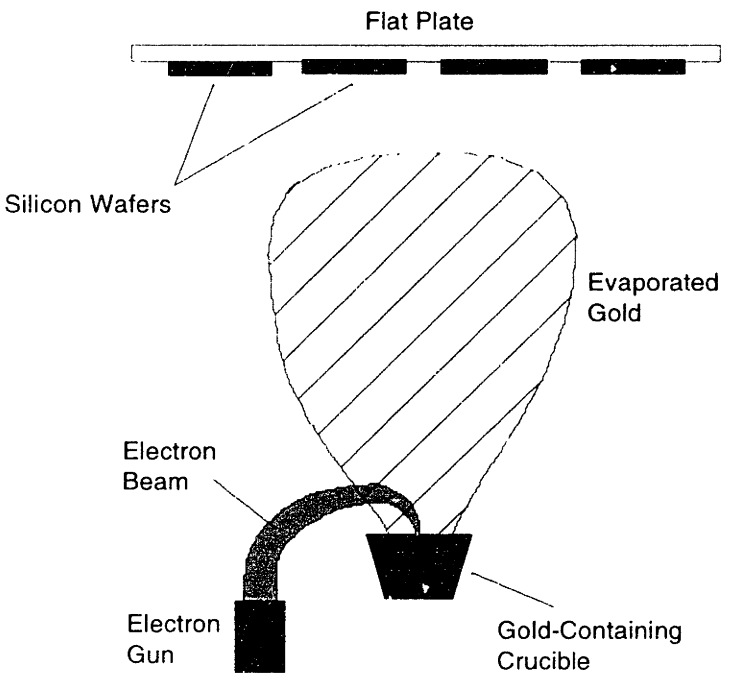

Figure 3-1. Diagram of an electron beam evaporation process (not drawn to scale).

A 2,500-3,000 Å (0.25-0.30 μm) thick layer of silicon dioxide (SiO_2) was deposited over the entire electrode containing surface of each Microlab prototype using the Microlab PECVD (Plasma-Therm 700 Series Waf'r/Batch Dual Chamber Plasma Processing System) at the conditions listed in table 3-5. Positive photoresist was patterned onto the newly deposited silicon dioxide layer using the same procedure described for positive photoresist patterning described at the beginning of this section. The photoresist was patterned so that some portions of the silicon dioxide located on the anode, cathode, and bonding pads were exposed. The photolithographically patterned wafers were exposed to an oxygen plasma in the RIE (Plasma-Therm 700 Series Waf'r/Batch Dual Chamber Plasma Processing System) for 30 sec at the conditions listed in table 3-4 to remove any residual photoresist over the portions of the SiO_2 layer that were to be etched. The SiO_2 was etched using a buffered oxide etchant (Ashland Chemical, 7:1 NH_4F:HF BOE) at room temperature for approximately 90 seconds. The devices were rinsed thoroughly in DI water. Any residual photoresist on the surface of the wafer after BOE etching was removed by a sequential solvent rinse using acetone and methanol, in that order. The devices were also etched in an oxygen plasma for 3 minutes at the conditions listed in table 3-4.

Table 3-5. Parameters for PECVD SiO_2 deposition in the Plasma-Therm 700 Series Waf'r/Batch Dual Chamber Plasma Processing system.

Gas Flows	
2% SiH_4 in N_2	400 sccm
N_2O =	900 sccm
RF Power =	20 W
Pressure =	900 mtorr
Temperature =	350°C

The devices were placed in the RIE with the electrode side facing down, exposing the nitride membrane under the gold membrane to the plasma. The silicon nitride membranes at the bottom of the reservoirs were etched for approximately 15 minutes at the conditions listed in table 3-3.

The Microlab prototype used in the chemical release studies presented in chapter 5 is referred to as Microlab prototype 091096-4. The Microlab prototypes used in the gold corrosion studies presented in chapter 4 are referred to as Microlab prototypes 091096-2 and 062696-2#3. Microlab prototype 062696-2#3 was fabricated as described above for Microlab prototypes 091096-2 and 091096-4, except that a thinner chromium layer was used (10 Å vs. 100 Å) and the silicon nitride layer was deposited using the Microlab PECVD, instead of the MIT Lincoln Labs PECVD.

3.2.1.2 TRL prototype. The Technology Research Laboratory (TRL) is a part of the Microsystems Technology Laboratory (MTL) at MIT. The TRL is a controlled environment, microelectronics fabrication facility with a particulate rating of class 100 (defined as <100, 1 μm particles per ft^3) and equipment designed for processing 4" diameter silicon wafers.

Fabrication of the TRL prototypes began by depositing approximately 0.12 μm of low stress, silicon-rich nitride on both sides of 4" diameter, 295-310 μm thick, prime grade, (100) oriented silicon wafers using a vertical tube reactor (VTR - SVG/Thermco 7000 Series vertical tube reactor). The VTR silicon nitride was deposited at a rate of 30 Å/min at the conditions given in table 3-6. The films were made silicon rich by using a 10:1 ratio of the gas flows of dichlorosilane (DCS) and ammonia (NH_3). The wafers were vapor coated with a photoresist adhesion promoter, hexamethyl-di-silazane (HMDS), in a vacuum oven (Yield Engineering Systems Model 310T vapor prime oven) at approximately 150°C for 30 minutes. A positive photoresist (Arch Chemicals OCG825-20) was spin coated (Solitec Inc. Model 5110 spinner) onto the silicon nitride layer on one side of each wafer at the conditions given in table 3-7. The photoresist was then "soft" baked at 90°C for 30 min. in an oven (Blue M Model DDC-146C). The "soft" baked photoresist was exposed to ultraviolet (UV) light at 320 nm for 32 seconds in a contact alligner (Karl Suss Model MA4) through an iron oxide photolithography mask (Advance Reproductions Corporation). The UV exposed photoresist was developed for 45 seconds using an ammonium hydroxide based developer (Arch Chemicals OCG934 1:1), rinsed with de-ionized (DI) water, and rinsed and dried in a spin rinse dryer (SRD). The developed wafers were "hard" baked at 120°C for 30 minutes in an oven (Blue M Model DDC-146C). The photolithographically patterned wafers were inserted into an electron cyclotron resonance (ECR)

enhanced reactive ion etching (RIE) unit (Plasmaquest Series II Reactor Model 145) to etch the portions of the silicon nitride layer not masked by photoresist. The silicon nitride was etched at approximately 350 Å/min at the conditions listed in table 3-8. Any residual photoresist on the surface of the wafer after etching was removed by a sequential solvent rinse using acetone, methanol, and isopropanol, in that order. The nitride layer of each wafer had 21, 17 mm square devices etched into it, with each device containing 34, 480 μm square reservoirs.

Table 3-6. Parameters for low stress, silicon-rich silicon nitride deposition in the SVG/Thermco 7000 Series vertical tube reactor (VTR).

Gas Flows	
SiH_2Cl_2 =	253 sccm
NH_3 =	24 sccm
Pressure =	268 mtorr
Temperature =	780°C

Table 3-7. Parameters for spin coating silicon wafers with Arch Chemicals OCG825-20 positive photoresist using a Solitec Inc. Model 5110 spinner.

Step	Spin Time (sec)	Spin Speed (rpm)
Coat	7	500
Spread	7	750
Spin	30	3,500

Table 3-8. Parameters for the ECR enhanced, reactive ion etching of VTR silicon nitride in the Plasmaquest Series II Reactor Model 145.

Gas Flows	
O_2 =	2 sccm
He =	15 sccm
CF_4 =	15 sccm
Power	
RF =	10 W
ECR =	100 W
Pressure =	20 mtorr
Temperature =	25°C

Silicon is readily etched by aqueous potassium hydroxide (KOH) solutions at high temperatures[2,3]. Silicon nitride is etched only slightly by the same solution. Therefore, the VTR nitride was used as a mask to protect the silicon from etching in KOH, except for those areas where reservoirs were to be located. The patterned nitride wafers were etched in a 38% (by weight) solution of KOH at 85°C. The resulting silicon etch rate was calculated to be approximately 1 μm/min. The KOH solution anisotropically etched square pyramidal reservoirs (as shown in fig 2-4b) into the silicon along the (111) crystal planes until the silicon nitride film on the opposite side of the wafer was reached. The newly fabricated silicon nitride membranes completely covered the 40-60 μm square openings of the reservoir.

Sodium, potassium, gold, copper, and other cations have traditionally been harmful to integrated circuits due to their capacity to diffuse rapidly through insulation layers[5]. Gold is tolerated in some equipment in the TRL that is specifically designated for gold use. However, potassium is not tolerated in any TRL equipment and must therefore be thoroughly cleaned to remove all traces of potassium ions before they can undergo further processing. The first step in the post-KOH cleaning process is a piranha etch, which consists of placing the wafers in a 3:1 (volume ratio) H_2SO_4:H_2O_2 solution for 15 minutes. The mixing of these two chemical results in a highly exothermic reaction, causing the solution to heat itself to near boiling. The wafers are

then rinsed three times with DI water in a dump rinser before being placed in a 50:1 (volume ratio) H_2O:HF solution at room temperature for 10 seconds. The wafers are again rinsed three times with DI water in a dump rinser and dried with heated N_2 (usually in a spin-rinse-dryer). The final step in the post-KOH cleaning process is exposing the wafers to the entire RCA cleaning process described in table 3-1. The cleaned wafers could then be used in designated, gold contaminated equipment in the TRL.

The next step in TRL prototype fabrication was the formation of the gold anodes and cathodes. The wafers are vapor coated with HMDS as described in the first photolithography step in TRL prototype fabrication. An image reversal photoresist (Crariant AZ 5214 E), which behaves like a negative photoresist, was spin coated (Solitec Inc. Model 5110 spinner) onto the side of the silicon wafers having the nitride membranes over the small opening of the reservoirs using the spinning parameters listed in table 3-9. The photoresist was "soft" baked at 90°C for 30 minutes in an oven (Blue M Model DDC-146C). The "soft" baked photoresist was exposed to UV light at 320 nm for 40 seconds in a contact alligner (Karl Suss Model MA4) through an iron oxide photolithography mask (Advance Reproductions Corporation). Each wafer was baked for 90 seconds on a metal plate in an oven (Blue M Model DDC-146C) at 120°C. The entire surface (no mask) of the wafer containing the image reversal photoresist was flooded with UV light at 320 nm for 200 seconds or UV light in the range of 365-405 nm for 30 seconds. The image reversal photoresist was developed for 75-90 seconds using an ammonium hydroxide based developer (Crariant AZ 422 MIF) and rinsed with DI water. The photoresist was "overdeveloped" for 30-45 seconds after the photoresist had cleared (approximately 45 seconds) to ensure that the patterned photoresist sidewalls had the negative slope required for the gold liftoff process. No "hard" bake was performed with image reversal photoresist wafers.

Table 3-9. Parameters for spin coating silicon wafers with Crariant AZ 5214 E image reversal photoresist using a Solitec Inc. Model 5110 spinner.

Step	Spin Time (sec)	Spin Speed (rpm)
Coat	6	500
Spread	6	750
Spin	30	4,000

The wafers patterned with the image reversal photoresist were placed in the vacuum chamber of an electron beam evaporator (Temescal Semiconductor Products Model VES 2550). The wafers were secured to a flat plate positioned above the crucible containing the metal to be evaporated (see figure 3-1). The chamber was pumped down to a vacuum of approximately 5.0 x 10^{-7} torr. First, a 100 Å (0.01 μm) thick layer of chromium was deposited at a rate of 2 Å/sec on the wafers to serve as an adhesion layer for gold[4]. Next, a 3,000 Å (0.3 μm) thick layer of gold was deposited at a rate of 5 Å/sec. Both metals were deposited with no external heating or cooling. The wafers were allowed to cool for 10 minutes after metal deposition and removed from the vacuum chamber. Each wafer was submerged in acetone to dissolve the image reversal photoresist and "lift off" the metals from wafer except in those areas where the metals were deposited directly on exposed silicon nitride. Residual photoresist on the surface of the wafer after lift off was removed by a sequential solvent rinse using acetone, methanol, and isopropanol, in that order.

The wafers were transported to the Building 13 Microlab for the deposition of a layer of silicon dioxide (SiO_2) over the entire side of the wafer containing the gold electrodes. The reasons for using the plasma enhanced chemical vapor deposition unit (Plasma-Therm 700 Series Waf'r/Batch Dual Chamber Plasma Processing System) in the Microlab is discussed in sections 3.3.2 and 3.4.4. The surface of each wafer was cleaned with an oxygen plasma in the Plasmaquest system in TRL or in the Plasma-Therm system in the Microlab prior to SiO_2 deposition. The oxygen plasmas in the Microlab and TRL were run between 50-120 seconds at the conditions listed in tables 3-4 and 3-10, respectively. A 6,000 Å (0.6 μm) thick layer of SiO_2 was deposited at 350°C over the entire electrode containing surface. The SiO_2 was deposited at approximately 250-500 Å/min at the conditions listed in table 3-5. The wafers were returned to TRL and solvent rinsed with acetone, methanol, and isopropanol, in that order. Positive photoresist was patterned onto the newly deposited silicon dioxide layer using the same procedure described for positive photoresist patterning described at the beginning of this section. The photoresist was patterned so that some portions of the silicon dioxide located on the anode, cathode, and bonding pads were exposed. The photolithographically patterned wafers were inserted into the ECR enhanced RIE (Plasmaquest Series II Reactor Model 145) to etch the portions of the silicon dioxide layer not masked by photoresist. The silicon dioxide was etched

at approximately 215 Å/min at the conditions listed in table 3-11. Any residual photoresist on the surface of the wafer after etching was removed by a sequential solvent rinse using acetone, methanol, and isopropanol, in that order.

Table 3-10. Oxygen plasma parameters for device cleaning in the Plasmaquest Series II Reactor Model 145.

Gas Flows	
O_2 =	25 sccm
He =	15 sccm
Power	
RF =	10 W
ECR =	200 W
Pressure =	20 mtorr
Temperature =	25°C

Table 3-11. Parameters for the ECR enhanced, reactive ion etching of Microlab PECVD SiO_2 in the Plasmaquest Series II Reactor Model 145.

Gas Flows	
He =	15 sccm
CF_4 =	15 sccm
Power	
RF =	10 W
ECR =	100 W
Pressure =	20 mtorr
Temperature =	15°C

A layer of positive photoresist was spin coated onto the electrode containing surface and "soft" baked. This photoresist layer was used to help keep the wafer surface clean during the wafer dicing process. The wafers were placed in a diesaw (Disco Automatic Dicing Saw Model DAD-2H/6T) and diced into 21, 17 mm by 17 mm devices. Residual photoresist was removed from individual devices by a sequential solvent rinse with acetone, methanol, and isopropanol, in

that order. The devices were placed in the ECR enhanced RIE with the electrode side facing down, exposing the nitride membrane under the gold membrane to the plasma. The silicon nitride membranes at the bottom of the reservoirs were etched at the conditions listed in table 3-8. The etch time was usually selected to be at least twice that needed to etch a given nitride thickness to account for transport limitations for etching at the bottom of a reservoir and to ensure that the nitride was completely removed. The devices were then turned over and exposed to an oxygen plasma for 50-120 sec at the conditions listed in table 3-10 to clean the electrode containing surface, resulting in finished TRL prototypes.

Three TRL prototypes were used in the chemical release studies presented in chapter 5. TRL prototypes 081297-1#10 and 081297-1#11 were fabricated as described in this section. TRL prototype 081897 used in the gold corrosion studies presented in chapter 4 was fabricated as described in this section except that the silicon substrate did not have reservoirs etched into it. Therefore, the anodes of this prototype were supported gold films rather than unsupported gold membranes. TRL prototype 021397-2#2 was fabricated as described in this section, with a few exceptions. The nitride film on TRL prototype 021397-2#2 was 0.3 μm thick and was deposited by PECVD at Lincoln Labs, similar to Microlab prototype 091096-4. TRL prototype 021397-2#2 also had a gold membrane that was only 2,000 Å thick, unlike the other TRL prototypes that had 3,000 Å thick gold membranes. Finally, the SiO_2 overlayer of TRL prototype 021397-2#2 was 4,900 Å thick and was deposited at low temperature (~85-90°C in the TRL Plasmaquest), instead of the 6,000 Å thick layer deposited at moderate temperature (~350°C in the Microlab PECVD) on the other TRL prototypes. TRL prototype 021397-1#6 used in gold corrosion studies presented in chapter 4 was fabricated the same as TRL prototype 021397-2#2 with one exception. The SiO_2 overlayer of TRL prototype 021397-1#6 was deposited by the Microlab PECVD at 350°C.

3.2.2 Reservoir filling. The gold membrane covering each reservoir was examined using a light microscope in reflected and transmission modes to determine if any defects (i.e. pinholes, tears, etc.) were present in the membrane. Membranes that were determined to be defect-free were filled as described in the next two sections.

3.2.2.1 Microlab prototype. Inkjet printing was used to fill the reservoirs of the Microlab prototypes. The black ink inside Hewlett Packard inkjet cartridges (HP 51626A) was removed with a vacuum hose and liquid trap through a hole drilled in the top portion of the cartridge. The cartridge was rinsed out several times with DI water until no black ink remained in the rinse water. The ink jet cartridge was filled with a solution of sodium fluorescein and DI water. The fill hole in the cartridge was sealed with wax and 5 minute epoxy.

Dr. Ben Wu and Bob Palozzolo designed an apparatus for attaching the HP inkjet cartridge to a three dimensional printing (3DP) system (figure 3-2) using parts from an inkjet printer (Hewlett Packard Deskjet 400). The 3DP system allowed the inkjet cartridge's position to be controlled by a computer to within 2.5 microns in the x and y directions. A piston allowed control over the distance between the prototype and the inkjet nozzle (z direction). The cartridge was positioned over a reservoir of the prototype by the 3DP system, the computer controlled the flow of electricity from a power supply to the inkjet cartridge, and a controlled number of drops of the fluorescein/water solution was deposited into the reservoir. The computer then moved the cartridge to another reservoir in the prototype and repeated the filling process. Volumes as small as approximately 150 pL could be deposited using this reservoir filling method.

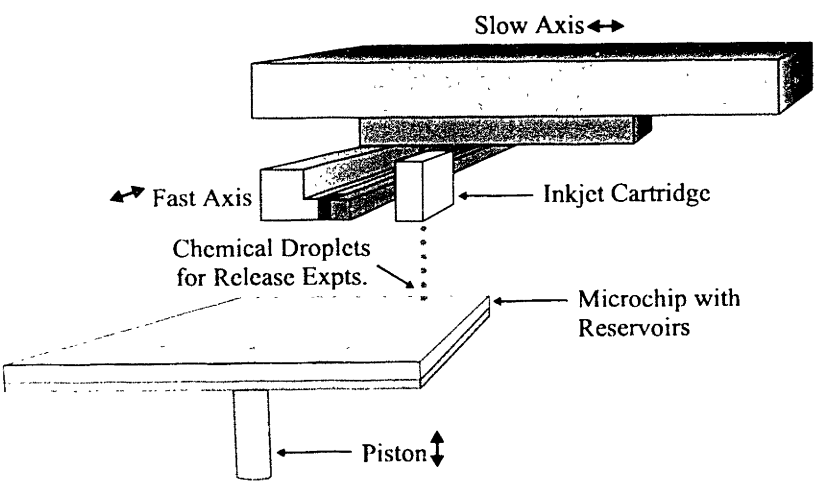

Figure 3-2. Diagram of three dimensional printing apparatus with an attached inkjet printhead. (Diagram provided by Scott Uhland.)

3.2.2.2 TRL prototype. The TRL prototypes were filled in one of two ways. The first method was inkjet filling as described for the Microlab prototype in section 3.2.2.1. The difference in the ink jet filling method between the Microlab and TRL prototypes involved the composition of the filling solution. Microlab and a few TRL prototypes were filled with fluorescein and water solutions only. Most TRL prototypes were filled with fluorescein, water, and a low molecular weight (mw = 200) liquid polymer such as poly(ethylene) glycol (Union Carbide Carbowax PEG 200). The purpose of the liquid polymer was to keep the solution in the reservoir in liquid form. The reason for this will be described in more detail in section 3.4.3.

The second reservoir filling method for TRL prototypes was microinjection. The microinjection system shown in figure 3-3 consisted of a 10 μL glass syringe (Unimetrics Laboratory Syringe with Luer Lock), a mechanical syringe pump (World Precision Instruments Ultramicropump #UMP), a micro-positioning unit (World Precision Instruments Taurus Micromanipulator), and a computerized controller (World Precision Instruments Ultramicropump Controller #UMC). Steel, 32 gauge gas chromatography needles (Hamilton #91032) with an outside tip diameter of 240 μm were attached to the glass syringe after filling the syringe with the filling solution. A stereomicroscope (World Precision Instruments PZMT) and the micro-positioning unit were used to position the needle tip at the edge of the large opening of a reservoir. A volume of the filling solution was pushed through the needle, forming a small droplet at the end of the needle. The needle was moved so that the droplet contacted the inner wall of the reservoir. Capillary action pulled the droplet from the needle tip and into the reservoir. The device was moved and the filling process was repeated for another reservoir. The manufacturers claim that volumes as small as 52 pL can be deposited (into another liquid) when using this filling method with specially manufactured, drawn glass capillary needles. However, it was found that ~10 nL was the practical volume limit that could be deposited when injecting the filling solution into air with larger metal needles.

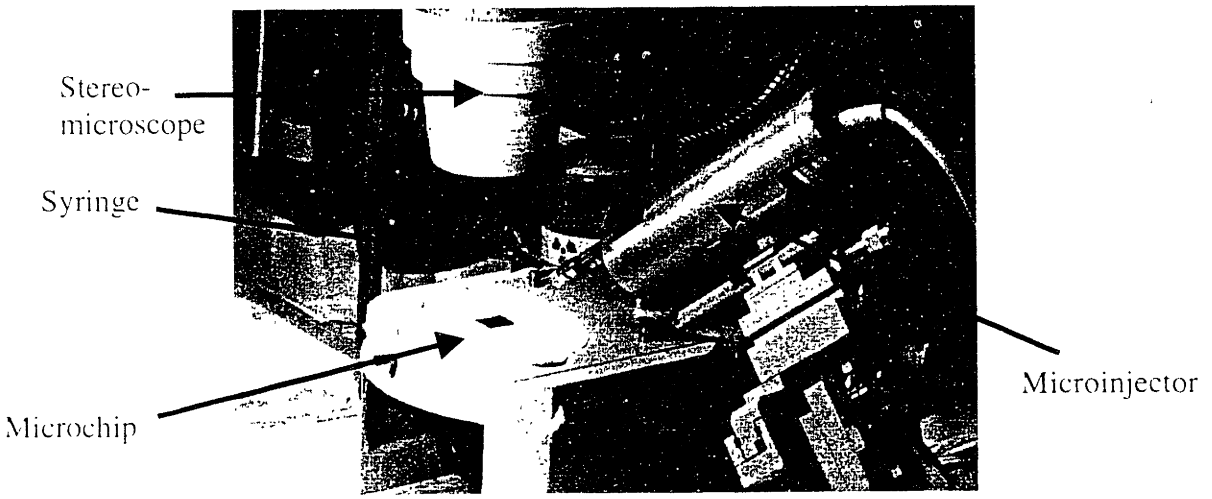

Figure 3-3. Photograph of a microinjection system.
(Photograph by Malinda Tupper.)

There were two main reasons for selecting microinjection over inkjet printing for the reservoir filling of some TRL prototypes. First, microinjection is not as sensitive as inkjet printing to the composition of the filling liquid. Inkjet printing involves the vaporization of small amounts of the filling solution to push the liquid drops out through the inkjet nozzle. The composition of the filling solution will affect its vaporization characteristics and ability to be printed. Solution composition may also affect viscosity, which will have a greater effect on inkjet printing than microinjection. Second, some inkjet printing methods may aerosolize a small amount of the filling solution and can create a potential safety hazard. For example, aerosolization of a radioactive filling solution, such as the radioactive ^{45}Ca (in the form of $^{45}CaCl_2$) used in the multiple compound release experiments described in section 5.2.3, can create a serious inhalation hazard. Microinjection does not aerosolize the filling solution and is therefore a better choice as a reservoir filling method for hazardous materials.

3.2.3 Reservoir sealing. The reservoirs of Microlab and TRL prototypes used in chemical release studies were sealed in one of three ways after they were filled. The first method (figure 3-4a) involved placing a small piece of a glass coverslip over the filled reservoir. The piece of

glass was held in place by a drop of 5 minute epoxy (Devcon 5 Minute Epoxy). A layer of waterproof epoxy (Masterbond EP21LP) was deposited over the entire back surface of the prototype and another piece of glass, either a glass microscope slide for Microlab prototypes or a glass coverslip for TRL prototypes, was placed on the waterproof epoxy.

The second method (figure 3-4b) of reservoir sealing was only used with later TRL prototypes for chemical release studies. The filled reservoir was covered with a small piece of an adhesive plastic sheet (Adwell G46 Lintec Tape). A layer of waterproof epoxy (Masterbond EP30HTF) was deposited on top of the pieces of plastic and a glass coverslip was placed on the waterproof epoxy. The device was then attached to a microchip package (see section 3.2.4.2) with waterproof epoxy.

Experiments were also conducted under a microscope in an attempt to videotape the corrosion of the gold membranes and the release of material from filled reservoirs (see chapter 6). Only TRL prototypes were used in these experiments. However, this third method (figure 3-4c) for sealing the reservoirs of TRL prototypes is slightly different from that described above for chemical release experiments. Each filled reservoir was surrounded by a small rubber O-ring (Greene Rubber Co., Size 001 or 002) attached to the back of the microchip with 5 minute epoxy. A glass microscope slide was attached to the other side of the O-ring with 5 minute epoxy. This method of reservoir sealing allowed each reservoir to be isolated from the other reservoirs and the surrounding solution, while also keeping the filling solution in contact with the gold membrane. This was important because we were trying to determine if the filling solution was exerting a force on the gold membrane. It was found that the filling solution gets pulled away from the gold membrane by capillary forces when a glass coverslip or plastic film is laid directly over the reservoir opening, as depicted in figure 3-4b. We would not be able to determine if the filling solution exerted a force on the gold membrane if the solution was not directly in contact with the gold membrane.

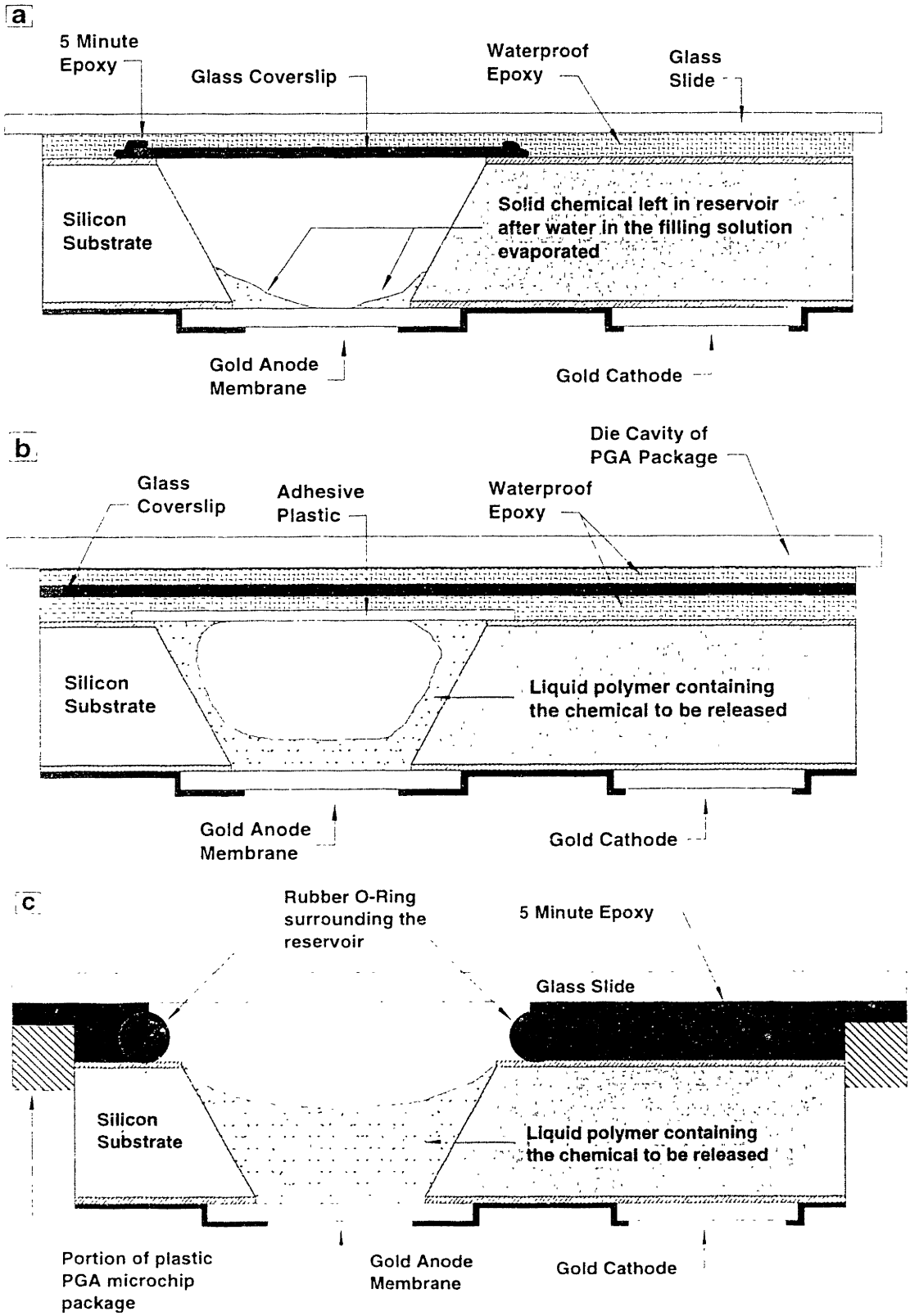

Figure 3-4. Three reservoir sealing methods for prototype devices.

3.2.4 Prototype packaging.

3.2.4.1 Microlab prototype. Sealed Microlab prototypes were attached to a glass microscope slide with a waterproof epoxy (Masterbond EP21LP). Plastic coated wires containing seven conductors were epoxied to the glass slide to hold them in place. A single conductor from each wire was attached to the wire bond pad of the Microlab prototype using silver paint (Ernest Fullam Inc. #14810). The electrical connections were sealed with waterproof epoxy after the silver paint was completely dried. The completed package for Microlab prototypes is shown in figure 3-5.

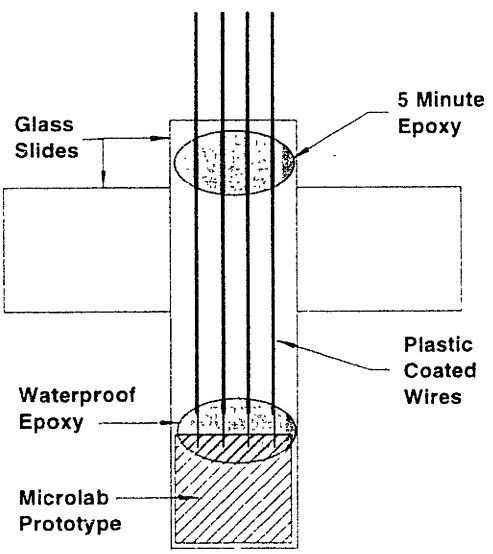

Figure 3-5. Microlab prototype packaging.

3.2.4.2 TRL prototype. Sealed TRL prototypes were placed in a 145 pin, pin grid array (PGA) package made of alumina (Kyocera Co.) or a 176 pin PGA made of alumina (NTK Technical Ceramics). The prototype was held into the PGA package using a waterproof epoxy (Masterbond EP21LP or EP30HTF). Electrical connections between the prototype and the package were made with a gold ball wirebonder (Kulicke & Soffa Industries Inc.. Model 4124). The completed package for most TRL prototypes is shown in figure 3-6. The packaging for the *in situ* corrosion experiments of chapter 6 was slightly different and is described in section 6.2.1.

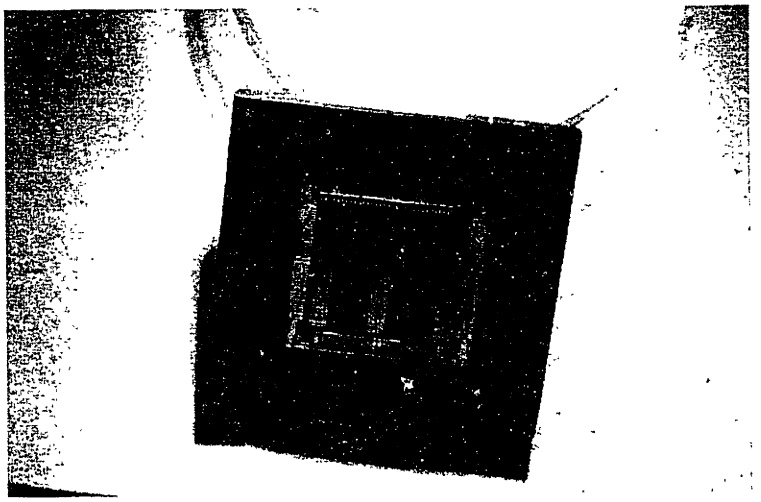

Figure 3-6. Photograph of TRL prototype packaging containing a TRL prototype microchip. (Photograph by Malinda Tupper.)

3.3 Experimental results.

3.3.1 Nitride membranes. A difference between the Microlab and TRL prototypes is the amount and type of stresses present in the silicon nitride membranes. The membranes of all Microlab prototypes and some TRL prototypes (021397 prototypes) were deposited using Plasma Enhanced Chemical Vapor Deposition (PECVD). This method produces uniform nitride films having good etch resistance to KOH solutions used to etch silicon. However, it was observed experimentally that the PECVD nitride films had high compressive stresses, as indicated by severe membrane buckling. This is shown clearly in figure 3-7a. The nitride membranes of TRL prototypes 081297-1#10 and 081297-1#11 were silicon-rich (Si:N > 3:4) and were deposited in a vertical tube reactor (VTR). According to the literature, silicon-rich nitride films deposited at somewhat similar conditions to the VTR nitride have a low tensile stress of approximately 60±50 MPa, which is small compared to the 1070±100 MPa or greater tensile stresses in stoichiometric (Si:N = 3:4) nitride films deposited by Low Pressure Chemical Vapor Deposition (LPCVD)[6]. Silicon-rich, VTR nitride membranes tend to be flat due to their small tensile stress, as shown in figure 3-7b.

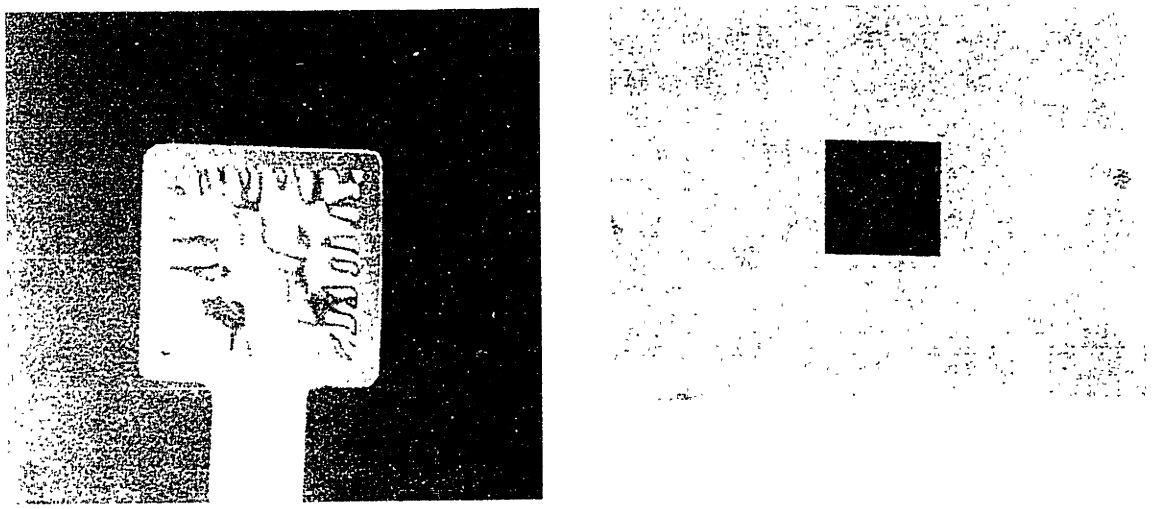

Figure 3-7. Comparison of a PECVD nitride membrane and silicon-rich VTR nitride membrane under a light microscope at 375x magnification. (a) the buckling of the gold membrane was caused primarily by the compressive stresses in the underlying PECVD nitride membrane and (b) the VTR nitride membrane was flat due to a small tensile stress.

3.3.2 SiO_2 overlayer. The adhesion of PECVD SiO_2 in water was affected by the deposition temperature. SiO_2 deposited by PECVD at low temperatures (<100°C) was found to delaminate from the microchips after less than one day in solution. This was most likely caused by the increased porosity of films deposited at lower temperatures. Only TRI prototype 021397 2#2 contained SiO_2 deposited at low temperature. SiO_2 deposited at moderate temperatures (approximately 350°C) remained adherent to the microchips in solution for at least nine days. Stress in PECVD SiO_2 films is dependent on deposition conditions[5]. However, the literature indicates that many plasma deposited SiO_2 films have compressive stresses[5], which may cause or increase buckling of the gold membrane.

3.3.3 Reservoir filling. Both methods of reservoir filling described in this thesis, inkjet printing and microinjection, deposit a small volume of liquid into the reservoir. It was found that depositing a solution consisting only of the chemical to be released (i.e. sodium fluorescein) and water sometimes caused the gold membranes to crack or tear. It is believed that the chemical

present in the reservoir during water evaporation exerts a stress on the gold membrane as it dries and shrinks. It was found that adding a small amount (approx. 15-25% by volume) of liquid polymer to the filling solution greatly reduces the incidence of membrane cracking or tearing after filling. This liquid polymer keeps the chemical in the reservoir from drying completely and decreases the stress exerted on the membrane by the drying process. The failure of gold membranes during the filling process is discussed in more detail in section 3.4.3.

3.4 Discussion. Device yield, as used in this thesis, is the ratio of the number of useable reservoirs in a device to the total number of reservoirs in a device. An unusable reservoir is one in which the gold membrane covering the reservoir contains holes, cracks, or is broken. A reservoir is also unusable if the gold traces away from the membrane are not protected from unwanted corrosion by SiO_2. Device yield is a good measure of the usefulness and robustness of a fabrication process. It is important to try to maximize the device yield when designing a fabrication process. Typical Microlab prototype yields ranged from 50-66%, and TRL prototype yields ranged from 73-88%. Four factors affecting device yield for the Microlab and TRL prototypes were fabrication environment cleanliness, the nitride membrane material, gold membrane strength, and the integrity of the SiO_2 overlayer.

3.4.1 Fabrication environment cleanliness. The cleanliness of the fabrication environment can greatly affect device yield. Holes can be formed in the gold membrane anodes if particulates (typically 1 μm or greater in size) are present on the surface of nitride membranes when the gold films ($\leq$ 0.3 μm thick) are deposited. The Building 13 Microlab is not a controlled environment like TRL, and therefore has a much higher particulate count. This may have contributed to the lower yields observed for Microlab prototypes. In addition, particulates and chemical residues on the surfaces of substrates can decrease adhesion of thin gold films and result in delamination. Poor film adhesion also decreases device yield.

3.4.2 Nitride membrane material. The selection of the nitride membrane material also has an affect on device yield. Membranes with large tensile stresses have a greater risk of breaking during reservoir filling or other fabrication processes. LPCVD deposited silicon nitride typically

has high tensile stresses. Membranes of LPCVD nitride of the sizes used for the prototype device (50 μm by 50 μm) do not survive most fabrication processes after they are formed with KOH etching. Stresses in PECVD nitride membranes are highly compressive, resulting in buckled membranes. Photolithography on buckled membranes can result in poor pattern generation and structures with delaminated edges. Prototypes incorporating PECVD nitride suffered from this type of buckling. Most TRL prototypes utilized silicon-rich VTR nitride, which is under a low tensile stress. The tensile component keeps the membranes flat, but its magnitude is low enough that the membrane does not have an increased tendency to break during processing. Therefore, prototypes using VTR nitride membranes typically had higher device yields than those that used LPCVD or PECVD nitride.

3.4.3 Gold membrane strength. The gold membranes of the prototype devices must be strong enough to withstand forces exerted on them during the fabrication process, reservoir filling, and chemical release studies. The forces exerted during the fabrication process and reservoir filling affect device yield if they cause gold membranes to fail. The types of forces exerted on the gold membranes during the microchip's use as a chemical release device are discussed in section 6.4.1.2. Estimations of gold membrane stress and failure can be found in section 6.4.1.3.

The gold membranes are supported by nitride membranes during most of the fabrication process. The nitride membranes provide additional structural integrity to the gold membranes, so the in-plane dimensions and gold thickness are not as critical during fabrication as they are for reservoir filling. The extent of the protection afforded by the nitride membrane is a function of the type of nitride and the stresses in the nitride membrane, as discussed in the previous section. Precautions are also taken during the fabrication process to limit the stresses put on the membranes. For example, an adhesive plastic film is put over the side of the wafer containing the large reservoir openings during photoresist spinning. This plastic film protects the membranes by forcing the vacuum of the spinner to be pulled on the plastic film and not directly on the membranes covering the reservoirs.

The silicon nitride membranes under the gold membranes are removed before reservoir filling, forming an unsupported gold membrane. The strength of the gold membrane is now dependent on its in-plane dimensions (i.e. the size of the reservoir opening), its thickness, and its

microstructure (i.e. grain size). It was discussed in section 3.3.3 that the gold membranes sometimes break when filled with a solution consisting only of the chemical to be released and water. It was observed that the water quickly evaporates from the 26 nL reservoir after it is filled. The chemical remaining in the bottom of the reservoir during water evaporation exerts a stress on the membrane. This stress may be caused by the transient formation of a liquid surface having a small radius of curvature (see the Young-Laplace equation in section 6.4.1.2 and the gold membrane stress estimates in section 6.4.1.3) when evaporation is nearly complete. This stress could cause the gold membrane to crack or tear, as shown in figure 3-8. The stress can be reduced and the device yield increased by not allowing the radius of curvature of the filling solution in a reservoir to get too small. This can be accomplished by adding some (15-25% by volume) liquid polymer to the filling solution to keep the filling solution from completely drying in the reservoir. In addition, decreasing the in-plane dimensions of the reservoir opening, increasing the thickness of the gold membrane, and/or modifying the gold membrane microstructure should make the membranes stronger and increase device yield during the filling process. This problem of membrane tearing is not encountered if a solid material is deposited in a reservoir as a solid, but only when it is deposited as a liquid solution that evaporates to form a solid.

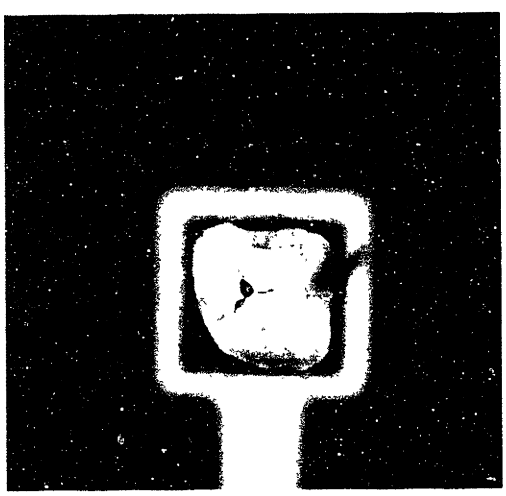

Figure 3-8. Light micrograph (at 375x magnification) of a gold membrane that has cracked (in the middle and at the edges) due to stresses exerted on the membrane by the filling solution. Notice the filling solution leaking from the cracks.

3.4.4 Integrity of the SiO_2 overlayer. Some portions of the gold electrodes must be protected from unwanted corrosion by an adherent, non-porous coating that isolates the electrode materials from the surrounding electrolyte. Silicon dioxide (SiO_2) was used as a model protective coating because its physical properties can be tailored to a particular application by selecting appropriate processing conditions. For example, SiO_2 deposited by PECVD at low temperatures (<100°C) tends to be porous and non-adherent in solution, while high temperature (>700°C) deposition or annealing results in denser SiO_2 but may also lead to thermal grooving and void formation in gold films[9]. PECVD deposition at moderate temperatures (350°C) increased device yield by addressing these problems and producing silicon dioxide films possessing adequate density and adhesion with negligible gold void formation. Light microscopy revealed no evidence of corrosion with applied potential on those areas of the gold electrodes covered by this SiO_2, except in those regions immediately adjacent to the exposed gold membrane.

The SiO_2 overlayer can have an indirect effect on the strength of gold membranes and device yield. It was mentioned in section 3.3.2 that PECVD SiO_2 deposited at moderate temperatures is highly compressive. These compressive stresses can cause the gold to buckle if the SiO_2 overlayer extends over the unsupported gold membrane. The compressive stresses, when combined with the stresses exerted by a drying liquid in the reservoir, can increase the susceptibility of the gold membrane to failure for a given membrane in-plane dimension and membrane thickness.

3.5 Conclusions. Sequential, multi-step processes for fabricating silicon-based, controlled release microchip prototypes in two different fabrication facilities were developed. These fabrication processes resulted in the production of controlled release microchip prototypes of sufficient quality for use in subsequent chemical release experiments presented in chapter 5.

A key process design feature built into the prototype fabrication procedures is that reservoir filling is not begun until all chemical and high temperature silicon processing of the microchip is complete. This process design feature is of critical importance if the chemicals to be delivered are sensitive to chemical exposure or to changes in temperature, as many protein drugs are. This feature also keeps the fabrication process generic for making microchips for a wide variety of applications.

Important areas for future research in controlled release microchip fabrication include the determination of the gold membrane thickness giving optimal strength and corrosion characteristics and improvement of reservoir filling and sealing methods.

3.6 References.

1. Wolf, S. & Tauber, R.N. in *Silicon processing for the VLSI era, volume 1: process technology* 516-517 (Lattice Press, Sunset Beach, CA, 1986).
2. Bean, K.E. "Anisotropic etching of silicon." *IEEE Transactions on Electron Devices* **ED-25**, 1185-1193 (1978).
3. Matsuoka, M., Yoshida, Y. & Moronuki, M. "Preparation of silicon thin diaphragms free from micropyramids using anisotropic etching in KOH solution." *Journal of Chemical Engineering of Japan* **25**, 735-740 (1995).
4. Wolf, S. & Tauber, R.N. "Mechanical properties of thin films - adhesion" in *Silicon processing for the VLSI era, volume 1: process technology* 113-114 (Lattice Press, Sunset Beach, CA, 1986).
5. Hummel, R.E. "Electromigration and related failure mechanisms in integrated circuit interconnects." *International Materials Reviews* **39**, 97-111 (1994).
6. Gardeniers, J.G.E., Tilmans, H.A.C. & Visser, C.C.G. "LPCVD silicon-rich silicon nitride films for applications in micromechanics, studied with statistical experimental design." *J. Vacuum Science & Technology A* **14**, 2879-2892 (1996).
7. Denison, D.R. "Dependence of high-density plasma deposited SiO_2 film properties on deposition temperature" in *Proceedings of the Electrochemical Society* (The Electrochemical Society, 1996).
8. Schliwinski, H.J., Schnakenberg, U. & Windbracke, W. "Thermal annealing effects on the mechanical properties of plasma-enhanced chemical vapor deposited silicon oxide films." *Journal of the Electrochemical Society* **139**, 1730-1735 (1992).
9. Jiran, E. & Thompson, C.V. "Capillary instabilities in thin, continuous films." *Thin Solid Films* **208**, 23-28 (1992).

4. GOLD CORROSION

4.1 Introduction. Gold was selected as the model membrane and electrode material for the prototype controlled release microchips primarily due to its unique electrochemical properties. Gold has long been considered to be a noble metal. It is easily deposited and patterned, has a low reactivity with other substances, and resists spontaneous corrosion in most aqueous solutions over the entire pH range. The fact that the gold surface remains clean (i.e. the native oxide layer on a gold surface, if present, is very thin) and does not corrode in most environments led to gold's widespread use in jewelry, currency, medical implants, and microelectronic devices. Pourbaix diagrams indicate the thermodynamically stable species at any combination of applied potential and solution pH. Pourbaix diagrams were generated from data and calculations obtained from a thermodynamics computer program (Outokumpu Research's HSC Chemistry program, ver. 3.0). The Pourbaix diagram shown in figure 4-1 for gold in aqueous solutions free from complexing substances (such as chloride ions) indicates that gold is immune to corrosion over the entire domain of water stability (the area between the dashed lines). The species in bold lettering in areas delineated by solid black lines shows the thermodynamically stable, solid species at each combination of applied potential and solution pH.

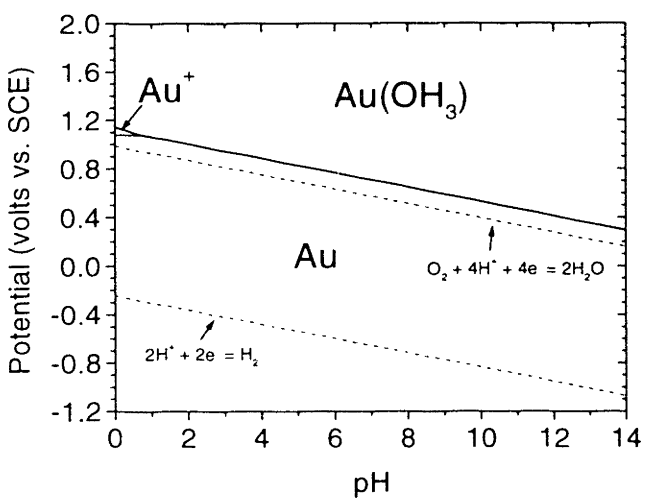

Figure 4-1. Pourbaix diagram for gold in water, free from complexing substances.

The presence of a small amount of chloride ion in solution creates an electric potential/pH region that thermodynamically favors the formation of water soluble gold chloride complexes[1]. Notice how the presence of a complexing substance such as chloride can change the Pourbaix diagram for gold in aqueous solutions (see figure 4-2). However, thermodynamics does not tell the whole story. It is also important to look at the kinetics of the formation of gold chloride complexes. Evans diagrams represent the kinetics of gold corrosion and indicate how the corrosion rate (shown as current density) changes with applied potential. A potentiodynamic Evans diagram for gold in 0.145 M NaCl solution shows a peak in current density corresponding to the formation of Au(III) chloride at an applied potential slightly above its thermodynamic barrier (see figure 4-3). Gold corrosion by the formation of water soluble Au(III) chloride is thermodynamically and kinetically favored and occurs rapidly in this potential region. This ability to corrode gold on demand led to its selection as the model membrane material for controlled release microchip prototypes. Figures 4-2 and 4-3 are placed next to one another so that the y-axes line up and the thermodynamics and kinetics can be easily compared.

4.2 Review of the gold corrosion literature. Gold corrosion in aqueous solution is difficult and requires the presence of both a complexing substance and highly oxidizing potentials. Gold corrosion received little attention until recently because such environmental conditions were not usually encountered in gold applications. However, the widespread use of gold in modern microelectronics over the last 25 years has led to a new interest in gold corrosion. Much of the gold corrosion research in microelectronics has focused on the role of chlorides in gold corrosion. For example, the combination of tiny amounts of chloride and high humidity may cause failure of gold metallizations in electronic circuits. Frankenthal & Becker have shown that chloride contamination, high humidity, and electric potential differences between adjacent gold structures on a microchip can lead to gold corrosion at one structure and gold redeposition at the adjacent structure[2]. This process continues until gold dendrites form between the adjacent gold metallizations and cause a short circuit and device failure.

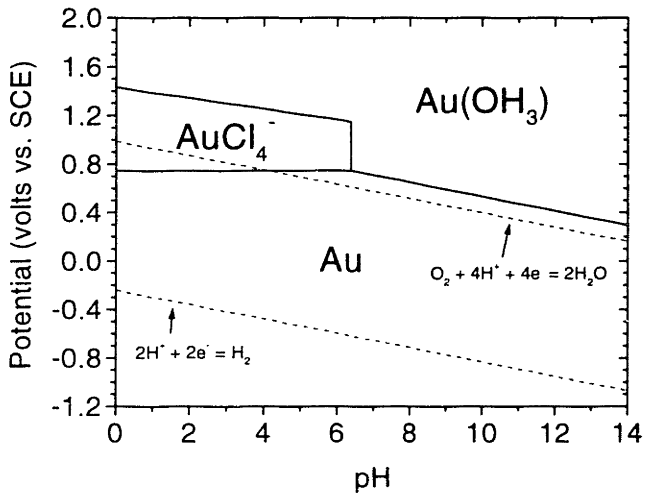

Figure 4-2. Pourbaix diagram for gold in water containing approximately 0.145 M chloride ions.

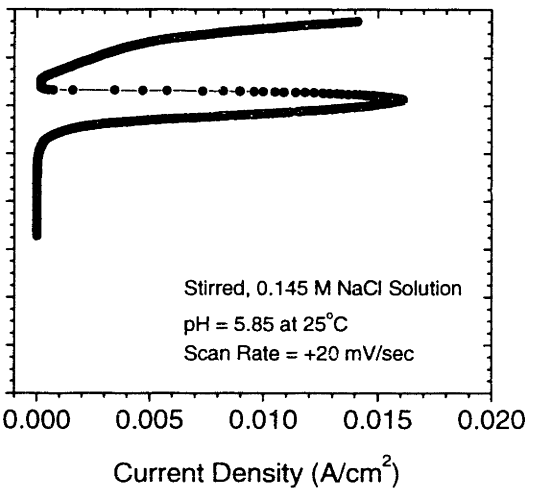

Figure 4-3. Evans diagram (potentiodynamic) for gold in water containing 0.145 M chloride ions.

Another example where the characterization of gold corrosion in chloride solutions is important is in the development of the controlled release microchips presented in this thesis. These microchips achieve chemical release in dilute saline solutions by the selective corrosion of a thin (~ 0.1-0.3 μm) gold membrane covering a reservoir containing the chemical[3]. A single device may contain thousands of such reservoirs and thin gold membranes. An understanding of gold corrosion is required to achieve the high reproducibility required to make such a controlled release device commercially viable.

The next several sections of this chapter review the most relevant literature on gold corrosion in aqueous, chloride containing solutions. Section 4.2.1 discusses the experimental data and theories relating to each of the four regions present in a typical electric potential vs. current plot (Evans Diagram) for gold in chloride containing solutions. The four regions are the pre-active region, the active region, the passive region, and the transpassive region (see figure 4-4). Section 4.2.2 presents proposed mechanisms from the literature for gold dissolution in the active region and gold dissolution/passivation in the passive and transpassive regions. Sections 4.4 and 4.5 present and discuss recent experimental results and SEM micrographs from gold

corrosion studies in dilute saline solutions. (Note: All electric potentials referred to in this chapter are relative to a saturated calomel reference electrode (SCE), unless otherwise noted.)

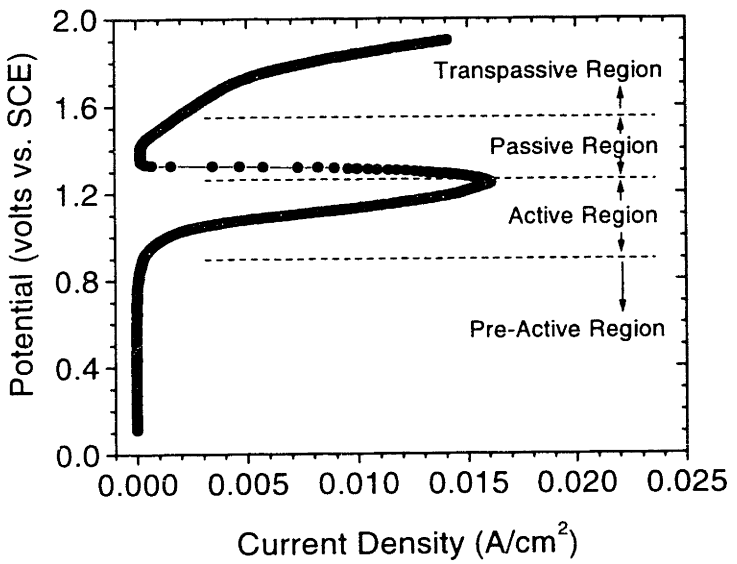

Figure 4-4. Four regions of gold's electrochemical behavior in chloride containing solutions.

4.2.1 Four regions of gold's electrochemical behavior in chloride containing solutions.

4.2.1.1 Pre-active region (E < +0.9 volts). Gaur & Schmid[4] observed that during anodic polarization experiments of gold in the absence of chloride ions, hydrogen oxidation occurred at the gold surface in the potential range from -0.1 to +0.4 volts. However, addition of chloride ions to the solution appeared to have stopped this reaction from occurring at the gold anode. It was believed that adsorption of chloride ions to the gold surface prevented the hydrogen oxidation reaction from occurring. Both Gaur & Schmid and Gallego *et al*[5] explained the chloride adsorption to gold by using the concept of potential of zero charge (E_z). This is the potential at which the metal has no charge with respect to the surrounding electrolyte. At potentials more noble than E_z, the metal is positively charged with respect to the solution, and anions in the electrolyte are attracted to the metal surface. Gallego *et al* reported that equation 4.1 for determining E_z for gold in chloride solutions is independent of pH for pH < 9.

$$E_Z(\text{vs.NHE}) = -0.15 + \left(\frac{2.3RT}{F}\right)\log a_{Cl^-} \qquad (4.1)$$

Nearly all chloride concentrations result in a negative E_z vs. SCE using this formula. Gallego *et al* stated that for the potential and chloride ranges used in their experiments, the gold potential will always be positive to E_z, resulting in a gold surface that is "practically saturated with chloride ions." It will become evident in the following sections that the adsorption of chloride ions onto the gold surface is a central component of current gold corrosion and passivation theories.

4.2.1.2 Active region (+0.9 volts < E < E_{pass}). The active region is characterized by a peak in the current corresponding to gold dissolution. Gaur & Schmid, Lovrecek *et al*[6], and Gallego *et al* state that gold dissolution in the active region probably occurs by the formation of a soluble Au(III) complex with chloride ($AuCl_4^-$), although the mechanism proposed by Gallego *et al* in section 4.2.2.1 does allow for the initial formation of a Au(I) chloride ($AuCl_2^-$). Frankenthal & Siconolfi[1] stated that "from a comparison of weight loss measurements and coulombs passed and assuming 100% current efficiency, it was established that gold dissolves as Au(I) below +0.80 V and as Au(III) at potentials above +1.1 V." Table 4-1 lists the reported active region start potentials and the locations of the current peak from several literature sources for dilute chloride solutions (~ 0.1 M).

Table 4-1. Literature values for the electric potential indicating the beginning of the active gold corrosion region and the potential at which the maximum gold corrosion rate occurs.

Source	Beginning Potential (V)	Peak Potential (V)
Gallego *et al*	0.9	1.05-1.1
Gaur & Schmid	1.0	1.1-1.2
Lovrecek *et al*	0.9	1.15-1.2
Fankenthal & Siconolfi	≤ 0.8	1.05

The magnitude of the peak current is an important quantity because it gives an indication of the rate of gold dissolution in the active region. In all cases, researchers have found that the peak current increases with chloride concentration. However, there is some disagreement in the literature concerning the extent to which chloride increases the rate (i.e. reaction order) and whether the reaction is activation or diffusion controlled. Gallego *et al* and Lovrecek *et al* have found that current (i.e. reaction rate) has a first order dependence on chloride concentration. Frankenthal & Siconolfi contend that the dependence is second order when Au(I) is the primary species formed ($E \leq +0.80$ V), and Gaur & Schmid state that peak current depends only "somewhat" on chloride concentration. Gallego *et al* and Gaur & Schmid are in the direct disagreement concerning diffusion vs. activation (surface reaction) control. Gallego *et al* believe that the dissolution reaction is controlled by the diffusion of chloride ions to the gold surface after the supply of chloride ions adsorbed to the surface begins to deplete. However, Gaur & Schmid calculated that the theoretical limiting current is approximately five times greater than the experimentally observed anodic peak current, suggesting that the dissolution reaction is surface reaction controlled. Frankenthal & Siconolfi and Lovrecek *et al* believe that gold dissolution can be surface reaction or diffusion controlled, depending on the particular situation. Frankenthal & Siconolfi found that the dissolution reaction is diffusion controlled for chloride concentrations above 0.1 M and surface reaction controlled for concentrations below 0.1 M. In other words, the reaction rate at the gold surface is so fast at concentrations above 0.1 M (due to their postulated 2^{nd} order dependence on chloride) that it exceeds the rate of diffusion, even though diffusion is relatively fast due to a high concentration gradient. Lovrecek *et al* found that the control mechanism varied with the angular velocity of their rotating disk electrode (i.e. solution agitation).

Except for very low pH, pH does not have a significant effect on the behavior of gold in the active region. Frankenthal & Siconolfi showed that for a given chloride concentration at +0.85 V, peak current in the active region is not a function of pH for $pH > 1.5$. However, the peak current does increase rapidly for $pH < 0$ (see figure 4-5). Gallego *et al* found that the anodic behavior of gold in the active region does not vary much with pH, except that the primary passivation potential (E_{pass}) is shifted. E_{pass} serves as the boundary between the active and passive regions. Anodic dissolution slows by up to several orders of magnitude as a protective

film is formed on the gold surface at this potential. The definition and location of E_{pass} and the nature of the passive film will be covered in the next section.

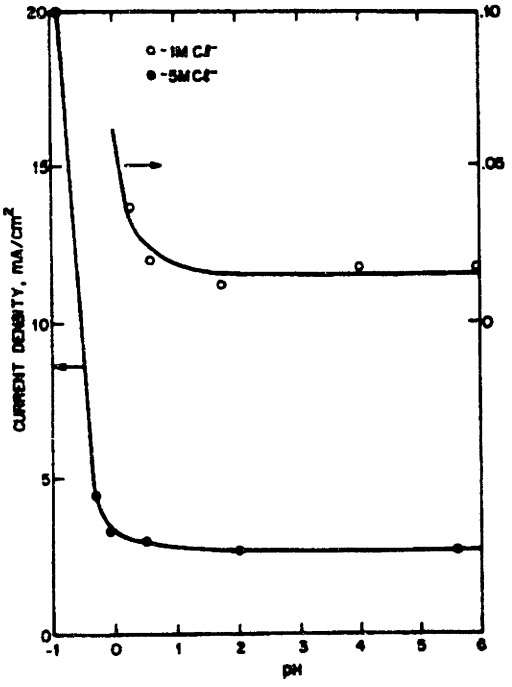

Figure 4-5. The variation of the peak current in the active corrosion region with solution pH. (Plot from Frankenthal & Siconolfi, "The anodic corrosion of gold in concentrated chloride solutions." Reproduced by permission of The Electrochemical Society, Inc.)

4.2.1.3 Passive region (E_{pass} < E < +1.4 to +1.6 V). There are two main theories concerning when and how the passive film forms on gold surfaces in chloride containing solution. Both theories have the competition of chloride ions and oxygen (possibly as hydroxide ions) for sites on the gold surface as their basis. However, the two theories differ in their specification of the species that plays the greater role in determining the onset of passivation.

The first theory states that the primary passivation potential is a function of chloride ion concentration and pH and therefore varies with system conditions. Frankenthal & Siconolfi demonstrate this in figure 4-6, while Gallego *et al* found an analytical expression for E_{pass} at 25°C as a function of chloride ion concentration and pH (see equation 4.2). Frankenthal & Siconolfi define E_{pass} as being the "potential of the current density minimum" occurring after the current peak, while Gallego *et al* define E_{pass} as "the break of the E/I profile occurring at high anodic potential." Jones[7] defines the primary passivation potential (E_{pass}) as the potential above which "the passive film becomes stable, and corrosion rate falls to very low values." In this case, E_{pass} corresponds to the potential at the current density peak. Although there is variation among

researchers about the definition and exact location of E_{pass}, it is generally recognized as the potential where passive film growth begins to predominate over corrosion and the resulting current drops to low values (possibly an order of magnitude or more).

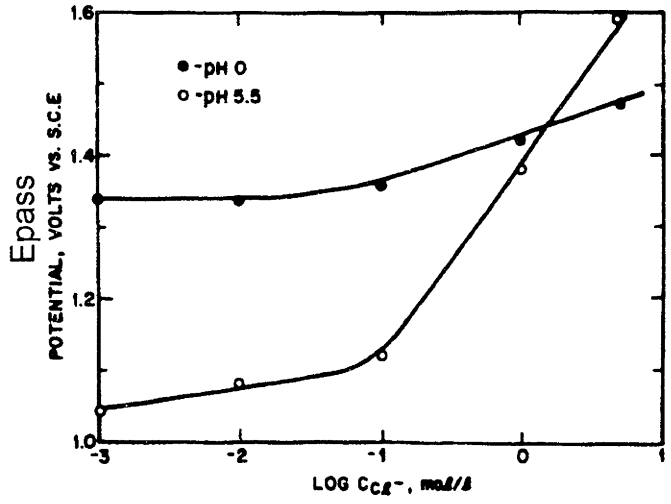

Figure 4-6. Effect of chloride concentration on the gold passivation potential (E_{pass}) in solutions at different pH. (Plot from Frankenthal & Siconolfi, "The anodic corrosion of gold in concentrated chloride solutions." Reproduced by permission of The Electrochemical Society, Inc.)

$$E_{pass} = 1.568 + 2.3\left(\frac{RT}{F}\right)\log c_{Cl^-} - 2.3\left(\frac{RT}{F}\right)pH \quad \text{at } 25^\circ C \tag{4.2}$$

Notice that Figure 4-6 and equation 4.2 both obey the general rule that as pH decreases, the size of the region of passivation decreases. In this case, this is shown by E_{pass} moving to more noble potentials with decreasing pH. This theory explains passive film formation as occurring only after chloride ions are depleted on the gold surface by diffusion limitations. Once the chloride is depleted, oxygen is able to adsorb onto the gold surface in the open sites. The adsorbed oxygen then serves to block chloride from these sites, causing gold dissolution to slow and the current to drop. This occurs at E_{pass}. Gallego *et al* believe that this "adsorbed oxygen," probably in the form of hydroxide ions or water, discharges on the gold surface to form a passivating oxide layer (Au_2O_3 or $Au(OH)_3$). Frankenthal & Siconolfi's mechanism for gold dissolution/passivation in the passive and transpassive regions presented in section 4.2.2.2 includes water as the only oxygen source for passive film formation (see equations 4.5b and 4.5c), while Gaur and Schmid do not speculate on the species comprising "adsorbed oxygen." Gaur and Schmid and Lovrecek *et al* observed normal gold passivation behavior in their chloride

solutions, even though their solutions were deaerated. This result, and the fact that the literature does not specifically mention dissolved molecular oxygen as a contributor to passive film formation in gold, does not rule out the possible contribution of dissolved molecular oxygen to passive film formation, but it does indicate that its presence is not required for normal passivation behavior.

The second theory describes E_{pass} as being much less variable than is proposed by the first theory. Gaur & Schmid found that E_{pass} did not vary appreciably from +1.2 V, even at different chloride concentrations. They also determined by polarization experiments in solutions without chloride, that oxygen began to adsorb onto the gold surface at approximately +1.0 V. A capacitance study of a gold electrode in chloride solution showed an increase in capacitance starting at approximately +1.0 V and ending at approximately +1.2 V (see figure 4-7). Gaur & Schmid recognized that this type of behavior is indicative of reactions such as the surface adsorption of oxygen. Gaur & Schmid proposed that chloride ions are adsorbed onto the gold surface at potentials greater than E_z and less than +1.0 V. Near +1.0 V, the competing processes of gold dissolution and oxygen adsorption began to occur simultaneously. As the potential is increased, Gaur & Schmid assume that the amount of adsorbed oxygen on the gold surface increases linearly until +1.2 V, where the gold surface is nearly saturated with adsorbed oxygen. Gold dissolution must stop at this point because there are no sites available on the gold surface for chloride ions. This explains the observation that E_{pass} varies little with chloride ion concentration and is always located near +1.2 V. Notice that in this theory, a preference for oxygen adsorption was the primary factor in determining the onset of passivation. This is in contrast to the first theory, which held that chloride ion depletion was the primary factor in determining the onset of passivation.

Cathodic polarization of the passivating film to potentials near +0.9 V will cause the reduction of the film and reactivation of the gold surface for subsequent corrosion. However, the oxide passivating film, once formed above E_{pass}, is stable in the active region between approximately +1.0 V and E_{pass}. Gaur & Schmid showed this experimentally by anodically polarizing gold in a chloride solution until a passive film was formed. They then cathodically polarized the gold to +1.0 V and anodically polarized it again through the active region. They observed no gold dissolution peak in the active region, demonstrating that a passive film was

present and that it was stable in the active region. However, the passive film was found to lose this stability in the active region over time. Gaur & Schmid observed that the passive film consistently began to break down in the active region after approximately ten minutes. When the film was left in the active region, the current eventually achieved the value that would be expected for un-passivated gold at that potential. This result lends support to the idea that chloride and oxygen compete for sites on gold surfaces and that this competition reaches an equilibrium over time. This result also supports the general observation that chloride ions contribute to passive film instability.

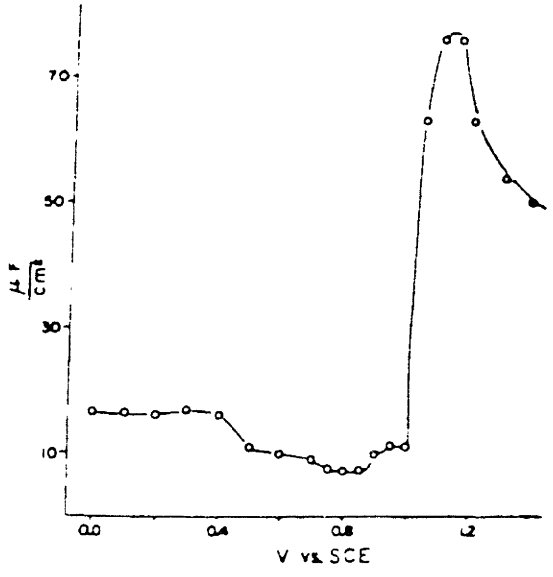

Figure 4-7. Capacitance vs. potential curve for gold in 0.1 M $HClO_4$ + 0.001 M KCl. (Plot reprinted from *Electroanalytical Chemistry and Interfacial Electrochemistry*, vol. 24, J.N. Gaur & G.M. Schmid, "Electrochemical behavior of gold in acidic chloride solutions," pages 279-286, 1970, with permission of Elsevier Science.)

Figure 4-8 from Gallego *et al* provides a graphical example of passive film stability using cyclic voltammograms of gold in chloride containing solutions. In this example, differences in cathodic sweep rate (V_c) serve as a measure of the time that the passive film is in the active region. In figure 4-8b, V_c is fast enough so that the passive film remains intact when passing through the active region and no dissolution peak is obtained. Notice also that there is a small peak at +0.9 V corresponding to the reduction of the passive film. In figure 4-8c, V_c is slow enough so that the passive film breaks down and gold corrosion is achieved in the active region. Notice also that there is no peak at +0.9 V for the reduction of the oxide film because the film had already been removed in the active region.

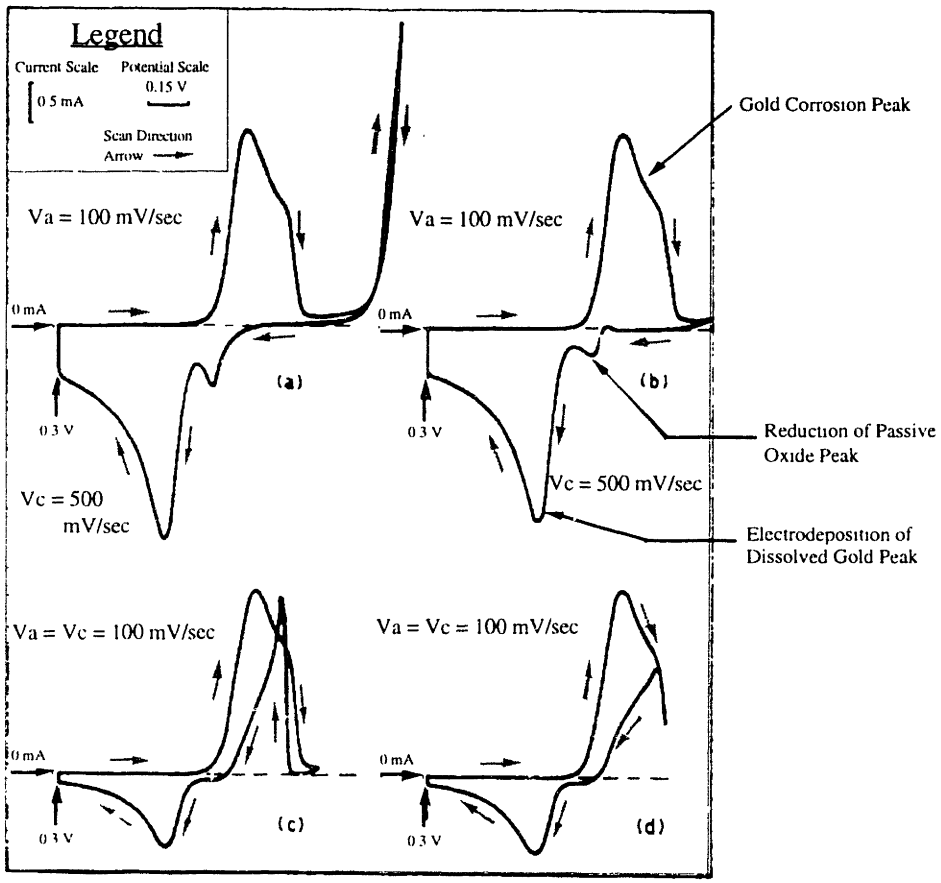

Figure 4-8. Cyclic voltammograms demonstrating the stability of gold's passive film by varying cathodic scan rate and the anodic scan potential limit in 1 M $NaClO_4$ + 0.0118 M HCl at 64°C. (Plot reprinted from *Journal of Electroanalytical Chemistry*, vol. 66, J.H. Gallego, C.E. Castellano, A.J. Calandra, & A.J. Arvia, "The electrochemistry of gold in acid aqueous solutions containing chloride ions," pages 207-230, 1975, with permission of Elsevier Science.)

4.2.1.4 Transpassive region (E > +1.4 to +1.6 V). This region is characterized by gold dissolution (higher relative to the passive region, but lower relative to the active region) and the evolution of gases such as chlorine and oxygen. The oxide passivating film becomes unstable in the transpassive region, particularly in the presence of chlorides. This results in local film breakdown, possibly by pitting, and an increase in gold dissolution. The evolution of chlorine gas is extremely dependent on chloride concentration. For example, chlorine evolution may become significant at potentials as low as +1.4 V for chloride concentrations ≥ 0.1 M. In these chloride containing solutions, oxygen is typically more difficult to evolve than chlorine and

requires higher potentials, > +1.6 V according to Gaur & Schmid or > +1.85 V according to Frankenthal & Siconolfi. However, Frankenthal & Siconolfi found that at a potential of +1.80 V, the current due to gas evolution was approximately one order of magnitude greater than the current due to gold dissolution (see figure 4-9).

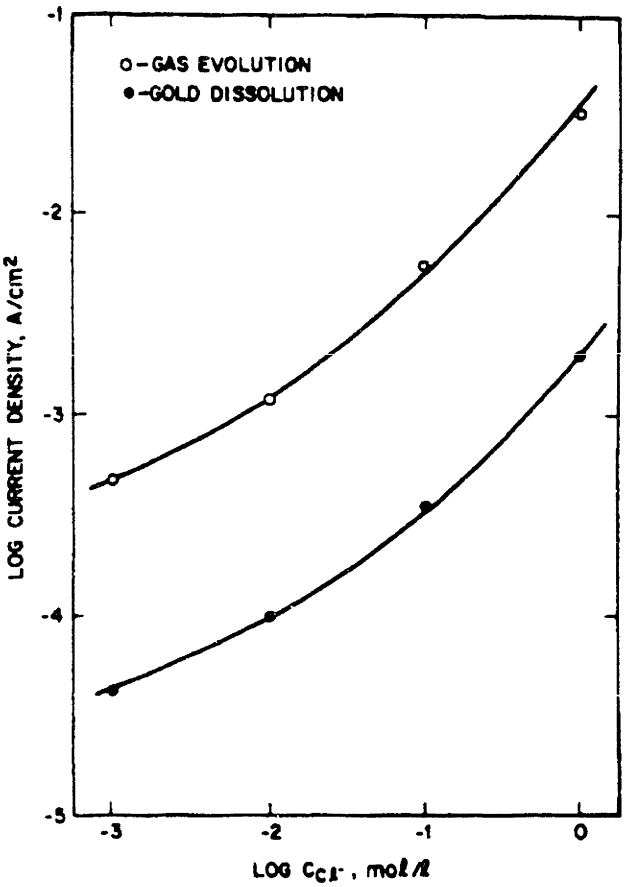

Figure 4-9. Effect of chloride concentration on the rates of gold dissolution and gas evolution at +1.80 V. (Plot from Frankenthal & Siconolfi, "The anodic corrosion of gold in concentrated chloride solutions." Reproduced by permission of The Electrochemical Society, Inc.)

4.2.2 Proposed gold dissolution/passivation mechanisms from the literature.

4.2.2.1 Mechanism for gold dissolution in the active region. A mechanism for gold dissolution in the active region was proposed by Gallego *et al* (see equations 4.3a-f). This mechanism allows for the heterogeneous and homogeneous formation of the soluble Au(III) corrosion product ($AuCl_4^-$) from a Au(I) compound ($AuCl_2^-$). The limiting step in this series of reactions is the formation of $(AuCl_2^-)_{ad}$ from $AuCl_{ad}$ in equation (4.3c). In addition, the surface is assumed to be nearly saturated with chloride ions in the form of $AuCl^-_{ad}$ due to the potential of

zero charge discussed in section 4.2.1.1. This mechanism led to the development of an expression for anodic current density that was first order in chloride concentration and directly dependent on the rate of constant of equation (4.3c) and the equilibrium constant of equation (4.3b). This expression is given as equation (4.4) and was reported by Gallego *et al* to have been in good agreement with experimental data.

$$Au + Cl^- \Leftrightarrow AuCl^-_{ad} \tag{4.3a}$$

$$AuCl^-_{ad} \Leftrightarrow AuCl_{ad} + e \tag{4.3b}$$

$$AuCl_{ad} + Cl^- \Leftrightarrow (AuCl^-_2)_{ad} \tag{4.3c}$$

$$3(AuCl^-_2)_{ad} \Leftrightarrow AuCl^-_4 + 2(AuCl^-)_{ad} \tag{4.3d}$$

$$(AuCl^-_2)_{ad} \Leftrightarrow AuCl^-_2 \tag{4.3e}$$

$$3AuCl^-_2 \Leftrightarrow AuCl^-_4 + 2Au + 2Cl^- \tag{4.3f}$$

$$i_a \approx FK_{3b}k_{3c}c_{Cl^-}\exp\left[\frac{FE}{RT}\right] \tag{4.4}$$

4.2.2.2 Mechanism for gold dissolution/passivation in the passive and transpassive regions. A mechanism describing the processes occurring at a gold surface in chloride containing solutions in the passive and transpassive regions (~ +1.35 to +1.85 V) was proposed by Frankenthal & Siconolfi (see equations 4.5a-e). This mechanism takes into account gold dissolution in the form of $AuCl_4^-$ ions, the formation and dissolution of oxide passivation layer in its hydrated ($Au(H_2O)_m^{3+}$) and non-hydrated (Au_2O_3) forms, and the evolution of chlorine gas. Oxygen gas evolution was not included because it was assumed that its contribution to the overall current in this potential range was negligible. These reactions were assumed to occur in parallel and each reaction in the mechanism may actually be a composite of several steps. According to Frankenthal & Siconolfi, good agreement with experimental data was obtained over a range of chloride concentrations using an expression for total current containing rate constants found by fitting experimental data.

$$Au + 4Cl^- \rightarrow AuCl_4^- + 3e \quad (4.5a)$$

$$Au + mH_2O \rightarrow Au(H_2O)_m^{3+} + 3e \quad (4.5b)$$

$$2Au + 3H_2O \rightarrow Au_2O_3 + 6H^+ + 6e \quad (4.5c)$$

$$2Cl^- \rightarrow Cl_2 + 2e \quad (4.5d)$$

$$Au_2O_3 + 8Cl^- + 6H^+ \rightarrow 2AuCl_4^- + 3H_2O \quad (4.5e)$$

4.2.3 Stress corrosion cracking of gold and gold alloys. Stress corrosion cracking (SCC) is a type of environmentally induced cracking (EIC). Environmentally induced cracking generally refers to "brittle mechanical failures that result from a synergism between tensile stress and a corrosive environment."[8] Other forms of EIC include corrosion fatigue cracking (CFC) and hydrogen induced cracking (HIC), also known as hydrogen embrittlement. It is generally accepted that three factors are required for stress corrosion cracking; a corrosive environment, a susceptible material, and a tensile stress. The corrosive environment factor usually involves a particular dissolved species. In the case of gold, chloride is a complexing agent that enables gold to dissolve with applied potential. However, extensive corrosion is not required for SCC to take place. In fact, corrosion rates are often low at the conditions favorable for SCC. The material is susceptible to SCC if it forms a passive surface film or if it is an alloy in which one component can be selectively dissolved. The tensile stress is usually a static stress and can be much lower than the yield stress for the material. The tensile stress does not have to be externally applied, but could consist of residual stresses present in the material itself (i.e. from processing conditions, at grain boundaries, etc.).

Stress corrosion cracking consists of two stages, crack initiation and crack propagation[9]. Crack initiation is primarily electrochemical in nature, while crack propagation is primarily mechanical. Crack initiation usually begins with the formation of a surface film. This could be a passivating oxide film, or it could be a porous, "ennobled" layer in an alloy that has been depleted of its more active component by selective dissolution[10,11]. The surface film or layer formed by oxidation or selective corrosion, if more brittle than the underlying material, can crack

with an applied tensile stress. The crack can propagate through the brittle film and extend into the underlying material, which would not normally crack due to its ductility. The cracks tend to be located near areas of stress concentration or high energy, such as grain boundaries or surface defects[12]. Cracks can also form in areas where alloyed materials have segregated[12] or by the local breakdown of passive films, as seen with pitting in the transpassive region.

Crack propagation is primarily a mechanical phenomenon, as evidenced by studies showing that both fracture surfaces tend to match up perfectly, with little or no material removed by corrosion. Two main mechanisms have been proposed in the literature for crack propagation in SCC. The first is film induced cleavage or cracking (FIC)[13]. This process is the same as the surface film induced crack initiation process. A crack forms, exposing a clean surface of the material. The surface forms a passive oxide layer, or an "ennobled" layer is formed by the corrosion and depletion of the more active material from the layer near the surface, just as in crack initiation. Tensile stresses cause the brittle film to crack again near the crack tip, which propagates the crack further into the material, exposes new material, and the process repeats until the material fails. Notice that electrochemistry can affect this method of crack propagation in that local chemistry in the crack tip may speed up or slow down the formation of surface films or "ennobled" layers. The second mechanism of crack propagation is based on surface mobility of lattice vacancies[14,15]. This proposed mechanism states that vacancies rapidly migrate toward the crack tip, causing the material at the crack tip to weaken and the crack to propagate. The rate of this type of crack propagation is dependent on the surrounding environment, which affects the surface self-diffusivity, and therefore the vacancy migration rate, of the material.

The literature contains numerous examples of SCC in gold alloys, typically copper-gold and silver-gold alloys[10,11,13-15]. Crack initiation for SCC in most of these cases is attributed to the selective dissolution of the more active metal (i.e. copper or silver) from the surface layers of the alloy, causing a gold rich layer to form. It is generally accepted that pure metals are comparitively more resistant to SCC than alloys[8], so it would seem that the gold rich layer should inhibit SCC in these alloys. Instead, this gold rich layer is weakened by porosity and can fracture under a tensile stress, resulting in the initiation of a crack into the alloy. Crack propagation by either mechanism will then lead to alloy failure. Interestingly, both intergranular and transgranular SCC were observed in gold alloys.

The literature does not report on the possibility of stress corrosion cracking in pure gold. This probably results from the fact that gold has more utility as a structural material (i.e. jewelry, dental materials, implants, etc.) in its alloyed, rather than pure, form. Pure gold is used in some microelectronic devices and may be exposed to conditions (i.e. tensile stresses and chloride) that could allow SCC to take place. However, this combination of conditions is not seen frequently because attempts are made in microelectronics to minimize chloride contamination. The controlled release microchip presented in this thesis purposely exposes pure gold to tensile stresses and chloride in its use as a material for its anode membranes. If gold is considered to be a material susceptible to SCC, then the conditions exist for SCC to occur in pure gold. This possibility is mentioned in section 4.5.2.2 and discussed in detail in section 6.4.1.3.

4.3 Experimental methods.

4.3.1 Selection of electrolyte. All electrolytes used for the corrosion studies presented in this chapter and the chemical release studies presented in chapter 5 contained chloride ions. The presence of chloride ions is required to corrode gold with low applied potentials in near neutral pH aqueous solutions. Two saline solutions were selected for corrosion and chemical release studies, one buffered with phosphate and the other non-buffered.

The controlled release microchips have possible applications in drug delivery. Therefore, phosphate buffered saline (PBS) was selected as an electrolyte as a first order approximation of a biological fluid. The PBS (Sigma #P-5886) was supplied in sterile, 100 mL bottles and had a NaCl concentration of 0.145 M and a phosphate concentration of 0.15 M. The source of phosphate in the PBS was mono-potassium phosphate, buffered to a pH of 7.2 with sodium hydroxide. The PBS was stored in a refrigerator at slightly above 0°C degrees until use.

The other electrolyte used for corrosion and chemical release studies was an un-buffered saline solution consisting of de-ionized (DI) water and 0.145 M NaCl. This electrolyte was prepared in the laboratory with DI water (made with a U.S. Filter water system) and NaCl crystals (Mallinckrodt #7532, granular, food grade). The ionic strength of this solution was 290 mM. However, some corrosion experiments with TRL prototype 081897 described in section 4.3.4.2.3 were conducted in this un-buffered saline solution with the addition of Na_2SO_4

(Mallinckrodt #8024, anhydrous, granular, analytic reagent grade) to adjust the ionic strength of the dilute saline solutions to a minimum value of 1.0 M.

Un-buffered saline solution was selected for chemical release experiments where the presence of phosphate ion would affect chemical release results due to interactions with one of the released chemicals. For example, the phosphate ions in PBS could react with the radioactive calcium ($^{45}Ca^{2+}$) ions released into solution during the multiple chemical release studies described in section 5.2.3. The calcium phosphate formed could fall out of solution as an insoluble salt, making detection of calcium release difficult and inaccurate. The pH of this un-buffered saline solution is typically 5.5-6.0. The absence of pH buffering does not significantly affect gold corrosion, but it can have an effect on the detection accuracy of pH sensitive materials such as the fluorescent dye, sodium fluorescein, as described in section 5.4.2.2.

4.3.2 Reference electrode. A reference electrode has a known, constant potential with respect to the equilibrium reaction between hydrogen ions and hydrogen gas. The equilibrium potential of this reaction has a value of +0.00 volts and is called the standard hydrogen electrode (SHE). Electrochemical reactions have an equilibrium potential that is either positive or negative with respect to the SHE. Reference electrodes enable the applied potential to be accurately controlled with respect to the SHE, allowing specific electrochemical reactions to take place in an electrolyte. A saturated calomel electrode (SCE) is composed of a platinum wire inserted into a mixture of mercury and mercury (I) chloride that is in contact with saturated KCl. The equilibrium reaction between mercury and mercury (I) chloride in contact with saturated KCl has a constant potential of +0.241 volts relative to the SHE. The fact that SCE's are easier to manufacture than SHE's and have a constant potential with respect to the SHE makes them useful as reference electrodes.

SCE's must maintain electrical contact with the working electrode (i.e. gold anode) through the electrolyte in which the corrosion reaction is taking place. This can be accomplished by the use of a salt bridge or by placing the SCE directly in the electrolyte. Electrical connection of the SCE through the electrolyte requires that a small amount of the saturated KCl in the SCE leak slowly into the electrolyte. Therefore, salt bridges are preferred for applications where minute amounts of chloride may affect the results of the experiment, such as in the study of

passive films. The electrolyte used for the gold corrosion experiments contains a significant amount of chloride (0.04 to 1.0 M, but usually 0.145 M) so a small amount of chloride ion leaking from the SCE into the electrolyte should not affect the gold corrosion results. For example, an SCE with a KCl leak rate of 8 μL/hr will change the chloride concentration of 100 mL of 0.145 M saline solution by 0.05% if left in the electrolyte for 15 minutes. As a point of reference, an SCE is usually left in the electrolyte for 5-15 minutes for each corrosion experiment, allowing little chloride ion to leak from the SCE into the electrolyte.

A saturated calomel electrode (Fisher #13-620-52) was used in all gold corrosion experiments to hold the applied potential in the gold corrosion region (+0.9 to +1.2 volts vs. SCE). The potential used in the potentiostatic gold corrosion experiments presented in the next several sections was typically +1.04 volts vs. SCE. The positioning of the SCE and the duration of its submergence in the electrolyte is detailed in the methods section for each experiment.

4.3.3 Gold foil corrosion. There are data published in the literature for the corrosion of bulk gold in the form of beads, wires, or foil in chloride containing solutions[1,4-6,16]. It was desired to verify that bulk gold corrosion could be achieved in several different chloride containing electrolytes and that the results resembled those published in the literature.

Gold foil (Englehard, 0.002" thick, minimum purity = 99.95%) was selected as the gold anode form for these initial corrosion experiments. The foil was cut into rectangular pieces (0.5 cm by 2 cm) and cleaned for 5 minutes in a 5:1:1 (volume ratio) solution of H_20:H_2O_2:NH_4OH at 75°C. The gold foil pieces were rinsed with DI water, dried, and stored in DI water until needed for electrode construction.

A diagram of a typical gold foil electrode is given in figure 4-10. Electrical connection between the gold foil and the potentiostat was achieved with an 18 gauge, 7 conductor wire soldered to one end of the gold foil. The soldered connection between the wire and gold foil was encapsulated in a plastic eppendorf tube filled with epoxy (Buehler Epo-Kwick). A glass tube was attached to the eppendorf tube to allow easier handling and positioning of the electrode in the electrolyte.

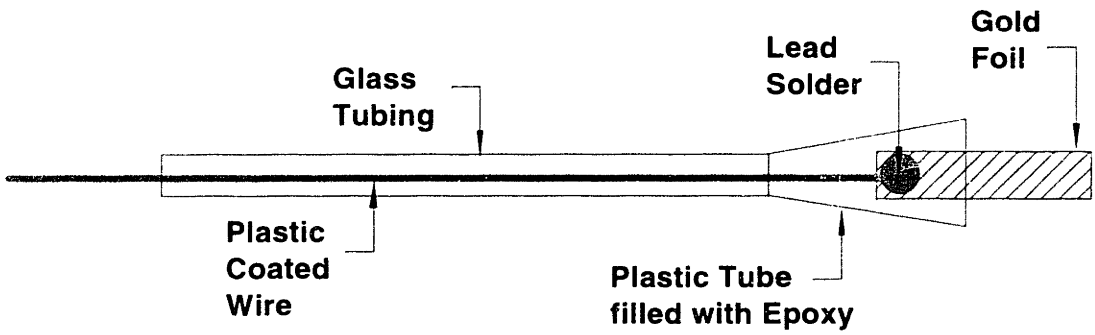

Figure 4-10. Typical gold foil electrode.

All corrosion experiments with gold foil anodes were conducted in 100 mL of electrolyte in a jacketed vessel (EG&G Jacketed Electrochemical Cell Kit #K0064). The temperature was held constant at 37°C (physiological temperature) by a controlled temperature water bath (Haake F3-K Digital) in all experiments except the experiment examining the effect of temperature on gold corrosion, which also included two runs at 25°C. The electrolyte was stirred with a magnetic stirring bar and stirrer (Corning Model PC-410) at the same rotation rate for all of the gold foil corrosion experiments except the experiment examining the effect of stirring rate on gold corrosion, which included two runs without stirring. The cathode was a platinum wire mesh electrode positioned 3-5 cm from the anode in the jacketed vessel. The tip of the saturated calomel reference electrode (SCE) was positioned 1-3 mm from the surface of the gold foil anode several minutes prior to the application of an electric potential. Cyclic voltammetry scans were conducted from +0.11 to +1.9 V vs. SCE at a scan rate of 20 mV/sec using a potentiostat/galvanostat (EG&G Model 273). Multiple scans in one electrolyte may have been completed using the same gold electrode, but a new gold foil electrode was used for each different electrolyte.

Two of the electrolytes used in the gold foil experiments, PBS and 0.145 M NaCl, were described in section 4.3.1. An acid chloride solution and a phosphate buffer solution without chloride were also used for gold foil corrosion experiments. The acid chloride solution was composed of 0.2 g NaCl and 0.7 mL concentrated HCl (Mallinckrodt #2062, 37.3 wt% HCl),

diluted to a total solution volume of 100 mL with DI water. The chloride concentration in this solution was 0.12 M, and the pH was measured with litmus paper to be 1-1.5. The phosphate buffer without chloride was made with a monobasic potassium phosphate solution (Sigma #P-8709, 1.0 M solution) diluted with DI water to a phosphate concentration of 0.15 M. Approximately 2.5 grams of potassium hydroxide pellets (Mallinckrodt #6984, pellets) were added to the solution to adjust the pH to 7.2. The phosphate buffer pH was measured with a pH electrode (Fisher 13-620-300). The phosphate concentration (0.15 M) and pH (7.2) were the same as that of the PBS used in several corrosion experiments. The difference between this phosphate solution and the PBS was that no chloride was added to this phosphate solution.

4.3.4 Gold thin film corrosion. Prototype controlled release microchips use the corrosion of thin gold membranes as the mechanism for releasing chemicals from reservoirs in silicon. It was desired to characterize the corrosion of gold thin films because gold thin film corrosion may differ from bulk gold corrosion.

The goal of the control experiments described in sections 4.3.4.1 was to verify that gold thin films do not corrode in a chloride containing electrolyte without an applied potential. The purpose of the patterned electrode experiments in section 4.3.4.2 was to characterize the corrosion of gold thin films in chloride containing solutions with an applied potential. The goal of the membrane experiments in section 4.3.4.3 was to demonstrate the proof-of-principle that unsupported gold membranes could be corroded on demand.

4.3.4.1 Controls. A thin film (3,000 Å) of gold was deposited at a rate of 5 Å/sec by electron beam evaporation onto the polished side of a (100) oriented silicon wafer coated with 1,800-1,900 Å of a low stress, silicon-rich nitride (VTR nitride). A thin film (100 Å) of chromium was deposited at a rate of 2 Å/sec by electron beam evaporation just prior to the gold to serve as an adhesion layer between the gold and silicon nitride. The metals were deposited without external heating or cooling, and the base vacuum achieved in the deposition system before evaporation was 5.0×10^{-6} torr.

The silicon wafer was scored with a diamond scribe and broken into small pieces (approximately 1 cm by 1 cm). Two pieces of gold coated silicon that were adjacent to one

another on the wafer were put into two glass scintillation vials; one vial was dry (i.e. contained only ambient air) and one was filled with phosphate buffered saline (PBS). The caps on all vials were sealed with parafilm (wax strip) and put aside for 45 days.

The vials were opened after 45 days, and the control samples were removed. The dry sample was broken into two pieces. The PBS sample and one of the dry pieces were put through a solvent rinse sequence to prevent water spots from forming on the gold films. Each sample went through the rinse sequence once. The rinse sequence consisted of DI water, acetone, methanol, and isopropanol, in that order. Each sample was dried with compressed gas (tetrafluoroethane, Falcon Dust Off Plus) and placed in a small plastic box. The two rinsed samples were mounted onto aluminum SEM stubs with copper tape. The remaining piece of the dry sample was also mounted onto a SEM stub with copper tape. This sample was never rinsed or soaked in a solution and was therefore, the "as deposited" control sample. The three samples were compared and examined for changes that may have occurred in the films over the 45 day experiment by light microscopy (Olympus BH-2 microscope) and high resolution scanning electron microscopy (JEOL 6320 Field Emission Scanning Electron Microscope). Comparision of the two dry samples (the un-rinsed "as deposited" sample and the rinsed "dry" sample) ensures that any observed differences between the as deposited gold sample and the PBS sample are not due to the rinse procedure.

4.3.4.2 Patterned electrodes.

4.3.4.2.1 Microlab prototype 062696-2#3. Microlab prototype 062696-2#3 contained a single gold electrode pair (10 A Cr and 952 Å Au) and was originally a portion of Microlab prototype 062696-2. The prototype was packaged with glass slides and silver paint as described in section 3.2.4.1. The electrical connections and most of the gold electrodes of the device were protected with 5 minute epoxy. The exposed gold electrodes of the prototype were submerged in 25 mL of room temperature PBS, stirred with a magnetic stirring bar. The electric potential scan was conducted between +0.85 and +1.15 volts vs. SCE at a scan rate of +2 mV/sec. The prototype was removed from the PBS, rinsed with DI water, and examined by light and scanning electron microscopy.

4.3.4.2.2 TRL prototype 021397-1#6. TRL prototype 021397-1#6 was packaged with glass slides and silver paint as described in section 3.2.4.1. The bond pads and silver paint were covered with epoxy to hold the wires in place during the experiment. The electrodes of the prototype were inserted into 100 mL of PBS at room temperature, stirred with a magnetic stirring bar. A constant potential of +1.04 volts vs. SCE was applied to the anode for approximately 42 seconds. The prototype was removed from solution, rinsed with DI water, and examined by light and scanning electron microscopy.

4.3.4.2.3 TRL prototype 081897. TRL prototype 081897 was fabricated as described in section 3.2.1.2, except that it did not have reservoirs etched into it. The anodes were simply patterned gold thin films (i.e. not membranes) completely supported by silicon nitride covered silicon. Each gold anode was examined and photographs were taken with a light microscope immediately preceding a corrosion experiment involving that anode.

The prototype was sealed into a PGA package as described in section 3.2.4.2 and connected to a potentiostat/galvanostat (EG&G Model 273) using the testing apparatus described in section 5.2.2.2 and shown in figure 5-3. The prototype was connected to the apparatus and placed in 100 mL of the electrolyte in a jacketed glass beaker until the water level covered the bottom half of the device (i.e. did not cover the gold wire bonds). The electrolyte was held at 25°C for the duration of the experiment using a temperature controlled water bath. The beaker was covered with parafilm (wax strip) to reduce the loss of electrolyte by evaporation. The electrolyte was gently stirred with a magnetic stirring bar throughout the experiment. The pH of the electrolyte was measured with a pH probe and removed before the insertion of the reference electrode. The SCE reference electrode was always placed in the electrolyte with its tip positioned approximately 1 cm from the surface of the anode approximately 10 minutes before the application of the potential. An electric potential of +1.04 V vs. SCE was applied to the anode for 90 seconds. The SCE was removed immediately after the potential corrosion experiment. The prototype was removed from the electrolyte, rinsed with DI water, gently dried with a can of compressed gas (tetrafluoroethane, Falcon Dust Off Plus). The anode was examined and photographs were taken with a light microscope.

Two types of corrosion experiments were conducted with this prototype, each with a different electrolyte. The first corrosion experiment examined the effect of changing chloride ion concentration ion on the corrosion of thin gold films. The chloride content of the electrolyte was varied between 1.0 M and 0 M by changing the amount of NaCl dissolved in DI water. However, all electrolytes were maintained at a minimum ionic strength of 1.0 M by the addition of Na_2SO_4. Therefore, all electrolytes with less than 0.5 M Cl^- (0.5 M NaCl has an ionic strength of 1.0 M) contained some amount of Na_2SO_4 to raise the ionic strength to 1.0 M. This procedure was used to keep the solution resistance from increasing at low chloride concentrations, and was similar to that used in the literature[1]. The pH and composition of the electrolyte used in the corrosion of each anode in this experiment is listed in table 4-2. All pH measurements were obtained with a pH electrode (Fisher 13-620-300).

Table 4-2. The electrolyte compositions used for corrosion of each gold anode of TRL prototype 081897.

Anode	NaCl	Na_2SO_4	pH	Ionic Strength (M)
1	1000	0	6.1	2.0
2	500	0	5.9	1.0
19	250	83.33	5.8	1.0
3	145	118.33	5.9	1.0
5	100	133.33	5.9	1.0
6	60	146.67	5.8	1.0
18	40	153.33	5.8	1.0
9	0	166.67	5.9	1.0

The second experiment examined the extent of gold corrosion as a function of time of applied potential. The electrolyte composition for this study was the same as that used for studies of release of multiple chemicals, 0.145 M NaCl in DI water, with no Na_2SO_4. The same electrolyte was used for the corrosion of multiple anodes (i.e. the electrolyte was not replaced with fresh solution after each anode was corroded). The pH of this electrolyte was 5.8 and the temperature was held constant at 25°C. An electric potential of +1.04 V vs. SCE was applied to each anode as given below in table 4-3.

Table 4-3. Time of application of +1.04 volts vs. SCE to the each anode of TRL prototype 081897.

Anode	Time (sec)
20	0
7	2
16	4
10	8
11	12

4.3.4.3 Membranes. The six gold membranes of Microlab prototype 091096-2 were examined for defects with reflected and transmission light microscopy. The membranes of reservoirs 1, 4, and 6 were defect free. The membranes of reservoir 2 and 3 had pinholes and the gold trace of reservoir 5 was broken. Reservoirs 1, 4, and 6 were filled with fluorescein powder and a drop of ethanol was added to dissolve the powder. The gold membrane of reservoir 4 was broken during this process and was sealed with waterproof epoxy. The large (filling) opening of each reservoir was covered with a piece of glass cover slip and held in place with 5 minute epoxy. The entire back of the prototype was sealed with and the prototype was packaged with glass slides and silver paint as described in section 3.2.4.1. The bond pads and silver paint were covered with 5 minute epoxy to hold the wires in place during the experiment. Waterproof epoxy was used to seal around the outside of the device and over the 5 minute epoxy covering the wires.

The electrodes of the device were submerged for 21.67 hours in 25 mL of room temperature PBS, stirred with a magnetic stirring bar. The solution was replaced with fresh PBS, and a potential of +1.04 V vs. SCE was applied 62.75 minutes later to reservoir #1 for 4 minutes. Another potential of +1.04 V vs. SCE was applied 11.5 minutes later to reservoir #1 for approximately 2.5 minutes. The prototype was removed from the PBS, rinsed with DI water, and examined with a light microscope to see if reservoir #1 had opened. The prototype was reinserted into the PBS, and +1.04 V vs. SCE was applied 25 minutes later to reservoir #6 for 1 minute. The prototype was removed from the PBS 20.0 minutes later, rinsed with DI water, and examined by light and scanning electron microscopy.

4.4 Experimental Results.

4.4.1 Gold foil corrosion. Figure 4-11 shows typical cyclic voltammetry data (only the anodic scan is shown) for gold foil anodes in three different chloride containing electrolytes. The gold foil in PBS is the first to form a passivating layer and the first to have its current rise after passivation. The current in the region from +1.4 to +1.7 V vs. SCE is much larger in the PBS than in the other electrolytes. Possible reasons for this behavior in PBS will be discussed in section 4.5.1.1. The acid chloride solution passivates at the highest potential of the three electrolytes. The electrolyte appeared to gain a slight yellow color after several potential scans, probably due to dissolved gold. The cathode also appeared to have metallic gold plated on it after several scans.

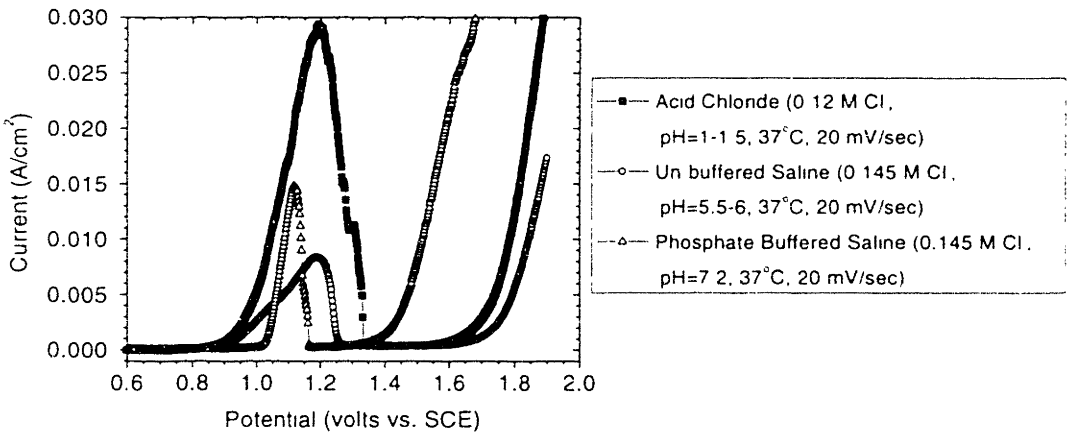

Figure 4-11. Cyclic voltammograms for gold foil in several electrolytes (only anodic scan is shown).

Figure 4-12 contains scanning electron micrographs (Hitachi S-530 SEM) showing the extent of corrosion sustained by gold foil during four consecutive cyclic voltammetry experiments conducted between +0.11 and +1.9 volts vs. SCE in un-buffered saline solution. The gold foil is polycrystalline and has been shown by x-ray diffraction to have a preferred orientation of (200). The corroded gold surface in figure 4-12b appears to contain many small facets. In addition, there were a number of larger pits in the gold that had facets and smooth side walls (figure 4-12c). These features may have formed from grains that were detached from the

gold surface by corrosion along grain boundaries. It is possible that the type of corrosion (i.e. uniform, transgranular, or intergranular) observed in gold foil in the active region may be different from that seen in the transpassive region. It is difficult to determine from these SEMs which type of corrosion dominates in either region because the cyclic voltammetry experiments included potentials in both the active and transpassive corrosion regions.

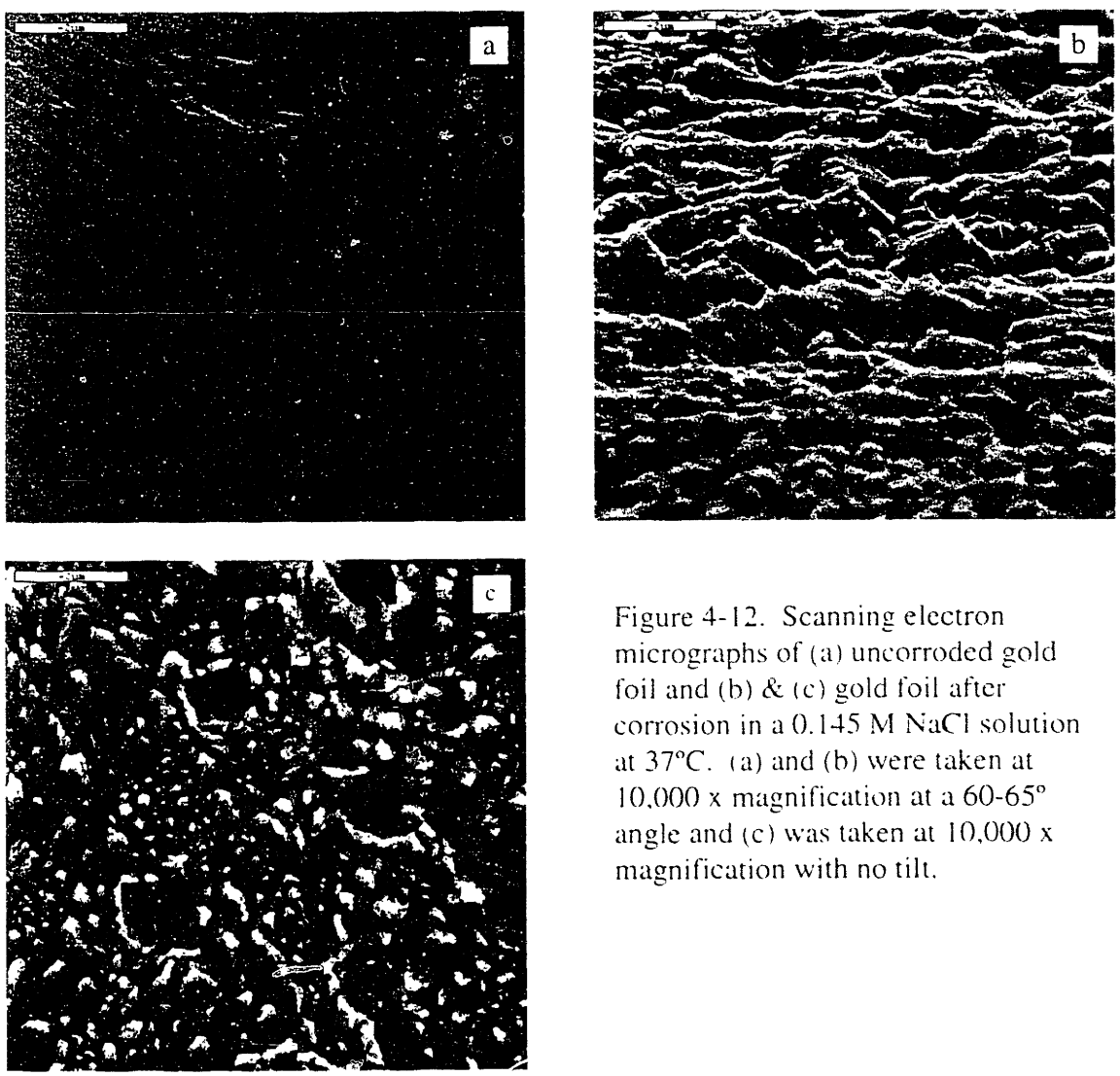

Figure 4-12. Scanning electron micrographs of (a) uncorroded gold foil and (b) & (c) gold foil after corrosion in a 0.145 M NaCl solution at 37°C. (a) and (b) were taken at 10,000 x magnification at a 60-65° angle and (c) was taken at 10,000 x magnification with no tilt.

4.4.2 Gold thin film corrosion.

4.4.2.1 Controls. Light micrographs and scanning electron micrographs for the "as deposited" and PBS gold control samples are given in figure 4-13. Both samples have small black spots and circular objects on their surface when viewed at 375x under a light microscope (figures 4-13a,b). These same features appear as white spots under a scanning electron microscope at low magnification (2,500x), as shown in figures 4-13c,d. These spots have diameters ranging from 0.3 to over 1.0 μm. They appear under high magnification (50,000x) in figures 4-13e.f to be particles on top of the gold film, as indicated by the shadowing on the gold surface. Scanning electron micrographs at 100,000x show the gold film texture and grain size (figures 4-13g,h).

4.4.2.2 Patterned electrodes.

4.4.2.2.1 Microlab prototype 062696-2#3. The gold anode and cathode for this prototype were not covered by a protective layer of SiO_2 like most prototype devices. Therefore, the exposed gold surface area of the anode used in current density calculations included a portion of the gold trace up to the epoxy and was 2.93×10^{-4} cm^2. A plot of applied electric potential vs. current density from the linear sweep voltammetry experiment is given in figure 4-14. The peak current density occurs at approximately +1.04 volts vs. SCE and is approximately two orders of magnitude higher than the current density between +0.85 and +0.95 volts vs. SCE. The current quickly decreases at potentials above +1.10 volts vs. SCE, as is expected due to gold passivation.

Scanning electron micrographs of the anode surface after the application of electric potential are given in figure 4-15 and show extensive gold corrosion, especially in those areas of the anode closest to the cathode. Figure 4-15b shows the edge of a portion of corroded gold. Notice how gold corrosion appears to have progressed around gold grains. This process caused the electrical connection between some gold grains to be cut off before they had finished corroding, leaving some isolated gold grains behind.

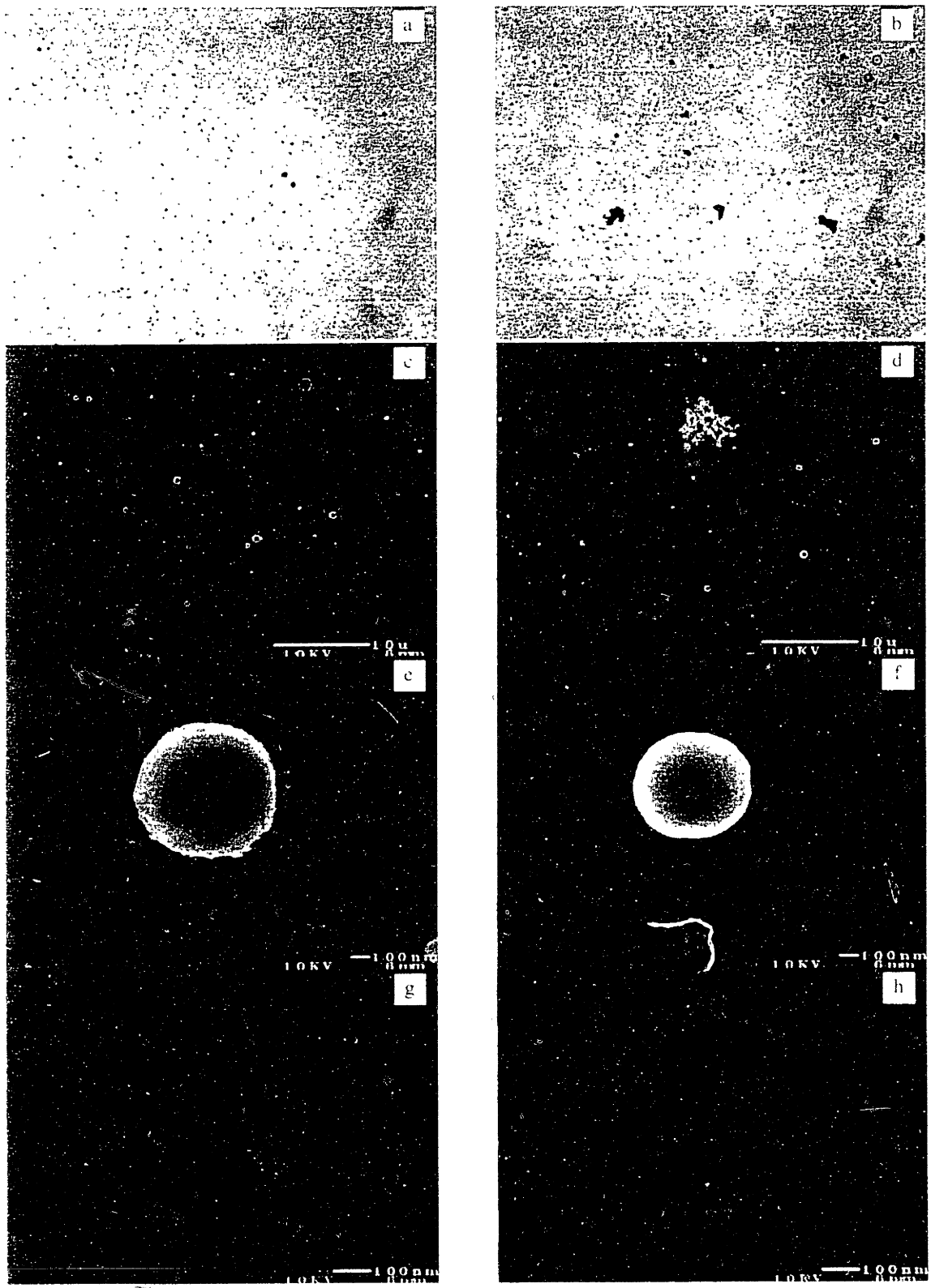

Figure 4-13 Light and scanning electron micrographs for gold controls. (a,c,e,g) "as deposited" controls and (b,d,f,h) PBS controls

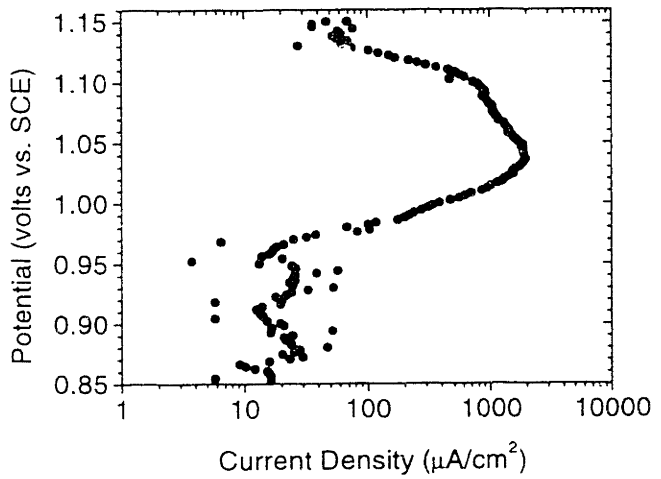

Figure 4-14. Linear sweep voltammogram for Microlab prototype 062696-2#3 in stirred, room temperature PBS open to air.

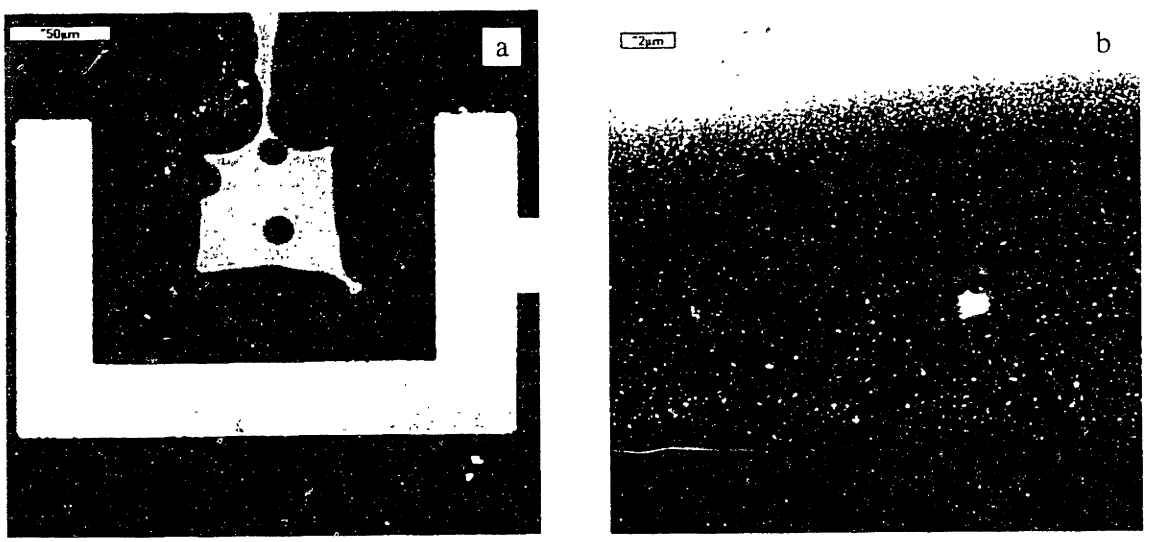

Figure 4-15. Scanning electron micrographs for Microlab prototype 062696-2#3. (a) overall view and (b) close-up of the edge of the corroded gold electrode.

4.4.2.2.2 TRL prototype 021397-1#6. This prototype did include reservoirs, so the gold anode would normally be considered a gold membrane instead of a gold thin film. However, the nitride support layer was not removed from below the gold film of this prototype, so the gold anode is better approximated as a supported gold thin film.

Figure 4-16 shows the current vs. time plot for the gold anode with an applied potential of +1.04 volts vs. SCE. Scanning electron micrographs of the gold anode after the application of the electric potential are shown in figure 4-17. Notice that corrosion occurred primarily in the grain boundaries of the large exposed region of gold and then extended beneath of the SiO_2 overlayer. The large peak in the current vs. time plot corresponds to the corrosion of the exposed gold membrane. The quick drop in current after 3 seconds corresponds to the breaking of electrical contact between the exposed gold surface and the current trace leading to the potentiostat supplying the electric potential. This breaking of electrical contact around the edges of the SiO_2 overlayer results in a large area of uncorroded gold remaining over the reservoir. Possible causes of this observed phenomenon and its implications on device reliability are discussed in detail in section 6.4.2.4.

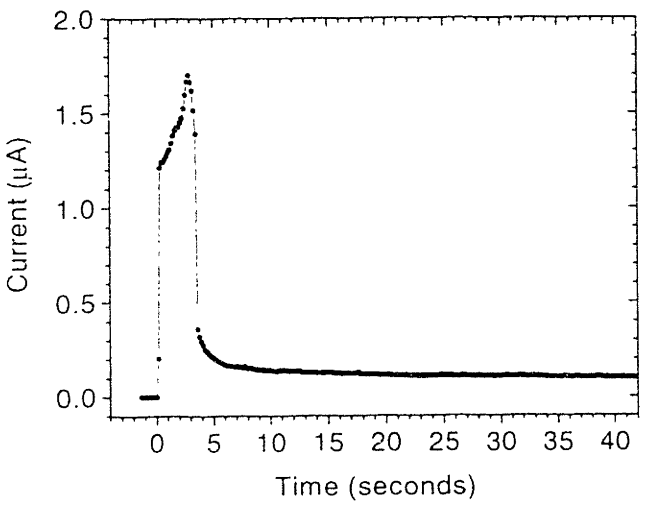

Figure 4-16.Chronoamperometry for TRL prototype 021397-1#6 in stirred, room temperature PBS open to air.

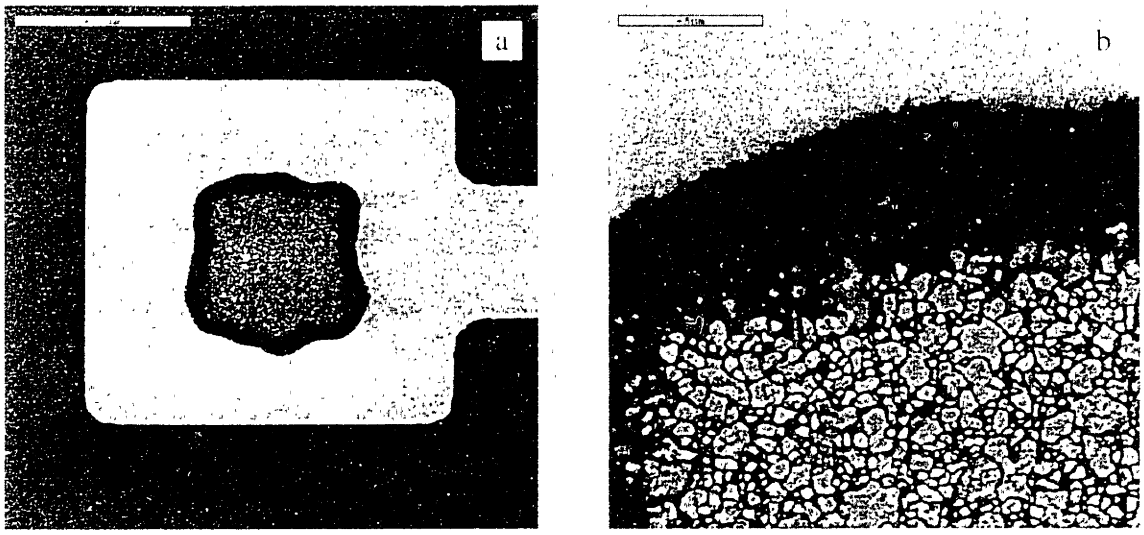

Figure 4-17. Scanning electron micrographs for TRL prototype 021397-1#6, (a) overall view and (b) close-up of the edge of the corroded gold electrode. The black region of (b) is the area of gold corroded under the SiO_2 overlayer.

4.4.2.2.3 TRL prototype 081897. The first experiment conducted with this prototype was designed to examine the effect of Cl^- concentration on thin film gold corrosion. The current density vs. time plots for gold thin film anode corrosion as a function of Cl^- concentration are given in figure 4-18. The current density peak decreases in height and increases in width as the Cl^- concentration decreases. The magnitude of the average peak current density and the time at which it occurred (i.e. location) are given in table 4-4 for each chloride concentration. (Note that the peak locations for 40 and 60 mM are only approximate due to the widening and flattening of the current density peak at those concentrations.)

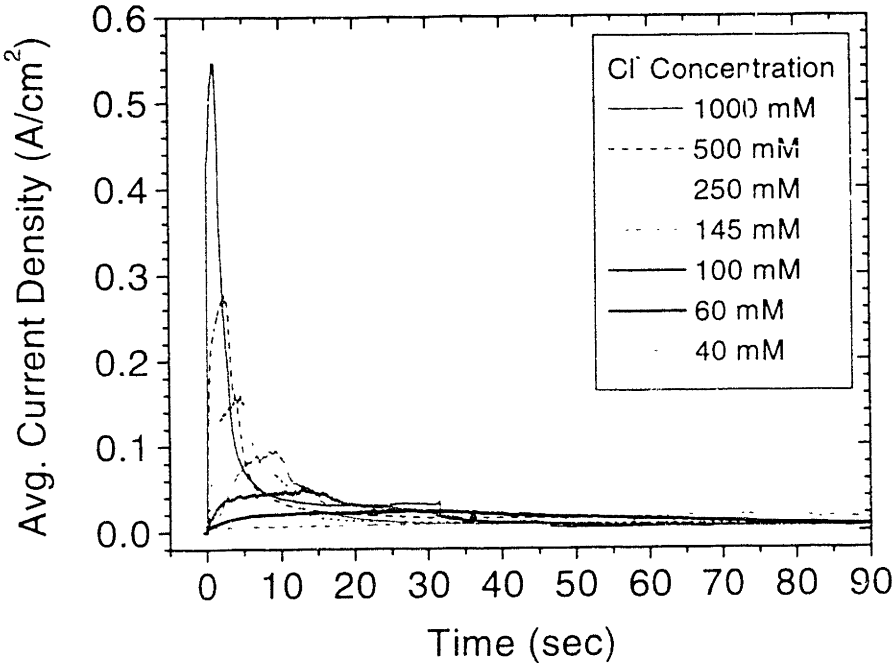

Figure 4-18. Average current density vs. time plot for different chloride concentrations.

Table 4-4. Average peak current density and peak current location for TRL prototype 081897 in electrolytes having different chloride concentrations.

Anode	Chloride Conc.(mM)	Average Peak Current Density (A/cm^2)	Peak Location (sec)
1	1000	0.548	1.0
2	500	0.278	2.4
19	250	0.161	4.6
3	145	0.097	9.1
5	100	0.051	12.8
6	60	0.025	27.1
18	40	0.020	74.4
9	0	$< i \times 10^{-8}$	na

Scanning electron micrographs of typical anodes are given in figure 4-19. The gold surrounding the 40 μm by 40 μm exposed gold surface of each gold thin film anode was covered by a protective layer of SiO_2 at the beginning of the experiment. However, some of this SiO_2 near the exposed gold delaminated during the experiment, allowing corrosion to take place under

the edges of the SiO_2 overlayer. There were also some portions of the exposed gold anode that did not corrode, probably due to the presence of a gas bubble on its surface during the experiment. The current density for each anode was calculated using the minimum exposed surface area (consisting of the 40 μm by 40 μm surface minus any uncorroded regions) and the maximum exposed surface area (as calculated from light micrographs taken at the end of the experiment). This provided a range in which the actual current density should be located. The current density data plotted in figure 4-18 and listed in table 4-4 are the average of the maximum and minimum values.

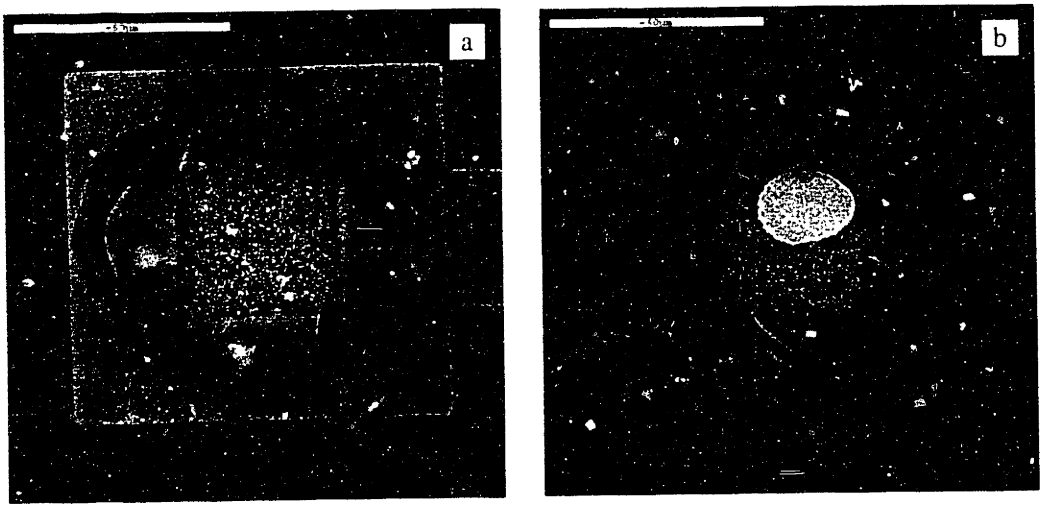

Figure 4-19. Scanning electron micrographs of corroded anodes from TRL prototype 081897, (a) anode #19 in 250 mM NaCl, and (b) anode #5 in 100 mM NaCl.

The second experiment conducted with this prototype was designed to examine changes in the gold anode's surface morphology with time of applied electric potential. Figure 4-20 contains scanning electron micrographs for anodes corroded for different amounts of time. The grain boundaries appear to be attacked preferentially, as indicated by the progression of grooving at the grain boundaries with corrosion time. Figure 4-21 shows the current vs. time data for the four corroded electrodes.

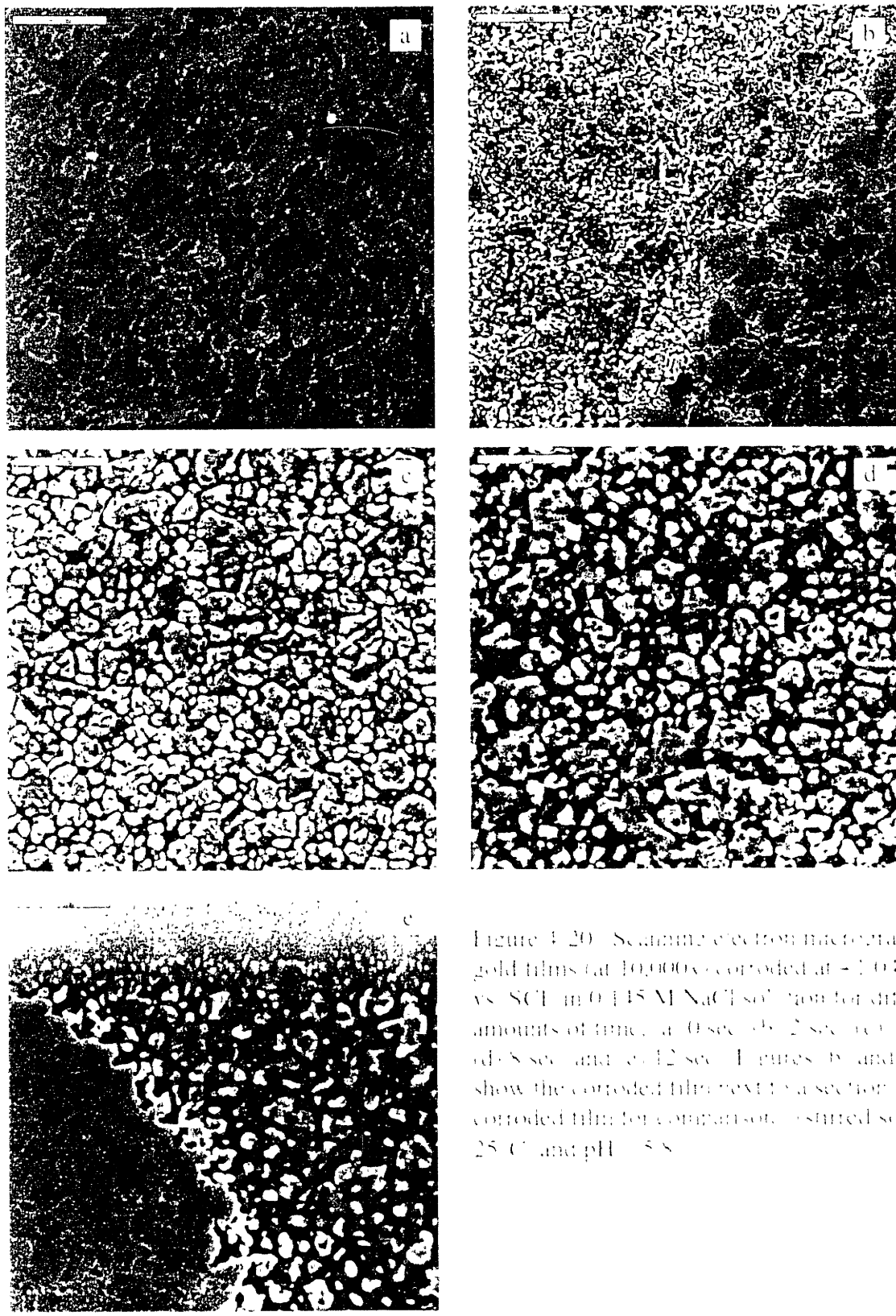

Figure 4.20 Scanning electron micrograph of gold films (at 10,000x) corroded at +1.04 volts vs. SCE in 0.145 M NaCl solution for different amounts of time: a) 0 sec, b) 2 sec, c) 4 sec, d) 8 sec, and e) 12 sec. Figures b and e show the corroded film next to a section of the corroded film for comparison. Stirred solution, 25 °C and pH = 5.8.

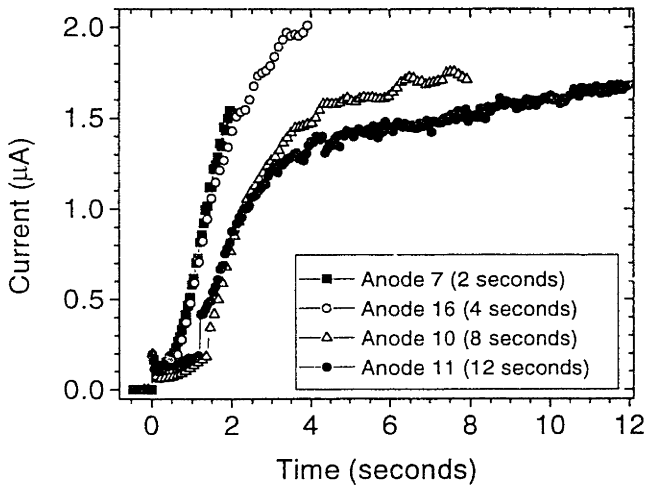

Figure 4-21. Chronoamperometry for TRL prototype 081897 in 0.145 M NaCl solution for different times. (stirred solution, 25°C, and pH = 5.8)

4.4.2.3 Membranes. Microlab prototype 091096-2 was originally going to be used for a chemical release experiment, so the experimental methods resemble those presented in chapter 5 for chemical release experiments. However, the most important aspect of this experiment with this prototype was the demonstration of corrosion and opening of unsupported gold membranes.

The current vs. time plots for reservoirs 1 and 6 of Microlab prototype 091096-2 are given in figure 4-22. The shape of the plots for the first application of electric potential to the gold membranes of reservoirs 1 and 6 resemble those presented in this chapter for other thin gold films. They both have a current peak that drops quickly to a low current value after the gold membrane corrodes to the point at which is breaks or loses electrical connection to the potentiostat at the edge of the SiO_2 overlayer. The magnitude of the peak current in the second application of electric potential to the membrane of reservoir 1 is more than an order of magnitude lower than for the first application (difficult to see in the figure) because the membrane has broken and the remaining exposed surface area for gold corrosion is small. The process of the gold membrane dissolving and falling apart is referred to as "disintegration" in chapter 6 and is described in more detail in section 6.4.1.

Figure 4-23 contains scanning electron micrographs for a reservoir covered with an intact gold membrane (reservoir 5), a reservoir covered by a partially corroded membrane (reservoir 6), and a reservoir whose membrane has corroded and fallen apart (reservoir 1).

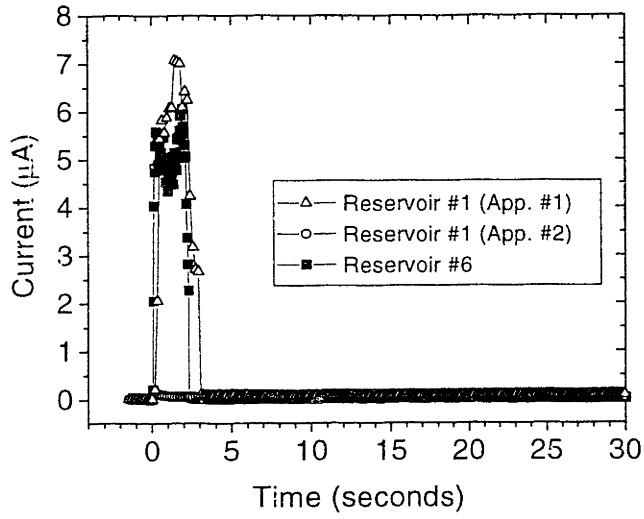

Figure 4-22. Chronoamperometry for Microlab prototype 091096-2 in PBS. (stirred solution, room temperature, pH=7.2)

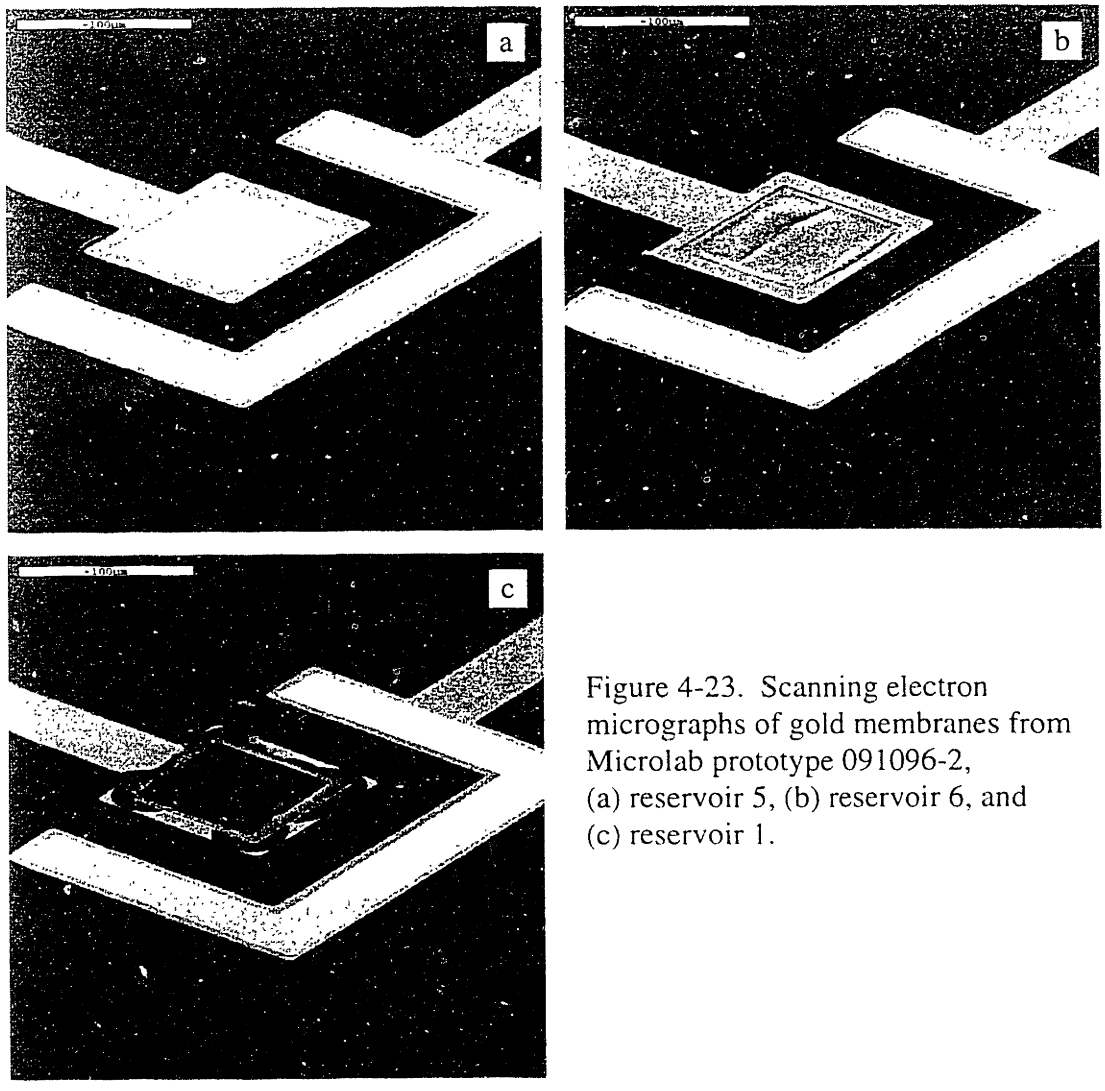

Figure 4-23. Scanning electron micrographs of gold membranes from Microlab prototype 091096-2, (a) reservoir 5, (b) reservoir 6, and (c) reservoir 1.

4.5 Discussion.

4.5.1 Comparison of experimental data with the gold corrosion literature.

4.5.1.1 Gold foil. Typical current vs. potential data from gold foil corrosion experiments were plotted in figure 4-24 with experimental data presented by Frankenthal & Siconolfi[1] having a similar chloride concentration. The results of the gold foil corrosion experiments agreed well with the trends shown in the literature data even though the experiments were conducted at slightly different conditions. All current vs. potential curves showed an active gold dissolution region with a current peak occurring between +1.0 and +1.2 volts, which agreed well with the literature values presented in table 4-1 in section 4.2.1.2. The experimental data also showed the characteristic drop in current density usually observed between +1.2 to +1.6 volts due to gold passivation. Figure 4-24 shows that the passive region for PBS is smaller than that for the other solutions. Anodic polarization of gold foil in phosphate buffer not containing chloride indicates that this difference can most likely be attributed to the presence of phosphate ion in solution. The early rise in current cannot be attributed to gold corrosion because no chloride is present in the phosphate buffer. The rise in current is possibly due to a chemical reaction taking place at the surface of the gold involving the phosphate ion. All experiments showed an increase in current density at high potentials (above +1.6 volts) due to the transpassive dissolution of gold and the evolution of oxygen and chloride gas[1].

A more detailed comparison of the gold foil corrosion can be accomplished by including data obtained by Frankenthal & Siconolfi at a chloride concentration of 1.0 M. Figure 4-25 contains the same data as figure 4-24 with the addition of the 1.0 M data and without the phosphate buffer data. The y-axis is plotted as the log of the current to allow easy comparison of data of significantly different current density. The data of Frankenthal & Siconolfi at chloride concentrations of 0.1 M and 1.0 M form an envelope in which the gold foil corrosion data, obtained at chloride concentrations of 0.12 M and 0.145 M, should fall. Variations in current peak height, the location in the active gold dissolution region, and the location of the passivation potential (E_{pass}) are attributed to differences in experimental conditions (see next paragraph) and agree well with trends presented in the literature.

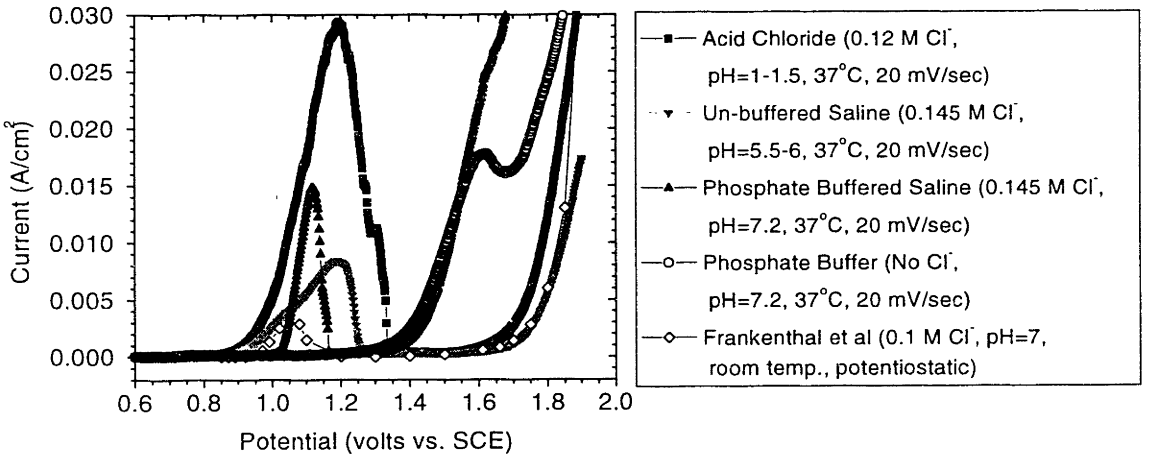

Figure 4-24. Cyclic voltammograms for bulk gold in several electrolytes plotted on a linear current scale (only anodic scan is shown).

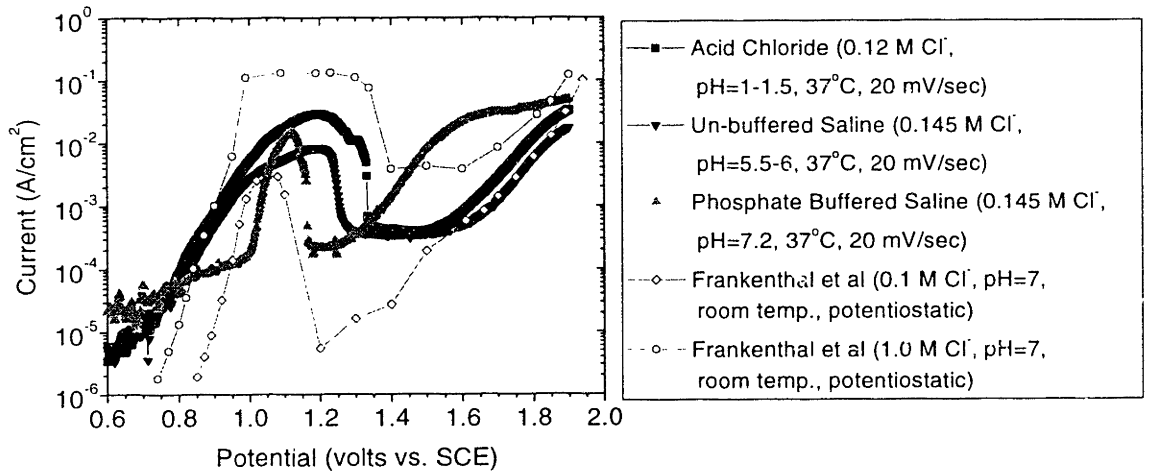

Figure 4-25. Cyclic voltammograms for bulk gold in several electrolytes plotted on a log current scale (only anodic scan is shown).

Frankenthal & Siconolfi's data was obtained potentiostatically in unstirred solutions at room temperature. The gold foil corrosion data was obtained potentiodynamically at a sweep rate of 20 mV/sec in well-stirred solutions at higher temperatures. Frankenthal & Siconolfi, Gaur and Schmid, and Gallego *et al* all report that peak current height (i.e. corrosion rate) increases

with chloride concentration and solution agitation. Frankenthal & Siconolfi also observed that potential sweep rates > 20 mV/sec can have an effect on current peak height similar to solution agitation. The experimental data in figure 4-26 show that current peak height increases with both stirring and temperature. Notice that stirring delays the onset of passivation, presumably by reducing mass transport limitations affecting chloride transport to the gold surface at higher potentials. Increases in temperature cause the gold surface to begin corroding and to begin passivating sooner, presumably by increasing the rate of the gold corrosion reaction at lower potentials and the rate of gold passivation at higher potentials. The experimental gold foil corrosion data in figure 4-25 were obtained at higher chloride concentrations, greater solution agitation (stirring with moderate potential scan rates), and higher temperatures, than Frankenthal & Siconolfi's data at 0.1 M. This could help explain the higher current peak heights observed for the gold foil experiments when compared with the literature.

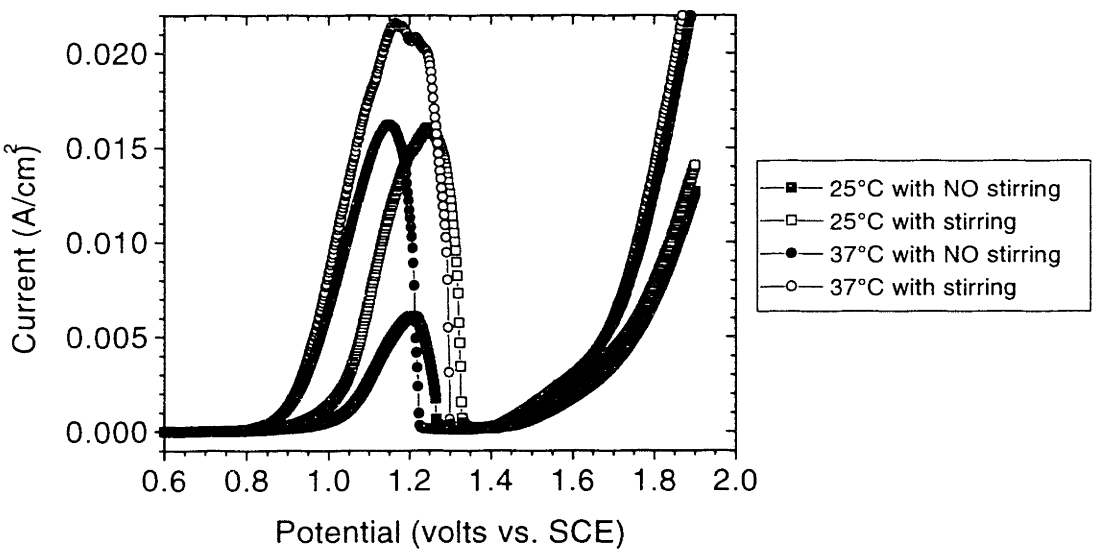

Figure 4-26. Linear sweep voltammetry of gold foil in 0.145 M NaCl solution examining the effect of solution temperature and stirring on the anodic current peak.

It was reported by Frankenthal & Siconolfi and Gallego *et al* that E_{pass} moves to higher (more noble) potentials with increasing chloride concentration and decreasing pH, resulting in a decrease in the potential range over which gold is passivated from corrosion. This agrees with

traditional corrosion theories that hold that the presence of chloride and low pH cause instabilities in passive (oxide) films. Gallego *et al* also reported an equation (see equation 4.2 in section 4.2.1.3) for predicting E_{pass} for gold at varying pH and chloride concentration at 25°C. Gallego *et al* define E_{pass} as "the break of the E/I profile occurring at high anodic potential." Gallego's definition for E_{pass}, for the purposes of this discussion, has been interpreted as meaning the potential at the sharp drop in current. Approximate values for E_{pass} were obtained from the data in figure 4-25 using this definition and are listed in table 4-5. The gold foil corrosion data were obtained at a higher temperature (37°C), but they do follow the trend predicted for pH and agree reasonably well with E_{pass} values calculated at 25°C using Gallego *et al*'s equation. The value of E_{pass} for Frankenthal & Siconolfi's data at 0.1 M agrees well with that predicted by equation 4.2, but the value predicted at 1.0 M is much lower than that observed experimentally.

Table 4-5. Comparison of experimental values for E_{pass} (from figure 4-25) and those predicted by equation 4.2 for several electrolytes.

Electrolytes	Cl^- (M)	pH	Observed E_{pass}(25°C)	Predicted E_{pass}(25°C)
Acid Chloride	0.12	~1.3	1.32 (at 37°C)	1.42-1.45
Un-buffered Saline	0.145	~5.8	1.25 (at 37°C)	1.17-1.19
Phosphate Buffered Saline	0.145	7.2	1.16 (at 37°C)	1.09
Frankenthal & Siconolfi ($NaCl + Na_2SO_4$)	0.1	7.0	1.14	1.10
Frankenthal & Siconolfi (NaCl)	1.0	7.0	1.38	1.16

4.5.1.2 Gold thin films. It is known that the mechanical properties of thin films can vary greatly from those of the same material in bulk form. The same may hold true for some electrochemical properties. Unfortunately, most gold corrosion literature presents studies on the electrochemical characteristics of the corrosion of bulk gold. A few papers do discuss the corrosion of gold thin films in the context of the failure of gold metallizations in electronic circuits[2,17]. However, these papers generally assume that electrochemical data obtained with bulk gold is sufficient for explaining corrosion in gold thin films. The objective of this section is to compare some of the electrochemical data obtained for gold thin films to that presented in the literature for bulk gold corrosion.

4.5.1.2.1 Location of peak current density. The success of the controlled release microchip is dependent upon the ability to achieve reproducible corrosion of gold thin films on demand. Gold corrosion in the active region (approximately +0.9 to +1.2 volts vs. SCE) is more uniform and reproducible than corrosion by pitting in the transpassive region (≥ +1.4 - +1.6 volts vs. SCE). Therefore, it is important to find the potential in the active gold corrosion region at which the maximum rate of thin film gold corrosion occurs. The current density vs. time plot for Microlab prototype 062696-2#3 in figure 4-14 shows that the peak current density occurs at a potential of +1.04 volts vs. SCE in PBS. The location of the current peak agrees well with the values shown in figure 4-24 for gold foil in PBS and Frankenthal & Siconolfi's data at a slightly lower chloride concentration. All subsequent experiments with gold thin films or membranes were conducted with an applied electric potential of +1.04 volts vs. SCE.

Another comparison can be drawn between bulk and thin film gold corrosion using the data from Microlab prototype 062696-2#3. The E_{pass} value of +1.12 observed experimentally for Microlab prototype 062696-2#3 agrees well with the value of +1.09 V predicted by equation 4.2 given by Gallego *et al* for a chloride concentration of 0.145 M and pH of 7.2.

4.5.1.2.2 Gold species formed during corrosion. Gold has two cationic forms, Au(I) and Au(III). The literature presented in section 4.2.1.2 states that gold probably dissolves as the Au(III) complex, $AuCl_4^-$, when potentials greater than approximately +1.0 V vs. SCE are applied to gold in chloride containing solutions. Frankenthal & Siconolfi believe that the ion formed depends on the magnitude of the applied potential and "established that gold dissolves as Au(I) at potentials below +0.8 V and as Au(III) at potentials above +1.1 V." The data obtained from TRL prototype 021397-1#6 can be used to determine whether the conclusions from the literature hold for gold thin films at +1.04 V.

The current vs. time data presented in figure 4-16 in section 4.4.2.2.2 can be broken into two different parts. The first part of the plot consists of the current peak occurring between 0 and 3.5 seconds. The peak corresponds to the corrosion of the 40 μm by 40 μm exposed (i.e. not covered by SiO_2) area of gold directly over the reservoir. Corrosion starts quickly and occurs primarily in the grain boundaries, as is shown in figure 4-17. The current begins to drop at the

point where portions of the film are electrically isolated from the electric potential source due to grain boundaries corroding to the substrate surface, or the potential at the center of the exposed gold film has fallen below the corrosion potential due to increases in the resistance across a thinning membrane (see section 6.4.1.1). The second part of the plot consists of the nearly constant current observed between approximately 5 and 42 seconds. This current of 0.1-0.2 μA results from the corrosion of the gold thin film under the SiO_2 overlayer after electrical isolation of the exposed gold explained above. The magnitude of the current is low because the approximate gold surface area exposed to the electrolyte under the SiO_2 (8.0×10^{-8} cm^2) is much smaller than the exposed gold surface area not covered by SiO_2 that is present at the beginning of the experiment (1.6×10^{-5} cm^2). The exposed gold surface area under the SiO_2 slowly increases as the corrosion front progresses, which would cause the resulting current to increase over time. However, the diffusion path for chloride ions to the gold surface and gold chloride ions away from the gold surface increases over time, keeping the resulting current nearly constant for the duration of the experiment. A discussion of why less gold is corroded when exposed than when under the SiO_2 can be found in section 4.5.2.2.

An estimate of the amount of gold corroded can be obtained using the area under the current vs. time plot and equation 4.6, where m = mass of gold corroded in grams, i = current in amps, t = time in seconds, mw = 196.97 g/mol, F = Faraday's constant, and n = number of equivalents per mole. It was assumed that the area under the first part of the plot (t = 0 to 3.62 seconds) represented corrosion of exposed, 40 μm by 40 μm gold surface only. It was also assumed that second part of the plot (t = 3.62 to 41.76 seconds) represented only the corrosion that occurred under the SiO_2 layer. These assumptions are reasonable given the observation that the current drop coincides with the electrical isolation and cessation of corrosion of the gold not covered by SiO_2. A 100% current efficiency was also assumed. This requires that all charge passed in this experiment was a result of gold dissolution and not side reactions, such as gas evolution.

$$m = \frac{i \cdot t \cdot mw}{n \cdot F} \tag{4.6}$$

The value of n in equation 4.6 is 1 for formation of Au(I) and 3 for formation of Au(III). The mass of gold corroded obtained using equation 4.6 and n=1 and n=3 for the two parts of the current vs. time plot are listed in table 4-6. The table also includes estimations of the mass of gold present in each area using dimensions obtained from the SEM micrograph given in figure 4-17a and the known gold film thickness of 0.2 μm. The estimate of gold corroded as Au(III) for the 40 μm by 40 μm gold surface is approximately half of the amount of gold present. This result could be interpreted as indicating that membrane failure would take place after approximately 50% of the gold is corroded when intergranular corrosion predominates and no mechanical stresses cause the membrane to break before it has corroded through its thickness. This is a reasonable result when the supported gold film of figure 4-17 is examined. The estimate of gold corroded as Au(III) for the gold under the SiO_2 is within 18% of the amount of gold present. This is good agreement considering that the area of corroded gold under the SiO_2 could only be roughly approximated from figure 4-17. Notice that both estimates assuming Au(I) formation are much higher (100-200%) than the amount of gold present. This is not physically possible. Therefore, the experimental data obtained with gold thin films is consistent with gold dissolving primarily as Au(III) ions.

Table 4-6. Calculation of mass of gold corroded as either Au(I) or Au(III) for TRL prototype 021397-1#6 and comparison with SEM observations.

	40 μm by 40 μm area of exposed gold (t = 0 to 3.62 sec)	Gold present under the SiO_2 overlayer (t = 3.62 to 41.76 sec)
Mass corroded as Au(I)	9.79 ng	9.63 ng
Mass corroded as Au(III)	3.26 ng	3.21 ng
Mass present (by SEM)	6.2 ng	3.9 ng

4.5.1.2.3 Order of reaction. The rate of gold corrosion is affected by changes in chloride concentration. The magnitude of the corrosion rate change with chloride concentration is represented by the reaction order, which is the exponent of chloride ion concentration in the gold corrosion rate equation. Gallego *et al* and Lovrecek *et al* both claim that the gold corrosion reaction has a first order dependence on chloride for concentration ranges of 0.005 to 1.0 M and 0.01 to 0.1 M, respectively. Frankenthal & Siconolfi found that the reaction was second order

(actually, 1.9) for chloride concentrations from 0.1 to 5.4 M, which they state was in good agreement with the value of 1.88 published in the literature by other researchers[18]. The thin film, current density data obtained with TRL prototype 081897 at +1.04 volts for chloride concentrations from 0.04 to 1.0 M can be used to estimate the reaction order for gold corrosion. A steady state corrosion current density cannot be achieved in gold thin films due to their small thickness. The current density increases rapidly after the application of the electric potential as the gold film corrodes and become thinner. The current density begins to drop as the gold film is corroded to the substrate surface, isolating uncorroded sections of gold and preventing further corrosion. However, a reaction order can be calculated if it is assumed that the peak current density obtained for a gold thin film at a given chloride concentration approximates the steady state gold corrosion current density that would be obtained if the gold film were much thicker, like bulk gold samples. The current density data from TRL prototype 081897 at varying chloride concentrations are plotted in figure 4-27 making this assumption. The slope of line for the average peak current densities for chloride concentrations ranging from 0.04 to 1.0 M is 1.0653, which agrees more closely with the first order dependence proposed by Gallego *et al* and Lovrecek *et al* determined using bulk gold samples. The error bars in figure 4-27 are due to uncertainties in the surface areas of the gold thin film anodes, as discussed in section 4.4.2.2.3.

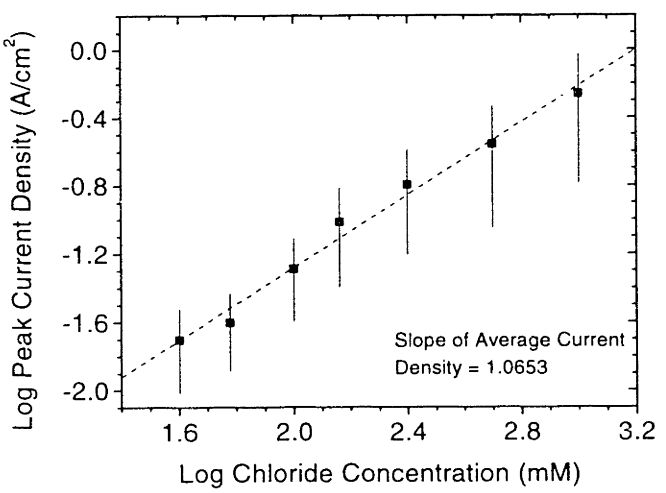

Figure 4-27. Average peak current density vs. chloride concentration for gold thin films.

An issue that should be addressed when comparing reaction order estimates from the literature and from the gold thin film experiments is the species formed during corrosion. First, Frankenthal & Siconolfi's estimate of a chloride reaction order of 2 was determined at a lower applied potential (+0.80 V) than the literature or gold thin film experiments reporting a reaction order of 1 (≥ +1.0 V). Frankenthal & Siconolfi state that at potentials lower than +0.80 V, gold dissolves primarily as Au(I) ions. Gallego *et al*, Lovrecek *et al*, and the gold thin film experiments presented in section 4.4.2.2.3 predict that gold dissolves as Au(III) ions at potentials greater than +1.0 V vs. SCE. Even Frankenthal & Siconolfi report that gold dissolves as Au(III) above +1.1 V. Frankenthal & Siconolfi further assume that the reaction order of 2 holds at potentials higher than +0.80 V. This may not be a good assumption because it is possible that the reaction order calculated where primarily Au(I) is formed may be different from the reaction order under conditions where primarily Au(III) is formed.

4.5.2 Observations of thin film gold corrosion.

4.5.2.1 Controls. The purpose of the control experiments was to examine whether gold thin films would be corroded or affected in any way by a chloride containing solution, in this case PBS, with no applied electric potential. This is important to determine because some applications may require that a controlled release microchip be submerged in solution for a long period of time before chemical release is desired. The only difference between the as deposited gold film and the PBS film revealed by high resolution scanning electron microscopy was a slight difference in average grain size. The average grain size for the as deposited sample was estimated from figure 4-13g to be approximately 50-75 nm. The average grain size for the PBS sample was estimated from figure 4-13h to be approximately 100 nm. It is thermodynamically and kinetically impossible for gold to corrode in saline solution without an applied potential, especially at near neutral pH (7.2). Therefore, it is unlikely that the grain size difference was caused by the PBS. Instead, it is postulated that the slight difference in average grain size results from thickness variations in the gold film. The gold film was deposited on the silicon wafer in an electron beam evaporator on a stationary flat plate (not a rotating planetary). It is possible that the gold film thickness varied slightly across the surface of the wafer. The 0.3 μm gold film is

only one grain thick, so slight variations in film thickness can cause the grain diameter to vary. A few additional experimental observations are explained in more detail below.

The control films had a different grain structure than the gold membranes of most finished prototype devices. The grains of the control films were approximately 0.03-0.10 μm in diameter and were relatively circular or oval in shape. Most prototype membranes had a wider distribution of grain sizes (approximately 0.2-2.0 μm) and were irregular in shape. This can be attributed to two factors. First, the control films were deposited at a much worse vacuum (5.0 x 10^{-6} torr vs. 5.0 x 10^{-7} torr for typical TRL prototypes), which can result in smaller grain sizes. Second, the control films did not go through any further processing that may have favored grain growth. For example, PECVD deposition of SiO_2 at 350°C for 1-3 hours may result in gold grain growth in the TRL prototype devices due to elevated temperatures.

4.5.2.2 Morphology of corroded gold thin films. It was discussed in section 4.5.1.2 that data obtained for thin gold films seem to agree well with experimental observations and reaction mechanisms proposed for bulk gold corrosion in chloride solutions. However, little data exist in the literature about the physical appearance of gold surfaces after corrosion. One paper shows oxidation rings on a piece of anodically polarized gold foil[16], while another shows how oxidation of gold traces in integrated circuits can cause device failure by spalling, increased conductor resistance, or short-circuiting due to spreading of conductive oxidation products between adjacent traces[2]. Another paper discusses how gold corroded in chloride solution can redeposit at adjacent conductors, causing conductive bridges to form and short-circuiting to occur[17]. However, no work, to the best of my knowledge, has been published detailing the morphology of gold thin films corroded in chloride containing solutions.

The most striking feature of gold thin film corrosion in chloride containing solutions is its preference toward intergranular corrosion. The intergranular nature of gold thin film corrosion is quite obvious when examining SEM micrographs of uncorroded and corroded gold (figures 4-28a and 4-28b, respectively) from TRL prototype 021397-1#6. Due to differences in surface contrast in the SEM, the grain boundaries of an uncorroded gold film appear light colored in figure 4-28a. Gold grains are clearly delineated in figure 4-28b by the preferential corrosion that occurred in the grain boundaries. The grain boundaries corrode quickly, causing the grains to

become isolated from the applied electric potential before they have had a chance to corrode significantly. The isolation of grains is seen most clearly when the corroded film is examined on an angle, as it is in figure 4-29. It is also clear in figure 4-29 that the edges of the grains are rounded and smooth. No faceting of the grain surface is observed in this thin film, but that does not rule out the possibility that stress corrosion cracking (SCC) may play a role in the opening of chemical reservoirs. The *in situ* experiments presented in chapter 6 utilize unsupported membranes, rather than supported thin films, and may contain fracture surfaces after reservoir opening. These experiments might provide additional data for the discussion of SCC.

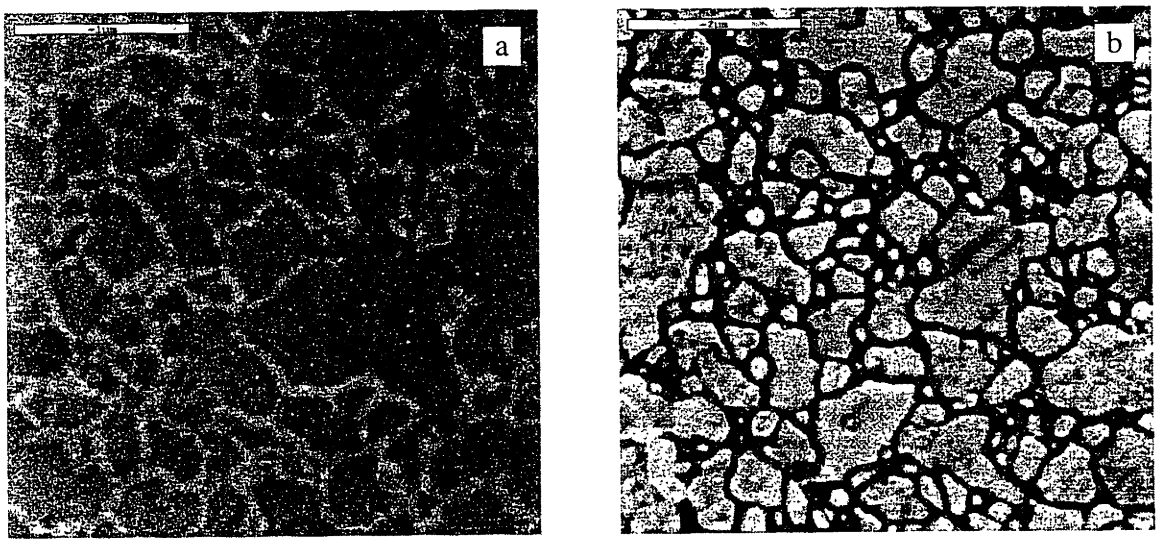

Figure 4-28. Scanning electron micrographs for TRL prototype 021397-1#6, (a) un-corroded gold thin film and (b) corroded gold thin film. Note that (a) is at 2x the magnification of (b).

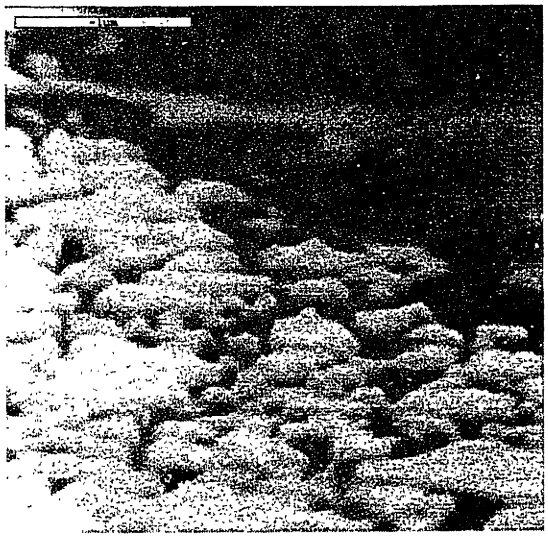

Figure 4-29. Scanning electron micrograph of TRL prototype 021397-1#6 showing the smooth texture of gold grains that stopped corroding due to electrical isolation caused by grain boundary corrosion.

The study of intergranular corrosion was the purpose of the corrosion experiments conducted with prototype 081897 in which gold films were corroded for varying amounts of time. The progression of the corrosion in the grain boundaries with time can be seen in figure 4-20. However, viewing the partially corroded gold thin films from an angle (figure 4-30) gives an even better perspective. The extent of grain boundary grooving and the exposed gold surface area increases steadily with time.

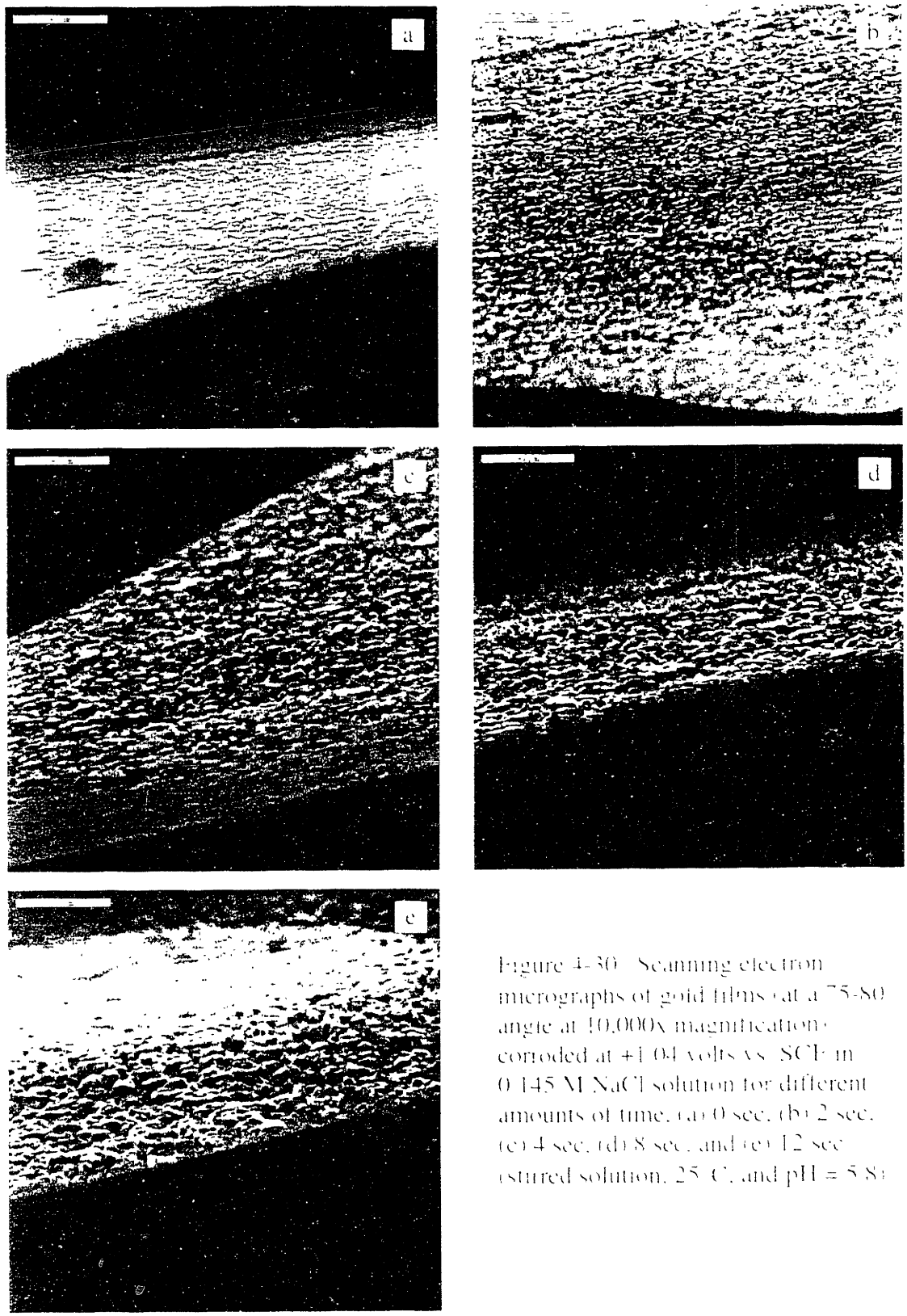

Figure 4-30. Scanning electron micrographs of gold films (at a 75-80 angle at 10,000x magnification) corroded at +1.04 volts vs. SCE in 0.145 M NaCl solution for different amounts of time, (a) 0 sec, (b) 2 sec, (c) 4 sec, (d) 8 sec, and (e) 12 sec (stirred solution, 25 °C, and pH = 5.8).

There is also a significant difference in the morphology of gold thin films corroded with one surface exposed or no surfaces exposed (except the cross-sectional surface). Notice in figure 4-31 for TRL prototype 021397-1#6 that corrosion occurred under the SiO_2 overlayer, resulting in nearly complete removal of the gold, while corrosion of gold with one exposed surface resulted in the removal of only a fraction of the gold. Corrosion from the top surface of the thin film requires only 0.2 μm of grain boundary to corrode for film perforation and electrical isolation of individual gold grains. Corrosion from the cross section of the film requires 1.6 to 6.2 μm of grain boundary (approximation based on average 0.5-2.0 μm diameter grains) to corrode for electrical isolation of individual gold grains. This concept is shown graphically in figure 4-32. The grain boundary corrosion path length increases by an order of magnitude when corrosion occurs in the cross sectional direction under the SiO_2. This increases the time required for electrical isolation of gold grains, allowing the grains themselves to corrode completely. It is predicted that gold thin films with smaller grains would corrode more completely if the above explanation holds true.

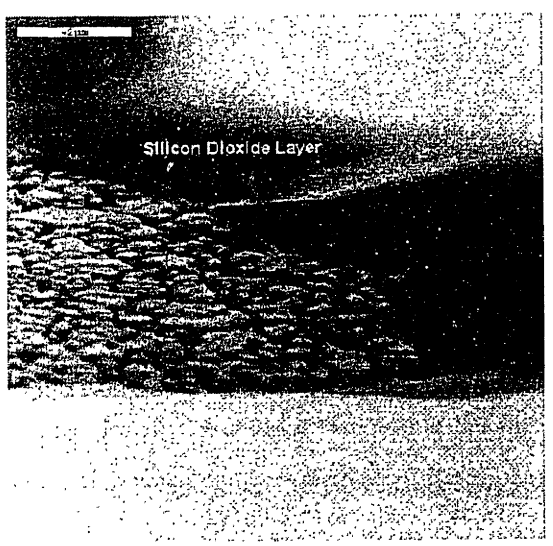

Figure 4-31. Scanning electron micrograph of TRL prototype 021397-1#6 showing the difference in corrosion between the exposed gold surface and the gold under the SiO_2 layer.

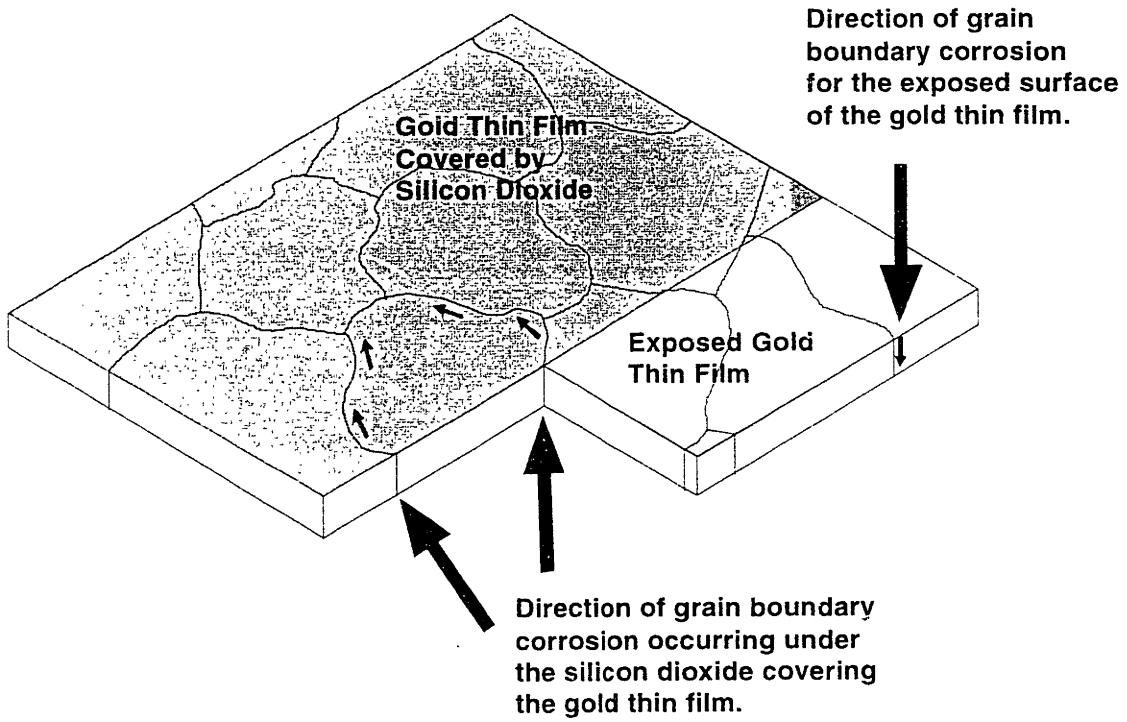

Figure 4-32. Diagram showing the direction of grain boundary corrosion for exposed and covered gold thin films.

4.5.2.3 Membranes. Much of the work presented in this chapter was carried out with gold foil or supported gold thin films. The gold foil experiments were used to verify some of the trends presented in the literature, while the gold thin film experiments were used to help understand the mechanism of gold thin film corrosion in chloride containing solutions. Prototype controlled release microchips release a chemical from a reservoir by the corrosion of an unsupported gold membrane. The experiments conducted with foil and thin films provide a basis for predicting the mechanism of gold membrane corrosion and reservoir opening, known in chapter 6 as gold membrane disintegration. The experimental results presented in section 4.4.2.3, and especially figure 4-23, demonstrate proof-of-principle for using the corrosion of gold membranes as a chemical release mechanism. Chapter 5 moves on to apply the concept of gold membrane disintegration to releasing chemicals from prototype microchips, while chapter 6 studies the mechanism of gold membrane disintegration.

4.5.3 Gold biocompatibility. The controlled release microchip concept is not limited to using any specific substrate or membrane material. Gold was selected as a model membrane material for proving the concept of a controlled release microchip primarily due to its favorable electrochemical properties. These include its low reactivity with other substances, its resistance to spontaneous corrosion in most aqueous solutions over the entire pH range, and its ability to quickly dissolve with a small applied potential in the presence of chloride ions. However, gold is also a relatively biocompatible material and may be useful in controlled release microchips for biological applications, such as implantable or oral drug delivery devices.

Gold's biocompatibility and toxicity is highly dependent upon its form[19,20]. Gold can exist as a metallic element, Au(0), or in its cationic forms, Au(I) and Au(III). Au(0) has been used extensively in jewelry and medical prostheses. The use of gold and gold alloys as dental materials is widespread, but they have also been used in other medical devices such as eyelid implants for individuals that lack the ability to voluntarily close an eyelid. Au(0) is considered to be a biologically inert material. However, some individuals may develop non-allergic skin conditions or allergic contact dermatitis (ACD) from prolonged contact with gold or gold alloys. Other metals such as nickel, mercury, or copper that are present in gold alloys or as contaminants are believed to be the cause of a large percentage of the reported cases of adverse reactions to gold[19].

Au(I) salts such as gold thiomaleate, gold thioglucose, and gold thiosulfate have found extensive use in the treatment of rheumatoid arthritis. The use of such salts in medical treatment is referred to as chrysotherapy. Many of the adverse reactions to chrysotherapy consist of non-allergic skin reactions, with a smaller percentage of patients developing a form of ACD[19] or delayed-type hypersensitivity[20]. Side effects from Au(I) salts are rarely seen in individuals that have received cumulative doses less than 250 mg, and some patients can receive well over 1000 mg without any problems. It is interesting to note that Au(I) complexes can be formed from Au(0) in cells and lysosomes by certain thiol-containing molecules at biological conditions (pH=7.2). These reactions occur very slowly, so it is unlikely that the gold membranes of a controlled release microchip would be affected by such processes. However, this reaction pathway should be investigated if microchips with gold membranes are used in biological applications for long periods of time.

Small amounts of Au(III) can be introduced into the body indirectly by the enzymatic conversion of Au(I) to Au(III) in phagolysosomes. For example, it was postulated by Shaw *et al*[21] that gold thiomaleate can be converted in phagolysosomes to gold (III) chloride ($AuCl_3$), which is a highly oxidizing molecule. They conducted *in vitro* experiments that suggested that the rate of formation of $AuCl_3$ is faster than its rate of reduction back to Au(I). This allows the $AuCl_3$ to diffuse away from the site of generation and react with methionine or cysteine residues in proteins, causing them to denature irreversibly. Interestingly, it is the denaturation of inflammation-enhancing lysosomal proteins or the disruption of the presentation of arthritogenic (self) proteins to T cells that is proposed to result in the therapeutic effect of reducing inflammation in rheumatoid arthritis[19,20]. The denaturation of self proteins may also result in auto-immunity, but this is a rare occurrence[22,23].

As a point of reference, approximately 3 to 9 ng of gold (primarily as Au(0) and Au(III)) are released with the opening of each chemical reservoir when covered by a 0.2-0.3 μm thick gold membrane. This is much smaller than the 250 mg cumulative dose usually required to see side effects when Au(I) drugs are given to rheumatoid arthritis patients. Therefore, it is uncertain whether the tiny amount of gold released by the microchip will cause any side effects or immune reactions in biological systems. The presence of side effects will most likely depend on the microchip's application, the form and total amount of gold released, the location of release in the body, and the potential for gold accumulation in particular tissues. The literature shows that gold is a relatively biocompatible material that has numerous biological applications, including its use in implants, drugs, and as a DNA delivery vehicle[19]. However, predictions about the biocompatibility of any material are difficult to make, so *in vivo* testing will be necessary to determine the suitability of gold for use in controlled release microchips designed for biological applications.

4.6 Conclusions. Gold is able to resist corrosion in solutions of nearly any pH, even those containing chloride ions, in the absence of an applied electric potential. The gold membrane covering a reservoir serves as an impermeable barrier to water and the chemical in the reservoir and remains intact until an electric potential in a specific range is applied to it. Gold is biocompatible, depending on the amount and form of the gold in contact or released into the

body. The experiments presented in this chapter agreed well with the literature and demonstrated that the application of an electric potential near +1.0 volt relative to a saturated calomel reference electrode causes gold membranes to corrode, opening chemical reservoirs in a matter of seconds. Gold's resistance to spontaneous corrosion, its impermeability to water, its biocompatibility, and its ability to quickly corrode on demand with an applied potential made it the best choice for a model membrane material for the proof-of-principle, chemical release experiments presented in chapter 5.

4.7 References.

1. Frankenthal, R.P. & Siconolfi, D.J. "The anodic corrosion of gold in concentrated chloride solutions." *Journal of the Electrochemical Society* **129**, 1192-1196 (1982).
2. Frankenthal, R.P & Becker, W.H. "Corrosion failure mechanisms for gold metallizations in electronic circuits." *Journal of the Electrochemical Society* **126**, 1718-1719 (1979).
3. Santini, J.T., Jr., Cima, M.J. & Langer, R. "A controlled-release microchip." *Nature* **397**, 335-338 (1999).
4. Gaur, J.N. & Schmid, G.M. "Electrochemical behavior of gold in acidic chloride solutions." *Electroanalytical Chemistry and Interfacial Electrochemistry* **24**, 279-286 (1970).
5. Gallego, J.H., Castellano, C.E., Calandra, A.J. & Arvia, A.J. "The electrochemistry of gold in acid aqueous solutions containing chloride ions." *J. Electroanal. Chem.* **66**, 207-230 (1975).
6. Lovrecek, B., Moslavac, K. & Matic, D.J. "Anodic dissolution and passivation of gold, particularly in presence of chloride." *Electrochimica Acta* **26**, 1087-1098 (1981).
7. Jones, D.A. *Principles and Prevention of Corrosion* 116-142 (Prentice Hall, Upper Saddle River, NJ, 1996).
8. Jones, D.A. *Principals and Prevention of Corrosion* 235-244 (Prentice Hall, Upper Saddle River, NJ, 1996).
9. Rapson, W.S. "Tarnish resistance, corrosion and stress corrosion cracking of gold alloys." *Gold Bulletin* **29**, 61-69 (1996).
10. Flanagan, W.F., Lee, J.B., Massinon, D., Zhu, M. & Lichter, B.D. "Role of selective dissolution in transgranular stress-corrosion cracking: studies of transient and steady-state dealloying in copper-gold alloys." *ASTM Spec. Tech. Publ. #1049* , 86-99 (1990).
11. Chen, J.S., Salmeron, M. & Devine, T.M. "Intergranular vs. transgranular stress corrosion cracking of Cu 30-Au." *Scripta Metallurgica* **26**, 739-742 (1992).
12. Dugmore, J.M.M. & DesForges, C.D. "Stress corrosion in gold alloys." *Gold Bulletin* **12**, 140-144 (1979).
13. Friedersdorf, F. & Sieradzki, K. "Film-induced brittle intergranular cracking of silver-gold alloys." *Corrosion* **52**, 331-336 (1996).
14. Duffo, G.S. & Galvele, J.R. "Stress corrosion cracking of Ag-20Au in $HClO_4$, $AgClO_4$, and KCl solutions by surface mobility." *Metallurgical Transactions A* **24A**, 425-433 (1993).

15. Galvele, J.R., Maier, I.A. & Fernandez, S.A. "Stress corrosion cracking of silver-gold alloys in 1 M potassium chloride, potassium bromide, and potassium iodide solutions." *Corrosion* **52**, 326-330 (1996).
16. Robinson, F.P.A. & Frost, F.A. "Anodic polarization characteristics of gold and silver in chloride and sulfate media." *Corrosion* **19**, 115t-119t (1963).
17. Frankenthal, R.P. "Electrolytic corrosion of gold, application to metallizations in electronic circuits" in *Equilibrium diagrams, localized corrosion* (eds. Frankenthal, R.P. & Kruger, J.) 284-293 (The Electrochemical Society, Pennington, New Jersey, 1984).
18. Heumann, T. & Panesar, H.S. "Beitrag zur frage nach dem auflosungsmechanismus von gold zu chlorkomplexen und nach seiner passivierung." *Z. Phys. Chem.* **229**, 84-97 (1965).
19. Merchant, B. "Gold, the noble metal and the paradoxes of its toxicology." *Biologicals* **26**, 49-59 (1998).
20. Best, S.L. & Sadler, P.J. "Gold drugs: mechanism of action and toxicity." *Gold Bulletin* **29**, 87-93 (1996).
21. Shaw, G.F., III, *et al.* "Redox chemistry and $[Au(CN)_2^-]$ in the formation of gold metabolites" in *Metal Based Drugs* (ed. Shaw, F., III) 351-362 (Freund Publishing House Ltd., London, England, 1994).
22. Druet, P.H. "Metal-induced auto-immunity." *Human Exper. Toxicol.* **14**, 120-121 (1995).
23. Bigazzi, P.E. "Auto-immunity and heavy metals." *Lupus* **3**, 449-453 (1994).

5. CHEMICAL RELEASE

5.1 Introduction.

One of the main goals of this research project was to design chemical release experiments that would provide support for claim that it was possible to make a microchip capable of storing and releasing multiple chemical substances on demand. This chapter presents the methods and results of these proof-of-principle release experiments.

5.2 Experimental methods.

5.2.1 Selection of model chemicals for release. There were two primary criteria in selecting chemicals to be used in release studies with the prototype microchips. The first criterion was the minimum chemical concentration that could be reliably detected (i.e. detection limit). We wanted to be able to detect concentrations as low as 1.0 nM. The second criterion was the ease of using a particular detection method. We preferred to use a method that would allow us to analyze our release samples with minimal sample preparation. This makes the release studies easier to conduct and reduces the opportunities for introduction of error into the experiment caused by complicated sample preparation. The two chemicals selected for proof-of-principle release studies were a fluorescent dye, sodium fluorescein, and a radioactive isotope of calcium, ^{45}Ca. The selection criteria for the model electrolytes for the corrosion and chemical release studies was presented in section 4.3.1.

5.2.1.1 Sodium fluorescein. Sodium fluorescein is the water soluble salt of a yellow fluorone dye (hydroxylated xanthene)[1]. Sodium fluorescein (Sigma #F6377) was selected as a model chemical for release from the microchip prototypes because of it high solubility in water (40 mg/mL) and its intense green fluorescence when exposed to visible light at a wavelength of 491 nm. A fluorescence spectrometer (Photon Technology International Model QM-1 Luminescence Spectrometer) was used to detect the light emitted from fluorescein solutions at a wavelength of 512-513 nm. A plot of fluorescein concentration vs. fluorescence emission intensity gives a

linear plot whose slope can be used to determine the fluorescein content of samples of unknown fluorescein content. An example of such a plot is given in figure 5-1.

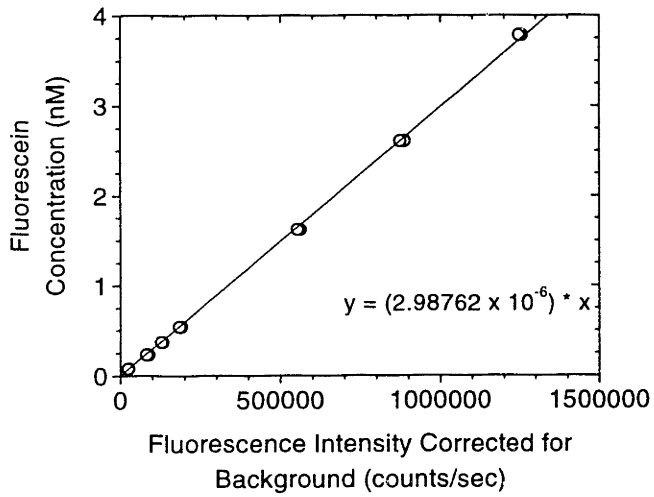

Figure 5-1. Plot of fluorescein concentration vs. fluorescence intensity.

The lower detection limit for sodium fluorescein using the fluorescence spectrometer in our lab ranged from 0.05 nM to 0.3 nM, depending on the age of the mercury lamp (i.e. excitation light source) and the background noise signal. The upper detection limit ranged from approximately 4 nM to 25 nM, depending on the slit-width settings selected for the excitation and emission monochromators. Fluorescein solutions with concentrations above the upper detection limit had to be diluted with fresh solution to bring the fluorescein concentration into the detectable range. The fluorescein concentrations of samples from release experiments were set to zero if the measured fluorescence was below the detection limit of the fluorescence spectrometer.

Fluorescein solutions can lose some of their fluorescence with time when exposed to light and/or dissolved oxygen[2]. This process is called photobleaching. The release medium, release samples, calibration samples, and stock solutions were protected from light exposure whenever possible to help minimize photobleaching. The effect of photobleaching on the results of chemical release studies is discussed in section 5.4.2.2 of this chapter.

5.2.1.2 Radioactive calcium. ^{45}Ca is a radioactive isotope of calcium. It was used in the chemical release experiments of TRL prototype 081297-1#11 in the form of a water soluble salt, $CaCl_2$ (NEN Life Science Products, #NEZ 013). ^{45}Ca was selected as a model chemical for release because it does not interact with fluorescein, it can be detected in very low quantities using a scintillation counter (Packard Tricarb 2700 TR), it has a half-life (~163 days) that is long compared to the length of a chemical release experiment, and it is a low energy beta radiation emitter (max. energy ~257 keV), which makes it safer to work with than gamma ray emitting materials such as ^{51}Cr or ^{125}I.

The method of scintillation counting is used to determine the (radio)activity present in a release sample. An aqueous sample is tested for activity by placing it in a small plastic vial containing a scintillation fluid (Packard Optifluor, Lot #47-7061, expires Dec. 1999). Scintillation fluid consists of a mixture of chemicals that fluoresce when excited by beta particles. A scintillation counter uses sensitive detectors (photomultiplier tubes) to measure the number of photons emitted from the scintillation fluid and outputs the data as counts per minute (CPM). The "true" activity in a sample (disintegrations per mintue or DPM) can be calculated by dividing the CPM by a counting efficiency specific to each isotope. The counting efficiency for ^{45}Ca is approximately 0.95, so DPM and CPM are nearly the same. DPM data can be converted to activity in nanocuries (nCi) by the conversion factor - 2,220 DPM/nCi. The activity of any ^{45}Ca sample can be calibrated to a specific date using the radioactive decay formula given as equation 5.1. This calibration is necessary to directly compare the activity of ^{45}Ca recovered from a reservoir to the activity loaded into that reservoir at an earlier date.

$$C = C_0 e^{-\lambda t} \tag{5.1}$$

where $\lambda = \frac{\ln 2}{t_0}$, C = current activity, C_0 = original activity, t = the time elapsed between C and C_0, and t_0 = the half-life of the radioactive material.

The lower detection limit for radioactivity by scintillation counting is usually accepted as 4.66 x sqrt(background counts)/(count time)/(counting efficiency). This definition gives an approximate detection limit of 0.01 nCi for ^{45}Ca. The upper detection limit is a few microcuries. ^{45}Ca solutions with concentrations above the upper detection limit have to be diluted with fresh solution to bring the ^{45}Ca activity into the detectable range. The activity of samples from release experiments were included in release calculations even if they weren't quite above the minimum detectable activity. The accuracy of these low activity values is questionable, but they are so close to background that they do not significantly affect the results.

5.2.2 Single chemical release.

5.2.2.1 Microlab prototype 091096-4. The six reservoirs of device 091096-4 were checked with a light microscope for defects as described in section 3.2.2. Reservoirs 1,3,4, and 6 were determined to be defect-free and were filled with a 90.8 mM solution of sodium fluorescein in de-ionized (DI) water using the inkjet printing method described in section 3.2.2.1. Table 5-1 lists the number of drops of solution deposited into each reservoir using inkjet printing at a frequency of 10 Hz.

Table 5-1. The number of drops of a 90.8 mM solution of fluorescein deposited into the reservoirs of Microlab Prototype 091096-4 by inkjet printing.

Reservoir #	Approx. # of Drops
1	810
3	410
4	510
6	820

The reservoirs looked completely filled with liquid immediately after filling when viewed under a light microscope. However, the water started to quickly evaporate, leaving the reservoir only partly filled. The reservoirs were quickly sealed while liquid was still present in the reservoirs. Glass coverslips were used to seal the reservoirs as described as the first method in

section 3.2.3. The Microlab prototype was then packaged as described in section 3.2.4.1 and shown in figure 3-5.

The amount of fluorescein deposited in each reservoir by inkjet printing was experimentally determined in the following way. Fluorescein calibration standards having concentrations from 1.82 nM to 20.28 nM were prepared in phosphate buffered saline (PBS - Sigma #P5886) two days after reservoir filling by serial dilution of the 90.8 mM fluorescein stock solution. The standards were analyzed for fluorescence emission intensity at a wavelength of 512 nm in a fluorimeter (Photon Technology International Model QM-1 Luminescence Spectrometer) using an excitation wavelength of 491 nm. Inkjet printed standards were made by printing 1 to 5 drops of the fluorescein stock solution used to fill the reservoirs into 3.0 mL of PBS in clear, polystyrene fluorimeter cuvettes. The cuvettes were analyzed in the fluorimeter, and their fluorescein content was determined using the fluorescein calibration standards. The mass of fluorescein per drop was determined to range from 5.9 ng to 6.7 ng.

The gold membranes covering the four filled reservoirs were examined with a light microscope for a few days while the waterproof epoxy was curing to make sure all four membranes were still intact. The membrane of reservoir 1 appeared to be pulled into the device and looked like it was about to tear. Waterproof epoxy was placed over this reservoir to ensure that this reservoir would not tear and leak fluorescein into the release medium when the release study was begun.

Electrical connection between the packaged prototype and the potentiostat/galvanostat (EG&G Model 273) used to apply the electric potential to the device was accomplished through plastic coated wires containing seven conductors that were epoxied to the glass slide containing the prototype. The prototype was placed in 35.0 mL of PBS (release medium) in a glass beaker at room temperature until the water level covered the bottom half of the device (i.e. did not cover the silver paste wire connections). The release medium (PBS) was gently stirred with a magnetic stirring bar throughout the experiment. 1.0 mL samples of the PBS release medium were taken at times before and after the activation of each reservoir. The samples were diluted to a total volume of 3.0 mL by the addition of 2.0 mL of fresh PBS before being analyzed in the fluorimeter. The 1.0 mL taken from the release medium for analysis was replaced immediately with 1.0 mL of fresh PBS to keep the release medium volume constant at 35.0 mL throughout the

experiment. The SCE reference electrode was always placed in the release medium with its tip positioned 1-3 mm from the surface of the anode just before the application of the potential. The setup for the release experiment is shown in figure 5-2. The SCE was removed immediately after the potential was turned off. Note that placing the reference electrode directly in the release medium should not affect the gold membrane corrosion process, as was discussed in section 4.3.2.

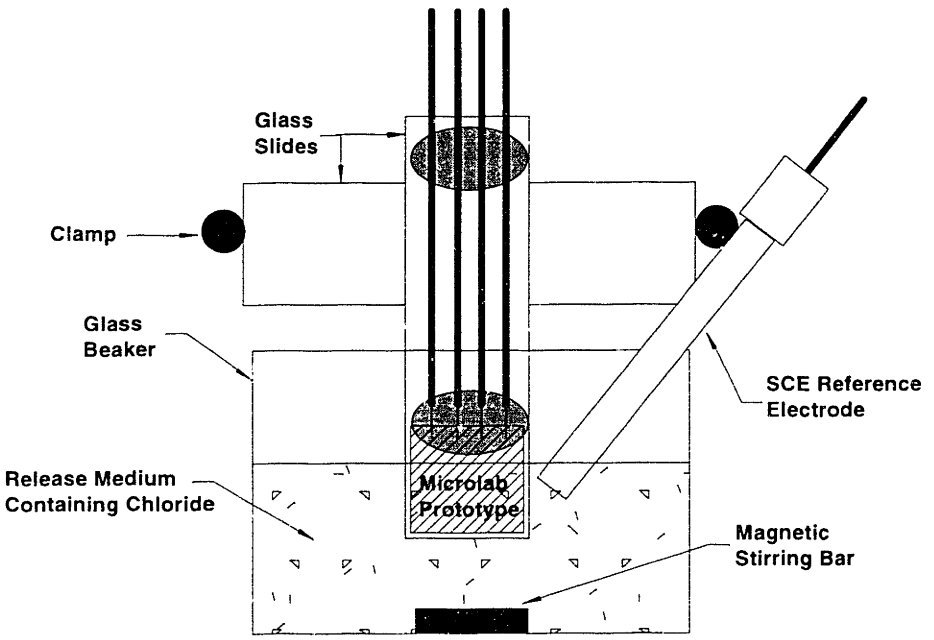

Figure 5-2. Release apparatus and set up for Microlab prototypes.

The Microlab prototype was inserted and allowed to stay in PBS for 17.55 hours. The prototype was then removed from the release medium, rinsed with DI water, gently dried with nitrogen, and the release medium was replaced with fresh PBS. The prototype was inserted into the fresh PBS for 35 minutes before an electric potential of +1.04 volts relative to (vs.) a saturated calomel reference electrode (SCE) was applied to the gold membrane anode of reservoir 6 for 75 seconds. The prototype was removed from the release medium, rinsed with DI water, gently dried with nitrogen, and the release medium was replaced with fresh PBS after 3.25 hours of fluorescein release. The prototype was inserted into the fresh PBS for 17.45 hours before +1.04 V vs. SCE was again applied to reservoir 6 for 5 minutes to make sure that it had

fully opened after the first application of electric potential. The prototype was again removed from the release medium, rinsed with DI water, gently dried with nitrogen, and the release medium was replaced with fresh PBS, 6 hours after the second application of an electric potential to reservoir 6. Reservoir 6 was sealed with epoxy to keep any residual fluorescein from leaking out during the release of reservoirs 3 and 4. The prototype was inserted into the PBS for 1.47 hours before +1.04 V vs. SCE was applied to reservoir 4 for 5 minutes. The prototype was removed from the release medium 24.87 hours later, rinsed with DI water, gently dried with nitrogen, and the release medium was replaced with fresh PBS. The prototype was inserted and allowed to stay in the fresh PBS for 95.8 hours. The prototype was then removed from the release medium, rinsed with DI water, gently dried with nitrogen, and the release medium was replaced with fresh PBS. The prototype was inserted into the PBS, and +1.04 V vs. SCE was applied four times to reservoir 3 for 5 minutes each at 40, 52, 60, and 80 minutes after insertion in the PBS. The prototype was removed from the release medium 26.47 hours after the last application of electric potential, rinsed with DI water, gently dried with nitrogen, and the release medium was replaced with fresh PBS. The prototype was inserted and allowed to stay in the fresh PBS for 12.72 hours. The prototype was then removed from the release medium, rinsed with DI water, and gently dried with nitrogen.

5.2.2.2 TRL prototype 021397-2#2. The thirty-four reservoirs of TRL prototype 021397-2#2 were checked with a light microscope for defects as described in section 3.2.2. Reservoirs 1-5,9,15,19 were determined to be defect-free and were filled with a 92.2 mM solution (made approx. 10 days prior to reservoir filling) of sodium fluorescein in DI water using the inkjet printing method described in section 3.2.2.1. Table 5-2 lists the number of drops of solution deposited into each reservoir using inkjet printing at a frequency of 10 Hz.

Table 5-2. The number of drops of a 92.2 mM solution of fluorescein deposited into the reservoirs of TRL Prototype 021397-2#2 by inkjet printing.

Reservoir #	Approx. # of Drops
9	50
1-5,15,19	100

The reservoirs had a noticeable amount of liquid in them immediately after filling. However, most of the water appeared to quickly evaporate, leaving the reservoir with only a small amount of solid fluorescein in the bottom of the reservoir. 100 drops of fluorescein were deposited in each reservoir. This resulted in a total mass deposited of approximately 253-385 ng per reservoir, as determined by inkjet printed fluorescein standards. There also appeared visually to be significant disparity between the amount of solid deposited in each reservoir. Reservoirs 1 and 19 had solid completely covering the bottom of the reservoir. Reservoirs 2-5 and 15 had solid at the bottom of the reservoir, but it did not completely cover the bottom. Reservoir 9 appeared to have nearly as much solid in it as reservoirs 2-5 and 15 even though it was only filled with half as many drops. The reservoirs were sealed by the first method described in section 3.2.3 using glass coverslips. The prototype was then sealed into a PGA package as described in section 3.2.4.2 and shown in figure 3-6.

The process of experimentally determining the amount of fluorescein deposited in each reservoir by inkjet printing is the nearly the same as that described in section 5.2.2.1 for the Microlab prototype. One difference is that the fluorescein calibration standards used for the inkjet calibration were made in DI water instead of PBS. This change should not affect the results as long as both the calibration standards and the inkjet-printed standards are made in the same liquid. The fluorescein calibration standards had concentrations from 0.67 nM to 21.94 nM in DI water and were prepared the day after filling by serial dilution of a 92.2 mM fluorescein stock solution. Inkjet printed standards were prepared on the day of reservoir filling by printing 50 or 100 drops of the 92.2 mM fluorescein stock solution into 3 mL of DI water in polystyrene cuvettes. The excitation wavelength used for fluorescence measurements was 491 nm. However, the fluorescence emission intensity was measured at a wavelength of 513 nm, instead of the wavelength of 512 nm used for Microlab prototype 091096-4.

The gold membranes covering the filled reservoirs were examined with a light microscope for a few days while the waterproof epoxy was curing to make sure all membranes were still intact. Reservoirs 4,9,15, and 19 had tiny cracks in their membranes, like that shown in figure 3-8, and a small amount of fluorescein was visible. Waterproof epoxy was placed over these cracked reservoirs to insure that they would not leak fluorescein into the release medium when the release study was begun.

Electrical connection between the PGA packaged prototype and the potentiostat/galvanostat used to apply the electric potential to the device was accomplished through a custom made apparatus consisting of a PGA socket, a PC board, and plastic coated wires containing seven conductors, as shown in figure 5-3. The prototype was connected to the custom made apparatus and placed in 100 mL of PBS (release medium) in a glass beaker at room temperature until the water level covered the bottom half of the device (i.e. did not cover the gold wire bonds). The release medium (PBS) was gently stirred with a magnetic stirring bar throughout the experiment. 3 mL samples of the PBS release medium were taken at times before and after the activation of each reservoir. These 3 mL samples were analyzed in the fluorimeter without dilution. However, the samples were diluted by taking 0.3 mL of the original 3 mL sample and diluting it to a total volume of 3 mL by the addition of 2.7 mL of PBS before being analyzed in the fluorimeter when the fluorescein concentration was too large to be detected by the fluorimeter. The 3.0 mL taken from the release medium for analysis were replaced immediately with 3.0 mL of fresh PBS to keep the release medium volume constant at 100 mL throughout the experiment. The SCE reference electrode was always placed in the release medium with its tip positioned 1-3 mm from the surface of the anode just before the application of the potential. The SCE was removed immediately after the potential was turned off.

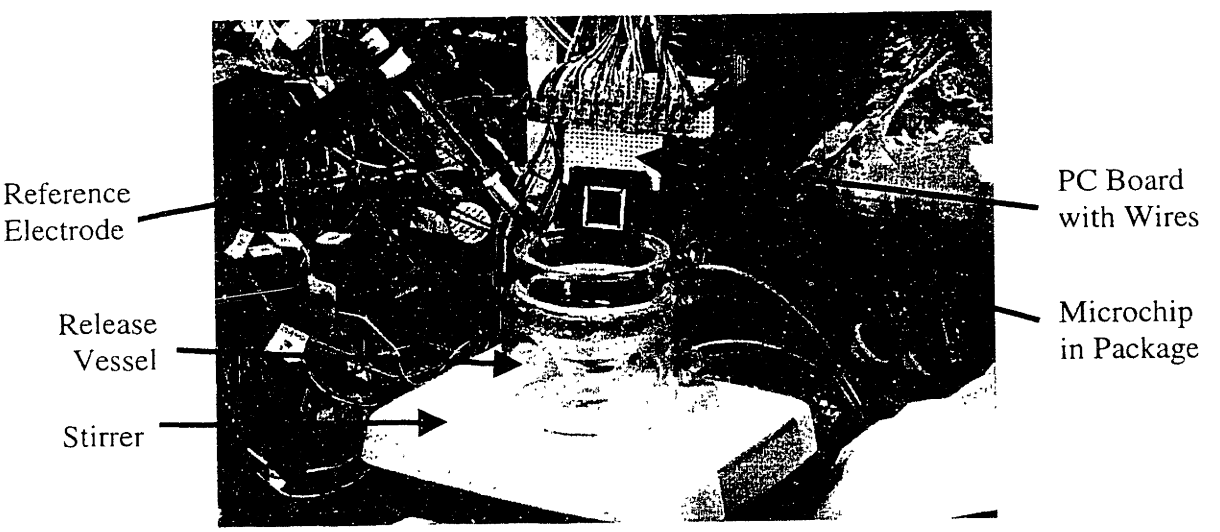

Figure 5-3. Photograph of release apparatus and set up for TRL prototypes. (Photograph by Malinda Tupper.)

An electric potential of +1.04 V vs. SCE was applied to the gold membrane anode of reservoir 5 for 32 seconds after being submerged in PBS for 24 hours. The prototype was removed from the release medium, rinsed with DI water, gently dried with nitrogen, and the release medium was replaced with fresh PBS after 3 hours of fluorescein release. The prototype was inserted into the fresh PBS for 10.83 hours before +1.04 V vs. SCE was applied to reservoir 3 for 3 minutes. The prototype was again removed from the release medium, rinsed with DI water, gently dried with nitrogen, and the release medium was replaced with fresh PBS after 3 hours of fluorescein release. The prototype was inserted into the PBS for 8.35 hours before +1.04 V vs. SCE was applied to reservoir 2 for 3 minutes. The prototype was removed from the release medium approximately 1 hour later, rinsed with DI water, and gently dried with nitrogen.

5.2.2.3 TRL prototype 081297-1#10. The thirty-four reservoirs of TRL prototype 081297-1#10 were checked with a light microscope for defects as described in section 3.2.2. Nearly all the reservoirs were determined to be defect-free and were filled with 100 drops of a 60.2 mM solution of sodium fluorescein in 75/25 v/v DI water/PEG 200 (prepared two weeks before) using the inkjet printing method described in section 3.2.2.1 at a frequency of 10 Hz.

The reservoirs had a noticeable amount of liquid in them immediately after filling. However, most of the water appeared to quickly evaporate, leaving the reservoir with only a small amount of fluorescein and PEG 200 (liquid polymer) in the bottom of the reservoir. The material in the reservoir remained in liquid form for the entire experiment because the polymer does not evaporate. No gold membranes were observed to crack or tear after reservoir filling. The total mass deposited in each reservoir was approximately 208-274 ng of fluorescein for 100 drops, as determined by inkjet printed fluorescein standards. The reservoirs were sealed by the second method described in section 3.2.3 using pieces of adhesive plastic and glass coverslips. The prototype was then sealed into a PGA package as described in section 3.2.4.2.

The process of experimentally determining the amount of fluorescein deposited in each reservoir by inkjet printing is similar to that described in section 5.2.2.1 for the Microlab prototype. The fluorescein calibration standards used for this TRL prototype had concentrations from 0.053 nM to 3.78 nM and were made in PBS on the day after reservoir filling by serial dilution of a 60.2 mM fluorescein stock solution. The concentration of the calibration standards

was much lower for this prototype than TRL prototype 021397-2#2 due to changes in the fluorimeter since the last prototype. Inkjet printed standards were prepared on the day of reservoir filling by printing 100 drops of the 60.2 mM fluorescein stock solution into 3 mL of PBS in polystyrene cuvettes. The fluorescence emission intensity was measured at a wavelength of 513 nm, using an excitation wavelength of 491 nm.

The gold membranes covering the filled reservoirs were examined with a light microscope for a few days while the waterproof epoxy was curing to make sure all membranes were still intact. No reservoirs had cracks or tears in their gold membranes, so all the filled reservoirs were viable for the release experiment.

Electrical connection between the PGA packaged prototype and the potentiostat/galvanostat using the testing apparatus described in section 5.2.2.2 and shown in figure 5-3. The prototype was connected to the apparatus and placed in 100 mL of PBS (release medium) in a glass beaker at room temperature until the water level covered the bottom half of the device (i.e. did not cover the gold wire bonds). The release medium was gently stirred with a magnetic stirring bar throughout the experiment. 3.0 mL samples of the PBS release medium were taken at times before and after the activation of each reservoir. These 3.0 mL samples were analyzed in the fluorimeter without dilution. However, the samples were diluted by taking 1.0 mL of the original 3.0 mL sample and diluting it to a total volume of 3.0 mL by the addition of 2.0 mL of PBS before being analyzed in the fluorimeter when the fluorescein concentration was too large to be detected by the fluorimeter. The 3.0 mL taken from the release medium for analysis were replaced immediately with 3.0 mL of fresh PBS to keep the release medium volume constant at 100 mL throughout the experiment. The SCE reference electrode was always placed in the release medium with its tip positioned 1-3 mm from the surface of the anode just before the application of the potential. The SCE was removed immediately after the potential was turned off.

TRL prototype 081297-1#10 was inserted and allowed to stay in PBS for 39.75 hours. The prototype was then removed from the release medium, rinsed with DI water, gently dried with nitrogen, and the release medium was replaced with fresh PBS. The prototype was inserted into the fresh PBS, and an electric potential of +1.04 V vs. SCE was applied to the gold membrane anode of reservoir 34 for 30 seconds after being submerged in the PBS for 0.37 hours.

The prototype was removed from the release medium, rinsed with DI water, gently dried with nitrogen, and the release medium was replaced with fresh PBS after 9.41 hours of fluorescein release. The prototype was inserted into the fresh PBS for 14.63 hours before +1.04 V vs. SCE was applied to reservoir 33 for 30 seconds. The prototype was again removed from the release medium, rinsed with DI water, gently dried with nitrogen, and the release medium was replaced with fresh PBS after 25.09 hours of fluorescein release. The prototype was inserted into the fresh PBS for 16.26 hours before +1.04 V vs. SCE was applied to reservoir 31 for 30 seconds. The prototype was removed from the release medium, rinsed with DI water, gently dried with nitrogen, and the release medium was replaced with fresh PBS after 9.01 hours of fluorescein release. The prototype was inserted into the fresh PBS for 20.98 hours before +1.04 V vs. SCE was applied to reservoir 21 for 30 seconds. The prototype was removed from the release medium, rinsed with DI water, gently dried with nitrogen, and the release medium was replaced with fresh PBS after 18.38 hours of fluorescein release. The prototype was inserted into the fresh PBS for 19.67 hours before +1.04 V vs. SCE was applied to reservoir 20 for 40 seconds. The device was removed from the release medium after 15 minutes of release, rinsed with DI water, gently dried with nitrogen, and examined under a light microscope. The prototype was re-inserted into the same PBS that it was just removed from. 9.29 hours later, an electric potential of +1.04 V vs. SCE was applied to reservoir 18 for 60 seconds. The prototype was removed from the release medium, rinsed with DI water, gently dried with nitrogen, and the release medium was replaced with fresh PBS after 11.46 hours of fluorescein release from reservoir 18. Reservoirs 16 and 17 were sealed with epoxy and allowed to cure. The electrodes of reservoirs 1, 2, 29, 31, and 32 were shorted to each other and to ground. The prototype was then inserted into the fresh PBS for 20.87 hours before +1.04 V vs. SCE was applied to reservoir 30 for 60 seconds. The SCE reference electrode was re-positioned and +1.04 volts vs. SCE was applied 8 minutes later to reservoir 30 for another 60 seconds. The prototype was removed from the release medium approximately 19.67 hours later, rinsed with DI water, and gently dried with nitrogen.

5.2.3 Multiple chemical release - TRL prototype 081297-1#11. The thirty-four reservoirs of TRL prototype 081297-1#11 were checked with a light microscope for defects as described in section 3.2.2. Reservoirs 1-3,5,16-18,20,21,23-25,29-31,33 (reservoirs 7-15 were not checked or used in the release experiment) were determined to be defect-free and were filled with stock solutions of sodium fluorescein and PEG 200 in DI water or radioactive calcium (^{45}Ca, in the form of $CaCl_2$ salt) and PEG 200 in DI water. The fluorescein stock solution had a fluorescein concentration of 63.2 mM in 85/15 v/v DI water/PEG 200. The ^{45}Ca stock solution had a radioactivity concentration of 13.7-14.6 nCi/nL in 85.7/14.3 v/v DI water/PEG 200. Known volumes of either stock solution were deposited in reservoirs by the microinjection method described in section 3.2.2.2. Table 5-3 lists the volume of each stock solution deposited into each reservoir using microinjection.

Table 5-3. The volume of solutions of fluorescein/PEG 200 and ^{45}Ca/PEG 200 deposited into the reservoirs of TRL Prototype 081297-1#11 by microinjection.

Reservoir #	Volume Deposited in Each Reservoir
2,5,16,17,20,29,31	25 nL (Fluorescein)
1,3,18,21,24,25,30,33	25 nL (^{45}Ca)

The reservoirs appeared completely filled with liquid immediately after injection. However, most of the water quickly evaporated, leaving the reservoir with only a small amount of fluorescein or ^{45}Ca in PEG 200 (liquid polymer) in the bottom of the reservoir. The material in the reservoir remained in liquid form for the entire experiment because the polymer does not evaporate. No gold membranes were observed to crack or tear after reservoir filling. The total mass of fluorescein deposited in each reservoir was calculated to be approximately 595 ng of fluorescein for 25 nL. The total activity of ^{45}Ca deposited in each reservoir was calculated to be approximately 344-366 nCi of ^{45}Ca for 25 nL. The reservoirs were sealed by the second method described in section 3.2.3 using pieces of adhesive plastic and glass coverslips. The prototype was then sealed into a PGA package as described in section 3.2.4.2.

It is not trivial to experimentally determine the amount of material deposited in each reservoir using microinjection. Therefore, estimates of the mass or radioactivity of the material

in each reservoir were obtained by calculations using the concentrations of the stock solutions and the volumes injected. The concentration of the fluorescein stock solution was known because the mass of sodium fluorescein in the solution was measured with a gram balance sensitive to four decimal places (Mettler AE200). The ^{45}Ca was supplied as a aqueous solution of $CaCl_2$ (NEN Life Science Products #NEZ 013) having an approximate activity of 16-17 mCi/mL. This estimate of activity was obtained by measuring the counts (i.e. detectable disintegrations) per minute (CPM) in diluted stock solution samples using scintillation analysis as described in section 5.2.1.2.

The gold membranes covering the filled reservoirs were examined with a light microscope for a few days while the waterproof epoxy was curing to make sure all membranes were still intact. No reservoirs had cracks or tears in their gold membranes, so all the filled reservoirs were viable for the release experiment.

Electrical connection between the PGA packaged prototype and the potentiostat/galvanostat using the testing apparatus described in section 5.2.2.2 and shown in figure 5-3. The prototype was connected to the apparatus and placed in 100 mL of 0.145 M NaCl solution (release medium) in a glass beaker at room temperature until the water level covered the bottom half of the device (i.e. did not cover the gold wire bonds). Note that a NaCl solution without phosphate buffer was used for the multiple release experiments due to the possible formation of insoluble calcium phosphate complexes upon release of ^{45}Ca into PBS. The precipitation of ^{45}Ca would have made detection of its release with time nearly impossible. A chloride ion concentration of 0.145 M was selected to keep the Cl^- concentration the same as in all previous release experiments. The release medium was gently stirred with a magnetic stirring bar throughout the experiment. 3.0 mL and 1.0 mL samples of the release medium were taken at times before and after the activation of each reservoir for fluorescein and ^{45}Ca detection, respectively. These 3.0 mL samples were analyzed in the fluorimeter without dilution. However, the samples were diluted by taking 1.0 mL of the original 3.0 mL sample and diluting it to a total volume of 3.0 mL by the addition of 2.0 mL of NaCl solution before being analyzed in the fluorimeter when the fluorescein concentration was too large to be detected by the fluorimeter. The 1.0 mL samples were added to 10 mL of Optifluor scintillation fluid (Packard, Lot #47-7061, expires Dec. 1999) and analyzed for activity content in the scintillation counter.

The 4.0 mL taken from the release medium for analysis were replaced immediately with 4.0 mL of fresh NaCl solution to keep the release medium volume constant at 100 mL throughout the experiment. The SCE reference electrode was always placed in the release medium with its tip positioned 1-3 mm from the surface of the anode just before the application of the potential. The SCE was removed immediately after the potential was turned off.

TRL prototype 081297-1#11 was submerged into the release medium for 24.34 hours before the application of an electric potential of +1.04 V vs. SCE to the gold membrane anode of reservoir 3 for 30 seconds. The prototype was removed from the release medium, rinsed with DI water, gently dried with nitrogen, and the release medium was replaced with fresh NaCl solution after 6.01 hours of ^{45}Ca release. The prototype was inserted into the fresh NaCl solution for 6.00 hours before +1.04 V vs. SCE was applied to reservoir 5 for 30 seconds. The prototype was again removed from the release medium, rinsed with DI water, gently dried with nitrogen, and the release medium was replaced with fresh NaCl solution after 6.00 hours of fluorescein release. The prototype was inserted into the fresh NaCl solution for 6.00 hours before +1.04 V vs. SCE was applied to reservoirs 24 and 25 for 30 seconds. (Reservoirs 24, 25, and 26 are all attached to a single gold trace. Therefore, the potential applied to a single gold trace will activate reservoirs 24, 25, and 26 simultaneously. Reservoir 26, however, was not filled with any material during this experiment.) The prototype was removed from the release medium, rinsed with DI water, gently dried with nitrogen, and the release medium was replaced with fresh NaCl solution after 6.00 hours of ^{45}Ca release. The prototype was inserted into the fresh NaCl solution for 6.02 hours before +1.04 V vs. SCE was applied to reservoir 20 for 30 seconds. The prototype was removed from the release medium 5.98 hours later, rinsed with DI water, and gently dried with nitrogen.

5.3 Experimental results.

5.3.1 Single chemical release.

5.3.1.1 Microlab prototype 091096-4. A plot of mass released vs. time for Microlab prototype 091096-4 is shown in figure 5-4. Reservoirs 6 and 4 began releasing fluorescein into the PBS release medium within 2 minutes after the application of the electric potential. Release was initially observed with the naked eye and later confirmed with fluorescence spectroscopy measurements of release samples. Light micrographs of reservoirs 6 and 4 are given in figures 5-5 and 5-6a. A scanning electron micrograph of the corroded membrane of reservoir 4 is given in figure 5-6b. No scanning electron micrographs of the membrane of reservoir 6 exist because reservoir 6 was sealed with epoxy after several hours of release in order to keep any residual fluorescein from leaking out during the release of reservoirs 4 and 3.

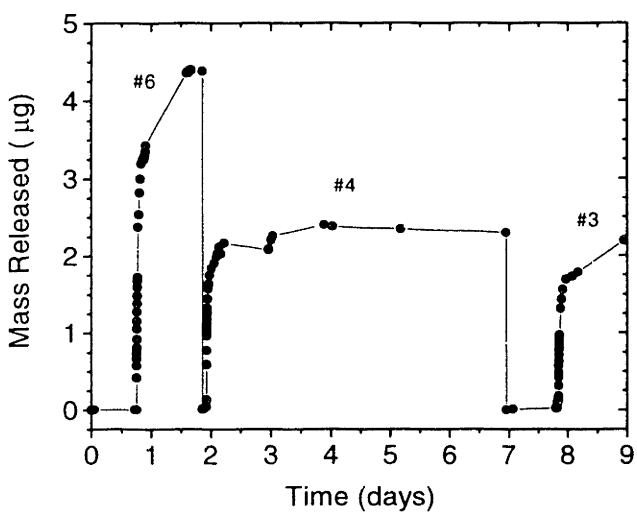

Figure 5-4. Mass of fluorescein released vs. time for Microlab prototype 091096-4. (The numbers on the plot refer to the reservoir from which the fluorescein was released.)

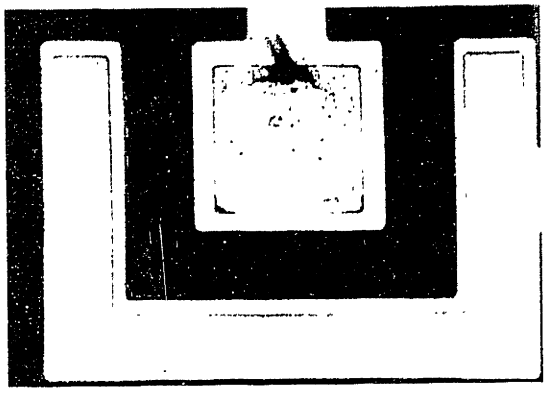

Figure 5-5. Light micrograph of reservoir 6 of Microlab prototype 091096-4.

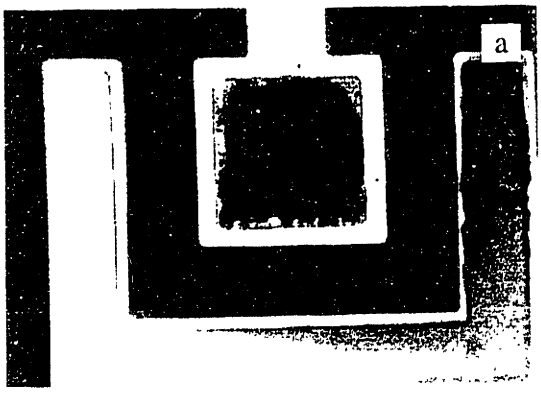

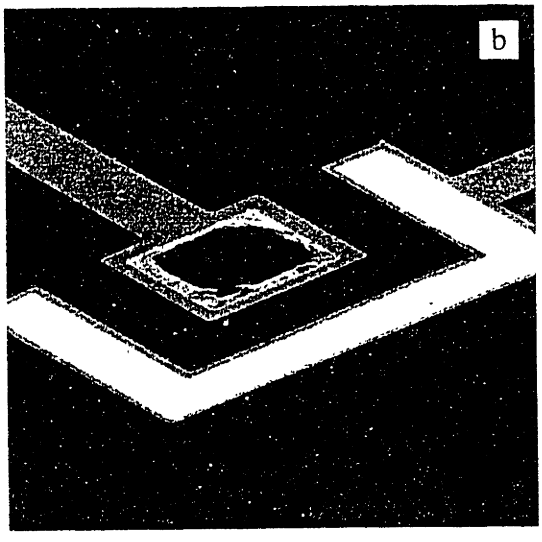

Figure 5-6. Reservoir 4 of Microlab prototype 091096-4, (a) light micrograph and (b) scanning electron micrograph.

Fluorescein release can often be detected from a reservoir with the naked eye. No fluorescein release was detected with the naked eye from reservoir 3, so the electric potential was applied multiple times to make sure that the reservoir was open. Release from reservoir 3 began approximately 6 minutes after the third application of electric potential to the gold membrane of reservoir 3. Light and scanning electron micrographs of the gold membrane of reservoir 3 taken after the multiple applications of an electric potential are given in figure 5-7.

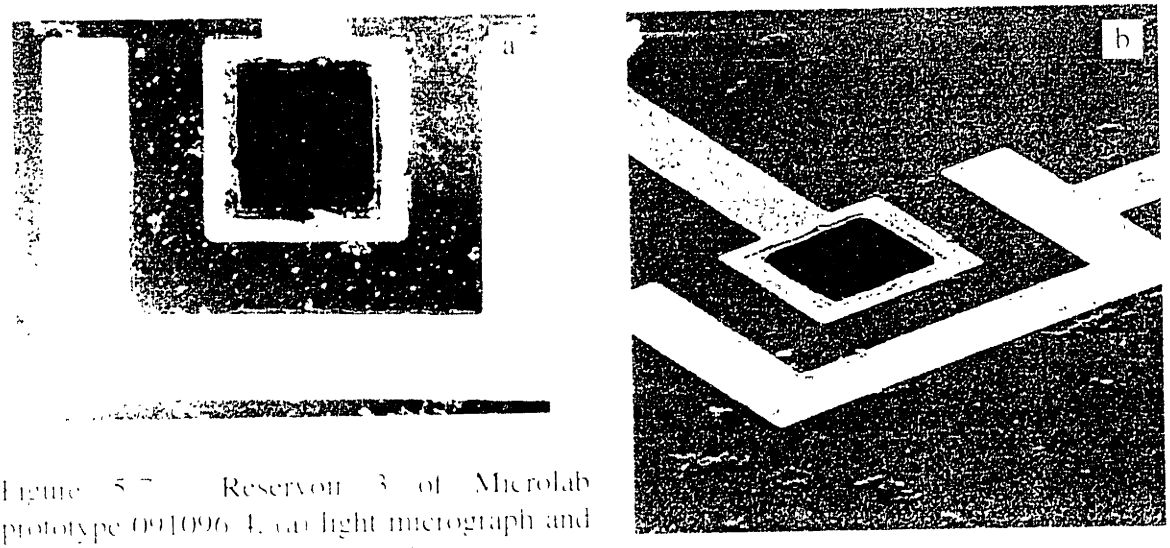

Figure 5-7 Reservoir 3 of Microlab prototype 091096-4: (a) light micrograph and (b) scanning electron micrograph

Release rate vs. time for Microlab prototype 091096-4 is given in figure 5-8. Reservoirs 6, 4, and 3 show that the release rate of fluorescein increases and decreases rapidly after reservoir opening.

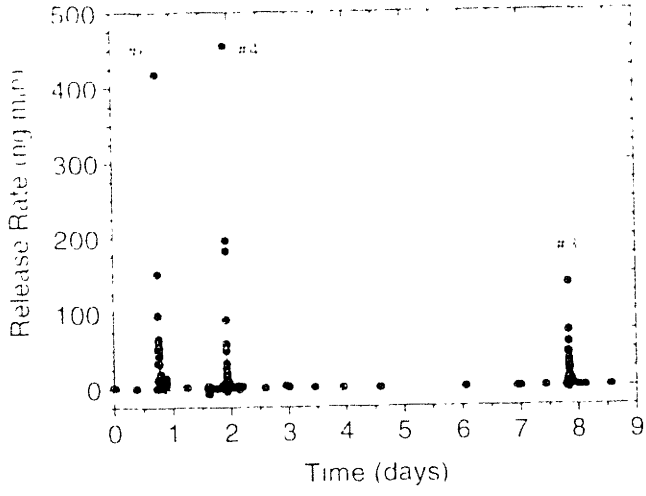

Figure 5-8 Fluorescein release rate vs. time for Microlab prototype 091096-4. (The numbers on the plot refer to the reservoir from which the fluorescein was released.)

Each reservoir of Microlab prototype 091096-4 was filled with a different amount of fluorescein, i.e. 820, 510, or 410 drops of a 90.8 mM solution from an inkjet cartridge. The varying peak heights in figure 5-4 show this clearly. A summary of the estimated mass in each reservoir and the observed mass released from reservoirs 6, 4, and 3 is given in table 5-4. The mass released from each reservoir is lower than expected from calculations using inkjet printed calibration data. A discussion of possible reasons for variation between the amount of fluorescein deposited into each reservoir and the amount released can be found in section 5.4.2. Appendix A shows the equations used to calculate mass released and release rates for Microlab prototype 091096-4. An example calculation spreadsheet for TRL prototype 081297-1#11 is also included in Appendix A.

Table 5-4. Estimates of mass deposited and mass released from each reservoir of Microlab prototype 091096-4.

Reservoir #	Mass in Reservoir (μg)	Mass Released (μg)
6	4.8-5.5	4.37-4.40
4	3.0-3.4	2.25-2.40
3	2.4-2.8	1.80-2.20

5.3.1.2 TRL prototype 021397-2#2. A plot of mass released vs. time for TRL prototype 021397-2#2 is shown in figure 5-9. Reservoirs 5 and 3 began releasing fluorescein into the PBS release medium within 2 minutes after the application of the electric potential. Release was sometimes observed with the naked eye and always confirmed with fluorescence spectroscopy measurements of release samples. Light micrographs of the membranes of reservoirs 5 and 3 are given in figure 5-10.

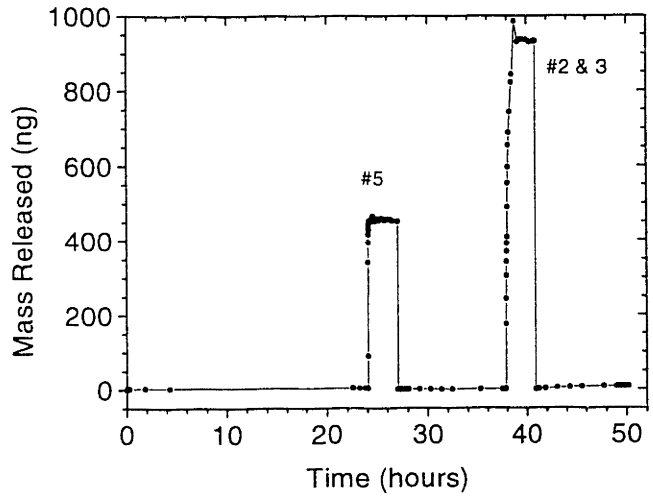

Figure 5-9. Mass of fluorescein released vs. time for TRL prototype 021397-2#2. (The numbers on the plot refer to the reservoir from which the fluorescein was released.)

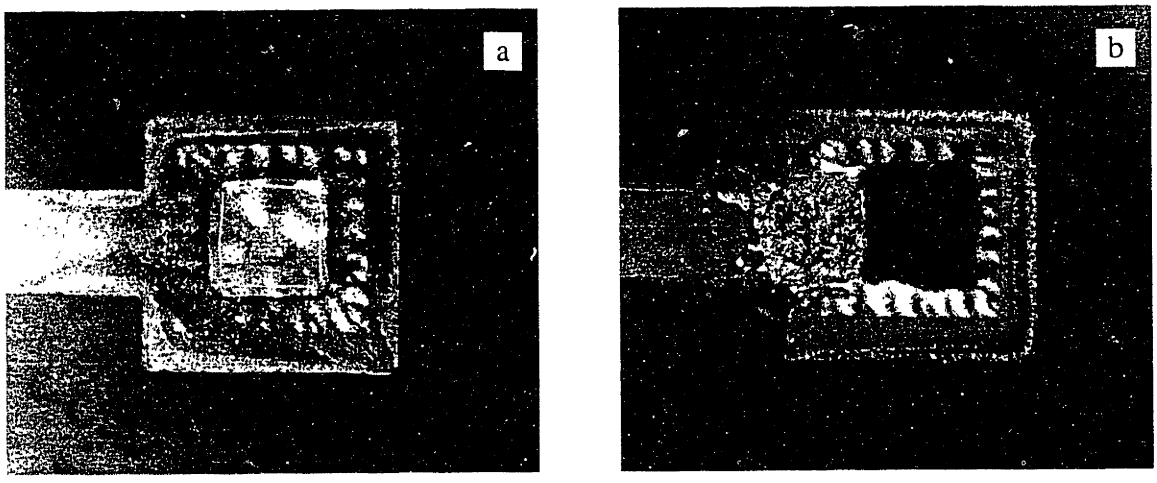

Figure 5-10. Light micrographs from TRL prototype 021397-2#2, (a) reservoir 5 and (b) reservoir 3.

The prototype was examined with a light microscope after the release of reservoir 5 and after the release of reservoir 3. It appeared that the gold membrane of reservoir 2 had corroded when an electric potential was applied to reservoir 3. The corrosion occurred over all portions of the gold anode of reservoir 2 because the SiO_2 layer on this anode had delaminated during the experiment. A light micrograph of reservoir 2 after the application of a potential to reservoir 3 is

given in figure 5-11. It appears that the membrane of reservoir 2 was perforated with the application of the electric potential to reservoir 3, indicating that the release peak for reservoir 3 may actually be a combination of the mass released from reservoirs 3 and 2. The device was inserted into fresh PBS and an electric potential of +1.04 vs. SCE was applied to reservoir 2 to make sure that it was open. No additional release of fluorescein was detected, lending support to the postulation that reservoir 2 had indeed released fluorescein with reservoir 3.

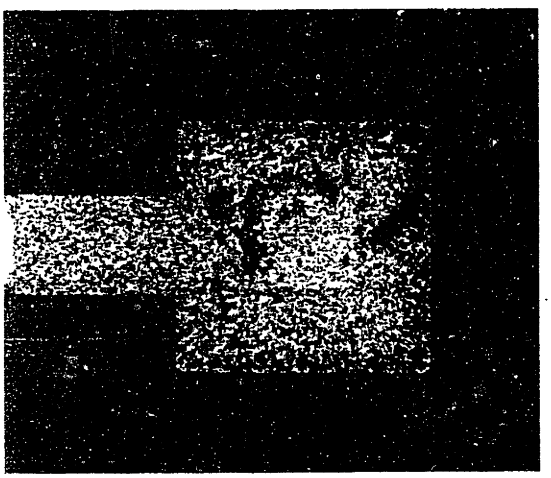

Figure 5-11. Light micrograph of reservoir 2 from TRL prototype 021397-2#2.

Release rate vs. time for TRL prototype 021397-2#2 is given in figure 5-12. Reservoirs 5, 3, and 2 show that the release rate of fluorescein increases and decreases rapidly after reservoir opening.

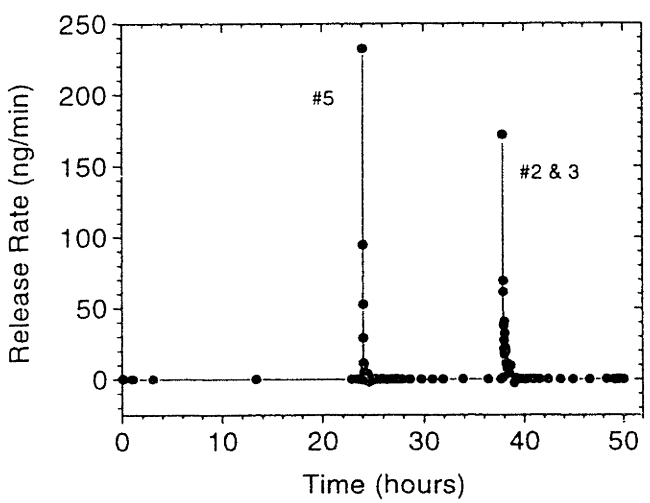

Figure 5-12. Fluorescein release rate vs. time for TRL prototype 021397-2#2. (The numbers on the plot refer to the reservoir from which the fluorescein was released.)

All reservoirs of TRL prototype 021397-2#2 were supposedly filled with the same amount of fluorescein, i.e. 100 drops of a 92.2 mM solution from an inkjet cartridge. The mass of fluorescein in each reservoir should have been between approximately 253 ng and 385 ng according to the minimum and maximum masses deposited in inkjet printed calibration samples. The mass released from reservoir 5 is slightly higher than expected from inkjet printed calibration samples. Also, the combined mass released from reservoirs 3 and 2 is slightly higher than that expected for two reservoirs released simultaneously. However, there is excellent agreement in the relative masses released, i.e. the combined amount released from reservoirs 3 and 2 is almost exactly twice as much released by reservoir 5 alone. A summary of the mass released from reservoirs 5, 3, and 2 is given in table 5-5. A discussion of possible reasons for deviations in the amount of fluorescein in each reservoir from that expected can be found in section 5.4.2. Appendix A shows the equations used to calculate mass released and release rates for TRL prototype 021397-2#2. An example calculation spreadsheet for TRL prototype 081297-1#11 is also included in Appendix A.

Table 5-5. Estimates of mass released from each reservoir of TRL prototype 021397-2#2.

Reservoir #	Mass Released (ng)
5	450-457
3 and 2	925-935

5.3.1.3 TRL prototype 081297-1#10. A plot of mass released vs. time for TRL prototype 081297-1#10 is shown in figure 5-13. Reservoirs 34, 33, 31, and 21 began releasing fluorescein into the PBS release medium within 2 minutes after the application of the electric potential. Release was initially observed with the naked eye and later confirmed with fluorescence spectroscopy measurements of release samples. Scanning electron micrographs of the membranes of reservoirs 34, 33, 31, and 21 are given in figure 5-14.

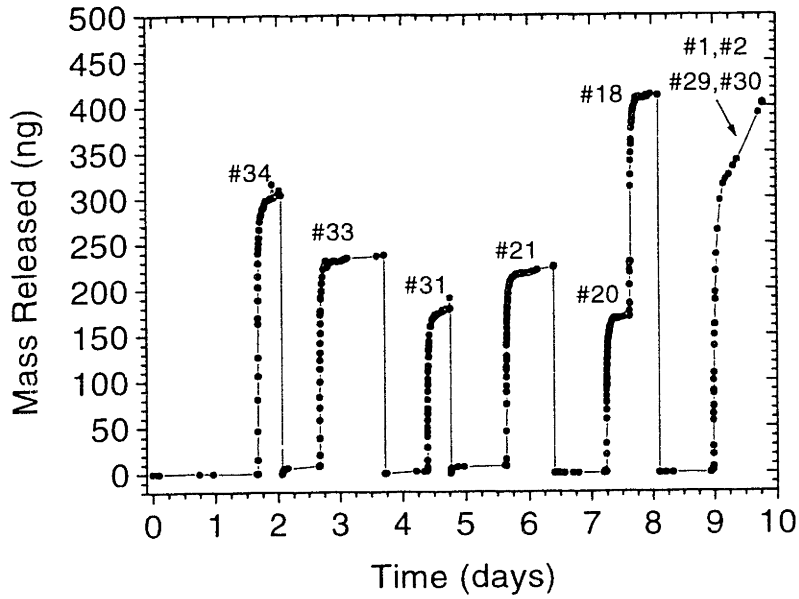

Figure 5-13. Mass released vs. time for TRL prototype 081297-1#10. (The numbers on the plot refer to the reservoir from which the fluorescein was released.)

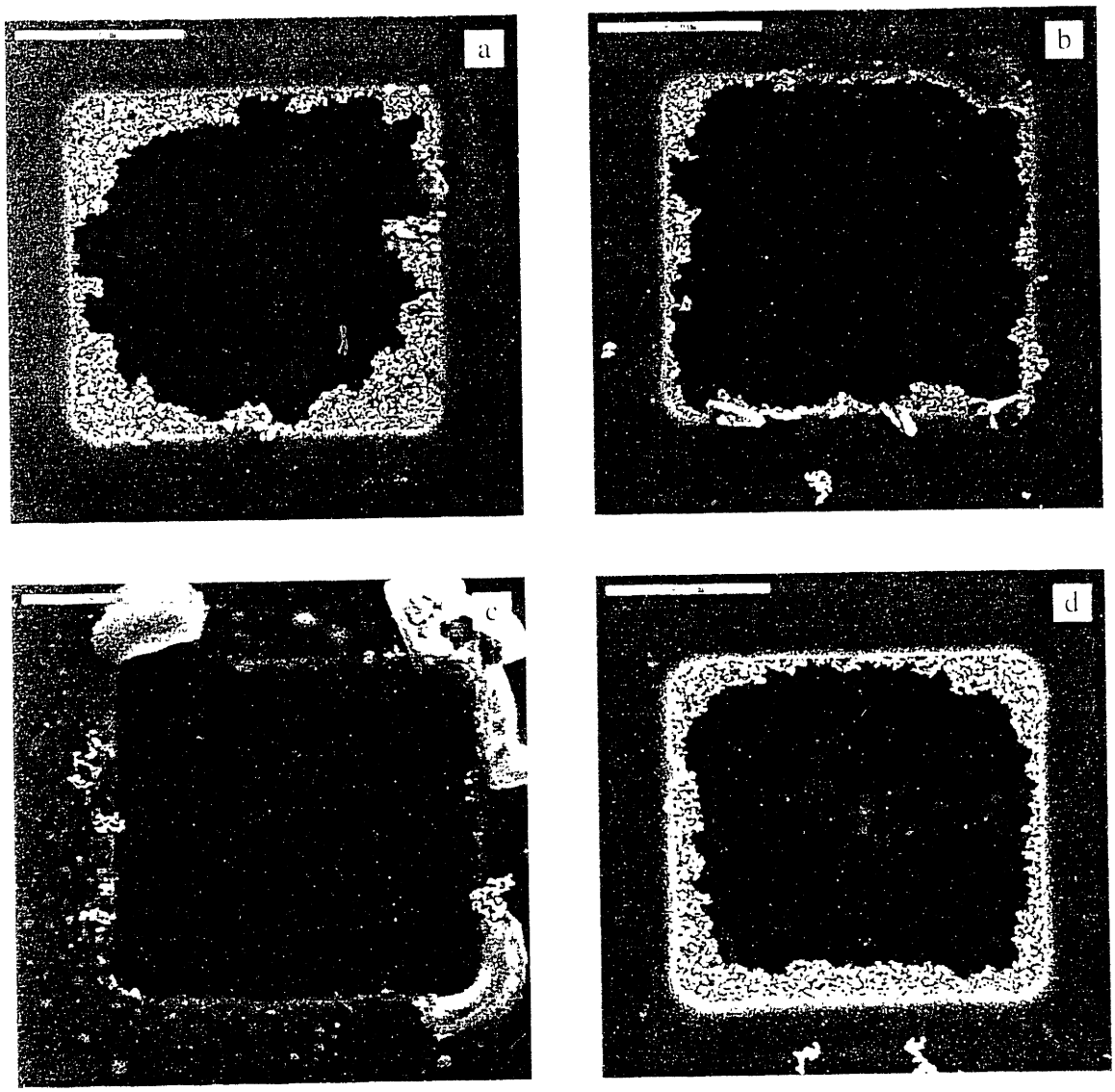

Figure 5.14 Scanning electron micrographs for TRL prototype 081297-1#10, (a) reservoir 34, (b) reservoir 33, (c) reservoir 31, and (d) reservoir 21

Reservoir 20 did not release fluorescein for the first 15 minutes after the application of the electric potential. The prototype was removed from the release medium, rinsed with DI water, gently dried with nitrogen, and examined under a light microscope. The membrane of reservoir 20 had partially corroded and had a number of holes in it as shown in figure 5.15. The prototype was returned to the release medium. Fluorescein release from reservoir 20 was observed with the naked eye immediately after prototype re-insertion into the release medium. This release was also confirmed with fluorescence spectroscopy measurements.

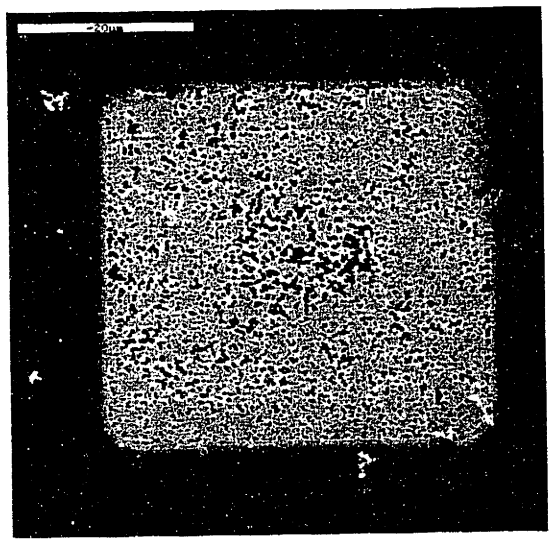

Figure 5-15. Scanning electron micrograph of reservoir 20 from TRL prototype 081297-1#10.

Reservoir 18 operated normally and released fluorescein within 2 minutes after the application of the electric potential. An SEM of the gold membrane of reservoir 18 is given in figure 5-16. However, light microscopy of the prototype after it was removed from solution showed that reservoir 17 had been partially corroded when the electric potential was applied to reservoir 18 (see figure 5-17). Light microscopy did not indicate that release had occurred from reservoir 17, although it is possible that a small amount of fluorescein may have leaked from this reservoir. Both reservoirs 16 and 17 were sealed over with epoxy before proceeding with the remainder of the release experiment to prevent any possible fluorescein leakage from those two reservoirs that might confound later release results.

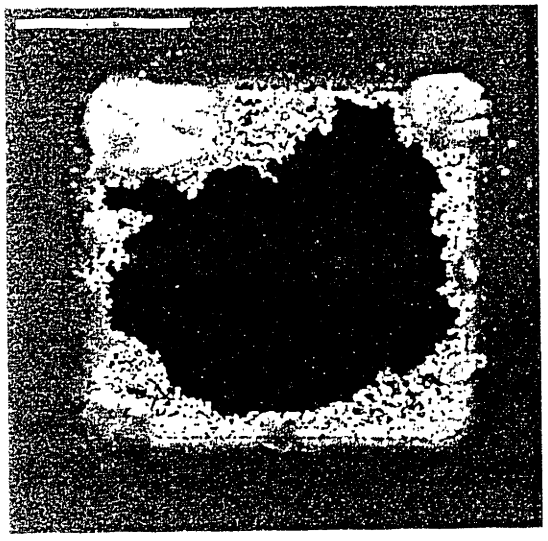

Figure 5-16. Scanning electron micrograph of reservoir 18 from TRL prototype 081297-1#10.

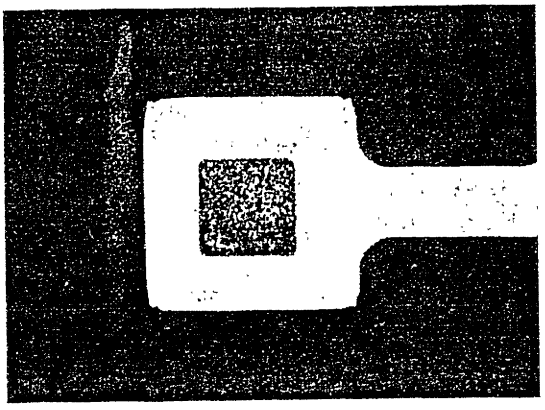

Figure 5-17. Light micrograph of reservoir 17 of TRL prototype 081297-1#10

The first application of electric potential to reservoir 30 did not result in fluorescein release. The current was approximately 10 times lower than that normally observed for gold membrane corrosion and reservoir opening (0.1 μA vs. 1-7 μA) and no release was observed visually. The reference electrode was re-positioned and an electric potential was applied to reservoir 30 again. No release was observed with the naked eye from this reservoir. However, release was observed visually from reservoir 1 within 2 minutes after the 2nd application of electric potential to reservoir 30. Fluorescein release was observed from reservoir 2 within 0.6 hours after the release from reservoir 1. Examination of the prototype with light microscopy after removal from the release medium showed that reservoir 30 had been corroded and opened (see figure 5-18), although it is unclear if this occurred during the 1st or 2nd application of electric potential. It was also observed that reservoirs 1, 2, and 29, which were electrically shorted (i.e. connected) together and to ground just before the application of potential to reservoir 30, had partially corroded and perforated (see figure 5-19). Interestingly, the corrosion and perforation only occurred at the 90° corners of interface between the gold membrane and the SiO_2 protective covering. Therefore, the last peak in figure 5-13 is made up of release from reservoirs 1, 2, 29, and 30.

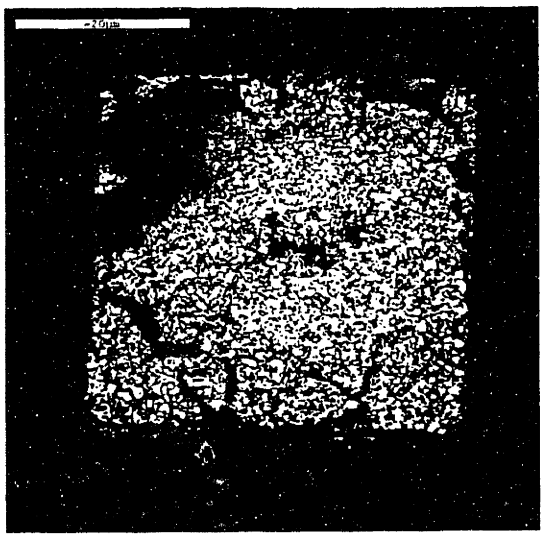

Figure 5-18. (left) Scanning electron micrograph of reservoir 30 from TRL prototype 081297-1#10.

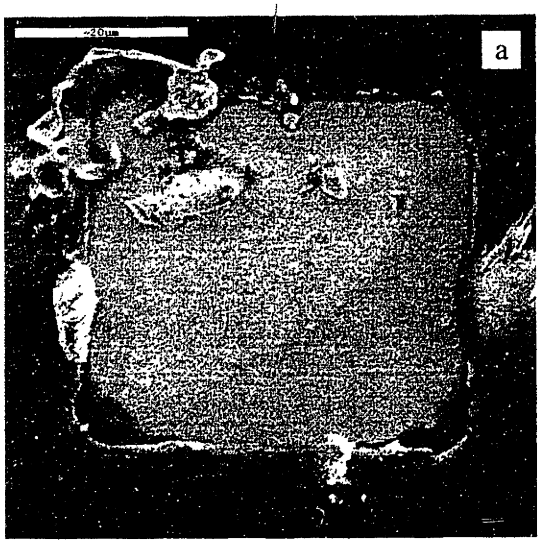

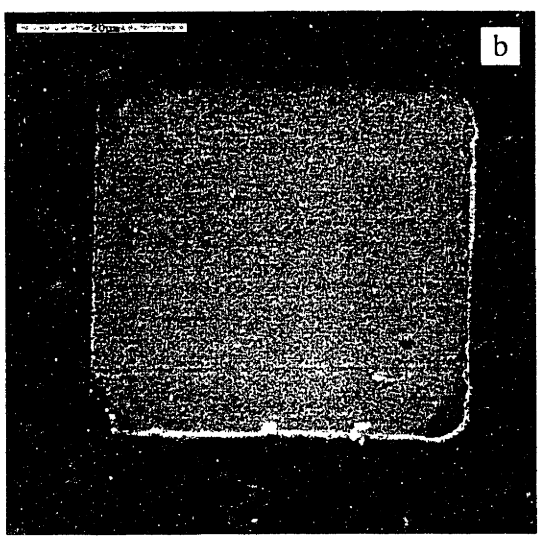

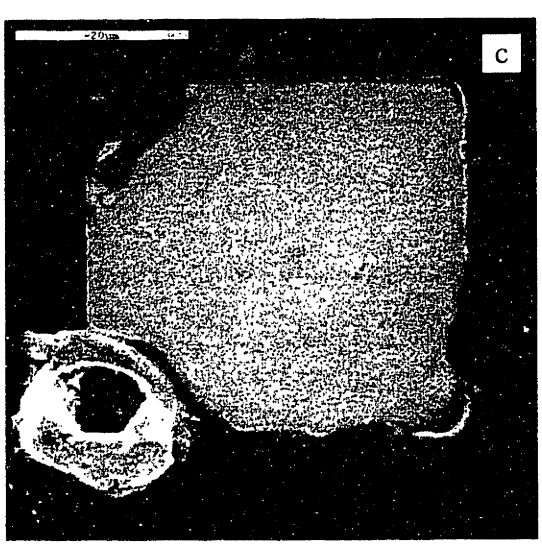

Figure 5-19. (above and left) Scanning electron micrographs of TRL prototype 081297-1#10, (a) reservoir 1, (b) reservoir 2, and (c) reservoir 29.

Release rate vs. time for TRL prototype 081297-1#10 is given in figure 5-20. Reservoirs 34, 33, 31, and 21 show that the release rate of fluorescein increases and decreases rapidly after reservoir opening. Reservoir 20 demonstrates the same release rate profile, but its onset is delayed by 15 minutes. Reservoir 18's release rate increases sharply after membrane opening, slows for approximately 24 minutes, then increases sharply one more time. It is easier to see this "double pulse" in the close up of the reservoir 18 release rate peak shown in figure 5-20b. An explanation for this observation can be found in section 5.4.1.

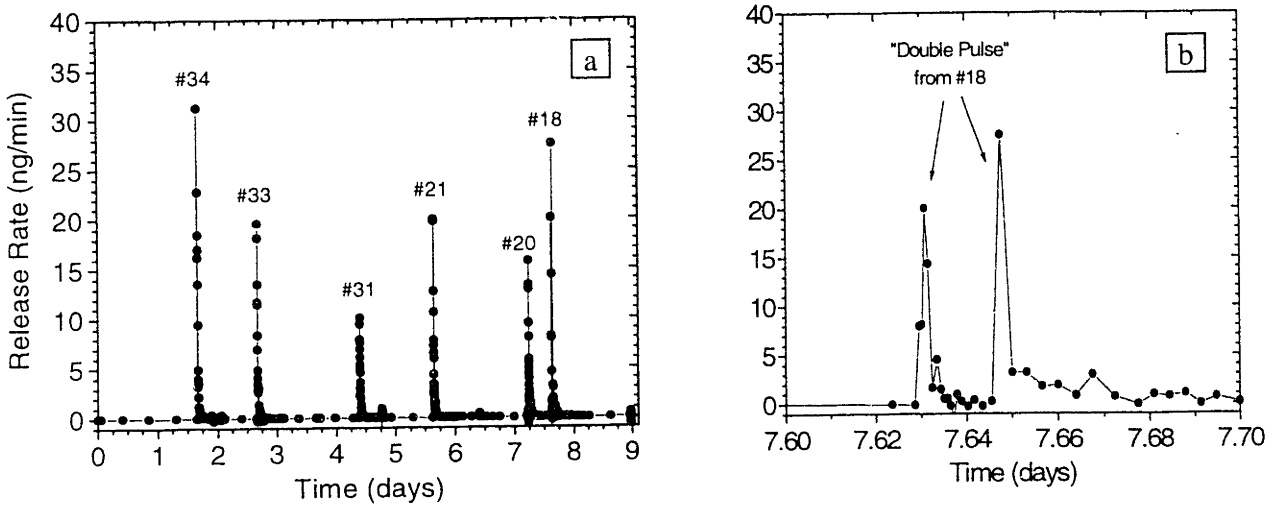

Figure 5-20. Release rate vs. time for TRL prototype 081297-1#10, (a) overall plot and (b) close up the reservoir 18 peak showing the "double pulse." (The numbers on the plots refer to the reservoir from which the fluorescein was released.)

All reservoirs of TRL prototype 081297-1#10 were supposedly filled with the same amount of fluorescein, i.e. 100 drops of a 60.2 mM solution from an inkjet cartridge. The peak heights in figure 5-13 indicate that there were variations in the amount of fluorescein released from each reservoir. The mass of fluorescein in each reservoir should have been between approximately 208 ng and 274 ng according to the minimum and maximum masses deposited in inkjet printed calibration samples. The mass released from three of the six reservoirs falls in this

range. Two of the reservoirs released slightly less than predicted and one reservoir released slightly more. A summary of the mass released from reservoirs 34, 33, 31, 21, 20, and 18 is given in table 5-6. A discussion of possible reasons for variation in the amount of fluorescein in each reservoir can be found in section 5.4.2. Appendix A shows the equations used to calculate mass released and release rates for TRL prototype 081297-1#10. An example calculation spreadsheet for TRL prototype 081297-1#11 is also included in Appendix A.

Table 5-6. Estimates of mass released from each reservoir of TRL prototype 081297-1#10.

Reservoir #	Mass Released (ng)
34	305-315
33	230-240
31	170-180
21	215-225
20	160-170
18	230-240

5.3.2 Multiple chemical release – TRL prototype 081297-1#11. A plot of amount of material (mass or activity) released vs. time for TRL prototype 081297-1#11 is shown in figure 5-21. Reservoirs 3, 5, 24-25, and 20 began releasing fluorescein or ^{45}Ca into the release medium in less than 5 minutes after the application of the electric potential. Release of fluorescein could sometimes be observed with the naked eye and was always confirmed with fluorescence spectroscopy measurements of release samples. Release of ^{45}Ca could not be observed visually and always had to be confirmed by scintillation analysis. Light micrographs of the membranes of reservoirs 3, 5, 24, 25, and 20 are given in figure 5-22. (Note: SEM photos could not be obtained for this device due to the possibility of contaminating the SEM vacuum chamber with radioactive material.)

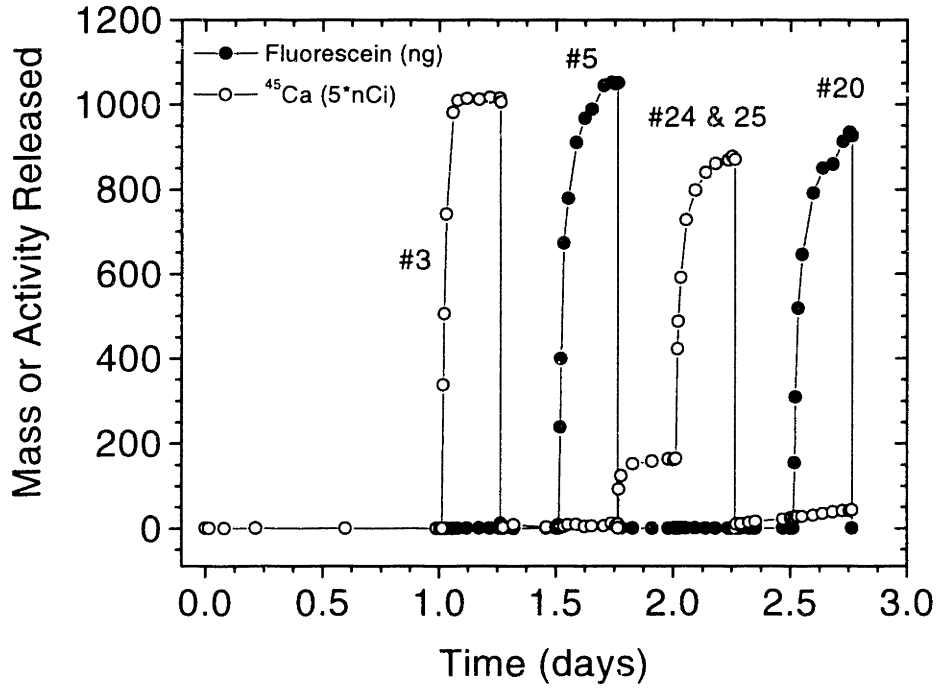

Figure 5-21. Mass or activity released vs. time for TRL prototype 081297-1#11. (The numbers on the plot refer to the reservoir from which the fluorescein or ^{45}Ca was released.)

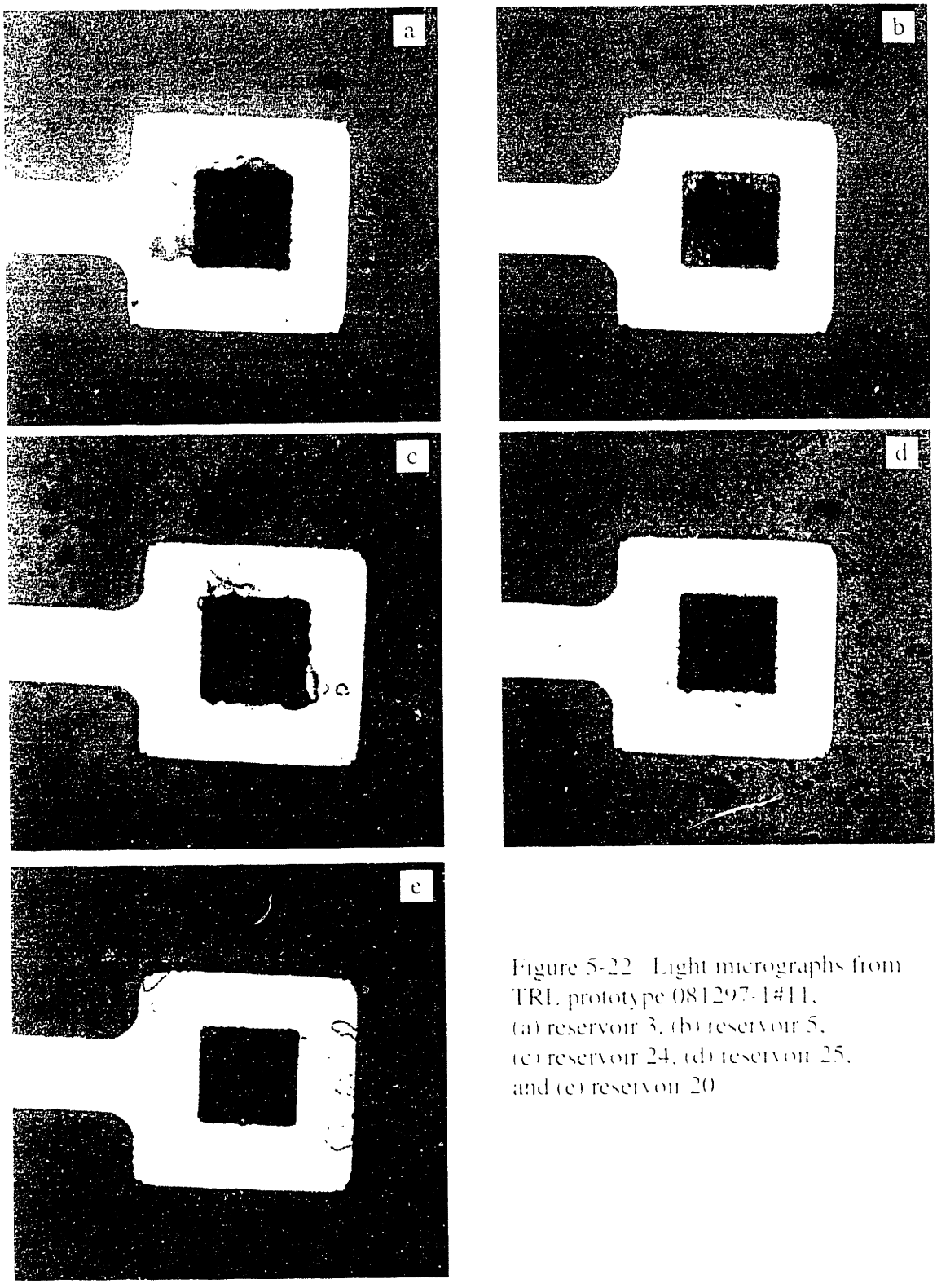

Figure 5-22 Light micrographs from TRL prototype 081297-1#11, (a) reservoir 3, (b) reservoir 5, (c) reservoir 24, (d) reservoir 25, and (e) reservoir 20

Release rate vs. time for TRL prototype 081297-1#11 is given in figure 5-23. This figure shows that the release rate of fluorescein and ^{45}Ca increases and decreases rapidly after reservoir opening.

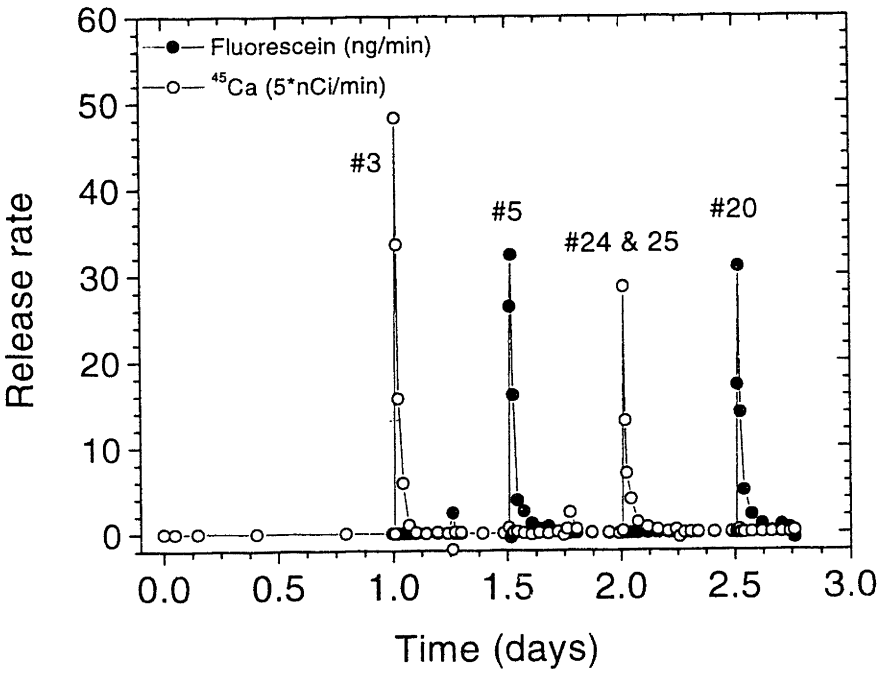

Figure 5-23. Release rate vs. time for TRL prototype 081297-1#11. (The numbers on the plot refer to the reservoir from which the fluorescein or ^{45}Ca was released.)

All reservoirs of TRL prototype 081297-1#11 were supposedly filled with the same amount of fluorescein or the same amount of ^{45}Ca, i.e. 25 nL of each stock solution by microinjection. The fluorescein peak heights in figure 5-21 indicate that the amount of fluorescein released from each reservoir was similar. The mass of fluorescein in each reservoir should have been approximately 595 ng according to calculations based on stock solution concentrations and injected volumes. The mass of fluorescein released from reservoirs 5 and 20 are nearly double that expected from these calculations. The activity of ^{45}Ca in each reservoir should have been approximately 334-359 nCi based on experimental measurements of stock

solution activity, volume injected, and half-life calculations. The peak height for reservoir 3 is lower than this value. The peak height from reservoirs 24 and 25 is much lower than expected for the release of two reservoirs simultaneously. The mass or activity released from reservoirs 3, 5, 24-25, and 20 are given in table 5-7. The small peak appearing before the peak for reservoirs 24 and 25 is believed to be some residual release from reservoir 3. However, even if this were the case, the total amount of activity released from reservoir 3 would still be lower (~237 nCi) than that expected (≥ 340 nCi). Also, the amount released from reservoirs 24 and 25 (~141 nCi) would be even further away from the amount expected from two reservoirs (≥ 680 nCi). The presence and possible origin of this extra release peak will be discussed in section 5.4.1. A discussion of possible reasons for deviations in the amount of fluorescein and ^{45}Ca in each reservoir from that expected can be found in section 5.4.2. Appendix A shows the equations and spreadsheet used to calculate mass or activity released and release rates for TRL prototype 081297-1#11.

Table 5-7. Estimates of mass or activity released from each reservoir of TRL prototype 081297-1#11.

Reservoir #	Material Released	Mass Released or Activity Released
3	^{45}Ca	196-204 nCi
5	Fluorescein	1040-1050 ng
24 & 25	^{45}Ca	167-175 nCi
20	Fluorescein	925-935 ng

5.4 Discussion.

5.4.1 Variation in reservoir opening and its effect on chemical release. Chapter 5 focuses on the release of chemicals from prototype, controlled release microchips. The purpose of this section of chapter 5 is to explain how observed differences in reservoir opening affected the release of chemicals from the prototype devices. This section does not provide detailed mechanistic explanations for the variations in membrane dissolution and reservoir opening, but will focus primarily on how these observed variations affect chemical release. Chapter 6 will build on the gold corrosion material of chapter 3 and the observed variations in reservoir opening

presented in this chapter in an attempt to develop a qualitative mechanism of gold membrane disintegration.

It was observed that most gold membranes were rapidly corroded along grain boundaries exposed to the chloride containing solution, leading to a local thinning and weakening of the membrane. Forces internal or external to the reservoir could then cause the weakened membrane to fail catastrophically. Forces internal to the reservoir could include tension exerted on the membrane by a curved liquid surface or intrinsic stresses in the membrane itself. Forces external to the reservoir could include shear forces due to solution mixing or pressure due to the weight of the solution on the membrane. The kind of membrane disintegration described here is clearly shown in figure 5-14a for reservoir 34 of TRL prototype 081297-1#10, which led to the immediate commencement of release from the reservoir with little resistance for the continued emptying of the reservoir. A more detailed discussion of the forces exerted on gold membranes during chemical release is found in section 6.4.1.2.

Reservoirs 20 and 18 of TRL prototype 081297-1#10 opened in a slightly different way. The gold membranes covering these two reservoirs appeared to have been corroded along grain boundaries as mentioned in the previous paragraph, but not evenly across the surface of the membrane. It appears as though boundaries around certain grains corroded, causing the entire grain to fall out of the membrane, forming small holes in an otherwise intact membrane. The membrane of reservoir 20 had many small holes in it, but remained intact throughout the release experiment. An angled view of this membrane clearly shows this and can be found in figure 5-24. Release did not begin from reservoir 20 immediately after the application of the potential as expected. Instead, release did not begin until the device was removed from the release medium, examined under a light microscope, and re-inserted into the release medium. It is possible that surface tension or air bubbles kept release from occurring through the holes of membrane 20. Removal of the prototype from solution may have disrupted the surface tension or bubbles preventing release, allowing release to commence upon re-insertion into the release medium. Reservoir 18 was also opened by the formation of small holes in the gold membrane, but unlike reservoir 20, release from reservoir 18 commenced almost immediately after the application of potential to that membrane. There does appear to be some resistance to release through a number of small holes, as compared to a fully opened reservoir. Release from reservoir 18 began shortly

after the application of the potential. Chemical release then began to slow over the next several minutes. Another sharp increase in release occurred 27 minutes after release began from reservoir 18. Examination of reservoir 18 with a light microscope after removal from the release medium shows that several large portions of the membrane were missing (see figure 5-25). (Note that the light micrograph in figure 5-25 looks slightly different from the SEM shown in figure 5-16. The SEM in figure 5-16 was taken after the completion of the entire release experiment. Some pieces of the membrane appear missing in figure 5-16 and would have most likely broken off and washed away during the frequent rinsing and drying of the device.) It is believed that release began through the small holes in the membrane and then began to slow due to the resistance of diffusion through the small holes. The membrane was weakened by the presence of the holes and catastrophically failed in several places approximately 27 minutes after release began. This membrane failure created a much larger area through which the chemical could diffuse, thereby increasing the release rate for a short time. This explains the "double pulse" observed for reservoir 18 in the release rate vs. time plot shown in figure 5-20b in section 5.3.1.3.

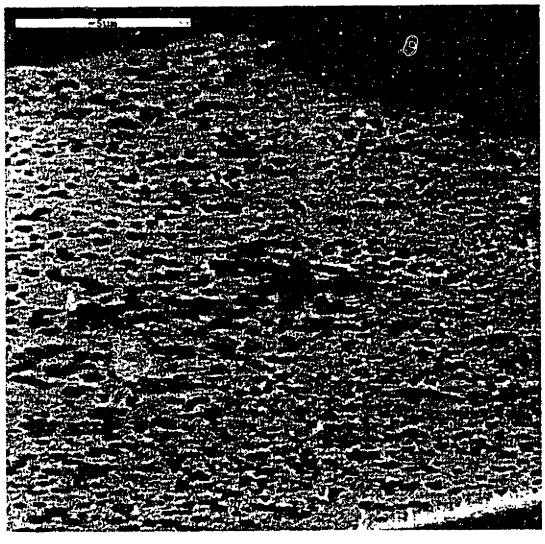

Figure 5-24. Scanning electron micrograph (at an angle) of reservoir 20 of TRL prototype 081297-1#10.

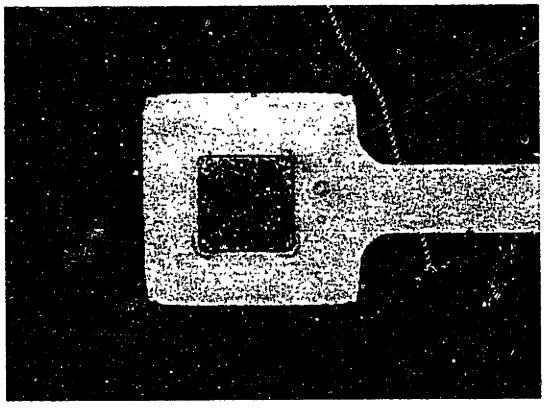

Figure 5-25. Light micrograph of reservoir 18 of TRL prototype 081297-1#10.

The presence of varying rates of corrosion for a gold membrane can have an effect on release from a reservoir. Possible explanations for variance in corrosion rate across a gold membrane are presented in more detail in section 6.4.1.1. Faster corrosion in controlled release microchip prototypes is most often observed along the interface between the exposed gold membrane anode and the SiO_2 layer protecting parts of the gold anode surface. Reservoir 3 of TRL prototype 021397-2#2 demonstrates this situation clearly. The corrosion at this interface can occur at a faster rate than across the rest of the membrane, causing the membrane to perforate first along the interface. Figure 5-10b shows how the membrane of reservoir 3 failed along the gold-SiO_2 interface, forming a gold membrane "flap" that opened to release the chemical. Release from this reservoir occurred rapidly because the entire membrane was removed. The formation of a "flap" can greatly affect release from a reservoir and will be discussed in more detail later in this section.

Corrosion can even occur under the SiO_2 layer. For example, the SiO_2 layer of TRL prototype 021397-2#2 was deposited at low temperature and did not adhere well to the gold. This allowed the chloride solution to penetrate between the SiO_2 and gold layers of reservoir 5. Extensive corrosion of the gold membrane occurred under the SiO_2 upon application of an electric potential, leaving most of the exposed membrane intact. However, release from reservoir 5 did not appear to be hindered by the SiO_2, probably because the SiO_2 adhered so poorly to the gold that there was a clear path for the chemical to diffuse out of the reservoir and into the release medium. The SiO_2 layer of reservoir 2 completely delaminated from the surface of the anode. The unprotected gold film corroded in all exposed areas, as expected. This reservoir appears to be similar to that of reservoir 20 of TRL prototype 081297-1#10 in that both reservoirs were perforated with holes but still retained their mechanical integrity. However, reservoir 2 is more like reservoir 18 of TRL prototype 081297-1#10 in that release began almost immediately after the application of the electric potential.

Areas of stress concentration in the gold membranes are vulnerable to local failures, such as cracks. The origins of these stresses were mentioned earlier in this section and can either be internal or external to the reservoir. One such stress concentration area is where the gold membrane meets the silicon at the edge of the reservoir opening. Reservoir 6 of device 091096-4 failed along this edge by forming a long crack, as shown in figure 5-5. The fluorescein diffused

out of this large crack with little resistance and a normal release profile was obtained. The interface of the SiO_2 layer of this reservoir with the gold anode was located at a point above silicon, not above the gold membrane. Therefore, faster corrosion at this interface did not play a direct part in the opening of the membrane, but it still played an indirect role in the activation of reservoir 6. Reservoir 6 began to corrode at the interface and on the membrane at the same time. The interface corroded at a faster rate than the rest of the membrane, causing the electrical connection between the anode membrane and the power source to be broken. This explains why a second application of electric potential to reservoir 6 caused no further corrosion of the gold membrane. Fortunately, fluorescein was released because enough gold in the membrane was dissolved before the circuit was broken to allow a crack to form in the gold membrane at the edge of the reservoir above the silicon.

The crack formation described in the previous paragraph can affect the release of a chemical from a reservoir. If cracks form along two or three sides of the anode membrane, a "flap" of gold can form. The extraneous bump of ^{45}Ca in the mass released vs. time plot for TRL prototype 081297-1#11 (see figure 5-21) occurring just before the second release of ^{45}Ca is believed to have resulted from the formation of a "flap" over reservoir 3. A "flap" of gold was noticed on reservoir 3 when it was examined with a light microscope after it was released. (The "flap" can barely be seen in the reservoir in the light micrograph of reservoir 3 in figure 5-22a. This photograph was taken after the completion of the entire release study. The "flap" is not as obvious at this time because the device had been subjected to frequent rinsing and drying during the release experiment.) It is believed that this flap closed before all the ^{45}Ca inside had been released. This flap remained closed during the release of reservoir 5, but popped open again when inserted into the release medium before the release of reservoirs 24 and 25, releasing a small amount of ^{45}Ca that was trapped inside reservoir 3 The likelihood of "flap" formation increases greatly if there is still a thin layer of silicon nitride present under the gold membrane, which can keep the membrane from falling apart during gold dissolution. Another discussion of "flap" formation is presented in section 6.4.2.2.

A final variation of observed reservoir opening is based on inadvertent, induced currents, which lead to the premature release of chemicals into the release medium. This problem was first encountered with TRL prototype 081297-1#10. Reservoir 17 was observed to partially

corrode when an electric potential was applied to reservoir 18. The wires connected to each reservoir were not specifically grounded or isolated from ground up to this point in the release experiment. It was postulated that the inadvertent, partial corrosion of reservoir 17 occurred because of a short circuit present on the surface of the device itself. It was decided that reservoirs not in use (i.e. not having a potential applied to them) should be shorted to each other and to ground. Reservoirs 1, 2, 29, 31, and 32 were the closest electrodes to the anode and cathode in use for the next experiment. Therefore, the reservoirs were shorted to each other and to ground when an electric potential was applied to reservoir 30. It was observed that bubbles formed on or near each of these grounded reservoirs during the application of potential to reservoir 30. Also, reservoirs 1, 2, and 29 had been corroded to the point of perforation, causing the fluorescein inside each of these reservoirs to release. It was postulated and later verified with a "dummy" microchip that electrodes could be polarized when potentials were applied to neighboring electrodes. The polarized reservoirs partially corroded because the connection to ground enabled electrons to flow away from the membrane, allowing the gold to form its cationic salt and dissolve into the release medium. Micrographs for these partially corroded membranes are given in figures 5-19. Notice that corrosion and release only occurred at the corners of the membrane. The corners are the place where the highest current density should be observed. It was also observed that more corrosion took place at electrodes closest to the negatively charged cathode, as expected. This type of induced current corrosion can be prevented by isolating all electrodes from each other and from ground when not in use. It is obvious that this type of reservoir opening will drastically affect the chemical release profile from a controlled release microchip.

5.4.2 Variation in chemical loaded and chemical recovered. There are a number of reasons for variation between the amount of chemical that was loaded into a reservoir and the amount of chemical recovered in a release experiment. This section will comment on three possible sources of variation: the reservoir filling method, the properties of the chemicals released, and the device or release experiment design.

5.4.2.1 Reservoir filling method.

5.4.2.1.1 Inkjet printing. The inkjet apparatus used to fill the reservoirs of Microlab prototype 091096-4, TRL prototype 021397-2#2, and TRL prototype 081297-1#10 was made from an off-the-shelf inkjet printer (Hewlett Packard Deskjet 400). These printers were not designed to deliver solutions other than inks or to accurately control the amount of ink deposited to within a few drops. As a result, the number of drops deposited by the inkjet printer into a reservoir can be a source of variation in chemical loading.

A study was done to examine the variance in the inkjet printing method. A solution of sodium fluorescein in water was prepared and inserted into an HP inkjet cartridge (HP 51626A). 100 total drops (50 + 50 drops) of this solution were deposited into PBS in each of thirty polystyrene cuvettes for analysis by fluorescence spectroscopy. The mean mass deposited in each cuvette was determined to be 416 ng with a standard deviation of 35 ng. However, the mass of fluorescein deposited in 100 drops of solution ranged from a low value of 355 ng to a high value of 509 ng. Also, there was a trend in the samples indicating that more mass was deposited in later samples than in earlier ones. This type of variation could explain both the situations where the fluorescein recovered is less than the calculated amount loaded (Microlab prototype 091096-4 and TRL prototype 081297-1#10) and where more fluorescein is recovered than the calculated amount loaded (TRL prototype 021397-2#2 and TRL prototype 081297-1#10).

5.4.2.1.2 Microinjection. The syringe microinjector used to fill the reservoirs of TRL prototype 081297-1#11 was designed to inject biological material (i.e. DNA, proteins, etc.) into a liquid environment (i.e. inside a cell). This is usually accomplished with a drawn glass capillary needle with an orifice diameter of 1-10 μm. Filling reservoirs involves injecting a liquid into air (instead of another liquid) through a metal needle having an internal orifice diameter of 110 μm. The method of inkjet printing allowed the user to determine a range of chemical deposited by experimental means. Experimental determination of mass deposited by microinjection is extremely difficult. Therefore, values for the mass loaded into a reservoir by microinjection are calculated by knowing the concentration of the filling solution and the volume of material injected into the reservoir. These calculations assume that the filling solution (usually water,

PEG 200, and the chemical to be released) is well mixed and the volume injected is accurate. Variations in concentration or volume injected could cause significant variation in the calculated amount loaded and the amount recovered in release experiments.

Evaporation of water is fast when dealing with nanoliter size drops. The operator has only several seconds to place the drop in the reservoir after it is formed on the tip of the needle before the water evaporates, possibly leaving some of the mass of chemical to be deposited in the reservoir on the tip of the needle. This may cause subsequent drops from the needle to be more concentrated and contain more chemical than expected. This problem can be exacerbated by the another possible source of variation, wetting of the outside surface of the needle. Drops are placed in reservoirs by touching the drop surface to the side wall of the reservoir. Capillary action pulls the drop off of the tip of the needle and into the reservoir. However, the filling solution will sometimes wet the outside surface of the needle, causing the drop on the tip to have less volume than expected. This material left on the outside of the needle may then be deposited in other reservoirs accidentally. Variations in volume injected are sometimes significant enough to be observed visually though a microscope.

Nearly twice as much fluorescein was recovered from TRL prototype 081297-1#11 than was calculated to have been loaded. This variation may be attributed to the reasons discussed in the previous paragraphs. However, the fact that these two reservoirs contained nearly the same mass of fluorescein shows that this filling method is precise (i.e. reproducible), but not accurate. There may exist another source of systemic error affecting accuracy of microinjection of fluorescein that has not been identified. The amount of ^{45}Ca recovered from TRL prototype 081297-1#11 is lower than the calculated amount loaded. This could be attributed to the sources of variation discussed in the previous paragraphs, or could have resulted from device or release experiment design specific sources discussed in section 5.4.2.3.

5.4.2.2 Properties of chemicals released. The inherent properties of the chemicals released can also affect calculations of mass deposited and recovered. Probably the most likely reason for variation in amount of fluorescein deposited and recovered is the process of photobleaching. Photobleaching is a process where a solution of a fluorescent dye, such as fluorescein, loses some of its fluorescence intensity over time. This can be caused by exposure to light and/or dissolved oxygen[2]. Exposure to light and dissolved oxygen for an extended period of time, such as that encountered during a release experiment extending over several days, may photobleach the fluorescein in solution. Therefore, the amount recovered would appear to be less than that originally loaded into the reservoirs, as seen with Microlab prototype 091096-4 and TRL prototype 081297-1#10.

It is known that the fluorescence of fluorescein is highly dependent on the pH of the solution it is dissolved in[3]. The pK_a of fluorescein's monoanionic form is 6.7. Therefore, fluorescein exists primarily as its less fluorescent monoanion in the pH range of 4.4 to 6.7 and as its highly fluorescent dianion at pH's greater than 6.7. The pH of PBS is buffered at 7.2, while the pH of 0.145 M NaCl solutions in DI water range approximately between 5.4-6.0. Fluorescein calibration standards were always made with the same solution as the sample being analyzed (i.e. calibration standards for release experiments conducted in PBS were made with PBS). Therefore, pH would not be expected to affect the results of fluorescein release studies. However, any changes in the pH of the release medium during the release experiment would cause the pH of the release samples to differ from the pH of the calibration standards. Such differences in pH could cause errors in the calculation of the amount of fluorescein released from a reservoir. This kind of pH dependent error would not be expected in experiments conducted in PBS because the solution is buffered at a pH of 7.2. However, the 0.145 M NaCl solution is not buffered, and its pH is near the pK_a of fluorescein. Therefore, small changes in release medium pH with respect to the pH of calibration standards could cause significant errors in fluorescence measurements. The amount of fluorescein recovered could appear to be greater than that deposited, such as that observed for TRL prototype 081297-1#11, if the pH of the release medium were somehow increased during the release study. This could happen in an unbuffered solution if, for example, the DI water system failed to operate properly when a plug of high pH water came into the system from the city water supply or if basic materials leached into the

release medium from the microchip package or epoxy. It is also possible that the error in fluorescein recovered from TRL prototype 081297-1#11 was caused by the filling method or a source of error not yet identified.

Other chemical related issues include the interaction of different chemicals released into solution and interaction of the released chemical with the release medium. First, experiments conducted with mixtures of fluorescein and ^{45}Ca showed no interaction effects between these two chemicals over the range of concentrations relevant to the prototype devices and the multiple chemical release studies. Second, there were no interaction effects between fluorescein and the release medium. Release of fluorescein into PBS or unbuffered saline solution should not affect release calculations as long as the fluorescence calibration standards are made with the same solution (PBS or unbuffered saline solution, with the same pH as the release medium) for the relevant range of fluorescein concentrations. There were, however, possible release medium interactions with ^{45}Ca. ^{45}Ca was released in its ionic form ($^{45}Ca^{2+}$) as its chloride salt, $CaCl_2$. As a result, PBS could not be used as the release medium for the multiple chemical release studies of TRL prototype 081297-1#11. The phosphate ion in PBS could cause the ^{45}Ca to fall out of solution as an insoluble calcium phosphate complex. Therefore, release studies involving ^{45}Ca had to be carried out in a saline solution not containing the phosphate ion.

5.4.2.3 Device or release experiment design. Variation in the amount of chemical deposited in a reservoir and the amount recovered in release experiments can also be attributed to the device or experiment design. One device design issue is that the square pyramid shape of the reservoir and small release opening may cause some material to remain in the reservoir due to surface tension effects, interfacial phenomena, or air bubbles. Another device design issue is that leakage from other filled reservoirs of a prototype could contribute to variations in mass of chemical recovered. Each reservoir is checked with a light microscope for evidence of membrane perforation and chemical leakage every time the prototype is removed from the release medium during a release experiment. However, it is possible that leak-causing defects might be missed if they are small or hidden. A release experiment design issue deals with the rinsing of prototypes during release experiments. The prototype is rinsed with DI water and gently dried with nitrogen after it is taken out of the release medium for examination with a light

microscope or for a change in release medium. Material that has not yet released into the release medium could be washed away during this rinsing process, making the mass released from a reservoir appear lower than the mass originally loaded. A final release experiment design issue involves the sealing of a reservoir before it is finished releasing. This issue applies only to reservoir 6 of Microlab prototype 091096-4. This reservoir was sealed with epoxy after the release of fluorescein was thought to be complete. However, it is possible that some fluorescein was left in this reservoir when it was sealed, possibly resulting in the recovery of a smaller amount of material than the reservoir was filled with.

5.5 Conclusions. The chemical release studies presented in this chapter demonstrate operational proof-of-principle for a prototype microchip in which multiple chemicals can be stored inside the microchip itself and can be released on demand. The "pulsatile" release of chemicals in their pure form or dissolved in a low molecular weight liquid polymer was achieved from prototype microchips without the use of moving parts. The release studies presented in this chapter also proved useful for defining key areas for future research including methods to improve the reliability of the membrane opening process and development of reservoir filling methods affording better control over the amount of chemical deposited in each reservoir.

5.6 References.

1. "Fluorescein" in *The Sigma-Aldrich Handbook of Stains, Dyes, and Indicators* (ed. Green, F.J.) 373-375 (Aldrich Chemical Co., Milwaukee, WI, 1990).
2. Herman, B. "Photobleaching" in *Fluorescence Microscopy* 42-43 (BIOS Scientific Publishers Limited / Springer-Verlag, Oxford, UK / New York, NY, 1998).
3. Martin, M.M. & Lindqvist, L. "The pH dependence of fluorescein fluorescence." *Journal of Luminescence* **10**, 381-390 (1975).

6. GOLD MEMBRANE DISINTEGRATION

6.1 Introduction. The first part of this chapter describes experiments for the *in situ* observation of the steps of gold membrane disintegration. Disintegration, as used herein, refers to the "falling apart" of a gold membrane over a reservoir resulting from gold corrosion and possibly, applied physical stresses. The visualization of the membrane disintegration process was achieved by videotaping the corrosion of gold membranes through a microscope. The results of the *in situ* membrane disintegration experiments are then combined with gold corrosion concepts and data from chapter 4 and observations about reservoir opening presented in chapter 5 to develop a qualitative mechanism for the disintegration of thin, gold membranes covering chemical reservoirs. The proposed mechanism should provide a better understanding of device operation, which may lead to improved device reliability.

6.2 Experimental Methods.

6.2.1 Apparatus for *in situ* monitoring of gold membrane disintegration. TRL prototypes for *in situ* experiments were fabricated as described in section 3.2.1.2. The gold membranes of each reservoir were examined for defects using light microscopy. Some of the reservoirs that were defect free were filled with a solution of PEG 200 (liquid polymer) in DI water (15/85 v/v) by microinjection as described in section 3.2.2.2. The TRL prototypes for the *in situ* experiments were then sealed using the third method of reservoir sealing described in section 3.2.3.

A large square hole was milled through the die cavity of a 149 pin, plastic PGA microchip package (Ibiden Co., Ltd.), leaving the bonding pads on only one side of the die cavity intact. The pins not connected to the remaining bonding pads were removed by milling. The glass microscope slide containing the filled and sealed TRL prototype was attached to the plastic package with 5 minute epoxy (Devcon 5 Minute Epoxy) so that the prototype sat in the hole milled through the die cavity of the package. The prototype was wire bonded to the bond pads on the package as described in section 3.2.4.2.

A hole the size of the plastic PGA package was milled though a clear plastic culture dish. The packaged prototype was sealed into the hole in the plastic culture dish with 5 minute epoxy.

More 5 minute epoxy was used to cover the wirebonds of the prototype to protect them from the solution that will eventually be placed in the culture dish. A completely packaged prototype for *in situ* membrane disintegration experiments is show in figure 6-1.

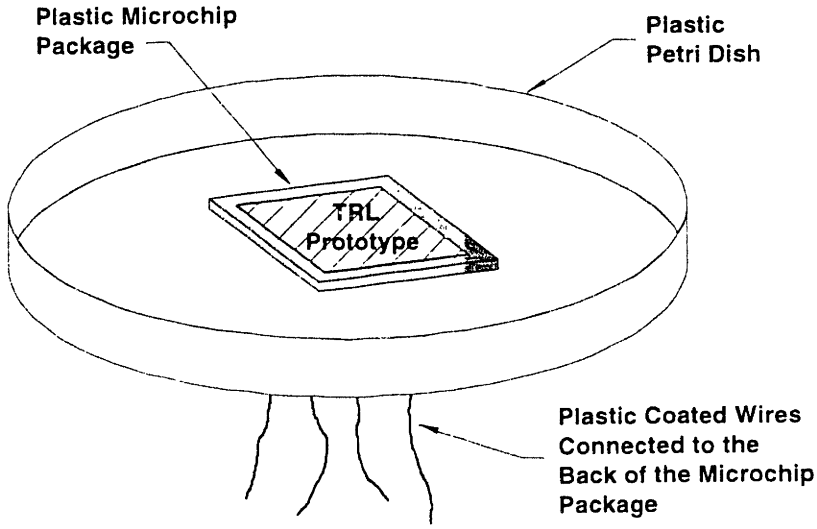

Figure 6-1. Diagram of packaged TRL prototype for *in situ* experiments.

The plastic culture dish was placed under a light microscope (Olympus BH with a ULWD MS Plan 20x objective and a 6.7x photo eyepiece) equipped with a black and white, CCD camera (Hitachi KP-111). The prototype was lit by the reflection light source of the microscope, and the output from the camera was recorded onto beta format videotape (Sony) using a beta recorder. The culture dish was filled with 0.145 M NaCl solution made with DI water. The top, electrode containing surface of the TRL prototype was completely covered with the electrolyte. A fiber optic light source (Dolan-Jenner Fiber Lite, Series 180) was positioned under the culture dish (for some experiments) so that light could be shined up through a reservoir as its membrane was disintegrating. The light would not be visible through the gold membrane until the membrane began to perforate and disintegrate. The appearance of light through the membrane could help determine how and when the membrane disintegrates. A diagram of the experimental set up including the microscope and fiber optic light can be found in figure 6-2.

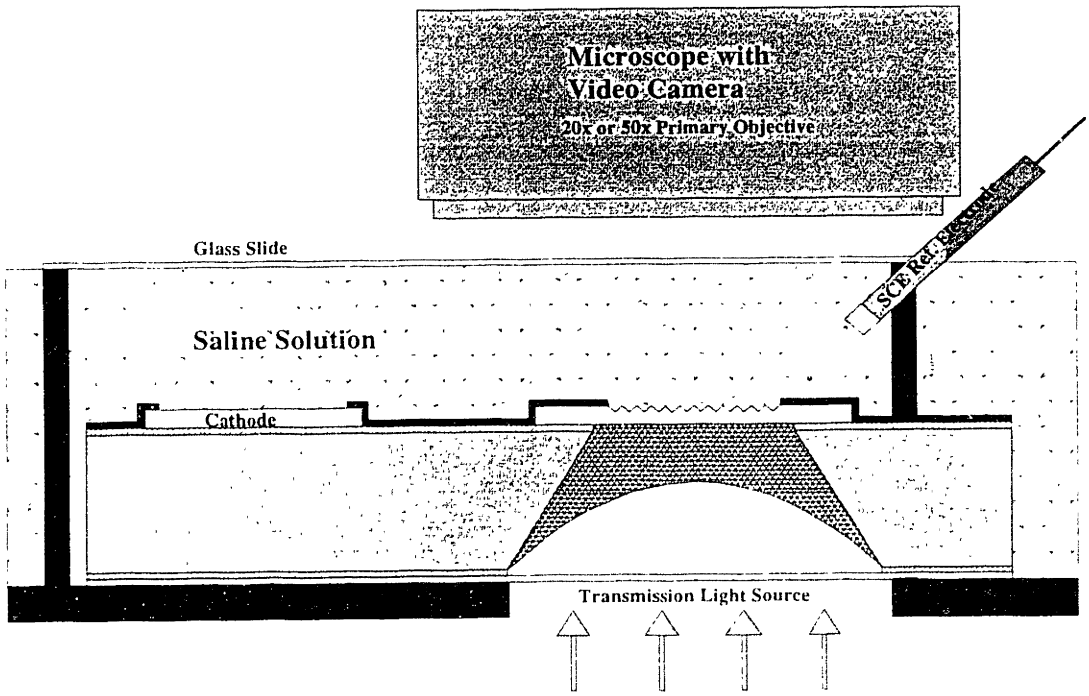

Figure 6-2. Diagram of microscope and *in situ* experiment set up.

A saturated calomel reference electrode (SCE - the same as that used for the chemical release experiments in chapter 5) was inserted into the electrolyte in the culture dish and positioned no more than 5-7 mm away from the anode membrane shortly before an electric potential was to be applied. An electric potential of +1.04 relative to the SCE was applied to the anode membrane for 30-60 seconds. The solution in the culture dish was not stirred before, during, or after the application of the electric potential. The SCE was positioned near the next anode membrane, and the process for application of an electric potential was repeated. The same solution was used for all the *in situ* experiments conducted with a single prototype. Information specific to each prototype will be presented in the next three sections.

6.2.2 TRL prototype 081297-2#6. Reservoirs 1,3,5,19,21,30 were filled with the PEG 200 solution described in section 6.2.1 using microinjection. Table 6-1 lists the volume of solution deposited into each reservoir.

Table 6-1. Volume of solution deposited in each reservoir of TRL prototype 081297-2#6 by microinjection.

Reservoir #	Volume Deposited in Each Reservoir
13,34	0 nL
21	≤ 10 nL
1,30	10 nL
3,19	30 nL
5	60 nL

The reservoirs had a noticeable amount of liquid in them immediately after filling. However, most of the water appeared to quickly evaporate, leaving the reservoir with only PEG 200 in the bottom of the reservoir. The material in the reservoir remained in liquid form for the entire experiment because the polymer does not evaporate. No gold membranes were observed to crack or tear after reservoir filling (see section 3.4.3). The prototype was sealed and packaged as described in section 6.2.1.

An electric potential of +1.04 volts vs. SCE was applied to the gold anode membranes of the reservoirs in the following order – 34, 19, 1, 5, 3, 13, 30, and 21. The fiber optic light source was used to shine light through each reservoir as the gold membrane disintegrated. This light was usually turned on a few seconds before the application of the electric potential. However, the light was hard to align correctly with the reservoir and had to be manually adjusted during several of the experiments to maximize the light intensity.

6.2.3 TRL prototype 081297-2#10. Reservoirs 2,5,17,21,29,32 were filled with the PEG 200 solution described in section 6.2.1 using microinjection. Table 6-2 lists the volume of solution deposited into each reservoir.

Table 6-2. Volume of solution deposited in each reservoir of TRL prototype 081297-2#10 by microinjection.

Reservoir #	Volume Deposited in Each Reservoir
17	≤ 10 nL
21	≤ 20 nL
2,5	30 nL
29,32	60 nL

The reservoirs had a noticeable amount of liquid in them immediately after filling. However, most of the water appeared to quickly evaporate, leaving the reservoir with only PEG 200 in the bottom of the reservoir. The material in the reservoir remained in liquid form for the entire experiment because the polymer does not evaporate. No gold membranes were observed to crack or tear after reservoir filling (see section 3.4.3). The prototype was sealed and packaged as described in section 6.2.1.

An electric potential of +1.04 volts vs. SCE was applied to the gold anode membranes of the reservoirs in the following order – 2, 5, 21, 17, 29, and 32. The fiber optic light source was used to shine light through each reservoir as the gold membrane disintegrated. The light was positioned very close to the back of the prototype in order to eliminate the light alignment problems encountered with TRL prototype 081297-2#6. This light was usually turned on a few seconds before the application of the electric potential.

6.2.4 TRL prototype 081297-2#4. The backside of this prototype was etched by reactive ion etching at a higher bias (425 volts, instead of 300 volts) and for a longer time (18 min. at 300 volts + 6 min. at 425 volts, instead of 16 min. at 300 volts) to ensure that the VTR SiN_x layer under the gold membrane anode was completely removed. Reservoirs 20 and 30 were then filled with a fluorescein solution that had a fluorescein concentration of 60.5 mM in 85/15 v/v DI water/PEG 200 using microinjection. Table 6-3 lists the volume of solution deposited into each reservoir.

Table 6-3. Volume of solution deposited in each reservoir of TRL prototype 081297-2#4 by microinjection.

Reservoir #	Volume Deposited in Each Reservoir
30	30 nL
20	60 nL

The reservoirs had a noticeable amount of liquid in them immediately after filling. However, most of the water appeared to quickly evaporate, leaving the reservoir with only fluorescein and PEG 200 in the bottom of the reservoir. The material in the reservoir remained in liquid form for the entire experiment because the polymer does not evaporate. No gold membranes were observed to crack or tear after reservoir filling (see section 3.4.3). The prototype was sealed and packaged as described in section 6.2.1.

An electric potential of +1.04 volts vs. SCE was applied to the gold anode membranes of the reservoirs in the following order – 14, 16, 34, 20, and 30. The fiber optic light source was not used for the *in situ* experiments of TRL prototype 081297-2#4. (Note: Reservoirs 14, 16, and 34 were empty and used only as test reservoirs before opening the fluorescein-filled reservoirs.)

6.3 Experimental Results.

6.3.1 TRL prototype 081297-2#6. The gold membranes of TRL prototype 081297-2#6 corroded with the application of the electric potential. This is evidenced by the transmission of light through the corroded membranes. However, the membranes did not completely disintegrate (i.e. they corroded, but did not "fall apart") due to the presence of a residual silicon nitride film under the gold membrane, which held in place the small gold pieces remaining after gold corrosion. The nitride membrane was not supposed to be present, but it did allow the visualization of how corrosion progresses across the gold membrane. Figure 6-3 shows a series of still photos from the filmed corrosion of reservoir 5 over a period of 11.0 seconds. Notice that the light begins to appear in the corners of the membrane first. Light then appears along the edges of the membrane. Finally, the light progresses toward the middle of the reservoir, indicating that the entire gold membrane surface has been perforated by corrosion. The gold membrane would have surely fallen apart if it were not supported by the nitride membrane.

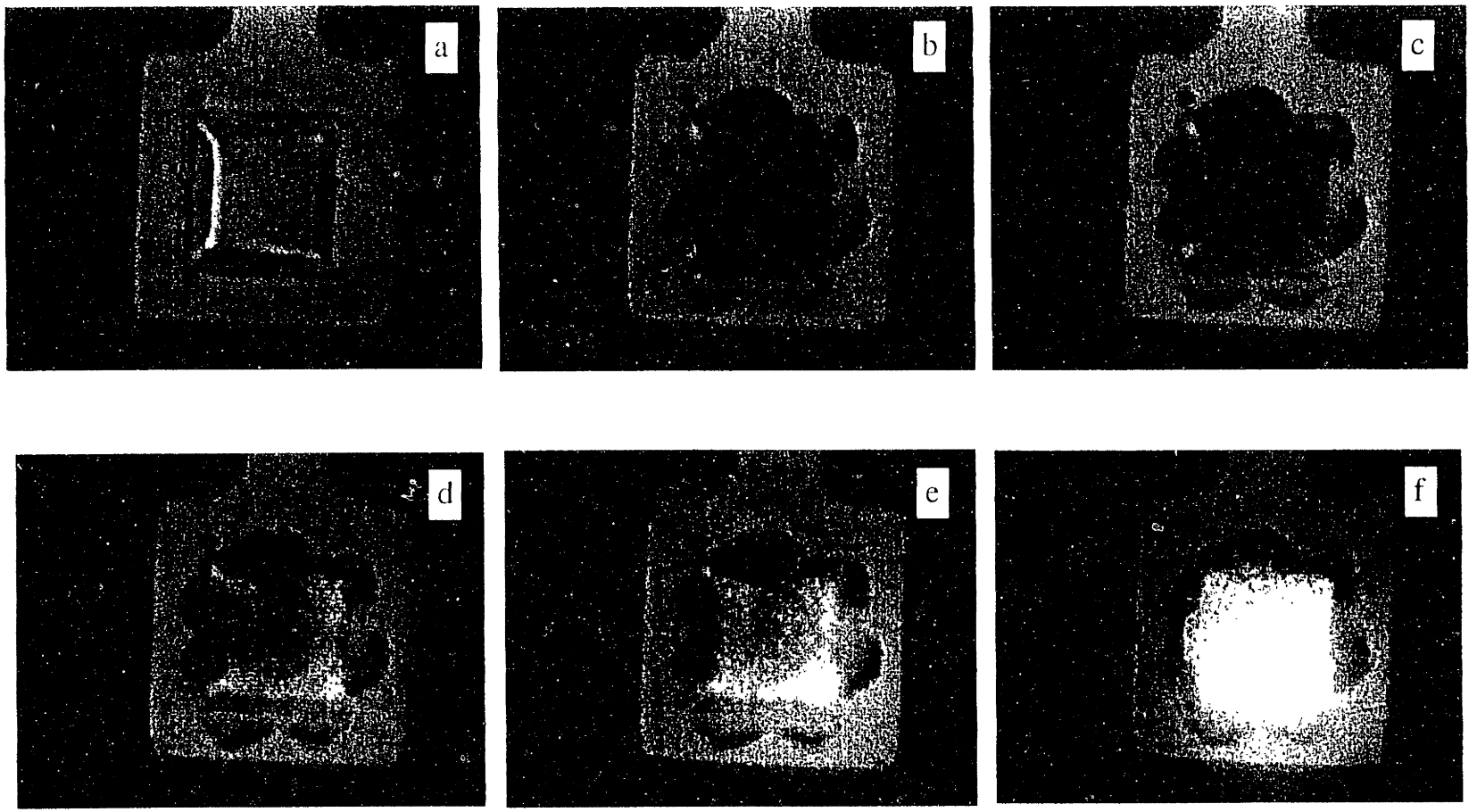

Figure 6-3. Light coming through the gold membrane of reservoir 5 of TRL prototype 081297-2#6 as the membrane corrodes during the *in situ* experiments. The membrane at (a) 0.0 sec, (b) 3.2 sec, (c) 4.6 sec, (d) 5.6 sec, (e) 6.4 sec, and (f) 11.0 sec after the application of +1.04 volts vs. SCE in 0.145 M NaCl solution..

Reservoir 30 of TRL prototype 081297-2#6 resembled the membrane of reservoir 5 in that it had been perforated across the entire gold surface after 11.5 seconds of applied potential. This is evidenced by the appearance of light passing though the membrane. However, reservoir 30 "popped" after 11.7 seconds of applied potential, quickly releasing the PEG inside it. Examination of the membrane 13.3 seconds later indicates that the membrane failed along 2 or 3 edges, giving rise to a "flap" of material. This flap was most likely made of the residual silicon nitride membrane also seen in reservoir 5 because the gold was perforated across its entire surface and would not have had the structural integrity to form such a flap. Figure 6-4 shows a series of still photos from the filmed corrosion of reservoir 30 over a period of 13.3 seconds.

The other reservoirs of TRL prototype 081297-2#6 corroded, but did not disintegrate, similar to reservoir 5. Therefore, no correlation between the amount of material in a reservoir and disintegration could be made.

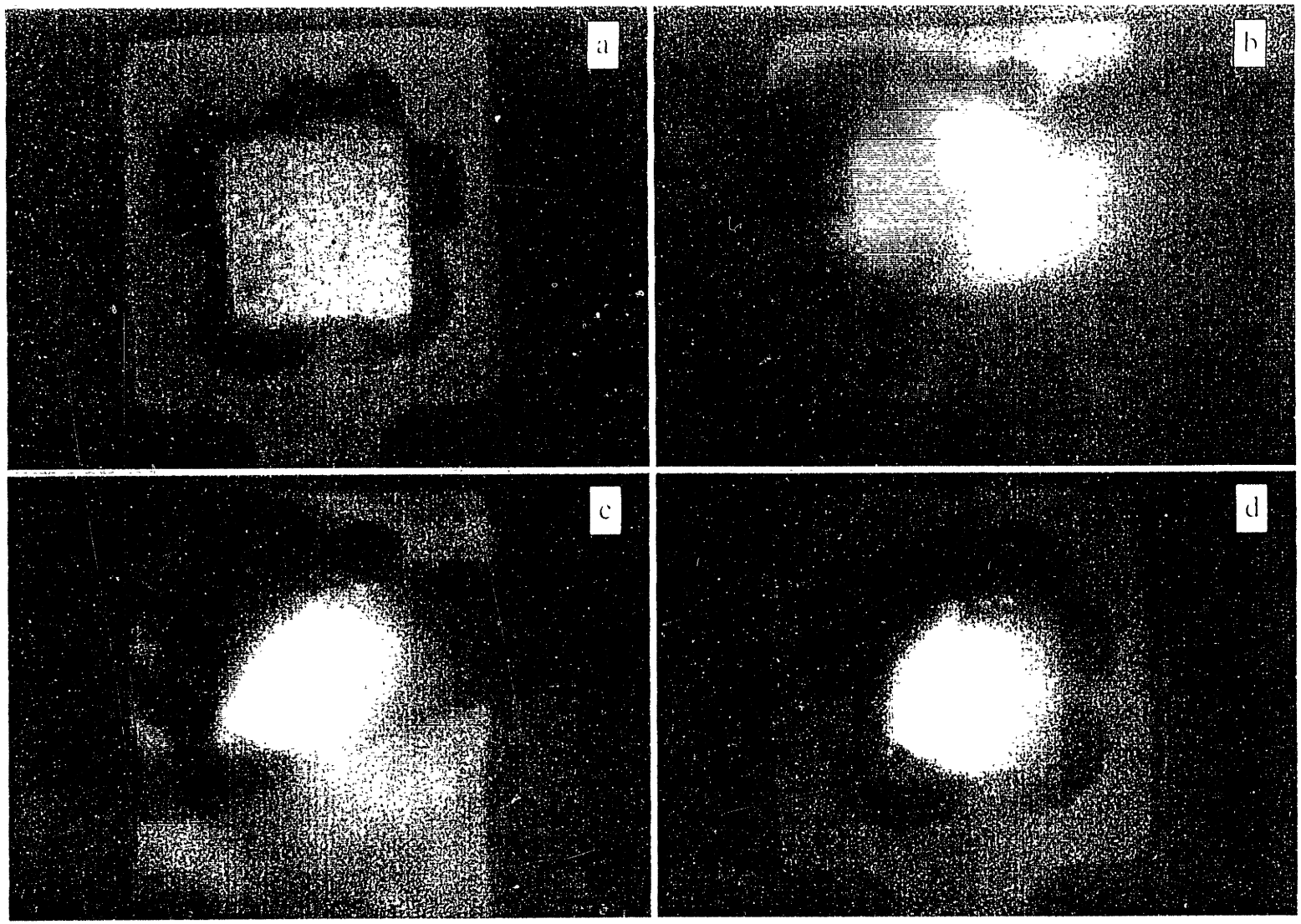

Figure 6-4. The "popping" of the gold membrane of reservoir 30 of TRI prototype 081297-2#6 after the weakening of the membrane during the *in situ* experiments. The membrane at (a) 11.53 sec, (b) 11.73 sec, (c) 11.93 sec, and (d) 13.33 sec after the application of +1.01 volts vs. SCE in 0.145 M NaCl solution.

6.3.2 TRL prototype 081297-2#10. The gold membranes of TRL prototype 081297-2#10 corroded with the application of the electric potential, but did not disintegrate, due to the presence of a residual silicon nitride film under the gold membrane. However, three of the six gold membrane anodes "popped", similar to reservoir 30 of TRL prototype 081297-2#6. The gold membranes of the other three reservoirs corroded, but did not pop. Therefore, no correlation between the amount of material in a reservoir and disintegration could be made.

Reservoir 32 opened in a slightly different way than the other reservoirs that popped, and a series of still photos of this opening process are given in figure 6-5. Figure 6-5b shows a small crack that has formed in the lower right portion of the gold membrane, as indicated by the passage of light through the crack. It appears in figure 6-5c that the corroded gold membrane partially detached from the nitride membrane, formed a gold flap, and was blown outward, probably due to the higher pressure in the reservoir escaping from the crack in the lower right portion of the membrane. The fiber optic light source is a possible source of this increased pressure in the reservoir is discussed in section 6.4.1.2. Figure 6-5d shows that the nitride membrane proceeded to fracture on three sides and blow out, forming a nitride flap and allowing light to freely pass through the reservoir opening. The nitride and gold flaps appear to be falling back down to cover the reservoir in figure 6-5e. The two flaps had returned to their original positions in figure 6-5f, with only the small crack on the lower right portion and a small hole in the lower middle portion of the membrane to indicate any perforation of the membranes. The whole process of flap formation and reservoir "popping" only took 0.16 seconds to complete.

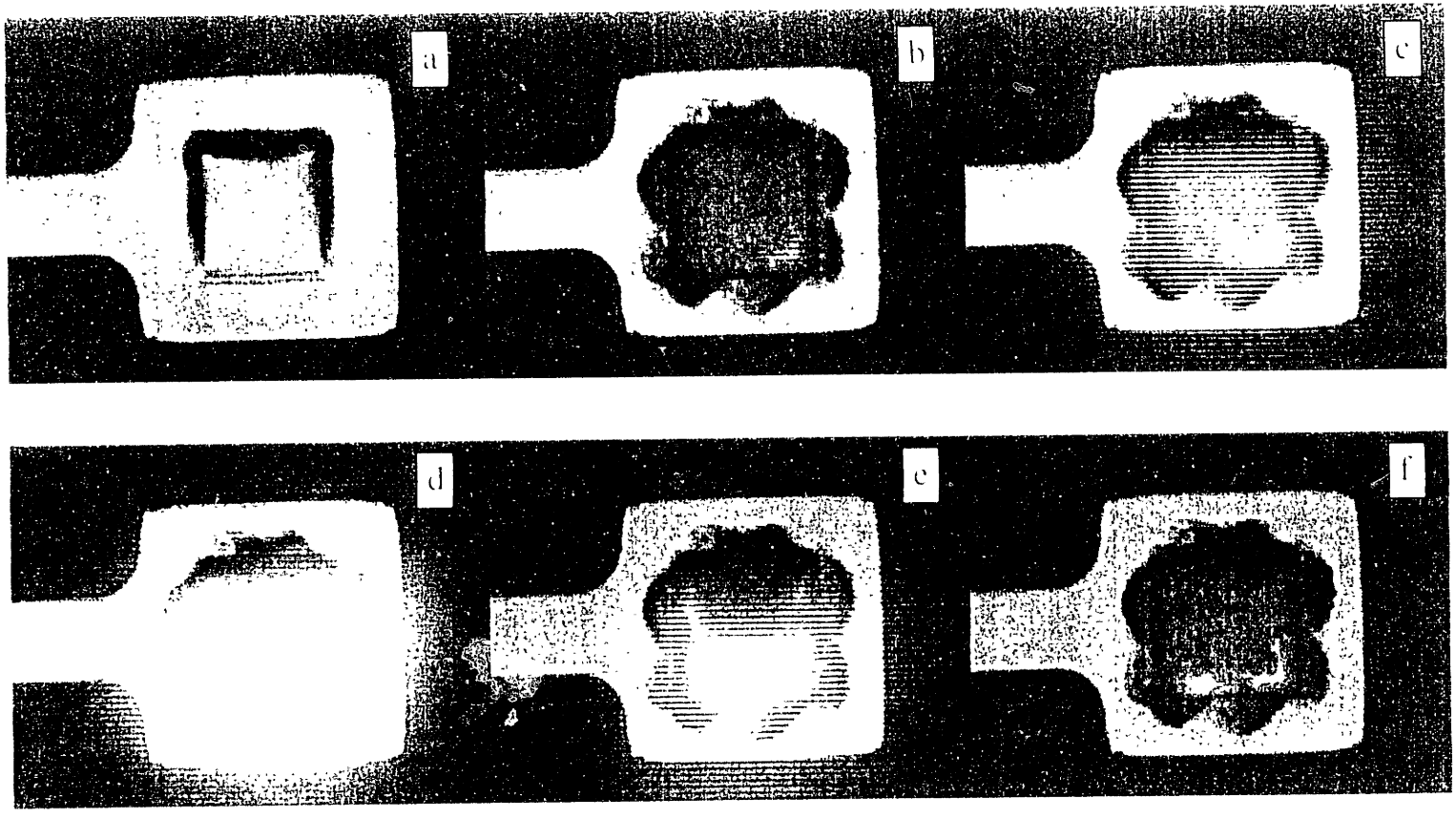

Figure 6.5 The "popping" of the gold membrane of reservoir 32 of TRI prototype 081297_2#10 after the weakening of the membrane during the *in situ* experiments. The membrane at (a) 0.00 sec, (b) 11.97 sec, (c) 12.00 sec, (d) 12.03 sec, (e) 12.10 sec, and (f) 12.13 sec after the application of +1.01 volts vs. SCE in 0.145 M NaCl solution

6.3.3 TRL prototype 081297-2#4. Scanning electron microscopy was used to verify that there was no residual silicon nitride membrane under the gold membranes of TRL prototype 081297-2#4. SEM micrographs of the reservoir facing side of a gold membrane from a piece of TRL prototype 081297-2#4 are given in figure 6-6. Notice that the surface appears free of any nitride film, as evidenced by the clearly visible gold grains. The gold grain boundaries appear to be slightly grooved. This may have been caused by physical sputtering of the gold due to the plasma etching at a higher power for an extended period of time. (The large white object in figure 6-6 is most likely a dust particle.)

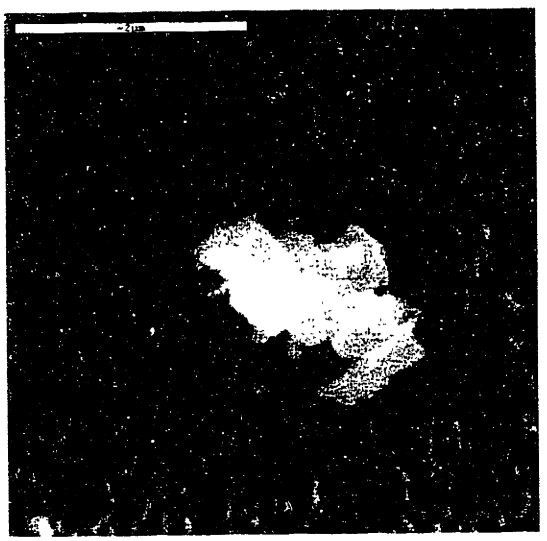

Figure 6-6. Scanning electron micrograph of the reservoir side of a gold membrane of TRL prototype 081297-2#4 whose silicon nitride layer has been removed by plasma etching. The membrane is viewed on an angle to show surface texture, indicating the complete removal of the nitride.

Figure 6-7 shows a series of still photos with time for reservoir 20. Notice that the gold membrane anode of this reservoir disintegrated ("fell apart") in several places after 10.60 seconds. Parts of the membrane appeared to fall into the reservoir when it failed, as shown in figures 6-7c and 6-7d. The videotape clearly showed the fluorescein/PEG 200 mixture releasing from this reservoir immediately after the gold membrane failed. However, this fluorescein release is too faint to be seen in any of the still images of figure 6-7.

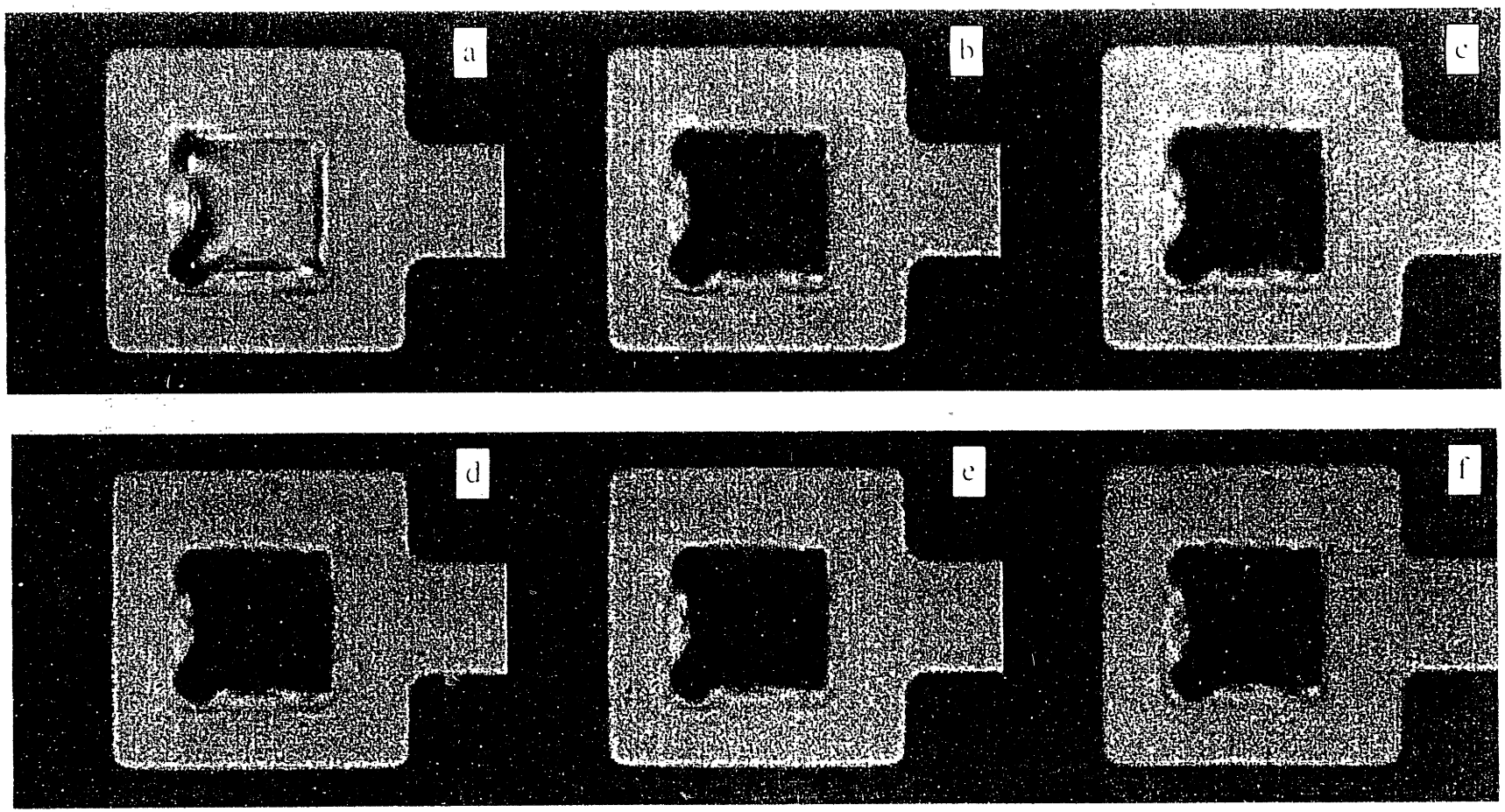

Figure 6.7. The disintegration of the gold membrane of reservoir 20 of TRI prototype 081297-2#4 after the weakening of the membrane during the *in situ* experiments. The membrane at (a) 0.00 sec, (b) 6.50 sec, (c) 10.60 sec, (d) 10.64 sec, (e) 10.67 sec, and (f) 11.50 sec after the application of +1.04 volts vs. SCE in 0.145 M NaCl solution

6.4 Discussion.

6.4.1 Gold membrane disintegration mechanism. This section combines the experimental observations presented in chapters 3 thru 6 in order to draw qualitative conclusions about how gold membranes corrode and fall apart ("disintegrate") with an applied electric potential in chloride containing solutions.

6.4.1.1 Role of corrosion. Gold membranes have repeatedly demonstrated preferential corrosion along grain boundaries (intergranular corrosion). Experiments from chapter 4 showed the progression of corrosion along grain boundaries in thin gold films with the duration of the applied electric potential, as seen in figure 4-20. Notice that the grooving at the grain boundaries increased with the duration of the applied potential. Figure 4-28 clearly demonstrates the intergranular nature of gold membrane corrosion by comparing an uncorroded and a corroded gold film from TRL prototype 021397-1#6.

The results presented in chapter 5 for reservoirs 18 and 20 of TRL prototype 081297-1#10 showed that not all membrane corrosion is uniform across the membrane surface. Localized attack can sometimes occur. However, reservoirs 18 and 20 still show signs of a preference for intergranular corrosion. The holes in these membranes appear to have formed by corrosion around a single grain or group of grains, causing them to fall out of the membrane and form a hole (see figures 5-15, 5-16, and 5-24).

The results of the *in situ* experiments of this chapter also provide evidence of intergranular corrosion. Notice in figure 6-3e that the light shining through the corroded membrane at 6.4 seconds is transmitted around what appear to be gold grains. This was observed in all *in situ* experiments.

Rapid corrosion also takes place along the interface between the edge of the patterned SiO_2 overlayer and the gold membrane, giving rise to non-uniform corrosion of the gold membranes. There are two possible reasons for this non-uniformity in gold corrosion across the membrane. One reason relates to the presence of a non-uniform, electric potential distribution across the membrane. An uncorroded, intact gold electrode will evenly distribute an applied electric potential across its surface due to its low resistivity, but this resistivity will increase as

the electrode corrodes and becomes thinner. The electric potential of the gold along the edge of the patterned SiO_2 overlayer will remain at the user defined potential because resistive losses along the protected (i.e. covered by SiO_2) gold trace are negligible. However, the increase in resistance across the thinning gold membrane will cause the potential to drop between the edge of the SiO_2 overlayer and the middle of the exposed gold membrane. This potential drop may increase to the point that the gold at the middle of the electrode is at a low enough potential so as to significantly slow the gold corrosion process there. This effect is observed as a more rapid corrosion of the gold along the border between the SiO_2 overlayer and the gold membrane than at the center of the membrane. This explanation is supported by the results of the *in situ* experiment shown in figure 6-3. Notice that the gold membrane is perforated and light is transmitted through the corners and edges of the gold membrane before the center of the membrane.

A second possible reason for increased corrosion rates at the interface of the patterned SiO_2 overlayer and the gold is the presence of crevice corrosion. The corrosion rate in a crevice can vary from that on the bulk material due to the formation of a micro-environment in the crevice that is much different from the surrounding medium[1]. For example, large differences in pH and dissolved oxygen between a crevice and bulk medium are not uncommon. These differences in pH or dissolved oxygen can cause the corrosion rate in a crevice to be much faster than that seen for metal exposed the bulk solution. Non-uniformities in corrosion rates caused by electrode thinning or crevice corrosion can seriously affect the reliability of microchip operation and will be discussed in section 6.4.2.4.

6.4.1.2 Role of physical stress. A number of different stresses can act on a gold membrane before, during, or after the reservoir filling process. The stresses caused by the fabrication process and by the drying of certain liquid materials in the reservoirs during the filling process were covered in section 3.4.3. Stresses acting on the gold membranes during its use as a chemical release device (after filling) can be broken down into internal and external stresses.

Internal stresses are those that are exerted on the gold membrane from inside of the reservoir. One such stress is that exerted by a curved liquid surface. This stress would be tensile if the liquid wetted the reservoir walls, as shown schematically in figure 6-8. The stress exerted perpendicular to the membrane surface (τ) is described by the Young-Laplace equation (see equation 6.1) and is dependent on the physical properties of the liquid (i.e. surface tension (γ) and radius of curvature (r)). Intact, uncorroded gold membranes of devices having a thickness of at least 2,000 Å that were filled with a material that remains in liquid form (i.e. the liquid polymer, PEG 200) were never observed to break due to the force exerted by the curved liquid surface. The stress exerted on a gold membrane by a curved liquid surface is estimated in section 6.4.1.3 using the Young-Laplace equation.

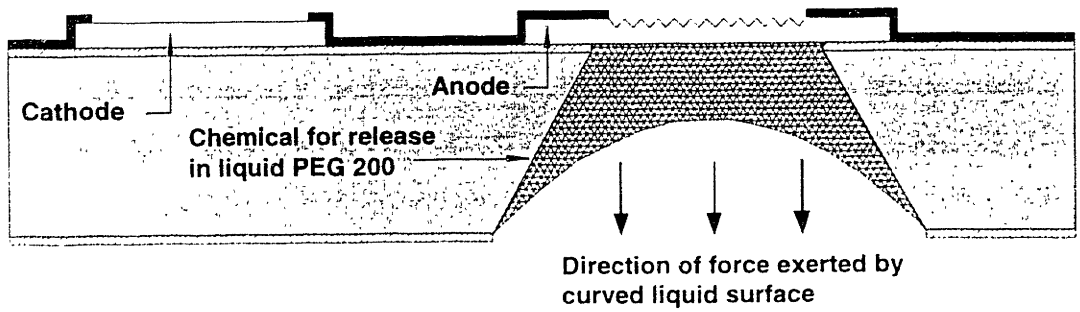

Figure 6-8. Diagram of a curved liquid surface in a filled reservoir.

$$\tau = \frac{2 \cdot \gamma}{r} \tag{6.1}$$

An internal stress observed only in the *in situ* experiments under the microscope was due to pressure build up inside the reservoir. Some of the *in situ* experiments required the use of a fiber optic light source, whose emitted light generated a significant amount of heat. This light was often placed near the glass slide sealing the back of the reservoirs to be opened in order to maximize the amount of light transmitted through the membrane when it corroded. The light most likely heated the air or the PEG 200 in the selected reservoir, causing a pressure build up. The failure of the gold membranes of TRL prototypes 081297-2#6 and 081297-2#10 that

"popped" after gold membrane corrosion during the *in situ* experiments were most likely caused by this pressure build up due to heating. Reservoirs "popping" can be observed in figures 6-4 and 6-5. It is not expected that this type of stress existed in any of the chemical release experiments and is limited to the *in situ* experiments only.

External stresses could also be exerted on the gold membranes. Shear stresses resulting from the stirring of the release medium in chemical release experiments would be one example. The flow of liquid release medium into a reservoir through holes formed in the membrane by corrosion could be an external stress on the membrane. An example from *in situ* experiments is the force exerted on the outside of the membrane by the hydrostatic pressure of the solution above it. The failure of the gold membrane of reservoir 20 of TRL prototype 081297-2#4 during the *in situ* experiments is shown in figure 6-7. The membrane fails after gold corrosion by having pieces of the membrane fall down into the reservoir, as shown in the rightmost portion of the membrane in figure 6-7c. This could have been caused by the hydrostatic pressure of the water above the weakened membrane, the stress exerted by the fluorescein/PEG 200 mixture inside the reservoir, or both.

It is important to note that the reservoirs of some devices did not open, even after the gold membrane had corroded. It was verified in nearly all of these cases that the reservoir did not open due to the presence of a nitride layer under the gold. Reservoir 5 of TRL prototype 081297-2#6 is a good example of a reservoir that did not open for this reason and is shown in figure 6-3. Reservoirs covered by a nitride layer could still open, depending on the thickness of the nitride layer and the magnitude of the stress exerted on it, but not until the gold membrane was corroded. For example, it was verified by SEM that TRL prototype 081297-2#6 had a nitride layer present under the gold layer. This would explain why some of these reservoirs did not appear to open during the *in situ* experiments. This also occurred with the reservoirs of TRL prototype 081297-2#10. However, some of these reservoirs did open after the gold membrane was corroded and enough stress was applied. The pressure build up that opened (in this case, "popped") the membranes of some of the reservoirs of TRL prototypes 081297-2#6 and 081297-2#10 (see figures 6-4 and 6-5) probably exerted large stresses on the nitride membrane. The key point is that no reservoirs (not even the ones that "popped") covered by a gold membrane were observed to open in any experiments until the gold had been weakened by corrosion.

6.4.1.3 Estimation of gold membrane stress and failure. The Young-Laplace equation can be used to estimate the stress exerted on gold membranes by a curved liquid surface, as was discussed in section 6.4.1.2. The model reservoir filling solution for these calculations is 30 nL of a 15:85 v/v PEG 200:water solution. (30 nL of solution can fit into a 26 nL reservoir due to surface tension, which keeps the reservoir from overflowing.) This filling solution will result in approximately 4.5 nL of liquid PEG 200 remaining at the bottom of the reservoir after the water evaporates. The calculation of the radius of curvature assumes a zero contact angle between the PEG 200 and silicon. This is a reasonable approximation because the PEG 200 wets the silicon surface very well. The radius of curvature (r) was estimated geometrically to be 356 μm for a reservoir in a 306 μm thick silicon wafer having a small opening of 40 μm by 40 μm and side walls sloped at 54.7°. The uniformly distributed stress exerted on the gold membrane (τ) can be calculated with equation 6.1 using a radius of curvature of 356 μm and a surface tension (γ) for PEG 200 of 43 dynes/cm (at 25°C, Union Carbide). The calculated stress on the membrane was 2,420 dyne/cm^2, or 3.51 x 10^{-2} psi.

Plate theory dictates that the stresses present in a fixed-edge, square plate of a given material due to a uniformly distributed load are determined by the in-plane dimensions of the plate and its thickness. Equation 6.2 calculates the maximum stress (which occurs at the center of each edge) for average-thickness plates, in which flexure stress predominates[2]. Membranes are somewhat different than average-thickness plates in that direct tension dominates in membranes. To the best of our knowledge, no one has yet developed equations for calculating the stress in square membranes subjected to a uniformly distributed, normal load. However, it is expected that the stress distribution in square membranes subjected to a uniformly distributed load will depend on the in-plane dimensions and membrane thickness, similar to average-thickness plates. Four assumptions[3] associated with equation 6.2 are: (1) the plate is flat, of uniform thickness, and of homogeneous material, (2) the thickness is not more than about ¼ of the least transverse dimension and the maximum deflection is not more than about ½ of the thickness, (3) all forces, both loads and reactions, are normal to the plane of the plate, and (4) the plate is no where stressed beyond the elastic limit. The gold membranes are believed to meet

each of these assumptions, so it is reasonable to use equation 6.2 to obtain rough estimates of the stresses in gold membranes and the point at which gold membranes will fail.

$$\sigma_{MAX} = \beta \frac{\tau b^2}{t^2} \tag{6.2}$$

σ_{MAX} is the maximum stress in the gold membrane (at the center of each edge) in psi, constant $\beta = 0.3078$ for a square plate, $\tau = 3.51 \times 10^{-2}$ psi and is a uniformly distributed load calculated at the beginning of this section using equation 6.1, $b = 40$ μm and is the length of one side of the square plate, and $t = 0.3$ μm is the thickness of the plate. $\sigma_{MAX} = 192$ psi for above the conditions.

The value of the yield strength for bulk gold varies widely in the literature, but ranges from approximately 500 psi to 7,980 psi (the upper limit was estimated by the yield stress of silver). The tensile strength of bulk gold is approximately 18,850 psi. The yield strength for gold thin films having a 60 Å TiO_2 layer on one side was estimated to be 21,800 psi in the unpublished work of a colleague[4]. Although these values for bulk gold and thin films vary considerably and none were determined using unsupported gold membranes, they can be used to estimate whether gold membranes will be plastically deformed or fractured by the stress exerted on the membrane by a curved liquid surface.

The previous analysis showed that the maximum stress in the gold membrane is approximately 192 psi. Therefore, when compared to the yield and tensile strength values in the previous paragraph, the stress exerted on the gold membrane by a curved liquid surface is too small to cause intact gold membranes to plastically deform or to fracture. However, the presence of membrane defects and stress concentrators such as pinholes or the reduction in membrane thickness due to grain boundary corrosion or thermal grooving could cause the membrane stress to exceed the yield or tensile strength of the gold. In other words, if corrosion caused local reductions in membrane thickness (i.e. corrosion in grain boundaries), the stress in the membrane could increase until it reached a point where the membrane stress exceeded the yield or tensile strength for gold, causing plastic deformation or membrane fracture. This "critical thickness" ($t_{critical}$) can be calculated using equation 6.2. Table 6-4 contains the values for $t_{critical}$ for each of the yield and tensile strengths reported for gold. The table also shows the percentage reduction

in the total membrane thickness required to reach $t_{critical}$ for a 3,000 Å membrane. It is interesting that a thickness reduction of only 38% could be sufficient to cause membrane failure.

Table 6-4. Values of the critical gold membrane thickness for estimated values of gold yield and tensile strength.

Yield or Tensile Strength (psi)	$t_{critical}$ (Å)	Thickness Reduction Required for a 3,000 Å Au Membrane to Yield or Fracture
500 (Au bulk yield)	1,860	38%
7,980 (Ag bulk yield)	470	84%
18,850 (Au bulk tensile)	300	90%
21,800 (Au thin film yield)	280	91%

It was pointed out in section 6.4.1.2 that no intact gold membranes having a thickness of at least 2,000 Å were observed to tear upon reservoir filling with a material that remains a liquid in the reservoir. This observation agrees well with the results presented in table 6-4. According to the plate theory calculations, the stresses in gold membranes begin to approach the critical thickness for yielding just below 2,000 Å. Therefore, for membranes thinner than 2,000 Å, the membrane stresses may be large enough to cause plastic deformation or failure. Also, if the radius of curvature of the liquid in the reservoir was smaller than the value used in these calculations (356 μm), which is the case when no liquid polymer is in the filling solution and all the water evaporates, the membrane stresses would be even larger and membranes thicker than 2,000 Å could fail.

The percentage reductions in the gold membrane thickness required for failure given in table 6-4 are consistent with experimental observations of membrane corrosion. It was shown in section 4.5.1.2.2 that approximately 50% of the mass of the exposed gold (not under the SiO_2) portion of the anode of TRL prototype 021397-1#6 was corroded. Figure 4-17 shows the extent of this corrosion in the 40 μm by 40 μm area of exposed gold. Figure 4-17b shows that large surfaces of this gold film remain uncorroded, which indicates that the corrosion in the grain boundaries must have extended deep into the film to account for corrosion of 50% of the mass of the exposed gold film. If this prototype were an unsupported gold membrane instead of a

supported gold film, such corrosion would cause local thinning of the gold membrane and a rapid increase in membrane stress. Figure 6-9 shows a section of the opened gold membrane of reservoir 34 of TRL prototype 081297-1#10. The grain boundaries of the opened gold membrane appear to be deeply corroded. The membrane also had sections that were still intact, indicating that the membrane opened before corrosion had progressed completely through the gold membrane. This is consistent with the analysis of this section, which says that membranes will fail due to applied stresses when the membrane is weakened, but not completely perforated, by corrosion.

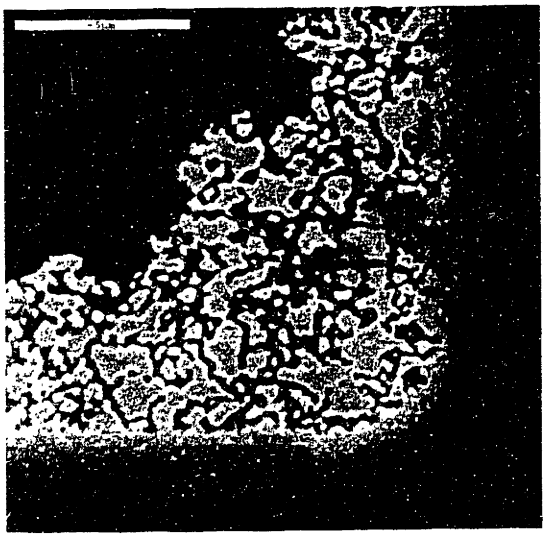

Figure 6-9. Scanning electron micrograph of reservoir 34 of TRL prototype 081297-1#10 showing grain boundary corrosion and the edge of the failed membrane.

6.4.1.4 Possible role of stress corrosion cracking. Sections 6.4.1.1, 6.4.1.2, and 6.4.1.3 discussed how corrosion and physical stress both contribute to the disintegration of gold membranes. However, it is not known whether corrosion and stress act independently, or if they act in conjunction with one another through stress corrosion cracking (SCC). It was stated in section 4.2.3 that the conditions under which the prototype controlled release microchips operate could potentially result in SCC cracking of the gold membranes. It is known that filled reservoirs have internal tensile stresses exerted on their gold membranes, as predicted by the Young-Laplace equation and evidenced by the deformation of the gold membranes after reservoir filling. The gold membranes also have external stresses exerted on them, such as the hydrostatic pressure of the electrolyte. If a thin oxide layer were present on the gold membrane

surface, it may be possible for these tensile stresses to initiate a crack in the oxide and extend it into the pure gold membrane. However, it is known that the native oxide present on gold is typically thin, and it is not known whether this oxide would be thick enough or brittle enough to initiate a crack. It was clearly demonstrated in chapters 4, 5, and 6 that gold membranes are preferentially corroded at the grain boundaries. It is possible that once corrosion is initiated at a grain boundary, mechanisms such as those mentioned in section 4.2.3 (i.e. film induced cracking or surface mobility of vacancies) could play a part in crack propagation.

The only way to determine if SCC is taking place would be to examine the membrane's fracture surfaces. If SCC were occurring, it would be expected that the fracture surfaces would be faceted, either intergranularly or transgranularly, and would show minimal signs of loss due to corrosion. General corrosion would be expected to have smoother surfaces due to extensive corrosion losses and more random fracture surfaces. Fracture by mechanical stresses after the membrane was thinned and weakened by general corrosion would tend to be ductile in nature, instead of the brittle fracture expected for SCC.

The fracture surfaces for the *in situ* devices, particularly TRL prototype 081297-2#4, should have provided evidence for or against SCC. However, there were factors that did not allow these fracture surfaces to be examined in detail. First, the devices were permanently mounted in their plastic microchip packages. These packages were large, and they made it impossible to view the devices under the SEM at an angle at small working distances. The resolution of the fracture surfaces was severely limited due to the large working distances in the SEM. Second, cleaning the devices after the *in situ* experiments sometimes damaged the fracture surfaces. The fractured membranes are only 0.3 μm thick, so even the process of gently rinsing and drying the device damaged the fracture surfaces enough so that they could not be adequately examined. It is important to make sure that issues such as these are addressed before future *in situ* experiments are conducted.

6.4.2 Device reliability. Device reliability, as used herein, is a measure of the ability of the controlled release microchip to operate as expected or desired and in a reproducible manner. This section will discuss aspects of device design, fabrication, or testing that can lead to unreliable device operation or unexpected results.

6.4.2.1 Pinholes. Tiny holes, or pinholes, in the gold membrane covering a reservoir can allow the chemical inside to leak out prematurely, causing the controlled release microchip to fail. The frequency of pinhole defects in gold membranes is directly related to the cleanliness of the fabrication facility (as measured by particulate count) and the processing habits of the person fabricating the devices. The author fabricated all of the controlled release prototypes presented in this thesis, so the variable of processing habits remained relatively constant for all devices. However, two processing facilities employing different methods of particulate control were used to make the prototypes.

The Building 13 Microlab at MIT is a facility that has the processing equipment necessary to make controlled release microchips, but it is not a controlled environment cleanroom. An effort is made to reduce particulates in the Microlab by using gowns and laminar flow hoods, but the particulate count cannot be tightly controlled. Consequently, one problem encountered with the Microlab prototypes was low yield. Most Microlab prototypes would have 3 or 4 viable reservoirs (out of six total reservoirs, for a 50-66% yield) after device processing. A portion of the low yield can be attributed to particulates forming holes in the gold membranes or defects in silicon nitride support membranes, causing them to break. (Stresses in nitride support membranes deposited in the Microlab could also contribute to the lower yield.) The Technology Research Laboratory (TRL) in the Microsystems Technology Laboratory (MTL) at MIT is a controlled environment cleanroom with a particulate rating of class 100 (defined as <100 1 μm particles per ft^3). This controlled environment greatly decreased the defects attributable to particulate contamination, resulting in significantly higher yields, typically (73-88%).

6.4.2.2 Nitride membrane. The presence of a residual silicon nitride membrane under the gold membrane covering a reservoir can greatly affect the reliability of a controlled release microchip. The presence of a nitride membrane can keep the reservoir from opening at all, as discussed at the end of section 6.4.1.2. Alternatively, a reservoir covered by a nitride membrane might still open (see figures 6-4 and 6-5), but the formation of a membrane "flap" could make chemical release from the reservoir erratic. The effect of a flap on the release kinetics of ^{45}Ca from TRL prototype 081297-1#11 was discussed in section 5.4.1. It is clear that reliable operation is not possible when a silicon nitride membrane is present under the gold membrane. Therefore, processing conditions must be optimized to ensure that no residual silicon nitride membrane remains under the gold membrane covering a reservoir.

6.4.2.3 Electrode placement. One difference between the Microlab prototypes and the TRL prototypes is the relative placement of the electrodes on the device surface. The Microlab prototype has an individual cathode close to (~ 40 μm) and surrounding each anode. Release studies conducted with the Microlab prototype indicated that having the anode and cathode this close together decreased the reliability of the gold corrosion reaction and reservoir opening. The diameter of the tip of the reference electrode is much larger (1 mm) than the distance across the anode and cathode area (260 μm). It is believed that the electric potential of the cathode interferes with the detection of the anode potential with the reference electrode because the anode and cathode are too close together. Consequently, the potentiostat is sometimes unable to precisely control the anode potential. The TRL prototype has the cathodes spaced farther (> 1 mm) from the anodes, resulting in greater reliability of the gold corrosion reaction.

6.4.2.4 Corrosion rate uniformity. It was discussed at the end of section 6.4.1.1 how non-uniformities in electric potential can form across the surface of a gold membrane during the corrosion process. This phenomenon can result in lower potentials and slower corrosion rates at the center of the membrane when compared to the edges. The formation of microenvironments in crevices can also result in non-uniform corrosion rates across a gold membrane. An extreme case of faster corrosion around the edges of the membrane or in crevices might result in the loss of electrical connection between the bulk of the membrane and the gold trace covered by SiO_2 at

the edge of the membrane. This would stop corrosion of the gold membrane prematurely, leaving a gold membrane over the reservoir that is weaker, but might still have some structural integrity. This membrane may not fall apart, which could prevent or impede the release of chemical from the reservoir.

6.4.2.5 Induced currents. The accidental release of chemicals must be prevented in order to consider the controlled release microchip reliable. It was shown in section 5.4.1 how currents induced in gold electrodes by the application of electric potentials to neighboring electrodes could result in premature chemical release by corrosion and perforation of the gold membrane. It was demonstrated that this type of failure could easily be prevented by isolating from ground all gold membranes from which release was not desired. This simple modification prevents induced gold corrosion by not allowing the electrons of neighboring electrodes to freely flow to ground.

6.5 Conclusions. Theory and experimental observations support the following conclusions about the disintegration of gold membranes in prototype controlled release microchips.

(1) The primary role of corrosion in gold membrane disintegration is to weaken the membrane by localized thinning of the membrane.

- Thin film, gold membranes are preferentially corroded along grain boundaries.
- Non-uniformities in the rates of corrosion across a gold membrane can result from a non-uniform potential distribution across the surface of the membrane formed as the membrane corrodes and thins or from the formation of microenvironments in crevices that favor faster corrosion rates.

(2) The primary role of physical stress in gold membrane disintegration is to cause the membrane to fail after it is weakened by corrosion.

- Stresses can be exerted on the gold membrane from sources both inside and outside the reservoir. These stresses are usually not large enough to break gold membranes that have not been weakened by corrosion.
- The role, if any, of stress corrosion cracking in the membrane disintegration process is still unclear and needs further study.

6.6 References.

1. Jones, D.A. *Principles and Prevention of Corrosion* 199-233 (Prentice Hall, Upper Saddle River, NJ, 1996).
2. Symonds, J. "Mechanical properties of materials" in *Marks' Standard Handbook for Mechanical Engineers* (eds. Avallone, E.A. & Baumeister, T.) 52-54 (McGraw-Hill, New York, NY, 1987).
3. Roark, R.J. & Young, W.C. *Formulas for Stress and Strain* Chapter 10 (McGraw-Hill, New York, NY, 1975).
4. Leung, O. "Personal Communication" (1998).

7. FUTURE WORK

This thesis describes the concept, theory, fabrication process, proof-of-principle release studies, and release mechanism observations for a controlled release microchip. Future work for the controlled release microchip spans a wide range of fields, from materials science to microelectronic fabrication and packaging to *in vivo* studies. The following sections present suggestions for future work to address some of the remaining issues in these areas.

7.1 Materials science. The most important aspect of any controlled release device is its chemical release mechanism. The prototype controlled release microchip presented in this thesis uses the disintegration of a thin gold membrane as the mechanism for chemical release. The process of disintegration was postulated in chapter 6 to have both electrochemical and mechanical components. Chapters 4, 5, and 6 clearly demonstrated the importance of the electrochemical corrosion of gold to the membrane disintegration process. Studies presented in chapter 6 seemed to indicate that mechanical stress on the membrane does contribute to its disintegration. However, it was difficult to draw conclusions about the importance of mechanical stresses exerted on the gold membranes by variable loading of the chemical inside the reservoir. It was also unclear as to whether stress corrosion cracking contributed to the membrane disintegration process through the combination of intergranular corrosion and applied mechanical stress.

Future work in this area should focus on evaluating the relative importance of the mechanical component of the membrane disintegration process. This may involve conducting additional experiments similar to the *in situ* experiments presented in chapter 6. The reservoirs should be filled with varying amounts of the chemical to be released to examine the effect of the stresses exerted on the gold membrane by the chemical inside the reservoir. If the stresses resulting from chemical loading are important in the membrane disintegration process, such studies should allow a correlation of membrane disintegration with gold structural/mechanical properties (i.e. strength, thickness, grain size, etc.) and chemical loading. Detailed scanning electron microscopy studies of gold membrane fracture surfaces may help determine whether the electrochemical and mechanical components of the disintegration process are independent of

each other, or if they work together through stress corrosion cracking. Studies where gold membranes covering filled reservoirs are exposed to chloride solutions and low applied voltages for extended periods of time may also help in determining the importance of SCC. Regardless, this work will necessarily require an understanding of the structural/mechanical properties of thin gold membranes. Work on grain growth in gold thin films was published by Thompson[1,2] and work on the mechanical properties of thin films has been conducted by Nix[3], including unpublished work on gold thin films. Such studies must be expanded to include unsupported membranes.

The determination of the structural/mechanical properties of thin gold membranes would not only be useful for the controlled release microchip, but may be useful in a number of MEMS applications. It was mentioned in section 3.4.3 that analytic expressions for the stress distribution in square membrane structures have not yet been developed. Correlation of membrane disintegration with membrane structural/mechanical properties and applied stresses (estimated by the Young-Laplace equation) due to chemical loading, could aid in the formation of mathematical models of stresses in square gold membranes.

7.2 Microelectronics fabrication and packaging. The previous section described the importance of the structural/mechanical properties of the gold membranes to the chemical release mechanism of the controlled release microchip. The structural/mechanical properties of these membranes can be significantly affected by processing conditions. For example, the grain size of the gold membranes can be affected by the pressure at which the gold is deposited and by the temperatures that the gold is exposed to during later processing steps. Grain size can affect the mechanical properties of the membrane and the proportion of exposed grain boundary to grain surface area. Because gold thin films corrode preferentially in the grain boundaries, changing the proportion of grain boundary to grain area will also affect the percentage of the membrane corroded with an applied electric potential. In addition, high processing temperatures may even form voids in the gold membrane, causing device failure[4]. Therefore, it is important to optimize processing conditions to achieve structural/mechanical membrane properties resulting in the most reliable microchip operation. The studies proposed in the previous section can be used to determine what these desired structural/mechanical properties might be.

The packaging of the controlled release microchip is important for its use in real applications, particularly in drug delivery. Implantable or orally administered controlled release microchips would potentially require the incorporation of a number of active components, such as a battery, a microprocessor, a demultiplexer, and a reference electrode, for the microchip to operate autonomously. Some of these components are used currently in medical devices such as implantable cardiac pacemakers and defibrillators. Pacemaker research could provide answers to some of the questions concerning implantable packaging. However, additional engineering challenges in the development of controlled release microchip packaging exist. These include decreasing the size of the packaging even further for implantation into smaller spaces (i.e. eye, brain, joints, etc.), interconnection between the microchip and the other active components in the hybrid (possibly, multi-level) package, and the type and location of a reference electrode on the chip or in the package. The development of an "on-chip" reference electrode is another interesting area for future work.

7.3 *In vivo* testing. The work presented in chapter 5 showed that chemicals could be stored and released from a microchip device on demand. This was a proof-of-principle demonstration. For application in human or veterinary drug delivery, it must be shown that the controlled release microchip operates in a living system (i.e. *in vivo*). The first step towards *in vivo* studies is the selection of the model system. The model system is composed of the drug or chemical to be released and the animal species. The most important requirement for the model drug or chemical is that it is detectable at low concentrations (i.e. in the blood or urine) or results in a physiological response that is easily quantifiable (i.e. increase in heart rate or blood pressure). The most important requirement for selection of the animal species for the *in vivo* studies is size of the animal. The animal must be large enough to allow the microchip and its associated electronics to be implanted. The size of the microchip will be dictated by the amount of the drug or chemical that must be contained in the microchip, which is directly related to the drug or chemical's detection limit and the duration of the experiment. Therefore, the device size and animal model can be selected after a model drug or chemical for release has been chosen.

The primary goal of initial *in vivo* studies would be to demonstrate qualitatively that drug or chemical release can be achieved *in vivo* with a controlled release microchip. However, it is

important to understand quantitatively how release is affected by a living system. Later *in vivo* studies could utilize measurements of release rate, total mass released, and the concentration vs. time profile in the animal to postulate the type of mass transport mechanisms dominating at the implant site. Factors such as local inflammation, immune reactions, or fibrous encapsulation, if present, could be quantified by histology and their effect on the transport kinetics of drugs out of the microchip could be correlated to observed changes in drug release profiles. It may even be possible to construct computer models to simulate *in vivo* drug release and to compare simulation results to experimental data.

7.4 References.

1. Wong, C.C., Smith, H.I. & Thompson, C.V. "Surface-energy-driven secondary grain growth in thin Au films." *Appl. Phys. Lett.* **48**, 335-337 (1986).
2. Thompson, C.V. "Grain growth in thin films." *Annu. Rev. Mater. Sci.* **20**, 245-268 (1990).
3. Nix, W.D. "Mechanical properties of thin films." *Metallurgical Transactions A* **20A**, 2217-2245 (1989).
4. Jiran, E. & Thompson, C.V. "Capillary instabilities in thin, continuous films." *Thin Solid Films* **208**, 23-28 (1992).

APPENDIX A – Chemical Release Calculations

This appendix contains the equations used to calculate the mass or activity released and the release rate for the chemical release studies presented in chapter 5. The calculation spreadsheet (Microsoft EXCEL 97) for TRL prototype 081297-1#11 is also included in this appendix as a representative example of how these calculations were conducted.

Fluorescence Calculations

Corrected Fluorescence

$$\left[\begin{array}{c}\text{Corrected Fluorescence}\\(\text{counts/sec})\end{array}\right]=\left[\begin{array}{c}\text{Release Medium}\\\text{Fluorescence (counts/sec)}\end{array}\right]-\left[\begin{array}{c}\text{Blank Medium}\\\text{Fluorescence (counts/sec)}\end{array}\right]$$

The release medium was the saline solution into which the device was inserted and fluorescein was released. The blank medium was used to obtain a background fluorescence signal and consisted of saline solution not containing any fluorescein.

Dilutions

$$\left[\begin{array}{c}\text{Fluorescein Concentration}\\\text{in a Dilution (nM)}\end{array}\right]=\left[\begin{array}{c}\text{Corrected Fluorescence}\\(\text{counts/sec})\end{array}\right]*\left[\begin{array}{c}\text{Slope of Fluorescence Calibration}\\\text{Line}\left(\dfrac{\text{nM}}{\text{counts/sec}}\right)\end{array}\right]$$

$$\left[\begin{array}{c}\text{Mass of Fluorescein}\\\text{in a Dilution (ng)}\end{array}\right]=\left[\begin{array}{c}\text{Fluorescein}\\\text{Concentration}\\\text{in a Dilution (nM)}\end{array}\right]*\left[\begin{array}{c}\text{Volume of the}\\\text{Sample (L)}\end{array}\right]*\left[\begin{array}{c}\text{Fluorescein Molecular}\\\text{Weight (ng/nmole)}\end{array}\right]$$

Dilution #1 was a sample taken directly from the release medium. If dilution #1 was too concentrated to be analyzed by the fluorescence spectrometer, dilution #1 was diluted to form a less concentrated solution, called dilution #2.

Release Vessel

$$\left[\begin{array}{c}\text{Fluorescein Concentration}\\\text{in Release Medium (nM)}\end{array}\right]=\frac{\left[\begin{array}{c}\text{Concentration in}\\\text{Dilution \#1 (nM)}\end{array}\right]*\left[\begin{array}{c}\text{Volume of Solution}\\\text{in a Cuvette (L)}\end{array}\right]}{\left[\begin{array}{c}\text{Volume of the Release Medium Transferred}\\\text{from the Release Medium to Dilution \#1 (L)}\end{array}\right]}$$

$$\left[\begin{array}{c}\text{Mass of Fluorescein}\\ \text{in the Release Medium}\\ \text{Immediately Before a}\\ \text{Sample was Taken (ng)}\end{array}\right]=\left[\begin{array}{c}\text{Fluorescein}\\ \text{Concentration}\\ \text{in Release}\\ \text{Vessel (nM)}\end{array}\right]*\left[\begin{array}{c}\text{Volume of the}\\ \text{Release Medium (L)}\end{array}\right]*\left[\begin{array}{c}\text{Fluorescein Molecular}\\ \text{Weight (ng/nmole)}\end{array}\right]$$

$$\left[\begin{array}{c}\text{Mass of}\\ \text{Fluorescein}\\ \text{Released}\\ \text{Between } T_1\\ \text{and } T_2 \text{ (ng)}\end{array}\right]=\left[\begin{array}{c}\text{Mass of Fluorescein}\\ \text{in the Release}\\ \text{Medium Immediately}\\ \text{Before a Sample was}\\ \text{Taken (ng)}\end{array}\right]_{T_2}-\left[\begin{array}{c}\text{Mass of Fluorescein}\\ \text{in the Release}\\ \text{Medium Immediately}\\ \text{Before a Sample was}\\ \text{Taken (ng)}\end{array}\right]_{T_1}+\left[\frac{4}{3}\right]*\left[\begin{array}{c}\text{Mass of}\\ \text{Fluorescein}\\ \text{in Dilution \#1}\\ \text{at } T_1 \text{ (ng)}\end{array}\right]$$

4 mL of the release medium were taken at each time point as samples for fluorescence spectroscopy and scintillation counting for the release calculation example presented in this appendix. Of these 4 mL, 3 mL were used for fluorescence spectroscopy and 1 mL was used for scintillation counting. The factor of 4/3 was included in the above calculation to account for the mass of fluorescein present in the 1 mL sample that was removed for scintillation counting.

Total Mass of Fluorescein Released as a Function of Time

$$\left[\begin{array}{c}\text{Total Mass of Fluorescein}\\ \text{Released into the Release}\\ \text{Medium up to Time } T_2 \text{ (ng)}\end{array}\right]=\left[\begin{array}{c}\text{Total Mass of Fluorescein}\\ \text{Released into the Release}\\ \text{Medium up to Time } T_1 \text{ (ng)}\end{array}\right]+\left[\begin{array}{c}\text{Mass of Fluorescein}\\ \text{Released Between } T_1\\ \text{and } T_2 \text{ (ng)}\end{array}\right]$$

Fluorescein Release Rate

$$\left[\begin{array}{c}\text{Fluorescein Release}\\ \text{Rate Between } T_1\\ \text{and } T_2 \text{ (ng/min)}\end{array}\right]=\frac{\left[\text{Mass of Fluorescein Released Between } T_1 \text{ and } T_2 \text{ (ng)}\right]}{\left[T_2 - T_1 \text{ (min)}\right]}$$

Averaged Time Point (used in plotting release rate vs. time)

$$\left[\text{Averaged Time Point (min)}\right]=\left[\frac{T_2 - T_1 \text{ (min)}}{2}\right]+\left[T_1 \text{ (min)}\right]$$

Radioactivity Calculations

Counting Efficiency

$$[\text{Counting Efficiency}] = \frac{[\text{Measured Activity (CPM)}]}{[\text{Estimated Activity (DPM)}]}$$

The (radio)activity of a sample was determined with a scintillation counter. The measured activity is given as counts per minute (CPM), which corresponds to the number of photons detected by the scintillation counter. These photons are emitted from the scintillation fluid of a sample when excited by beta particles from the decay of the radioactive compound. However, not every disintegration is detected. The scintillation counter estimates the actual activity of the sample, given as disintegrations per minute (DPM), from the counts per minute, the type of isotope, and the characteristics of the sample fluid. Therefore, counting efficiency is a measure of the fraction of total disintegrations per minute that were detected by the scintillation counter.

^{45}Ca Activity

$$[\text{Activity (nCi)}] = \frac{[\text{Estimated Activity (DPM)}]}{[2{,}220\ (\text{DPM}/\text{nCi})]}$$

Radioactive Decay Formula – See equation 5.1 in chapter 5.

Release Vessel

$$\begin{bmatrix}\text{Activity of } ^{45}\text{Ca}\\ \text{in the Release Medium}\\ \text{Immediately Before a}\\ \text{Sample was Taken (nCi)}\end{bmatrix} = \begin{bmatrix}\text{Activity of } ^{45}\text{Ca in}\\ \text{0.001 L Sample (nCi)}\end{bmatrix} * \begin{bmatrix}\text{Volume of the}\\ \text{Release Medium (L)}\end{bmatrix}$$

$$\begin{bmatrix}^{45}\text{Ca Activity}\\ \text{Released}\\ \text{Between } T_1\\ \text{and } T_2 \text{ (nCi)}\end{bmatrix} = \begin{bmatrix}^{45}\text{Ca Activity}\\ \text{in the Release}\\ \text{Medium Immediately}\\ \text{Before a Sample was}\\ \text{Taken (nCi)}\end{bmatrix}_{T_2} - \begin{bmatrix}^{45}\text{Ca Activity}\\ \text{in the Release}\\ \text{Medium Immediately}\\ \text{Before a Sample was}\\ \text{Taken (nCi)}\end{bmatrix}_{T_1} + [4] * \begin{bmatrix}\text{Activity of } ^{45}\text{Ca in}\\ \text{0.001 L Sample}\\ \text{taken at } T_1 \text{ (nCi)}\end{bmatrix}$$

4 mL of the release medium were taken at each time point as samples for fluorescence spectroscopy and scintillation counting for the release calculation example presented in this appendix. Of these 4 mL, 3 mL were used for fluorescence spectroscopy and 1 mL was used for scintillation counting. The factor of 4 was included in the above calculation to account for the ^{45}Ca activity present in the 3 mL sample that was removed for fluorescence spectroscopy.

Total Activity of ^{45}Ca Released as a Function of Time

$$\begin{bmatrix}\text{Total Activity of } ^{45}\text{Ca} \\ \text{Released into the Release} \\ \text{Medium up to Time } T_2 \text{ (nCi)}\end{bmatrix} = \begin{bmatrix}\text{Total Activity of } ^{45}\text{Ca} \\ \text{Released into the Release} \\ \text{Medium up to Time } T_1 \text{ (nCi)}\end{bmatrix} + \begin{bmatrix}^{45}\text{Ca Activity} \\ \text{Released Between } T_1 \\ \text{and } T_2 \text{ (nCi)}\end{bmatrix}$$

^{45}Ca Release Rate

$$\begin{bmatrix}^{45}\text{Ca Release} \\ \text{Rate Between } T_1 \\ \text{and } T_2 \text{ (nCi/min)}\end{bmatrix} = \frac{\left[^{45}\text{Ca Activity Released Between } T_1 \text{ and } T_2 \text{ (nCi)}\right]}{\left[T_2 - T_1 \text{ (min)}\right]}$$

Release Experiment Summary Sheet

John T Santini, Jr

Start Date =	7/19/98
Device =	081297-1#11
Release Medium =	0.145 M NaCl
Compounds =	Na-Fluorescein and ^{45}Ca
Fluorescein MW =	376 28

Fluorescence Spectroscopy Parameters

Excitation =	491	nm
Emission =	513	nm
Slit Width =	5	nm
Scan Time =	10	sec
Scan Increment =	10	points/sec

Soln Vol per Cuvette =	0.003	L
Vol. from Rel Med. to Dilution #1 =	0 003	L
Vol from Dilution #1 to Dilution #2 =	0.001	L
Vol of Release Medium =	0 100	L

	Sample Taken				Measured	Average Fluorescence (counts/sec)				Dilution #2	
Sample #	Date	Time (min)	Total Time (min)	Total Time (days)	Date	Blank Medium	Release Medium	Range	Corrected Flourescence	Concentration (nM)	Mass (ng)
1	7/17/98	0 00	0 00	0 00000	7/19/98	50064.00	35248 70		-14815 31		
2	7/17/98	23 75	23 75	0 01649	7/19/98	49917 03	38521.81		-11395 23		
3	7/17/98	118 00	118 00	0 08194	7/19/98	49797.22	32564 65		-17232.57		
4	7/17/98	308.00	308 00	0 21389	7/19/98	48418 31	35994 64		-12423 67		
5	7/18/98	863 00	863 00	0 59931	7/19/98	48534 86	24814.89		-23719 97		
6	7/18/98	1424 00	1424 00	0 98889	7/19/98	48322 41	37386.19		-10936.22		
7	7/18/98	1444 00	1444 00	1 00278	7/19/98	48366 18	46977 14		-1389 04		
8	7/18/98	1458 00	1458 00	1 01250	7/19/98	48423 25	32160 33		-16262 92		
9	7/18/98	1465 00	1465 00	1 01736	7/19/98	48646 19	27814 12		-20832 06		
10	7/18/98	1470 00	1470 00	1 02083	7/19/98	49472 82	22510 34		-26962 48		
11	7/18/98	1485 00	1485 00	1 03125	7/19/98	50235.95	23267 16		-26968 79		
12	7/18/98	1526 00	1526 00	1 05972	7/19/98	50534 42	46037 76		-4496 66		
13	7/18/98	1555 00	1555 00	1 07986	7/19/98	51771 55	20136 07		-31635 48		
14	7/18/98	1613 00	1613 00	1 12014	7/19/98	52712 97	21411.13		-31301.84		
15	7/18/98	1687 00	1687 00	1 17153	7/19/98	51423 61	27371.90		-24051 71		
16	7/18/98	1755 00	1755 00	1 21875	7/19/98	52435.50	31091 03		-21344 47		
17	7/18/98	1816 25	1816 25	1 26128	7/19/98	53103 88	34207.71		-18896 18		
18	7/18/98	1821 25	1821.25	1 26476	7/19/98	48695.69	69351 66		20655 97		
19	7/18/98	0 01	1821 26	1 26476	7/19/98	52415.76	52607 47		191 71		
20	7/18/98	5 00	1826 25	1 26823	7/19/98	52441.78	24222 36		-28219.42		
21	7/18/98	16 00	1837 25	1 27587	7/19/98	53094 86	38380.22		-14714 64		
22	7/18/98	82 00	1903 25	1 32170	7/19/98	53460 63	39287 37		-14173.26		
23	7/18/98	284.00	2105 25	1 46198	7/19/98	53387 95	30058.38		-23329 58		
24	7/18/98	345.50	2166 75	1 50469	7/19/98	53405 16	27997 61		-25407.55		
25	7/18/98	356 00	2177.25	1 51198	7/19/98	53071.68	24975 67		-28096.02		
26	7/19/98	365.00	2186 25	1 51823	7/19/98	53233 92	470249.05		417015 13		
27	7/18/98	370 00	2191 25	1 52170	7/19/98	53957 80	738459 78		684501 98		
28	7/19/98	387.00	2208 25	1 53351	7/19/98	53594 26	1191088 80		1137494 54		
29	7/19/98	415 00	2236 25	1 55295	7/19/98	54039 28	1333402 50		1279363 23		
30	7/19/98	467 00	2288 25	1.58906	7/19/98	54017 69	1514140.10		1460122 41		
31	7/19/98	517 00	2338 25	1 62378	7/19/98	54099 38	1555887 60		1501788.22		
32	7/19/98	560 00	2381 25	1 65365	7/19/98	54508.11	1534096 10		1479587.99		
33	7/19/98	632 00	2453 25	1 70365	7/19/98	52287 23	1570713 80		1518426.57		
34	7/19/98	682 00	2503.25	1 73837	7/19/98	53991.29	1524697.90		1470706.61		
35	7/19/98	710 00	2531 25	1 75781	7/19/98	54850.94	1460484 10		1405633.16		
36	7/19/98	720.00	2541 25	1 76476	7/19/98	54640 76	1408658 80		1354018.04		
37	7/20/98	0.01	2541 26	1 76476	7/21/98	61595.41	29922 47		-31672 94		
38	7/20/98	7.00	2548 25	1 76962	7/21/98	54898 42	29641 97		-25256.45		
39	7/20/98	20 00	2561 25	1 77865	7/21/98	62939.15	30291 60		-32647 55		
40	7/20/98	91 50	2632 75	1 82830	7/21/98	54854.42	31685 42		-23169 00		
41	7/20/98	211 50	2752 75	1 91163	7/21/98	55413 21	33177.49		-22235.72		
42	7/20/98	311 00	2852.25	1 98073	7/21/98	53616.75	47311 18		-6305 57		
43	7/20/98	344 00	2885.25	2 00365	7/21/98	55223.67	43260.10		-11963.57		
44	7/20/98	356 00	2897 25	2 01198	7/21/98	55131 86	37277 79		-17854 07		
45	7/20/98	365 00	2906 25	2 01823	7/21/98	52569 18	41933 25		-10635.93		
46	7/20/98	370.00	2911 25	2 02170	7/21/98	51942 46	51510 47		-431.99		
47	7/20/98	385 00	2926 25	2.03212	7/21/98	53089 17	54675.12		1585.95		
48	7/20/98	420 00	2961.25	2 05642	7/21/98	51981 36	47108 66		-4872.70		
49	7/20/98	476 00	3017 25	2 09531	7/21/98	55005.48	50219 54		-4785 94		
50	7/20/98	540 00	3081 25	2 13976	7/21/98	50217 54	30318 84		-19898.70		
51	7/20/98	603 00	3144.25	2 18351	7/21/98	50489 24	55116 19		4626 95		
52	7/20/98	677.00	3218 25	2 23490	7/21/98	56641 41	43474.20		-13167.21		
53	7/20/98	704 00	3245 25	2 25365	7/21/98	59626.15	31333 44		-28292.71		
54	7/20/98	720 00	3261 25	2.26476	7/21/98	57997 94	44776 74		-13221.21		
55	7/20/98	0.01	3261.26	2 26476	7/21/98	58636.27	40842 30		-17793.97		
56	7/20/98	6 00	3267 25	2 26892	7/21/98	51071.25	33897 81		-17173 44		

57	7/20/98	36.00	3297 25	2 28976	7/21/98	51339 50	36980 51		-14359 00		
58	7/20/98	88 00	3349.25	2 32587	7/21/98	51621 96	39303 81		-12318 16		
59	7/20/98	126 00	3387.25	2.35226	7/21/98	51429 06	38396 27		-13032.79		
60	7/20/98	294 00	3555 25	2 46892	7/21/98	61233 20	27516 93		-33716 27		
61	7/20/98	344 00	3605 25	2 50365	7/21/98	64686 08	23973 11		-40712 98		
62	7/20/98	356.00	3617 25	2 51198	7/21/98	62201 63	39786 63		-22415 01		
63	7/20/98	365 00	3626 25	2.51823	7/21/98	64762 11	154177 26		89415.15	1 3676	1.5438
64	7/20/98	370.00	3631.25	2 52170	7/21/98	54207 45	229635.76		175428.31	2 6832	3.0289
65	7/20/98	385 00	3646 25	2 53212	7/21/98	53831.32	343260 61		289429 29	4.4268	4.9971
66	7/20/98	411 00	3672 25	2 55017	7/21/98	56819 97	408400 33		351580 36	5 3774	6.0702
67	7/20/98	480 00	3741.25	2 59809	7/21/98	56522.45	478119 02		421596.57	6.4483	7 2791
68	7/20/98	540.00	3801 25	2 63976	7/21/98	55094.31	494139 42		439045 11	6 7152	7.5803
69	7/20/98	602.00	3863.25	2 68281	7/21/98	65701.43	492270 03		426568.60	6 5243	7.3649
70	7/20/98	662.50	3923 75	2 72483	7/21/98	54254 77	494680.97		440426.20	6.7363	7.6042
71	7/21/98	707.00	3968 25	2.75573	7/21/98	55609.14	491213 94		435604 80	6.6625	7.5209
72	7/21/98	720.00	3981.25	2.76476	7/21/98	54707.72	468015 63		413307.91	6.3215	7.1360

Important Notes:

The **BOLD** lines indicate when the PBS solution was changed

All of the calculations in this spreadsheet are based on the assumption that the solution in the release vessel is well mixed

The release medium was stirred with a small magnetic stirring bar at a setting of ~3 33 The release medium was at room temperature

Slope of Calibration Line [conc(nM) = m * corrected fluorescence(cts/sec)]

Date	Slope (m)
7/19/98	1 51094E-05
7/21/98	1 52949E-05

Dilution #1		Concentration in Release Vessel (nM)	Mass of Compound in Soln Before Sample was Taken (ng)	Mass of Compound Released Since Previous Time Point (ng)	Total Mass of Compound Released into Solution as a Function of Time (ng)	Averaged Time Point (min)	Averaged Time Point (days)	Approximate Release Rate at Averaged Time Point (ng/min)		Radioactivity Measured CPM
Concentration (nM)	Mass (ng)								Sample #	
0 0000	0 0000	0 0000	0 0000	0 0000	0 0000				1	29 80
0 0000	0 0000	0 0000	0 0000	0 0000	0 0000	11 88	0 00825	0 000	2	0 00
0 0000	0 0000	0 0000	0 0000	0 0000	0 0000	70 88	0 04922	0 000	3	0 00
0 0000	0 0000	0 0000	0 0000	0 0000	0 0000	213.00	0 14792	0 000	4	0.00
0 0000	0 0000	0 0000	0 0000	0 0000	0 0000	585 50	0 40660	0 000	5	0 00
0 0000	0 0000	0 0000	0 0000	0 0000	0 0000	1143 50	0 79410	0 000	6	0 00
0 0000	0 0000	0 0000	0 0000	0 0000	0 0000	1434 00	0 99583	0.000	7	0 00
0 0000	0 0000	0 0000	0 0000	0 0000	0 0000	1451 00	1 00764	0 000	8	0.00
0 0000	0 0000	0 0000	0 0000	0 0000	0 0000	1461 50	1 01493	0.000	9	1396.90
0 0000	0.0000	0 0000	0 0000	0 0000	0 0000	1467 50	1 01910	0 000	10	2049 10
0 0000	0 0000	0 0000	0 0000	0.0000	0 0000	1477 50	1.02604	0 000	11	2963 20
0 0000	0 0000	0.0000	0 0000	0 0000	0 0000	1505 50	1 04549	0.000	12	3862 10
0 0000	0 0000	0 0000	0 0000	0 0000	0 0000	1540 50	1 06979	0 000	13	3817.90
0.0000	0.0000	0 0000	0 0000	0.0000	0.0000	1584.00	1 10000	0 000	14	3687.30
0 0000	0 0000	0 0000	0 0000	0.0000	0 0000	1650 00	1.14583	0 000	15	3523 20
0 0000	0 0000	0 0000	0 0000	0 0000	0 0000	1721 00	1 19514	0 000	16	3413 30
0 0000	0 0000	0 0000	0 0000	0 0000	0 0000	1785.63	1.24002	0.000	17	3265.40
0 3121	0 3523	0 3121	11 7437	11.7437	11 7437	1818 75	1 26302	2 349	18	3093 40
0 0000	0.0000	0 0000	0 0000	0 0000	0 0000				19	24 300
0 0000	0 0000	0.0000	0 0000	0 0000	0 0000	1823 76	1 26650	0 000	20	0.000
0 0000	0 0000	0.0000	0 0000	0 0000	0 0000	1831.75	1.27205	0.000	21	2.600
0 0000	0 0000	0 0000	0 0000	0 0000	0 0000	1870 25	1 29878	0.000	22	7.700
0 0000	0 0000	0 0000	0 0000	0 0000	0 0000	2004.25	1 39184	0 000	23	2 400
0 0000	0 0000	0 0000	0 0000	0 0000	0.0000	2136 00	1 48333	0 000	24	1 000
0 0000	0 0000	0.0000	0 0000	0 0000	0.0000	2172 00	1 50833	0 000	25	3 700
6 3008	7.1126	6.3008	237 0883	237 0883	237 0883	2181.75	1 51510	26 343	26	3 900
10 3424	11.6749	10 3424	389 1644	161 5596	398.6479	2188 75	1 51997	32 312	27	1,900
17 1869	19.4012	17 1869	646 7072	273.1094	671 7573	2199 75	1.52760	16.065	28	5 200
19 3304	21 8209	19.3304	727 3647	106.5258	778 2831	2222 25	1 54323	3.804	29	5 600
22 0616	24 9040	22 0616	830 1329	131 8628	910 1459	2262.25	1 57101	2 536	30	5.900
22.6911	25 6146	22 6911	853 8214	56 8939	967.0397	2313 25	1 60642	1 138	31	2 900
22.3557	25 2360	22 3557	841.1908	21 5312	988.5709	2359.75	1 63872	0 501	32	6 300
22 9425	25 8984	22 9425	863 2809	55 7291	1044 3001	2417 25	1 67865	0.774	33	6 200
22 2215	25 0845	22.2215	836 1504	7 4007	1051 7008	2478 25	1 72101	0 148	34	14.000
21 2383	23 9746	21 2383	799 1538	-3 5506	1048 1502	2517 25	1 74809	-0 127	35	4 900
20.4584	23 0943	20 4584	769 8087	2 6211	1050.7712	2536 25	1 76128	0 262	36	5.300
0 0000	0 0000	0 0000	0 0000	0 0000	0 0000				37	26.00
0 0000	0.0000	0 0000	0 0000	0 0000	0 0000	2544.76	1 76719	0 000	38	358 60
0 0000	0 0000	0 0000	0 0000	0 0000	0 0000	2554 75	1 77413	0 000	39	475 90
0 0000	0 0000	0 0000	0 0000	0 0000	0 0000	2597 00	1 80347	0 000	40	582 20
0 0000	0.0000	0 0000	0 0000	0 0000	0 0000	2692 75	1 86997	0 000	41	587.30
0.0000	0.0000	0 0000	0 0000	0 0000	0 0000	2802 50	1 94618	0 000	42	579.20
0 0000	0 0000	0 0000	0 0000	0 0000	0.0000	2868 75	1 99219	0.000	43	547.60
0 0000	0 0000	0 0000	0 0000	0 0000	0 0000	2891 25	2 00781	0 000	44	535 00
0 0000	0.0000	0 0000	0 0000	0 0000	0 0000	2901 75	2 01510	0.000	45	1606.70
0 0000	0 0000	0 0000	0 0000	0 0000	0 0000	2908 75	2 01997	0 000	46	1821.00
0 0000	0 0000	0 0000	0 0000	0 0000	0 0000	2918 75	2 02691	0 000	47	2177 90
0.0000	0 0000	0 0000	0 0000	0 0000	0.0000	2943 75	2 04427	0 000	48	2677.60
0.0000	0 0000	0 0000	0 0000	0 0000	0 0000	2989.25	2 07587	0 000	49	2855 00
0 0000	0 0000	0 0000	0 0000	0 0000	0 0000	3049 25	2.11753	0.000	50	2919.10
0 0000	0 0000	0 0000	0 0000	0 0000	0 0000	3112 75	2.16163	0.000	51	2893.30
0 0000	0.0000	0.0000	0 0000	0 0000	0 0000	3181.25	2.20920	0 000	52	2802.60
0 0000	0 0000	0 0000	0 0000	0.0000	0 0000	3231.75	2 24427	0.000	53	2734.60
0 0000	0 0000	0 0000	0 0000	0 0000	0 0000	3253.25	2 25920	0 000	54	2599 60
0 0000	0.0000	0 0000	0 0000	0 0000	0.0000				55	25.70
0 0000	0.0000	0 0000	0 0000	0 0000	0 0000	3264 26	2.26684	0.000	56	12 70

0.0000	0 0000	0 0000	0 0000	0 0000	0 0000	3282.25	2.27934	0.000	57	4.80
0.0000	0.0000	0.0000	0.0000	0 0000	0.0000	3323 25	2 30781	0.000	58	24.90
0.0000	0.0000	0 0000	0.0000	0.0000	0.0000	3368 25	2.33906	0.000	59	34.30
0.0000	0.0000	0.0000	0.0000	0 0000	0.0000	3471 25	2.41059	0.000	60	53.20
0.0000	0 0000	0.0000	0 0000	0 0000	0 0000	3580 25	2.48628	0.000	61	64.70
0.0000	0.0000	0 0000	0 0000	0 0000	0 0000	3611 25	2.50781	0.000	62	59.00
4.1028	4.6314	4.1028	154.3797	154.3797	154.3797	3621.75	2.51510	17.153	63	62.80
8.0495	9.0866	8.0495	302.8857	154.6812	309.0608	3628 75	2.51997	30.936	64	66.30
13.2804	14.9914	13 2804	499.7140	208.9438	518.0046	3638.75	2 52691	13.930	65	64.40
16.1322	18.2106	16.1322	607 0209	127 2955	645 3001	3659.25	2.54115	4.896	66	59.40
19 3448	21.8372	19.3448	727 9073	145 1673	790.4674	3706.75	2.57413	2.104	67	70.20
20.1455	22.7410	20.1455	758.0331	59 2421	849.7094	3771.25	2.61892	0.987	68	82.60
19.5730	22.0948	19.5730	736.4918	8.7800	858.4894	3832 25	2.66128	0 142	69	91.80
20.2088	22 8125	20.2088	760.4176	53 3855	911.8749	3893.50	2.70382	0 882	70	99.70
19.9876	22.5628	19 9876	752.0932	22 0923	933.9673	3946 00	2.74028	0.496	71	97.40
18.9645	21.4079	18.9645	713 5966	-8.4130	925.5543	3974.75	2.76024	-0.647	72	101.40

Measurements and Calculations (from first scans)								
Calculated DPM	Calculated Efficiency	tSIE Factor	Activity (nCi) (from DPM)	Activity of ^{45}Ca in Release Vessel Before Sample was Taken (nCi)	Activity of ^{45}Ca Released Since Previous Time Point (nCi)	Total Activity of ^{45}Ca Released into Solution as a Function of Time (nCi)	Approximate Release Rate at Averaged Time Point (nCi/min)	Additional Comments/Notes
BKG		390.43	0 0000	0 0000	0 0000	0 0000		
0 00		391.49	0.0000	0 0000	0 0000	0 0000	0 0000	
0 00		392.49	0 0000	0 0000	0.0000	0 0000	0 0000	
0.00		393 01	0.0000	0 0000	0 0000	0 0000	0 0000	
0 00		388.99	0 0000	0 0000	0 0000	0 0000	0.0000	
0.00		389.95	0 0000	0 0000	0 0000	0 0000	0 0000	
0 00		390.93	0.0000	0 0000	0.0000	0 0000	0.0000	SCE in @ 1449.17 min
0 00		393.01	0 0000	0 0000	0 0000	0.0000	0.0000	Applied 1 04 V vs SCE to Res #3 for 30 sec @ 1460.33 min
1499.73	0.93	392.18	0.6756	67.5554	67 5554	67 5554	9.6508	SCE out @ 1461 33 min
2185 45	0.94	391 89	0.9844	98 4437	33 5905	101.1459	6.7181	
3144.15	0.94	394.25	1 4163	141 6284	47 1224	148 2683	3.1415	
4083.78	0.95	394.95	1 8395	183 9541	47.9908	196 2592	1.1705	
4046.01	0 94	391.61	1 8225	182.2527	5.6568	201 9160	0.1951	
3903 67	0.94	391.12	1 7584	175 8410	0 8784	202.7944	0 0151	
3735.13	0.94	393.85	1 6825	168 2491	-0.5583	202 2361	-0.0075	
3611.32	0 95	394.28	1.6267	162 6721	1.1529	203 3890	0.0170	
3458.21	0.94	392.15	1 5578	155 7752	-0 3900	202.9991	-0.0064	
3278.87	0 94	393 21	1.4770	147.6968	-1.8474	201.1517	-0.3695	
BKG		393.400	0.0000	0 0000	0 0000	0 0000		
0.000		391.780	0 0000	0 0000	0 0000	0 0000	0.0000	
6 250	0.42	391.120	0 0028	0 2815	0.2815	0 2815	0.0256	
35.320	0.22	390.410	0.0159	1.5910	1 3207	1 6023	0.0200	
5.760	0.42	391.300	0 0026	0 2595	-1 2679	0.3344	-0.0063	
2.400	0.42	392.100	0.0011	0 1081	-0.1410	0.1934	-0 0023	SCE in @ 350 min
30.300	0.12	390.150	0 0136	1.3649	1 2611	1.4545	0.1201	Applied 1.04 V vs SCE to Res #5 for 30 sec @ 360 min
9.370	0 42	390 830	0 0042	0 4221	-0.8882	0 5663	-0 0987	SCE out @ 360 75 min
4 560	0 42	392.210	0 0021	0 2054	-0 1998	0 3665	-0 0400	
12.440	0.42	393.560	0.0056	0 5604	0.3632	0 7297	0 0214	
31 920	0.18	390.270	0.0144	1 4378	0.8999	1.6295	0.0321	
33.060	0 18	392.250	0.0149	1 4892	0.1089	1.7384	0 0021	
6.900	0 42	396.980	0 0031	0 3108	-1.1188	0.6196	-0.0224	
15.050	0.42	394 350	0 0068	0 6779	0 3795	0 9992	0 0088	
14.840	0 42	393 200	0 0067	0.6685	0.0177	1 0168	0 0002	
40 760	0 34	389 430	0.0184	1 8360	1.1943	2.2111	0 0239	
11.710	0.42	393.910	0 0053	0 5275	-1 2351	0.9760	-0 0441	
31.530	0.17	392 220	0 0142	1 4203	0 9139	1.8899	0 0914	
BKG		390 55	0.0000	0.0000	0 0000	0 0000		
407 20	0.88	390 70	0 1834	18 3423	18 3423	18.3423	2 6241	
528 79	0.90	394 51	0 2382	23.8194	6 2107	24.5531	0.4777	
635.28	0.92	395.04	0.2862	28 6162	5 7496	30 3027	0 0804	
639.31	0.92	392.90	0 2880	28 7977	1.3262	31.6289	0 0111	
635 23	0.91	392 01	0 2861	28 6140	0 9681	32.5970	0.0097	
601.28	0.91	394 71	0 2708	27.0847	-0 3847	32.2123	-0.0117	SCE in @ 349 min
589.43	0.91	393 18	0 2655	26.5509	0.5496	32.7619	0 0458	Applied 1 04 V vs SCE to Res #24,25,26 for 30 sec @ 360 min
1709.95	0.94	391.05	0.7702	77 0248	51 5359	84 2978	5.7262	SCE out @ 361 min
1930 77	0.94	393.64	0 8697	86 9716	13 0278	97.3256	2.6056	
2314.46	0.94	392.82	1.0425	104.2550	20.7622	118.0878	1.3841	
2828.73	0.95	395.88	1 2742	127 4203	27.3355	145 4233	0.7810	
3027.16	0.94	395.05	1 3636	136.3586	14 0351	159.4584	0.2506	
3091.31	0 94	394.48	1.3925	139 2482	8.3440	167.8024	0 1304	
3062.64	0 94	390 37	1 3796	137.9568	4 2785	172 0809	0.0679	
2977.32	0.94	393.09	1 3411	134.1135	1.6750	173.7559	0 0226	
2897.72	0 94	391.56	1 3053	130 5279	1.7790	175.5349	0 0659	
2750.09	0.95	391.85	1 2388	123 8779	-1.4289	174.1060	-0.0893	
BKG		390.51	0.0000	0 0000	0.0000	0 0000		
40 75	0.31	394.89	0.0184	1.8356	1 8356	1 8356	0.3064	

44.06	0 34	394 94	0.0198	1.9847	0.2225	2 0581	0.0074	
55.42	0 45	393 67	0 0250	2 4964	0.5911	2 6492	0.0114	
64.70	0.53	392.18	0 0291	2 9144	0 5179	3.1671	0 0136	
84.32	0.63	395.55	0 0380	3 7982	1 0004	4.1674	0.0060	
95.02	0.68	392.88	0 0428	4 2802	0 6339	4 8014	0.0127	SCE in @ 348 min
89 44	0 66	392.46	0.0403	4 0288	-0 0801	4 7212	-0.0067	Applied 1 04 V vs SCE to Res #20 for 30 sec @ 361
93.65	0.67	394.90	0.0422	4.2189	0.3512	5 0725	0.0390	SCE out @ 361 min
97.34	0.68	392 56	0.0438	4.3847	0 3345	5.4070	0.0669	
93.55	0.69	392 08	0.0421	4.2140	0 0047	5.4116	0.0003	
90.52	0 66	391.49	0 0408	4.0775	0 0321	5 4437	0 0012	
100.77	0 70	391.78	0.0454	4 5392	0 6248	6 0685	0 0091	
114.27	0.72	391.09	0.0515	5 1473	0 7897	6.8582	0.0132	
124.00	0.74	392.57	0.0559	5 5856	0 6442	7.5024	0.0104	
131.96	0.76	395.62	0.0594	5.9441	0 5820	8 0844	0 0096	
129 53	0 75	394 55	0.0583	5.8347	0.1283	8.2127	0.0029	
133.08	0.76	393 32	0.0599	5 9946	0 3933	8 6060	0.0303	

THESIS PROCESSING SLIP

FIXED FIELD: ill. _____ name _____

index _____ biblio _____

► **COPIES:** Archives Aero Dewey Barker Hum

Lindgren Music Rotch Science Sche-Plough

TITLE VARIES: ► ☐ _____

_____

_____

NAME VARIES: ► ☐ _____

_____

IMPRINT: (COPYRIGHT) _____

_____

► **COLLATION:** _____

_____

► **ADD: DEGREE:** _____ ► **DEPT.:** _____

► **ADD: DEGREE:** _____ ► **DEPT.:** _____

SUPERVISORS: _____

_____

NOTES:

_____ cat'r: _____ date:

page:

► **DEPT:** _____

► **YEAR:** _____ ► **DEGREE:** _____

► **NAME:** _____

_____